National Aeronautics and Space Administration

Program Annual Technology Report

Physics of the Cosmos Program Office
Astrophysics Division
Science Mission Directorate

October 2017

PCOS Program

Program Office

Program Manager: *Mansoor Ahmed (mansoor.ahmed@nasa.gov)*
Deputy Program Manager: *Azita Valinia (azita.valinia-1@nasa.gov)*
Chief Scientist: *Ann Hornschemeier (ann.hornschemeier@nasa.gov)*
Deputy Chief Scientist: *Terri Brandt (t.j.brandt@nasa.gov)*
Chief Technologist: *Harley Thronson (harley.a.thronson@nasa.gov)*
Technology Development Manager: *Thai Pham (thai.pham@nasa.gov)*
PATR Production Lead and Editor: *Opher Ganel (opher.ganel@nasa.gov)*
PATR Co-Editor: *Russell Werneth (russell.l.werneth@nasa.gov)*
PATR Graphics: *Herbert Eaton (herbert.e.eaton@nasa.gov)*
DeLee Smith (delee.i.smith@nasa.gov)
PATR Admin Support: *Kay Deere (kay.m.deere@nasa.gov)*

Headquarters

Program Executive: *Shahid Habib (shahid.habib-1@nasa.gov)*
Program Scientist: *Rita Sambruna (rita.m.sambruna@nasa.gov)*
Deputy Program Scientist: *Daniel Evans (daniel.a.evans@nasa.gov)*

http://pcos.gsfc.nasa.gov

The report cover reflects the breadth of science topics pursued by the Physics of the Cosmos Program. Modern astrophysics has expanded beyond the spectrum visible to the human eye, depicted by the spiral galaxy. Searches for B-mode polarization in the cosmic microwave background, an expected signature of the inflationary period immediately following the Big Bang, are symbolized by vectors at the top right of our cover. X rays, generated by some of the most energetic and violent cosmic phenomena, such as active galactic nuclei, are represented by the artist's impression at the bottom left of the cover. Gravitational waves, vibrations in the very fabric of space-time caused by events involving supermassive black holes, are depicted by the artist's impression at the bottom right of the cover.

The Strategic Astrophysics Technology (SAT) project images, shown on the edges of the three-dimensional PCOS letters, demonstrate our ongoing efforts to identify and develop the technologies that will advance humankind's ability to observe and understand our universe.

Table of Contents

Executive Summary 4

1. Program Science Overview 7

2. Strategic Technology Development Process and Portfolio 11

3. Technology Gaps, Priorities, and Recommendations 18

4. Benefits and Successes Enabled by the PCOS SAT Program 24

5. Closing Remarks 29

References 30

Appendix A – Technology Gaps Evaluated by the TMB in 2017 31

Appendix B – Program Technology Development Quad Charts 64

Appendix C – Program Technology Development Status 78

Appendix D – Acronyms. 199

PCOS 2017 PATR Executive Summary

What is NASA's Physics of the Cosmos (PCOS) Program?

From ancient times, humans have looked up at the night sky and wondered: Are we alone? How did the universe come to be? **How does the universe work?** PCOS focuses on that last question. Scientists investigating this broad theme use the universe as their laboratory, investigating its fundamental laws and properties. They test Einstein's General Theory of Relativity to see if our current understanding of space-time is borne out by observations. They examine the behavior of the most extreme environments – supermassive black holes, active galactic nuclei, and others – and the farthest reaches of the universe, to expand our understanding. With instruments sensitive across the spectrum, from radio, through infrared (IR), visible light, ultraviolet (UV), to X rays and gamma rays, as well as gravitational waves (GWs), they peer across billions of light-years, observing echoes of events that occurred instants after the Big Bang.

Last year, the LISA Pathfinder (LPF) mission exceeded expectations in proving the maturity of technologies needed for the Laser Interferometer Space Antenna (LISA) mission, and the Laser Interferometer Gravitational-Wave Observatory (LIGO) recorded the first direct measurements of long-theorized GWs. Another surprising recent discovery is that the universe is expanding at an ever-accelerating rate, the first hint of so-called "dark energy," estimated to account for 75% of mass-energy in the universe. Dark matter, so called because we can only observe its effects on regular matter, is thought to account for another 20%, leaving only 5% for regular matter and energy. Scientists now also search for special polarization in the cosmic microwave background to support the notion that in the split-second after the Big Bang, the universe inflated faster than the speed of light! The most exciting aspect of this grand enterprise today is the extraordinary rate at which we can harness technologies to enable these key discoveries.

Why is PCOS Technology Development Critical?

A 2008 Space Review paper noted that robust technology development and maturation are crucial to reducing flight project schedule and cost over-runs: "*…in the mid-1980s, NASA's budget office found that during the first 30 years of the civil space program, no project enjoyed less than a 40% cost overrun unless it was preceded by an investment in studies and technology of at least 5 to 10% of the actual project budget that eventually occurred*" [1]. Such a technology maturation program is most efficiently addressed through focused R&D projects, rather than in flight projects, where "marching armies" make the cost of delays unacceptably high. The National Academies of Sciences 2010 Decadal Survey, *New Worlds, New Horizons in Astronomy and Astrophysics* (NWNH) stressed that *"Technology development is the engine powering advances in astronomy and astrophysics… Failure to develop adequately mature technology prior to a program start also leads to cost and schedule overruns"* [2].

NASA requires flight projects to demonstrate technology readiness level (TRL) 6* for required technologies by their preliminary design review. However, this can only occur if we correctly identify and adequately fund development of relevant "blue sky" technologies to TRL 3†, and then mature them to TRL 5‡ or 6, across the so-called "mid-TRL gap," where sustained funding frequently falls short.

* TRLs are fully described in NPR 7123.1B, Appendix E, with TRL definitions reproduced in Appendix A below; TRL 6 is defined as: "System/sub-system model or prototype demonstration in a relevant environment."

† TRL 3 is defined as: "Analytical and experimental critical function and/or characteristic proof-of-concept."

‡ TRL 5 is defined as: "Component and/or breadboard validation in relevant environment."

What's in this Report? What's New?

This seventh Program Annual Technology Report (PATR) summarizes the Program's technology development activities for fiscal year (FY) 2017. It lists technology gaps identified by the PCOS community and two mission-concept studies with priorities assigned by the PCOS Technology Management Board (TMB; see p. 22). Following this year's prioritization, the Program Office recommends that NASA Astrophysics Division at HQ solicit and fund the maturation of the following technologies with the highest priority:

- Highly stable, low-stray-light telescope;
- Low-mass, long-term-stability optical bench;
- Large-format, high-spectral-resolution, small-pixel X-ray focal plane arrays;
- Precision microthrusters;
- High-power, narrow-line-width laser sources;
- Phase measurement system (PMS);
- Fast, low-noise, megapixel X-ray imaging arrays with moderate spectral resolution;
- High-efficiency X-ray grating arrays for high-resolution spectroscopy;
- High-resolution, large-area lightweight X-ray optics;
- Non-deforming, X-ray-reflective coatings; and
- Long-wavelength-blocking filters for X-ray micro-calorimeters.

These recommendations represent technologies most critical for substantive near-term progress on strategic priorities. They take into account potential NASA contributions to the European Space Agency (ESA) Advanced Telescope for High ENergy Astrophysics (Athena), selected for ESA's L2 slot planned to launch in 2028, and the LISA GW mission selected for ESA's L3 slot planned to launch in the mid-2030s. The latter were captured by recommendations from the NASA L3 Study Team (L3ST). Technology needs for X-ray missions such as Athena and Lynx, an X-Ray Surveyor (XRS) concept, are represented by gaps submitted by the Lynx Science and Technology Definition Team (STDT). The Lynx STDT, along with STDTs for a Large UV/Optical/IR (LUVOIR) Surveyor; the Origins Space Telescope, a Far-IR Surveyor; and a Habitable Exoplanet (HabEx) imaging mission, were charged by the Astrophysics Division Director to develop the science case, technology assessment, design reference mission with strawman payload, and cost assessment. This is being done in preparation for the upcoming 2020 Astronomy and Astrophysics Decadal Survey. These Surveyors are three of five described in the Astrophysics Roadmap, "*Enduring Quests, Daring Visions*," released in December 2013, while HabEx was described in the NWNH. A LISA Study Office was established to manage NASA's efforts to develop technologies intended to serve as the US contribution to LISA.

Meanwhile, the Program is pleased to announce two newly awarded PCOS Strategic Astrophysics Technology (SAT) projects for FY 2018 start (alphabetically, by PI name):

- "*High-Speed, Low-Noise, Radiation-Tolerant CCD Image Sensors for Strategic High-Energy Astrophysics Missions*," Mark Bautz, MIT; and
- "*Superconducting Antenna-Coupled Detectors for CMB Polarimetry with the Inflation Probe*," James Bock, JPL.

Including these, the Astrophysics Division has awarded 28 PCOS SAT projects to date, funded by PCOS Supporting Research and Technology (SR&T), intended to develop telescopes, optics, detectors, electronics, micro-thruster subsystems, and laser subsystems, applicable to future strategic PCOS missions. Nine projects continue from previous years, each reporting significant progress, with several

prepared for TRL advancement review. Along with four new projects begun in FY 2017 that continue previous efforts, this PATR reports on the progress, current status, and planned activities for 13 projects funded in FY 2017. We thank the PIs for their informative progress reports (Appendix B – Quad Charts, p. 64; Appendix C – Development Status, p. 78), and welcome our new awardees, both of whom are returning SAT PIs (abstracts of the new SATs are included at the end of Appendix C).

The following are examples where PCOS-funded technologies were infused, or are planned to be infused, into projects and missions:

- Advancements made to X-ray detectors and readout technologies are allowing meaningful NASA contributions to Athena;
- REgolith X-ray Imaging Spectrometer (REXIS), an MIT student instrument on the Origins-Spectral Interpretation-Resource Identification-Security-Regolith Explorer (OSIRIS-REx), incorporated Program-funded directly deposited X-ray blocking filter technology on its CCDs (launched September 8, 2016);
- Antenna-coupled transition-edge superconducting (TES) bolometer technology was deployed in the ground-based Background Imaging of Cosmic Extragalactic Polarization (BICEP) experiment to measure B-mode polarization, and performance-tested in a realistic environment on a long-duration balloon flight of the Suborbital Polarimeter for Inflation Dust and the Epoch of Reionization (Spider) during the 2014/15 Antarctic season; and
- High-efficiency 40-GHz feedhorn-coupled TES-based detector architecture being matured by another SAT project was deployed in the Cosmology Large Angular Scale Surveyor (CLASS) telescope in the Atacama Desert.

Additionally, SAT-funded advances in X-ray detectors, high-stability lasers, low-scattered-light stable telescopes, micro-propulsion, phase-measurement systems, and others are allowing potential significant US contributions to ESA's Athena and LISA missions.

While infusion into ground-based and suborbital projects is not the goal of the SAT program, these are successes in that they support actual projects while proving technical performance on the path to infusion into space-based missions.

1. Program Science Overview

PCOS lies at the intersection of physics and astronomy. It uses the universe–the cosmic scale, the diversity of conditions, and the extreme objects and environments–as a laboratory to study the basic properties of nature. PCOS science addresses the fundamental physical laws and properties of the universe. The science objectives of the PCOS Program are to probe Einstein's General Theory of Relativity and the nature of space-time, to better understand the behavior of matter and energy in the most extreme environments, to expand our knowledge of dark energy and the accelerating universe, to precisely measure the cosmological parameters governing the evolution of the universe, to test the Big Bang inflation hypothesis, and uncover the connection between galaxies and supermassive black holes.

The Program encompasses multiple missions aimed at meeting Program objectives, each with unique capabilities and goals. The Program was established to integrate those missions into a cohesive effort, enabling each project to build on the technological and scientific legacy of its predecessors and contemporaries. Each project operates independently to achieve its unique set of mission objectives, which contribute to overall Program objectives.

Current Operating Missions

The Chandra X-ray Observatory

The *Chandra X-ray Observatory* is one of NASA's "Great Observatories," launched and deployed by Space Shuttle Columbia on July 23, 1999. It is the most sophisticated X-ray observatory built to date, and was specially designed to detect X-ray emission from very hot regions of the universe. Chandra's scientific impact has been enormous. Its discoveries include the first observation of an X-ray-emitting ring around the pulsar at the center of the Crab Nebula, the first X-ray emission seen from the supermassive black hole in the center of the Milky Way, and the first image of the compact object (neutron star or black hole) at the center of the Cassiopeia A supernova remnant.

The X-ray Multi-Mirror Mission-Newton (XMM–Newton)

XMM-Newton, named after physicist and astronomer Sir Isaac Newton, was launched on December 10, 1999, the second cornerstone mission of ESA's Horizon 2000 program. The observatory's science objectives include investigating interstellar X-ray sources, performing narrow- and broad-band spectroscopy, and the first simultaneous imaging of objects in both X-ray and optical (visible and UV) wavelengths. NASA funded elements of the instrument package and provided the Guest Observer Facility (GOF) at Goddard Space Flight Center (GSFC). The GOF provides a clearinghouse for project-generated technical information and analysis software, as well as budget support for US astronomers who receive observation time through a competitive process. XMM-Newton's scientific legacy includes the determination that the black hole at the center of the Milky Way "woke up" violently about 400 years ago, "turning off" about 100 years later. The observatory also acquired the first large-scale map of the dark matter and baryon distributions in the universe, and constructed the largest catalog of cosmic X-ray-emitting objects.

The Fermi Gamma-ray Space Telescope

The *Fermi Gamma-ray Space Telescope*, launched on June 11, 2008, bringing together astrophysicists and particle physicists. Fermi is a NASA-led mission built, launched, and initially operated in collaboration with the Department of Energy, with contributions from France, Germany, Japan, Italy, Sweden, and Iceland. Its science objectives are to explore the most extreme environments in the universe; search for signs of

new laws of physics; explain how black holes accelerate relativistic jets; help understand the physics of gamma-ray bursts; and answer long-standing questions across a broad range of topics such as solar flares, pulsars, and the origin of cosmic rays. Fermi made numerous discoveries, including the first observation of gamma-ray emission from a pulsar (Vela), evidence that supernova remnants are acceleration sites for lower-energy cosmic rays, and the first detection of the two gamma-ray and X-ray "Fermi Bubbles" extending 25,000 light years above and below the center of the Milky Way.

LISA Pathfinder (LPF)

LPF, launched on December 3, 2015, is a technology demonstration mission and the first PCOS mission to launch since the Program was created in 2009. The LPF launch, coupled with the momentous direct detection of GWs by the LIGO collaboration, made 2015 a watershed year for GW astrophysics. LPF validated a number of key technologies for space-based GW observatories, including inertial reference sensors, ultra-low-noise drag-free flight, and micro-Newton thrusters, retiring technical risks for a LISA-like mission. LPF contains two payloads, the European LISA Technology Package (LTP) and NASA's Space Technology 7 (ST-7) experiment, the latter managed by JPL. Science operations at the Earth-Sun L1 Lagrange point began on March 1, 2016. Results from the European phase of the mission were announced on June 7, 2016 and published in Physical Review Letters [3]. LTP's measured acceleration noise performance far exceeds its requirement and approaches that of a full-scale observatory such as LISA. ST-7 operations were conducted later in 2016 and were deemed similarly successful: in February 2017, the ST-7 experiment underwent a Level 1 requirements review by the PCOS program, and was recommended to pass. In late 2016/early 2017 an extended mission phase allowed a deeper understanding of instrument performance by cooling down the experiment to explore residual unexplained noise in components, and undertaking experiments deemed too risky for the prime mission. The mission completed its extended phase in summer 2017, turning off after these highly successful operations.

Mission in Development

Euclid, a dark energy survey mission led by ESA, is the sole mission currently in development addressing PCOS science. The NASA portion of Euclid is a PCOS project managed by JPL. Scheduled for a 2020 launch, Euclid will perform a six-year photometric and spectroscopic survey of about a third of the sky. To achieve Euclid's scientific objectives, improving our understanding of dark energy, gravity, and dark matter, NASA will provide detectors and associated cryogenic electronics for one of Euclid's two instruments, the Near-Infrared Spectrometer and Photometer (NISP). NASA also supports the Euclid NASA Science Center at IPAC (ENSCI; IPAC is the Infrared Processing and Analysis Center, located on the campus of the California Institute of Technology), which supports US users and contributes to the Euclid Science Ground Segment.

Planning for Future Missions

The PCOS portfolio currently focuses on technology studies in support of the priorities of the Astrophysics Division as outlined in the *Astrophysics Implementation Plan* (AIP), updated in December 2016. The highly ranked NWNH priorities addressing PCOS science are:

- *LISA*–large mission category (currently incarnated as ESA's L3);
- *International X-ray Observatory* (IXO)–large mission category (study led to Athena and XRS concepts); and
- *Inflation Probe* (IP)–medium-size mission category.

The decadal committee ranked as the highest-priority large space mission the *Wide-Field Infrared Survey Telescope* (WFIRST). Managed by the Exoplanet Exploration Program (ExEP) Program Office at JPL, with the implementation project located at GSFC, WFIRST is envisioned and designed to settle fundamental questions about the nature of dark energy, to perform studies of exoplanets, and to produce large-field Near-IR surveys. Following ESA's announcement of themes for its large-class L2 and L3 launch opportunities, scheduled for 2028 and 2034, respectively, NASA is pursuing partnerships on the X-ray mission Athena for L2 and a future space-based GW observatory for L3 (details below). PCOS and the Astrophysics Division continue to support IP-related technologies through SAT and Astrophysics Research and Analysis (APRA) funding.

Activities related to NASA-ESA collaboration on Athena continue, with US-funded participation through the Athena Science Study Team (ASST) and its science working group, and the NASA PCOS Athena Study Office. Mission Consolidation Review (MCR) activity was held in 2016. NASA members of the ASST and the science working group have been involved in different aspects of the MCR process. NASA contributions to Athena, centered upon the calorimeter array for the X-ray Integral Field Unit (X-IFU), will continue to be refined. NASA is also providing components of the Wide Field Imager (WFI). Work has now also begun on defining possible contributions to the observatory and Science Ground Segment.

The L3 theme is "The Gravitational Universe", and there was significant NASA participation in the official mission proposal submitted to ESA in January 2017. A cost, risk, and feasibility study of the proposal in ESA's Concurrent Design Facility (CDF) resulted in a recommendation for formal selection of the proposal by ESA's Science Program Committee (SPC) at their June 2017 meeting. This selection was formalized by the SPC on June 20, 2017 and the mission will henceforth be referred to as LISA. ESA will next establish a LISA Mission Office. A Phase 0 study by the CDF of the proposed instrument design will proceed during the summer and fall with support from NASA while requirements documents are prepared for an Invitation to Tender (ITT) to European contractors for a competitive Phase A formulation study. Awards for the 18-month Phase A study are expected by February 2018. In support of this activity, a final L3 study team technology report was delivered to the NASA HQ Astrophysics Division in December 2016 and an L3 science roadmap was delivered to the NASA HQ Astrophysics Division Director in April 2017. Work has begun on defining potential contributions to the Science Ground Segment and preparations are being made to stand up a NASA LISA team to support Phase A activities.

The large-scale mission-concept studies commissioned by NASA HQ continue, as described in the *Management Plan For Large Mission Concept Studies*. These large missions explore the nature of the universe in its earliest moments, in its most extreme conditions, and at the largest scales, as well as search for habitable planets beyond our solar system. The four studies are:

- *Origins Space Telescope* (formerly Far-IR Surveyor);
- *Habitable-Exoplanet Imaging Mission*;
- *LUVOIR Surveyor*; and
- *Lynx* (formerly X-Ray Surveyor).

For more information about study team activities and progress, follow the relevant mission-concept link(s) above.

In the medium-scale category, i.e., Probe-class, with total cost between approximately $400M and $1B, NASA solicited proposals to conduct concept studies for Astrophysics Probe missions. Following peer review, NASA selected 10 proposals for detailed study. The results of the selected studies will also be provided as input to the 2020 Decadal Survey. Note that technology needs of Probe missions are not regarded as "Strategic" for the purpose of guiding PCOS SAT funding.

The ten Probe mission concepts and their PIs are:

- Transient Astrophysics Probe, Jordan Camp (GSFC)
- Cosmic Dawn Intensity Mapper, Asantha Cooray (UC Irvine)
- Cosmic Evolution through UV Spectroscopy, William Danchi (GSFC)
- Galaxy Evolution Probe, J. Glenn (University of Colorado)
- Inflation Probe Mission Concept Study , Shaul Hanany (University of Minnesota)
- High Spatial Resolution X-ray Probe , Richard Mushotzky (University of Maryland)
- Multi-Messenger Astrophysics , Angela Olinto (University of Chicago)
- Precise Radial Velocity Observatory, P. Plavchan (Missouri State University)
- X-ray Timing and Spectroscopy, Paul Ray (Naval Research Lab)
- Starshade Rendezvous , Sara Seager (MIT)

2. Strategic Technology Development Process and Portfolio

The PCOS, COR, and ExEP Program Offices were set up by NASA HQ Science Mission Directorate (SMD) Astrophysics Division to manage all aspects of these focused astrophysics programs. The Program Offices shepherd critical technologies toward infusion into Program-relevant flight projects. The Offices follow Astrophysics Division guidance, and base their recommendations on science community input, ensuring the most relevant technologies are solicited and developed. The PCOS Program Office, located at GSFC, serves as HQ's implementation arm for PCOS Program-related matters. The Astrophysics Division achieves efficiency by having the same staff and physical facilities serve both the COR and PCOS Program Offices. The Astrophysics Division funds technology development at all TRLs. Early-stage development (TRL ≤ 3) and technologies related to non-strategic missions and suborbital projects are typically funded by APRA. Final maturation (TRL ≥ 6) is mission-specific and thus handled by flight missions. The SAT program, launched in 2009, funds maturation of technologies across the mid-TRL gap (3 ≤ TRL < 6).

The PCOS Technology Development Process

The PCOS Program Office is charged to develop and administer a technology development and maturation program, moving innovative technologies across the mid-TRL gap to enable strategic PCOS missions. The Program Office facilitates, manages, and implements the technology policies of the Program. Our goal is to facilitate technology infusion into PCOS missions, including the crucial phase of transitioning nascent technologies into targeted projects' technology programs during mission formulation. PCOS SAT projects are funded by the PCOS SR&T budget. Our work is guided by the priorities set forth in the AIP, the Astrophysics Roadmap, and other strategic guidance from the NASA Astrophysics Division. The AIP describes the Astrophysics Division's planned implementation of space-based priority missions and activities identified in NWNH, updated due to more-recent budgetary developments. The Roadmap strives to inspire and challenge the community to pursue the missions and technologies needed over the next three decades to address NWNH-identified science goals.

Our technology development process (Fig. 2-1) places the science community's inputs at the center of our efforts through the Decadal Survey process and ongoing identification of technology gaps. The community is encouraged to submit gaps at any time via the PhysPAG or directly through the PCOS Technology website. The PhysPAG Executive Committee (EC) reviews gaps submitted before the annual June 1 cutoff date, consolidating, enhancing, and adding to them as needed to create a complete, accurate, and compelling set of gaps for TMB evaluation. The Program Office charges its TMB annually to evaluate and determine which of the submitted technology developments would meet Program objectives, and to prioritize them for further development consideration. The TMB ranks gaps based on Program objectives, strategic ranking of relevant science/missions, benefits and impacts, and urgency. The TMB, a Program-level functional group, thus provides a formal mechanism for input to, and review of, PCOS technology development activities.

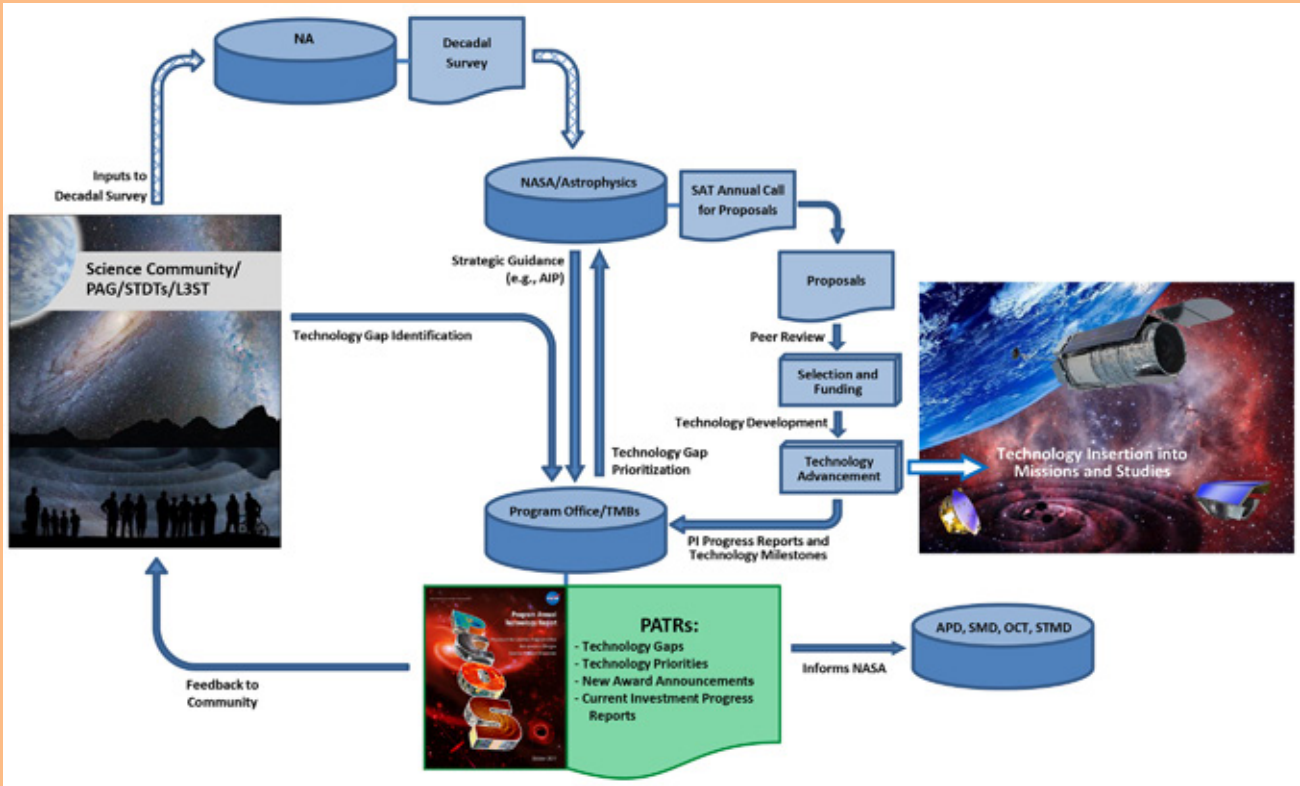

Fig. 2-1. *The PCOS technology development process receives community input on technology gaps, recommends priorities, manages SAT-funded activities, and informs NASA and the science community about progress (NA, National Academies; PAG, Program Analysis Group; APD, Astrophysics Division; OCT, Office of the Chief Technologist; STMD, Space Technology Mission Directorate).*

TMB priority recommendations inform Astrophysics Division decisions on what technologies to solicit in the upcoming annual SAT call for proposals, and help guide proposal selections. HQ's investment considerations are made within a broader context, with programmatic factors apparent at the time of selection affecting funding decisions. HQ evaluates submitted technology development proposals, considering overall scientific and technical merit, programmatic relevance, and cost reasonableness given the scope of work. Awardees work to mature their technologies from their initial TRL, normally 3 or 4[§], through TRL 5. PIs report progress and plans to the Program Office periodically, and submit their technologies for TRL advancement review as appropriate. Progress in these projects allows infusion of newly mature technologies into NASA missions and studies, enabling and enhancing their capabilities with acceptable programmatic costs and risks.

As seen in Fig. 2-1, the PATR plays an important role in our process. Through PI reports and quad charts, it describes the status of all current investments in strategic PCOS technologies. It reports technology gaps articulated by the scientific community and the large-mission-concept study teams, with a prioritized list of technologies for future solicitation and funding. The PATR is an open source for the public, academia, industry, and the government to learn about the status of enabling technologies required to fulfill PCOS science objectives. The report informs NASA organizations, including but not limited to the Astrophysics Division, and updates the community regarding technology development

[§] TRL 4 is defined as: "*Component and/or breadboard validation in laboratory environment.*"

progress, as input for future technology-gap submissions. Technological progress and programmatic decisions change the landscape of requirements for PCOS needs; therefore, the process is repeated annually to ensure continued relevance of priority ranking. Indeed, in any given year, new SAT award decisions are informed by PATRs published over the prior two years, a new SAT solicitation is informed by the prior-year PATR and the current year's TMB priority ranking, and the current PATR provides recommendations for next year's SAT.

This technology development and maturation process identifies existing and emerging needs in a transparent manner, improves the relevance of PCOS technology investments, provides the community a voice in the process, and promotes targeted external technology investments by defining needs and identifying NASA as a potential customer for innovative technologies. It also identifies providers of technologies and expertise, the Program PIs, to potential customers and collaborators within and beyond NASA. This encourages industry and other players to invest in enabling technologies for future missions, and promotes formation of productive collaborations. Beyond involvement in the Decadal Survey process and technology gap submission, the science and technical community is a key stakeholder in Program technology development activities. The community provides feedback and inputs to the technology development process; and participates in PhysPAG and other committees and workshops, ad hoc studies, and in technology development by responding to SAT solicitations.

TRL Vetting

SAT funding helps mature technologies expected to enable and/or significantly enhance future strategic astrophysics missions. These technologies typically enter the SAT program at TRLs 3 or 4, and are intended to progress toward higher TRLs. TRL assertions above a technology's approved entry level are not official until a TRL-vetting TMB concurs with the development team's assessment. When PIs believe their team has demonstrated the required progress, they may request a review to present their case for TRL update. The Program Office then convenes a TMB, consisting of Program Office and HQ senior staff along with subject matter experts, to assess the request and, when warranted, approve the new TRL. The typical forum for such a request is during the PI's end-of-year presentation to the Program Office, but it can be made at any time. Several projects in the PCOS portfolio have already gone through this process (see below), and the PIs of several more are planning to undergo TRL vetting this coming year.

Why review TRLs?

TRLs are used throughout the agency to help assess the maturity of technologies. The Program Office's charge includes a requirement that it monitor the progress of the Astrophysics Division's investments in technology maturation through SAT projects relative to the TRL plan and milestones submitted by the PI in the SAT proposal. A key indicator of such progress is TRL advancement as vetted by the Program Office, providing a consistent method of assessing progress across our full portfolio of projects.

What does our vetting mean?

When the Program's TMB approves a higher TRL asserted by the PI, it provides an independent assessment and verification that the project has achieved that TRL. The TMB consists of scientists, technologists, and systems engineers from the Program; as well as subject matter experts from the community and Aerospace Corporation, who provide an objective and informed assessment. The primary purpose for issuing this assessment is to inform the Program Office of significant progress in preparing the technology for possible infusion into strategic missions. It also informs the community of an improved state of readiness.

What is expected?

The TRL vetting process is initiated when a PI notifies the Program Office that the milestones necessary for TRL advancement have been met. The PI team prepares a brief but compelling presentation that makes the case for the higher TRL, and the PI presents it to the TRL-vetting TMB, which considers the TRL assertion. The TMB is guided by TRL definitions in *NASA Systems Engineering Processes and Requirements*, also known as NASA Procedural Requirement (NPR) 7123.1B. Recognizing that PI teams are busy and must concentrate their efforts on the work of maturing their technology, the Program Office is satisfied to rely on a cogent exposition of the same reports, graphs, and test results the team captures for its own records.

The Program Office has tools to help PIs assess their progress and is available to provide information on the TRL process. Finally, if the project is still ongoing, we recommend the PI present a plan for further TRL advances, if any, allowing the TMB to offer feedback and make recommendations.

What are the benefits for the PI and the Program?

The Program Office's TRL-vetting process serves as an opportunity to capture and collect the needed documentary evidence and present it to a group of independent experts. This can strengthen a potential future TRL case presentation, whether in person or in writing, to flight projects, proposal teams considering adding the technology to their mission, and/or proposal reviewers. Another leveraging opportunity might be in collaboration opportunities. As alluded to above, the TMB can help the PI team fine-tune its plan for future work to achieve the claimed TRL if the current claim was not vetted, or for the next TRL if it was.

Finally, TRLs are NASA's technology-development-assessment language, and TRL advancement is one of the key success criteria for SAT projects. Our TRL vetting is an objective process, rendering an independent verification of achievement, increasing the credibility of the technology's maturity and its potential for continued funding, infusion into flight missions, and consideration by community assessments such as STDT studies and Decadal Surveys.

The PCOS Technology Development Portfolio as of 2017

For FY 2017, the driving objective is to maintain progress in key enabling technologies for possible contributions to ESA L-class missions, such as Athena and LISA, Lynx, and a Cosmic Microwave Background (CMB) polarimetry mission.

Twenty-eight PCOS SAT grants have been awarded to date. Table 2-1 provides top-level information on the 13 projects that received funding in FY 2017, including where each is described in detail in the appendices. Appendix B provides one-page "quad chart" project summaries, while Appendix C provides in-depth reports detailing development status, progress over the past year, and planned near-term development activities. Abstracts for the two recently awarded projects, slated to begin in FY 2018, are included at the end of Appendix C. The appendices provide technology overviews and status, not flight implementation details. For additional information, please contact the PCOS Program Office or the PIs directly. Contact information for each PI appears at the end of his or her report.

Technology Development Title	PI/Project Scientist	Institution	Start Year; Duration	Current TRL	Quad Chart & Status Report Page Locations
Demonstration of a TRL-5 Laser System for eLISA	Jordan Camp	GSFC	FY14; 3 yrs	3	65, 79
Gravitational-Wave-Mission Phasemeter Technology Development	William Klipstein	JPL	FY17; 2 yrs	4	66, 89
Telescopes for Space-Based Gravitational-Wave Observatories	Jeffrey Livas	GSFC	FY16; 2 yrs	3	67, 95
Directly Deposited Optical-Blocking Filters for Imaging X-ray Detectors	Mark Bautz	MIT	FY12; 6 yrs	5	68, 106
Fast Event Recognition for the Athena Wide-Field Imager	David Burrows	PSU	FY15; 3 yrs	3	69, 121
Providing Enabling and Enhancing Technologies for a Demonstration Model of the Athena X-IFU (directed funding)	Caroline Kilbourne	GSFC	FY16; 2 yrs	4	70, 126
Reflection Grating Modules: Alignment and Testing	Randall McEntaffer	PSU	FY15; 2 yrs	4	71, 136
Development of 0.5-Arcsecond Adjustable Grazing-Incidence X-ray Mirrors for the SMART-X Mission Concept	Paul Reid	SAO	FY15; 3 yrs	3	72, 145
Development of Critical-Angle X-ray Transmission Grating Spectrometer	Mark Schattenburg	MIT	FY17; 2 yrs	4	73, 157
Technology Development for an AC-Multiplexed Calorimeter for Athena	Joel Ullom	NIST	FY15; 2 yrs	3	74, 165
Next-Generation X-ray Optics: High Angular Resolution, High Throughput, and Low Cost	William Zhang	GSFC	FY17; 2 yrs	4	75, 174
Planar Antenna-Coupled Superconducting Detectors for CMB Polarimetry	James Bock	Caltech/JPL	FY16; 2 yrs	3-6	76, 181
High-Efficiency, Feedhorn-Coupled, TES-Based Detectors for CMB Polarization Measurements	Edward Wollack	GSFC	FY16, 2 yrs	3	77, 191

Table 2-1. *PCOS Technology Development Portfolio as of FY 2017 (organized by science topic and PI name). Project durations include approved no-cost extensions.*

When possible, PCOS has leveraged its limited funding by joining with other programs, e.g. the Game-Changing Development Program of NASA's STMD, to co-fund projects that meet both programs' technology goals. Such collaborative investments are "win-win-win" opportunities for the Astrophysics Division, STMD, and the PI. The PCOS Program looks forward to continued relationship with STMD, creating more such opportunities in the future.

Similarly, the PCOS Program Office manages a project that transitioned from SAT to directed funding. Another SAT project, developing 0.5-arcsec adjustable X-ray optics, follows up on a related project led by the same PI and co-funded by the APRA program and STMD.

Strategic Astrophysics Technology Selection for FY 2018 Start

The PCOS Program funds SAT projects to advance the maturation of key technologies to make feasible their implementation in future space-flight missions. The Program focuses on advancing those technologies most critical for substantive near-term progress on strategic priorities. The PCOS SAT proposals selected for FY 2018 start, announced in September 2017, advance two technologies

(Table 2-2). The two efforts advance CMB polarization measurement capabilities (superconducting antenna-coupled detectors), and X-ray science (high-speed radiation-tolerant X-ray sensors). These are identified by the NWNH and Astrophysics Roadmap as key areas for technology maturation toward implementation of an Inflation Probe and an X-ray Surveyor.

Technology Development Title	PI	Institution	Duration	Initial TRL	Abstract Page Locations
High-Speed, Low-Noise, Radiation-Tolerant CCD Image Sensors for Strategic High-Energy Astrophysics Missions	Mark Bautz	MIT	2 years	3	197
Superconducting Antenna-Coupled Detectors for CMB Polarimetry with the Inflation Probe	James Bock	JPL	2 years	3-4	198

Table 2-2. *PCOS SAT Development Starts in FY 2018 (alphabetically by PI).*

These new SAT selections were based on the following factors:

- Overall scientific and technical merit;
- Programmatic relevance of the proposed work; and
- Cost reasonableness of the proposed work.

Since these projects have only recently been selected for funding, their status is not presented yet. First-year progress for each will appear in the 2018 PCOS PATR.

Large-Mission-Concept Studies toward the 2020 Decadal Survey

As mentioned in Section 1, the Astrophysics Division has set up STDTs to study four large-mission concepts – OST, HabEx, LUVOIR, and Lynx. The STDTs are each charged to develop the science case and design reference mission, assess technology development needs, and estimate the cost of their mission concept. These studies will guide our efforts to mature technology components and architectures required to offer four equally compelling cases for the 2020 Decadal Survey's consideration. Similarly, the L3ST was chartered to help us understand how NASA might participate in ESA's LISA mission, inform our engagement through its earliest stages, and prepare for the 2020 Decadal Survey. NASA has set up a LISA Study Office to manage technology development projects intended to provide the US contribution for LISA, and is in the process of transitioning several PI-led SAT projects to direct-funded projects led by product development leads (PDLs).

Each of these ambitious mission concepts promises breakthrough science results, but implementing them will require us to overcome daunting technology development challenges. The SAT program is certain to play a major role in funding these technology development efforts. We encourage all members of the community to support our efforts to identify the highest-priority technology gaps we need to close in order to make these missions feasible, and continue to submit proposals in response to SAT solicitations. As of this writing, notices of intent to submit for the next SAT round are due January 18, 2018, with proposals due March 15, 2018.

As described in Section 3, the Lynx STDT and the L3ST provide their own technology gap lists to the PCOS Program Office. The Program Office combines these lists with the one consolidated by the PhysPAG EC, and submits the resulting list to the TMB for prioritization.

Historical Record of TPCOS Proposals and Awards

As shown in Table 2-3, the Technology development for Physics of the Cosmos (TPCOS) section of the SAT program received 21 proposals in response to the 2010 solicitation, its first year; 26 for 2011; 10 for 2012; eight for 2013; six for 2014, nine for 2015, and five for 2016. Of the first set, five proposals were selected, with five more the following year, three in the third year, six in year four, three in year five, four last year, and two this year. This makes the historical selection rate for PCOS SAT proposals 33%, with the three most recent selection rounds hitting 50%, 44%, and 40% respectively.

Solicitation Year	TPCOS Proposals		Proposal Success Ratio
	Submitted	Awarded	
2010	21	5	24%
2011	26	5	19%
2012	10	3	30%
2013	8	6	75%
2014	6	3	50%
2015	9	4	44%
2016	5	2	40%
Total to Date	85	28	33%

Table 2-3. *Numbers of TPCOS SAT Proposals and Awards.*

3. Technology Gaps, Priorities, and Recommendations

Enabling strategic astrophysics missions that are decades away requires identifying and closing gaps between state-of-the-art (SOTA) performance and that required for those missions. As current technologies develop and mature, and as our understanding of the missions' concept designs mature, those gaps evolve.

As shown in Fig. 2-1, we solicit technology gaps from the community on an ongoing basis. Anyone may submit a technology gap directly to the Program Office by *downloading a form* from the PCOS website, or through the PhysPAG. Gaps may be submitted throughout the year; however, since gaps are assessed and prioritized annually in late July or early August, the Program Office set a June 1 cutoff date for consideration in the same year. This allows the PhysPAG EC to review the list of gaps for completeness, merge overlapping gaps, and complete and improve entries where the submission did not adequately address the requested information. Then, the EC returns the list to the Program Office for final preparation for the TMB's assessment.

To maximize the likelihood of high-priority ranking, the Program Office encourages submitters to include as much of the information requested as possible. Importantly, we ask submitters to describe a capability gap, not a specific implementation process or methodology. The goals and objectives should be clear and quantified. Additionally, a complete description of the needed capability with specific performance goals based on mission needs is very valuable. Such information serves several important purposes:

1. The TMB is best able to understand and thus correctly assess the identified technology gap.
2. NASA HQ is best able to develop accurate technology development proposal calls.
3. The community is clearly informed and best able to match candidate technologies to mission needs.

Aside from submitter information, the technology gap form requests the following information:

- **Technology gap name**: Identifies the gap, and optimally the type of mission filling it would enable;
- **Brief description**: Summarizes the technology gap and associated key performance criteria; in general, well-defined technology gaps receive higher priority than vague ones;
- **Assessment of current SOTA and TRL**: Describes the SOTA with justification, allowing the TMB to appreciate the gap between what's available and what's needed; SOTA TRL specifies the current TRL per NPR 7123.1B Appendix E of relevant SOTA technology; and Full-Solution TRL specifies the current TRL of candidate technologies that could provide a full solution; the SAT program funds projects to advance technologies from TRL 3 up through TRL 5, so those with full solutions already at TRL 6 rank lower unless the existing technology is significantly deficient in some way (e.g., cost, complexity, yield, etc.); note that full-solution TRL can never exceed the SOTA TRL, else this full-solution technology would be the SOTA;
- **Target goals and objectives**: Details the quantifiable goals and/or objectives for a candidate technology to fill the described gap. For example, "*The goal is to produce a detector with a sensitivity of X over a wavelength of Y to Z nm*"–technology gaps with clearly quantified objectives may receive higher priority than those without quantified objectives;
- **Scientific, engineering, and/or programmatic benefits**: Describes the benefits of closing the technology gap; for enabling technology, this describes how and why it is such; for an enhancing technology, it describes, and if possible quantifies, the impact; benefits could be better science,

lower resource requirements (e.g., mass, power, etc.), and/or programmatic (e.g., reduced risk, cost, or schedule); for example, "*Material X is 50% stronger than the current state of the art and will enable the optical subsystem for a 2-m telescope to be Y kg lighter*;" technology gaps with greater potential mission benefits receive higher scores;

- **Application and potential relevant missions**: Technologies enabling or enhancing missions ranked highly by the AIP, Astrophysics Roadmap, or NWNH, will score higher; technologies applicable to a wide range of PCOS missions, as well as COR and/or ExEP missions will rank better; and
- **Urgency**: Specifies when the strategic mission enabled or enhanced by the technology is planned to launch; in cases where there is a more immediate driving need (e.g., ESA requirements for achieving TRL 5 or 6 by a certain date to be considered for inclusion in a mission considered strategic by NASA Astrophysics Division), this driving requirement is also considered; technology gaps with shorter time windows relative to required development times receive higher priority.

Technology Gaps Submitted to the 2017 TMB

As in prior years, the PhysPAG EC reviewed the list of technology gaps compiled by the Program Office. The Program Office forwarded to the EC 25 gaps from the 2016 TMB prioritized list plus nine new community entries, some of which simply suggested edits to 2016 gaps. We thank the community for their engagement in this process and for their meaningful gap submissions. The EC returned to the Program Office a gaps list with notes indicating concurrences or disagreement as to strategic relevance of gaps and suggestions to merge similar/overlapping gaps or drop duplicate ones. In parallel, L3ST submitted seven gaps to the Program Office, while the Lynx STDT submitted six gaps. To facilitate and streamline the TMB prioritization process, a subset of the full TMB consolidated the gap entries into 31 distinct gaps. After determining that all practicable and Program-relevant aspects of two of these entries were already covered in other entries, the TMB prioritized the remaining 29.

Almost all technologies developed to close these gaps would enable and/or enhance high-priority strategic missions per the AIP, the Astrophysics Roadmap, and/or NWNH. We deeply appreciate the efforts of the EC, L3ST, and Lynx STDT, and look forward to continued collaboration in the future. Having the EC and study teams review gap entries and propose new ones where appropriate, prior to TMB prioritization, serves several important purposes:

- Providing a set of expert-vetted, unique, and compelling technology gaps, such that the resulting entries potentially merit higher priority ranking;
- Ensuring the gaps accurately reflect the current situation per the community and study teams; and
- Making the process of generating unique technology gaps more transparent to the community.

Prioritizing Technology Gaps

In its prioritization meeting, the TMB followed an agreed-upon set of evaluation criteria, resulting in the priorities shown below. TMB membership included senior staff from NASA HQ Astrophysics Division, the Program Office, STMD, and the Aerospace Corporation. The TMB used a prioritization approach similar to that used in prior years, with a streamlined set of four criteria. These included strategic alignment, benefits and impacts, scope of applicability, and urgency.

- **Strategic alignment**: How well does the technology align with PCOS science and programmatic priorities of current programmatic guidance (i.e., AIP, Roadmap, and NWNH)?
- **Benefits and impacts**: How much impact does the technology have on PCOS-relevant science in applicable mission(s)? To what degree does the technology enable and/or enhance achievable science objectives, reduce cost, and/or reduce mission risks?

- **Scope of applicability**: How crosscutting is the technology? How many Astrophysics programs and/or mission concepts could it benefit?
- **Urgency**: When are launches and/or other schedule drivers of missions enhanced or enabled by this technology anticipated?

The TMB assigned weighting factors, reflecting the relative importance of each criterion. Each gap received a score of 0 to 4 for each criterion. The scores were multiplied by their respective weights, and the products were summed. Technologies that could be scored based on several missions or mission classes were scored for each scenario independently, assigning the highest overall score (e.g., if a gap could receive an overall score of 91 for one mission and 75 for another, it would be assigned the higher score). Table 3-1 details the criteria descriptions, weighting factors, and TMB scoring guidelines.

Criterion	Weight	Max Score	Max Weighted Score	General Description/ Question	4	3	2	1	0
Strategic Alignment	10	4	40	How well does the technology align with PCOS science and programmatic priorities of current programmatic guidance (i.e., AIP, Roadmap, NWNH)?	Technology enables PCOS-relevant science within mission concept receiving highest current programmatic consideration	Technology enables PCOS-relevant science within mission concept receiving mid to high current programmatic consideration in AIP or Roadmap	Technology enables PCOS-relevant science within mission concept receiving low current programmatic consideration in AIP or Roadmap	Technology enables PCOS-relevant science within mission concept not considered in AIP or Roadmap, but positively addressed in NWNH	Technology does not enable PCOS-relevant science within any mission concept considered by current programmatic guidance
Benefits and Impacts	8	4	32	How much impact does the technology have on PCOS-relevant science in applicable mission(s)? To what degree does the technology enable and/or enhance achievable science objectives, reduce cost, and/or reduce mission risks?	Critical and key enabling technology; required to meet PCOS-science-relevant mission concept objectives; without this technology mission would not launch or PCOS science return would be significantly impaired	Highly desirable; not mission-critical to PCOS-science-relevant objectives, but significantly enhances PCOS science capability, reduces critical resources needed, and/or reduces mission risks; without it, missions may launch, but PCOS science return would be compromised	Desirable - not required for PCOS-relevant mission success, but offers moderate PCOS-relevant science or implementation benefits; if technology is available, would almost certainly be implemented in missions for PCOS purposes	Minor PCOS-relevant science impact or implementation improvements; if technology is available would be considered for implementation in missions for PCOS purposes	No PCOS-relevant science impact or implementation improvement; even if available, technology would not be implemented in missions for PCOS purposes
Scope of Applicability	3	4	12	How cross-cutting is the technology? How many Astrophysics programs and/or mission concepts (including Explorers and Probes) could it benefit?	Applies widely to PCOS mission concepts and both COR and ExoPlanet mission concepts	Applies widely to PCOS mission concepts and either COR or ExoPlanet mission concepts	Applies widely to PCOS mission concepts	Applies to a single PCOS mission concept	No known applicable PCOS mission concept
Urgency	4	4	16	When are launches and/or other schedule drivers of missions enhanced or enabled by this technology anticipated?	Launch anticipated in next 4-8 years (2021-2025) or other schedule driver requires progress in 2-3 years (2019-2020)	Launch anticipated in next 9-13 years (2026-2030) or other schedule driver requires progress in 4-8 years (2021-2025)	Launch anticipated in next 14-18 years (2031-2035)	Launch anticipated in next 19-23 years (2036-2040)	Launch anticipated in 24 or more years (2041 or later)

Table 3-1. *Clear, strategic criteria provide a rigorous, transparent process for prioritizing technology gaps.*

This process provides a rigorous and transparent ranking of technology gaps based on the Program's goals, community scientific rankings of relevant missions, Astrophysics Division priorities as outlined in the AIP and Astrophysics Roadmap, and the external programmatic environment. Since the SAT

program is intended to promote development and maturation of technologies relevant to missions and concepts identified as strategic, the strategic alignment criterion is driven by strategic documents such as the AIP, the Astrophysics Roadmap, and the NWNH. The AIP details highly ranked science missions and technology developments, which for PCOS includes dark energy, GWs, X-ray astronomy, and Cosmic Inflation; and prioritizes those based on current budget realities. This year, the TMB considered technologies identified by the Lynx STDT and the L3ST as having the highest possible strategic alignment. The CMB Polarization Surveyor mentioned in the Astrophysics Roadmap was also given points for strategic alignment, as were the Astrophysics Roadmap's GW and X-ray Mappers.

Prioritization Results

As mentioned above, in 2017, the PCOS TMB scored 29 technology gap entries. Reviewing the scores, the TMB binned the technology gaps into four groups based on a number of factors, including primarily a natural grouping of overall scores.

Priority Tier 1: Technologies the TMB determined to be of the highest interest to the PCOS Program. Advancing these key enabling technologies is judged as most critical to making substantive near-term PCOS-science-relevant progress on the highest-priority strategic astrophysics missions, including the XRS and GW missions such as participation in ESA's L3 mission. The TMB recommends SAT calls and award decisions address these technology gaps first.

Priority Tier 2: Typically, technologies the TMB believes would be highly desirable or desirable for a variety of strategic missions. The TMB recommends that should sufficient funding be available, SAT calls and award decisions address closing these technology gaps as well.

Priority Tier 3: Technologies the TMB deemed supportive of PCOS objectives, but scoring lower than Priority 1 and 2 technology gaps.

Priority Tier 4: Recognizing that a reasonable way of "sunsetting" gaps that have no strategic alignment has become necessary, the TMB created a new "Priority Tier 4." Gaps that the TMB deems legitimate PCOS technology gaps, but that are not currently aligned with any strategic mission, are assigned to this new tier and will not be reprioritized in following years. The Program Office will contact submitters of such gaps to inform them of what happened, why, and what changes are needed before their gap can be resubmitted.

Table 3-2 lists the gaps prioritized by the TMB, including 2017 assigned priorities, gap names, science topics addressed, gap submission sources, and where in Appendix A you can find detailed gap entries.

2017 Priority	Technology Gap Name	Science Addressed	Submitted By	Gap Detail Page Location
Priority Tier 1	Highly stable low-stray-light telescope	GW	L3ST	45
	Low-mass, long-term-stability optical bench	GW	L3ST	46
	Large-format, high-spectral-resolution, small-pixel X-ray focal plane arrays	X Ray	Lynx STDT	33
	Precision microthrusters	GW	L3ST	50
	High-power, narrow-line-width laser sources	GW	L3ST	44
	Phase measurement subsystem (PMS)	GW	L3ST	47
	Fast, low-noise, megapixel X-ray imaging arrays with moderate spectral resolution	X Ray	Lynx STDT	32
	High-efficiency X-ray grating arrays for high-resolution spectroscopy	X Ray	Lynx STDT	36
	High-resolution, large-area, lightweight X-ray optics	X Ray	Lynx STDT	37
	Non-deforming X-ray reflective coatings	X Ray	Lynx STDT	38
	Long-wavelength-blocking filters for X-ray micro-calorimeters	X Ray	Lynx STDT	61
Priority Tier 2	High-efficiency, low cost cooling systems for temperatures near 100 mK	X Ray, IP	General Community	62
	Advanced millimeter-wave focal plane arrays for CMB polarimetry	IP	General Community	42
	Non-contact charge control for Gravitational Reference Sensors (GRS)	GW	L3ST	48
	Rapid readout electronics for X-ray detectors	X Ray	General Community	35
	Optical-blocking filters (OBF)	X Ray	General Community	59
	Polarization-preserving millimeter-wave optical elements	IP	General Community	43
Priority Tier 3	Gravitational reference sensor (GRS)	GW	L3ST	49
	Very-wide-field focusing instrument for time-domain X-ray astronomy	X Ray	General Community	40
	Ultra-high-resolution focusing X-ray observatory telescope	X Ray	General Community	39
	Advancement of X-ray polarimeter sensitivity using negative ion gas	X Ray	General Community	34
Priority Tier 4	High-performance gamma-ray telescope	Gamma Ray	General Community	51
	Fast few-photon UV detectors	UHECR	General Community	52
	Lightweight, large-area reflective optics	UHECR	General Community	53
	Low-power time-sampling readout	UHECR	General Community	54
	Low-power comparators and logic arrays	UHECR	General Community	55
	Lattice optical clock for Solar Time Delay (STD) mission and other applications	STD	General Community	56
	Low-power, low-resolution continuous GSa/s direct RF digitizer	CR	General Community	58
	Tileable 2-D Proportional-Counter Arrays	Gamma Ray	General Community	63

Table 3-2. *Summary of 2017 PCOS technology gaps and their TMB-assigned priorities. Gaps shown by priority tier and science theme. All gaps within a specific tier have equal priority. Tier 4 gaps will not be prioritized again in 2018 (UHECR, ultra-high-energy cosmic rays; CR, cosmic rays).*

From 2011 through 2017, nearly all gaps achieving Priority 1 maintained that rank, or changed by one level due to minor shifts in how priority scores break up naturally into groups. In addition, funded projects have addressed high-priority gaps, mostly Priority 1, and occasionally Priority 2. For example, seven of the 11 2017 Priority 1 gaps have already been addressed by SAT projects or will be addressed by 2018-start SATs, as have four of the six Priority 2 gaps.

The Program Office continues to solicit and compile technology gap submissions from the community, and as was done this year, will maintain its collaboration with the EC and study teams to ensure the gaps ranked by the TMB continue to be complete, distinct, and compelling. As mentioned above, the next cutoff date for community gap submissions is June 1, 2018. Notices of intent to submit SAT proposals are due January 18, 2018, with proposals due March 15, 2018.

Independent TRL Assessment of STDT Technology Gaps

Early this year, NASA HQ Astrophysics Division tasked the PCOS, COR, and ExEP Program Offices to provide an independent assessment of the current TRLs of technologies applicable to all gaps submitted by the four large-mission-concept STDTs. The Program Offices called on over 50 subject matter experts, including from the Aerospace Corporation. Following Astrophysics Division direction, the Program Offices briefed each of the STDTs on the independent TRL assessment of its gaps, allowing the teams to remove, add, split, or merge gaps; and/or update gap requirements where and as they saw fit. The TRL assessments were then updated per those changes. The Program Offices reported the resulting independent TRL assessments to the Astrophysics Division and briefed the study teams at the June 2017 Pause and Learn meeting.

4. Benefits and Successes Enabled by the PCOS SAT Program

The main benefit of the SAT program is in maturing technologies across the mid-TRL gap, so that they can be infused into strategic PCOS missions and/or international collaborative missions relevant to Program goals, as part of a US contribution. Mark Schattenburg's project, "*Advanced Packaging for Critical-Angle X-ray Transmission Gratings*," was vetted on May 17, 2016 as having advanced from TRL 3 to 4. Similarly, Randall McEntaffer's project, "*Reflection Grating Modules: Alignment and Packaging*," was also vetted on June 14, 2016 as having advanced fom TRL 3 to 4. All other SAT projects have also made significant progress in maturing their technologies, with at least two active projects asserting TRL advances that have yet to be vetted by a TMB.

Where appropriate, newly matured technologies may also be implemented in ground-based projects, suborbital experiments, Explorers, and Probe-class missions. These often extend beyond the PCOS Program to COR, ExEP, and even beyond missions managed by Astrophysics Division.

The following are examples of TPCOS SAT project developments contributing to missions and projects:

- TES micro-calorimeter is expected to be a major US contribution to the ESA *Athena* mission's X-IFU (PI, Caroline Kilbourne);
- Continued development of time-division Superconducting QUantum Interference Device (SQUID) multiplexing supported by SAT funding is viewed as a backup to *Athena X-IFU's* baseline readout, which is currently at a lower TRL (PI, Joel Ullom);
- An SAT project is maturing a Field-Programmable-Gate-Array (FPGA) -based fast X-ray event recognition that NASA Astrophysics selected for work on a US contribution for *Athena's Wide-Field Imager* (PI, David Burrows);
- Phasemeter technology funded by the PCOS SAT program, including phase locking and laser stabilization, was infused into the Laser-Ranging Interferometer (LRI) on the *Gravity Recovery and Climate Experiment (GRACE) Follow-On mission*. Advances from this LRI work were then leveraged by the PI back into his SAT project (PI, William Klipstein);
- Antenna-coupled TES bolometer technology developed with SAT support was deployed in the *BICEP2* experiment in Antarctica, helping search for B-mode polarization in the CMB signal; this provided an order-of-magnitude increase in measurement speed compared to the BICEP1 experiment; detector-array technology from this SAT project was then incorporated into *BICEP3* and Keck Array, and flown on the *Spider* long-duration balloon mission during the 2014/15 Antarctic season, measuring CMB polarization at 90 and 150 GHz with excellent low-frequency stability and low cosmic-ray event rates (PI, James Bock);
- Directly deposited optical blocking filters developed by another SAT project were incorporated into flight CCDs of *REXIS*, an MIT student instrument on the *OSIRIS-REx* mission (launched September 8, 2016; expected to rendezvous with asteroid 10195 Bennu in late 2018; with the REXIS aperture door expected to open in early 2019); the instrument successfully completed initial calibrations; this filter technology meets the experiment's stringent performance requirements without straining its technical budgets; as a bonus, this provides the SAT project a nearly free opportunity to space-qualify its development, with environmental testing leading to the discovery and subsequent resolution of unexpected light leaks (PI, Mark Bautz);

- High-efficiency 40-GHz feedhorn-coupled TES-based detector architecture matured by another SAT project was deployed in the *CLASS* telescope in the Atacama Desert (PI, Edward Wollack);
- SAT team member, R.S. Shiri, has applied for a patent (GSC-17289-1, "Design and fabrication of partially transparent petaled mask or occulter using grayscale lithography," filed May 23, 2016), which may one day be used for flight missions (PI, Jeffrey Livas); and
- The Arcus MIDEX proposal, based on Critical-Angle-Transmission (CAT) -grating technology, was selected for a Phase A concept study (CAT grating PI, Mark Schattenburg).

As mentioned above, SAT-funded advances in X-ray detectors, high-stability lasers, micro-propulsion, low-scattered-light stable telescopes, and others also allow potential significant US contributions to ESA's Athena and LISA missions.

As in prior years, the Program Office surveyed current PIs about additional benefits resulting from their SAT funding. Of the 13 PIs represented in this PATR, 11 provided information about collateral benefits. Of these, six reported they were able to leverage SAT funding to generate matching internal research and development funding (e.g., GSFC IRAD); fellowships (e.g., Smithsonian Astrophysical Observatory, SAO, internal funding including two Leon Van Speybroeck, LVS, Fellowships in X-ray Optics; an NRC fellowship; a National Science Foundation, NSF, post-doctoral fellowship; NASA Postdoctoral Program, NPP; and university funding for undergraduate research); cost sharing with a flight project; and/or funded parallel efforts on related projects (e.g., APRA). Ten PIs responding report having hired students and/or post-doctoral fellows to assist their technology development work (on average about one undergraduate student, two graduate students, and one post-doctoral fellow per project), helping train the next generation of researchers and technologists needed to support future missions (Fig. 4-1). Students have received their PhDs, were accepted into graduate programs, and/or have gone on to full-time research positions at universities and government labs; proving that the SAT Program is helping train and shape the future astrophysics work force. Several PIs went on to successfully propose additional technology development projects through both the SAT and APRA programs, and several have led and/or participated in Explorer and other proposals based on their SAT work.

Fig. 4-1. *SAT projects hire many students and post-doctoral fellows, helping train the future astrophysics workforce.*

In January 2017, the Program presented a poster of COR and PCOS technology development at the AAS meeting in Grapevine, TX (Fig. 4-2), displaying the breadth of scope of our SAT investment and placing it visually in the progression of astronomy and astrophysics from ancient times to the coming decades. The poster explained the Programs' technology development priorities, and how the four large-mission-concept STDTs are involved in technology development.

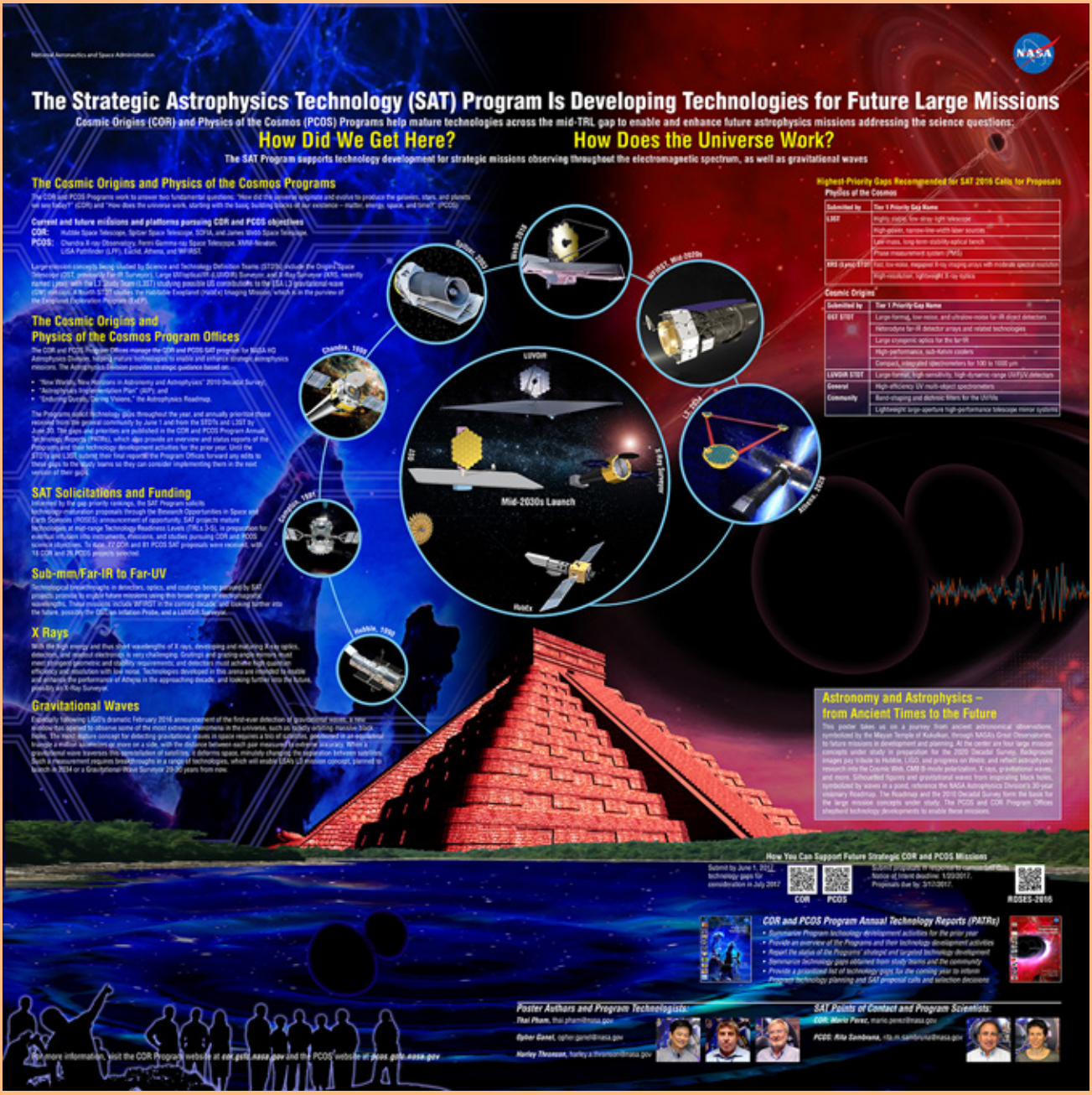

Fig. 4-2. *Poster presented at the January 2017 AAS meeting in Grapevine, TX. The Program promotes exposure of current technology developments and investment priorities at national and international meetings, and informs the community of upcoming SAT funding opportunities.*

The Broad Impacts of the SAT Program

Figure 4-3 depicts the geographic breadth of SAT program (both COR and PCOS) impacts, showing the locations of our PI institutions, their collaborators and partners, and the universities and colleges where the students and post-doctoral fellows involved in SAT projects attend school and work.

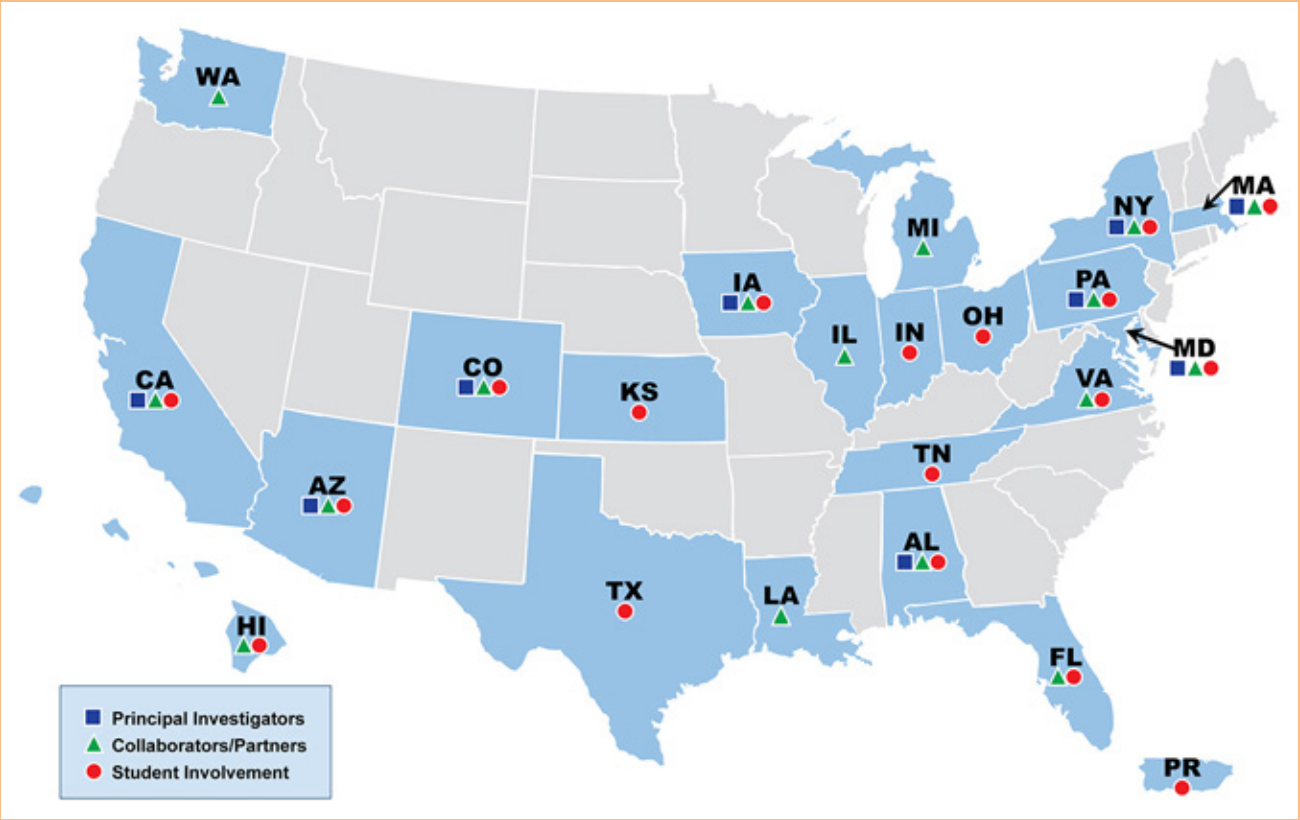

Fig. 4-3. *SAT Program Impacts Map. The Program supports research efforts of PIs and collaborators/partners, and develops our future astrophysics workforce through student involvement (locations shown for both COR and PCOS Programs).*

5. Closing Remarks

This 2017 PCOS PATR serves as a snapshot of the dynamic state of technology development managed by the Program Office and provides future directions for technology planning and maturation. As we complete another year of PCOS technology development activities, we see many positive developments.

Our technology development portfolio is growing, and continues to deliver significant advancements. All funded technologies are maturing toward higher TRLs, with several providing direct benefit to ground-based experiments and flight missions. New SAT awards slated to start in FY 2018 will fund additional CMB and X-ray detector technology work. PCOS SAT investments are also generating benefits beyond direct advancement of strategic technologies. This includes leveraging internal and external (including non-NASA) funding; using contributed materials, parts, and facility/equipment; hiring students and post-docs, thereby training our future astrophysics workforce; and generating research collaborations and industry partnerships, in support of PCOS science goals.

Our technology gap prioritization process continues to adhere to strategic guidance based on the AIP; Astrophysics Roadmap "Surveyor" concepts, especially those being studied by STDTs and the L3ST; and NWNH, with the TMB assigning the most significant weight in technology gap prioritization to strategic alignment. As a result, the Astrophysics Division is likely to continue to fund SAT proposals addressing technology gaps identified by the TMB as having the highest priority. The latest set of highest-priority TMB recommendations, submitted to the Astrophysics Division and reported here, includes technology developments related to GW missions, as well as X-ray focal plane arrays and optics.

To support the ever-evolving technology needs of the PCOS community, we continue to interact with the broad scientific and technical communities through the PhysPAG, through various workshops, via public outreach activities, and at scientific conferences. These activities identify and incorporate the astrophysics community's ideas about new science, current technology progress, and new needs for technology in an open and proven process. Each year, we incorporate new lessons learned and make appropriate improvements to our process. In parallel, we incorporate the technology needs identified by the large-mission-concept study teams into our technology gaps identification and prioritization process.

We would like to thank the PCOS scientific and technical communities, the PIs and their teams, the PhysPAG EC, and the large-mission-concept study teams for their efforts and inputs that make this annual report current and meaningful. We welcome continued feedback and inputs from the community in developing next year's PATR, which should be sent to the *Program Office Technology Development Manager*. For more information about the PCOS Program and its activities, please visit the *PCOS website*.

References

[1] J. Mankins, "*The critical role of advanced technology investments in preventing spaceflight program cost overrun*," The Space Review, December 1, 2008. Available at *http://www.thespacereview.com/article/1262/1*. Accessed May 2014.

[2] National Research Council, "*New Worlds, New Horizons in Astronomy and Astrophysics*," Washington, DC: The National Academies Press, 2010. Available at *http://www.nap.edu/catalog/12951/*. Accessed May 2014.

[3] M. Armano et al., "*Sub-Femto-g Free Fall for Space-Based Gravitational Wave Observatories: LISA Pathfinder Results*," Phys. Rev. Lett. **116**, 231101, DOI: 10.1103/PhysRevLett.116.231101 (2016).

Appendix A
Technology Gaps Evaluated by the TMB in 2016

This appendix details the technology gaps prioritized by the Physics of the Cosmos (PCOS) Program Technology Management Board (TMB) in 2017. These are gaps between the current state-of-the-art (SOTA) technologies, as assessed by technology readiness levels (TRLs, see Table A-1) and capabilities needed for future missions.

The order of the gaps is similar to that of prior-year Program Annual Technology Reports (PATRs). Specifically, we've grouped the gaps by science topic, and within that, by technology type. Where submitted gaps had significant overlap, they were merged into a single gap by the PCOS Program Analysis Group (PhysPAG) Executive Committee (EC) or by the TMB. Gap priority ranking is shown on p. 22 above. Submitted entries not ranked may have been merged into others; deemed outside the purview of the PCOS program (e.g., better addressed by Strategic Astrophysics Technology, SAT, programs other than PCOS; or associated with launch vehicles, rovers, avionics, spacecraft systems, etc.); deemed as not being technology gaps (i.e., specific implementations or not technologies at all); or deemed too mature for the SAT program.

Each entry lists the source of the gap next to the gap name. Sources include the general community or a large-mission-concept study team. We thank the EC, the Lynx Science and Technology Definition Team (STDT), the L3 Study Team (L3ST), and the general community for their engagement in and support of our technology gap identification process.

The Program Office considers gaps submitted by a study team as "owned" by the study team until the team submits its final report. In practical terms, this means that the Program Office will forward to the study team any edits to such a gap that are submitted by the general community by the June 1 deadline. The study team will then consider these edits for possible inclusion into the following-year version of the gap. The study teams' unmatched expertise in the technology needs of their respective mission concepts gives great credibility to their opinions on such technologies; increasing the likelihood of higher priority ranking for gaps owned by the teams.

TRL	Definition
1	Basic principles observed and reported.
2	Technology concept and/or application formulated.
3	Analytical and experimental critical function and/or characteristic proof-of-concept.
4	Component and/or breadboard validation in laboratory environment.
5	Component and/or breadboard validation in relevant environment.
6	System/subsystem model or prototype demonstration in a relevant environment.
7	System prototype demonstration in an operational environment.
8	Actual system completed and "flight qualified" through test and demonstration.
9	Actual system flight proven through successful mission operations.

Table A-1. *TRL definitions from NASA Procedural Requirements (NPR) 7123.1B Appendix E, which provides a full description of the TRLs.*

Gap Name		Fast, low-noise, megapixel X-ray imaging arrays with moderate spectral resolution *Submitted by Lynx STDT*
Description		Lynx requires X-ray imaging arrays covering wide fields of view (> 60 x 60 mm) with excellent spatial resolution (i.e. < 16 micron pixels, or equivalent X-ray position resolution), and moderate spectral resolution (comparable to modern scientific CCDs). These detectors must have good detection efficiency across the soft X-ray band pass, from 0.2-10 keV, and excellent detection in the low-energy (0.2–1 keV) end of this band pass is essential. Therefore, optical blocking filters with minimal attenuation of soft X-ray will also be required. Fast frame rates (i.e. > 30 -100 frame/s) to minimize pile-up for demanding effective areas that are ~30x that of Chandra are also required.
Current State-of-the-Art (SOTA)		Silicon active pixel sensors (APS) currently satisfy some of the requirements, but further work is needed to meet all requirements simultaneously. APS with 36-μm pixels are at TRL 6, but noise levels are still too high, and sensitivity to soft X rays needs to improve. Sparsified readout, limited to pixels with signals, allows fast frame rates and is at TRL 3.
TRL	**SOTA**	2–3
	Solution	3
Performance Goals and Objectives		• Lynx requires large format X-ray detectors with sufficient spatial resolution so as not to compromise the imaging performance of the Lynx optics (notionally with 0.5" half power diameter, HPD); • Multi-chip abuttablility to build detector surface approximating best focal surface for the mirrors; • Roughly Fano-limited spectral resolution in the 0.2-10 keV energy band; actual energy resolution requirement is still TBD, but it will be roughly CCD-like or perhaps slightly less stringent • Frame rates > 30~100 frames/s; • Optical-blocking filters with minimal X-ray absorption above 0.2 keV; and • Radiation hardness supporting 5-20 years of science operations at Chandra-like or L2 orbit.
Scientific, Engineering, and/or Programmatic Benefits		Enables X-ray imaging of wide fields with high spatial resolution and sufficient spectral resolution to meet science goals of strategic X-ray missions.
PCOS Applications and Potential Relevant Missions		Lynx, Joint Astrophysics Nascent Universe Satellite (JANUS) / X-ray Time Domain Explorer (XTiDE) -like, or any other focused X-ray optics, or coded-aperture wide-field X-ray-monitoring, or X-ray-grating mission.
Time to Anticipated Need		Need to demonstrate credibility before the 2020 Decadal Survey, and would require TRL 6 by mission Preliminary Design Review (PDR) anticipated in the mid-2020s.

Gap Name		Large-format, high-spectral-resolution, small-pixel X-ray focal plane arrays *Submitted by Lynx STDT*
Description		X-ray microcalorimeters are needed to allow spatially resolved spectroscopy with Lynx. The arrays need to cover a wide field (> 5 arcmin) and with spatial resolution matching future X-ray optics (<~ 1 arcsec). The X-ray focal-plane-array pixels need to provide excellent spectral resolution (<~ 4 eV Full-Width at Half-Maximum, FWHM, in the 0.2 – 10 keV band). Different regions of the array should be optimized for different types of measurements in a hybrid configuration. The innermost region should have the smallest pixels with an energy range extended to > 7 keV. The outer region should be optimized for soft X-rays up to 2 keV, ideally extending the field-of-view to ~ 20 arc-minutes.
Current State-of-the-Art (SOTA)		Fabrication of arrays with 1024 transition-edge sensors (TESs), each connected to nine absorbers on a 75-μm pitch has been demonstrated (9216 pixels). Smaller arrays have been fabricated with a 50-μm pitch. Small arrays with nine absorbers attached to a single TES have demonstrated < 3 eV FWHM energy resolution, and with twenty absorbers attached to a single TES have demonstrated 3.4 eV FHWM energy resolution. Much larger arrays are needed. In the context of the required array size, the array fabrication is currently TRL 3. Small arrays (36 pixels) of much larger microcalorimeter pixels, is at TRL 9 (Hitomi). Multiplexing with microwave Superconducting QUantum Interference Devices (SQUIDs) in resonator circuits at GHz frequencies will accommodate the read out of hundreds or maybe a thousand sensors per readout channel, and thus provides a path to reading out much larger arrays. This has been demonstrated reading out 130 pixels (TRL 4). TESs and magnetically coupled (micro-)calorimeters (MCC) are two of the leading thermal-sensor technologies with potential to meet the Lynx requirements, and both can be read out using microwave SQUIDs in GHz resonators.
TRL	**SOTA**	
	Solution	3
Performance Goals and Objectives		The primary objective for Lynx is large-format arrays with pixel count > 100k and spectral resolution < 4 eV FWHM at 0.2 – 10 keV. This likely requires a high degree of multiplexing, both thermal and electrical: Thermal multiplexing: Sensors attached through varying thermal conductances (hydras) to multiple absorbers, allowing pixel identification across the entire energy band, up to a multiplexing factor of 25:1, with energy resolution < 4 eV and pixel pitch < 50 μm. Electrical multiplexing: • Readout using microwave resonators, such as with microwave SQUIDs. Desired multiplexing factor is > 1000:1 for TESs with low slew rates, and > 400:1 for high slew-rate hydras.
Scientific, Engineering, and/or Programmatic Benefits		Science benefits identified for International X-ray Observatory (IXO) in "New Worlds, New Horizons in Astronomy and Astrophysics" (NWNH) and Lynx in the 2014 Astrophysics Roadmap update. The more advanced the multiplexed readout becomes, the more engineering benefits there are. These benefits include having less-demanding cryogenic requirements; and also lower instrument mass, power, and cost for the cryogenics and readout.
PCOS Applications and Potential Relevant Missions		Lynx. The technology is also synergistic with an enabling technology for the US contribution to Athena.
Time to Anticipated Need		Need to demonstrate credibility before the 2020 Decadal Survey, and would require TRL 6 by mission PDR anticipated in the mid-2020s.

Gap Name		Advancement of X-ray polarimeter sensitivity using negative-ion gas *Submitted by General Community*
Description		Standard photoelectric X-ray polarimeter designs are both quantum-efficiency (QE) -limited and challenging to calibrate due to diffusion of electron signal as it drifts through the gas. Drifting negative ions decreases diffusion to the thermal limit, thereby decoupling sensitivity from drift distance, and enabling larger detector areas that can be at the focus of larger-diameter mirrors and single-reflection concentrator. Negative-Ion Time-Projection-Chamber (NITPC) polarimeters also allow the selection of constituent gases and pressures to be based on optimization of modulation and QE rather than diffusion properties. This versatility enables a large improvement in sensitivity without driving cost and with only moderate increase to mass and power of the detector and/or instrument. Furthermore, the energy band will be tunable to maximize science return.
Current State-of-the-Art (SOTA)		Several photoelectric polarimeter concepts such as Polarimeter for Relativistic Astrophysical X-ray Sources (PRAXyS, previously Gravity and Extreme Magnetism Small Explorer, GEMS), Imaging X-ray Polarimeter Explorer (IXPE), and Polarimetry of Energetic Transients (POET) etc. were proposed in 2014 to provide the next substantial step exploiting X-ray polarization to answer key scientific questions for some of the brightest sources in the sky. However, proposed measurements remain photon-limited and the need for higher-sensitivity polarimeters for both faint persistent sources such as Active Galactic Nuclei (AGN) and bright transient sources such as Soft-Gamma Repeaters (SGRs) by way of Explorer missions and probe-class missions in the next decade remains critical. The goal of this development is to make practical the technology that will provide an order-of-magnitude improvement in polarization sensitivity over current-generation instruments.
TRL	**SOTA**	4
	Solution	
Performance Goals and Objectives		Development of gas electron multipliers optimized for negative ion gas. Development of finer-pitch strip readouts to improve the sensitivity at lower energies and higher pressures. Optimization of gas mixtures to maximize sensitivity (QE vs. track length). Demonstrate lifetime of gas and detector materials is commensurate with mission requirements.
Scientific, Engineering, and/or Programmatic Benefits		These developments will allow a factor-of-10 improvement in sensitivity without decreasing the sensitivity per unit mass and without increasing the relative cost of an instrument.
PCOS Applications and Potential Relevant Missions		Flagship and Probe-class X-ray missions. Explorer-class X-ray missions. Sounding rocket experiments.
Time to Anticipated Need		**Named missions:** **Development needed for 2020 Decadal:** No **Other drivers:** Explorers, Probes, and Missions of Opportunity (MOs).

Gap Name		Rapid readout electronics for X-ray detectors *Submitted by General Community*
Description		Future NASA X-ray missions in both the long term (Lynx, which is endorsed by Enduring Quests Daring Visions Report and currently under STDT study) and nearer term (Probe and Explorer-class opportunities), as well as the Athena mission, led by the European Space Agency (ESA), will have focal-plane instruments that have many pixels (> 10 Mpix) and very fast frame rates. A key technology that will need further development to support these focal planes will be electronics boards that can read out and process the events from these detectors at very rapid rates.
Current State-of-the-Art (SOTA)		The concept for a board that would accomplish the requirements for both JANUS and Athena was initially developed when JANUS was in a phase-A study and Athena had a potential opportunity for US contribution to these electronics. The need still exists for such a board for other future missions such as Lynx, Arcus, or other upcoming Explorer and/or Probe-class missions. A design was developed using a Xilinx Field Programmable Gate Array (FPGA) and parallel event processing that enables the required speeds. A prototype board was built, with firmware being finalized. Current TRL is assessed by the team as 4, and planned to be at TRL 5 in summer 2017.
TRL	**SOTA**	4–5
	Solution	4–5
Performance Goals and Objectives		Development of digital electronics that can accept data and detect and characterize X-ray events at rates required by Lynx (> ~ 100 Mpix/s)
Scientific, Engineering, and/or Programmatic Benefits		Enable rapid detector readout and event characterization for a variety of possible X-ray missions, large and small: flagship, Probes, Small Explorer (SMEX), Medium-class Explorer (MIDEX), and CubeSats. In particular, this will enable missions such as Arcus, which is being proposed, and/or Lynx, which is endorsed by Enduring Quests Daring Visions and under study by an STDT in preparation for the 2020 Decadal Survey. It would also be useful for other possible missions such as probe-class missions like TAP or AXIS; SMEX and Explorer like Arcus; and even CubeSat opportunities. These developments could also contribute to efforts by our European colleagues on technology needed for the Athena mission.
PCOS Applications and Potential Relevant Missions		Lynx (currently under study by a NASA STDT as a large strategic mission concept) is one example of a potential mission requiring rapid readout electronics with these characteristics (Kouveliotou et al. 2014, "Enduring Quests, Daring Visions;" & Vikhlinin et al. 2012 gives a possible strawperson example of how this mission might look). The large-FOV instrument on this mission specifically required large-format APS. This instrument would provide a large FOV with excellent spatial and temporal resolution and moderate spectral resolution. The heart of the instrument is a > 16 Mpix focal plane with a readout requirement of >100 frames/second and is comprised of an array of X-ray photon-counting APS. Similar requirements would apply to any other similar mission that couples large effective area with a need for large-format/many-pixel detectors, or missions that require rapid readout of many pixels for other purposes such as timing resolution or background suppression. Examples: Lynx, Arcus, Athena, Probe-class X-ray missions with more targeted capabilities, JANUS-like missions, XTiDE-like missions.
Time to Anticipated Need		**Named Missions:** Lynx and Athena (2020) **Development needed for 2020 Decadal:** Yes **Other drivers:** to ready this technology for a future mission that could begin development as early as 2018, technology design and testing would need to achieve TRL 5/6 between 2018 and 2035, depending on specific mission.

Gap Name		High-efficiency X-ray grating arrays for high-resolution spectroscopy *Submitted by Lynx STDT*
Description		Light-weight, high-efficiency (> 40-50%), large-format X-ray grating arrays enable high spectral resolving power R > 5000 in the soft X-ray band (~ 0.2 - 2 keV) for absorption- and emission-line spectroscopy using large X-ray telescopes. These would provide the resolving power needed to address key science goals in the soft X-ray band, such as studying the physical state of baryons in galactic halos and in the Cosmic Web, detailing matter and energy feedback from supermassive black holes (SMBH), and characterizing stellar lifecycles from birth to death.
Current State-of-the-Art (SOTA)		Proven technologies (grating spectrometers on Chandra and X-ray Multi-mirror Mission-Newton, XMM-Newton) fall short in efficiency, collecting area, and resolving power, by factors of 5-10. High-efficiency gratings have been demonstrated that place > 40% of the incident soft X-ray light into the diffracted orders. Separately, high-spectral-resolving-power gratings have achieved resolving powers > 10,000 in the soft X-ray band Current technology readiness is assessed to be at TRL 4.
TRL	**SOTA**	4
	Solution	4
Performance Goals and Objectives		Lightweight, high efficiency (~40% or more), large-format grating arrays with high spectral resolving power (R > 5000) in the soft X-ray band (0.2 - 2 keV) for absorption- and emission-line spectroscopy using large X-ray telescopes.
Scientific, Engineering, and/or Programmatic Benefits		Spectrometers achieving R > 5000 throughout the soft X-ray band are mission-enabling, as microcalorimeters cannot achieve that. Priority science goals for soft X-ray spectroscopy are studying the physical state of baryons in galactic halos and in the Cosmic Web, detailing matter and energy feedback from SMBH, and characterizing stellar lifecycles from birth to death.
PCOS Applications and Potential Relevant Missions		A spectrometer using gratings with this performance is envisioned for Lynx, has been studied by NASA as a Probe, has been proposed for an Explorer, and will be flown on the Off-plane Grating Rocket Experiment (OGRE).
Time to Anticipated Need		Need to demonstrate credibility before the 2020 Decadal Survey, and would require TRL 6 by mission PDR anticipated in the mid-2020s.

Gap Name		High-resolution, large-area, lightweight X-ray optics *Submitted by Lynx STDT (Enabling)*
Description		The science of Lynx requires a large-throughput mirror assembly with sub-arcsec angular resolution. These future X-ray mirrors have a set of requirements, which collectively represent very substantial advances over any currently in operation or planned for missions other than Lynx. Of particular importance is achieving low mass per unit collecting area, while maintaining Chandra-like angular resolution.
Current State-of-the-Art (SOTA)		• High Resolution Chandra optics: • Angular resolution <~ 0.5 arcsec; • Effective area 750 cm2 at 1 keV; and • Mirror mass 951 kg. There are multiple efforts underway to develop lightweight, high angular resolution X-ray optics. These efforts include single substrate development to full assemblies, and includes silicon and glass segmented, adjustable segmented and full-shell solutions, among others. TRL 2-3 for various technologies for high-resolution, lightweight mirrors mentioned above. To date, no effort has demonstrated, with X-ray testing sub-arcsec, lightweight optics. No effort has yet demonstrated sub-arcsec resolution for an optical assembly with reasonable effective area of lightweight X-ray optics.
TRL	**SOTA**	2–3
	Solution	2–3
Performance Goals and Objectives		• Mirror technologies must be scalable to at least 2m^2 effective area-class assemblies; and • Overall mirror angular resolution of order 0.5 arcsec or better on-axis. • A demonstration is desired in the form of an adequate engineering unit involving a subset of the outermost and innermost elements. The goal would be to provide realistic and adequate X-ray measurements that do not rely on optimistic extrapolations.
Scientific, Engineering, and/or Programmatic Benefits		These X-ray optics will enable study of the early universe to complement the James Webb Space Telescope (JWST) and other observatories, maintain US leadership in lightweight X-ray optics for space, and facilitate future missions. Most of the Lynx observations do not require significantly better resolution than the proven Chandra capabilities. Rather, it is the significant increase in collecting area at a reasonable mass, combined with unprecedented spectral performance, while maintaining high angular-resolution that makes Lynx a true successor to Chandra and synergistic to a multitude of other observatories (both in-space and ground-based).
PCOS Applications and Potential Relevant Missions		This is an enabling technology for Lynx. This technology is also applicable to Probe-class and Explorer-class missions.
Time to Anticipated Need		Need to demonstrate credibility before the 2020 Decadal Survey, and would require TRL 6 by mission PDR anticipated in the mid-2020s. The community and the world need not wait until a potential launch for Lynx (probably 20 years after the Decadal survey that ranks it number 1). Once developed there are numerous potential scientific applications). Once developed (and no longer virtual optics) cost estimates will become much more realistic and lower. Moreover, the development is urgent for the future of X-ray Astronomy in the USA. Without adequate development, proposed missions will be costed based on virtual optics, and thus priced much higher than they would be given an adequate development program.

Gap Name		Non-deforming X-ray reflective coatings *Submitted by Lynx STDT*
Description		Lynx requires a light-weight X-ray telescope with large collecting area and ~0.5 arc-second angular resolution. The X-ray mirrors used to construct the Lynx telescope will comprise thin, curved substrates (either segmented or full-shell) coated with X-ray reflective thin films. The thin-film coatings must provide high reflectance over the Lynx energy band, and must maintain or improve the high-frequency surface roughness of the substrate (to minimize losses due to X-ray scattering.) Additionally, and crucially, coating stress must be minimized or controlled in order to mitigate stress-driven substrate deformations that degrade angular resolution.
Current State-of-the-Art (SOTA)		Iridium single-layer, and boron-carbide/iridium bilayer films, both have been demonstrated to have high X-ray reflectance over the Lynx energy band. Additionally, preliminary work on more complex Ir-based multilayer coatings has demonstrated even better X-ray performance. However, all these coatings have exceedingly high stress when deposited under sputtering conditions that give high film density and low surface roughness, and thus maximal X-ray performance. Ir-based coatings having low net stress (as measured on flat test substrates) have been demonstrated through various methods. However, preservation of figure error on curved, thin mirror segments has not yet been demonstrated at the 0.5-arcsecond-level. (Chandra substrates are ~50x thicker than those required for Lynx, so Ir coating stress did not degrade angular resolution in that case.) Additionally, coating thickness uniformity better than 2% in two-dimensions on shell segments has not yet been demonstrated, and almost certainly will be required to achieve acceptable figure preservation. Current TRL: 2-3. Advancement to TRL 4 will require demonstration of X-ray reflective coating deposition on thin, curved substrates (segmented or full-shell) with acceptable figure preservation, demonstration of preservation (or improvement) of high-frequency substrate surface roughness, and demonstration of acceptable X-ray reflectance, using techniques that are scalable for mass production.
TRL	**SOTA**	3
	Solution	3
Performance Goals and Objectives		Thin-film coatings deposited onto figured, thin-shell substrates that (a) provide high X-ray reflectance up to 10 keV, (b) have low high-frequency surface roughness (to minimize losses due to X-ray scattering), and (c) preserve the underlying substrate figure after coating deposition to minimize or eliminate coating-stress-driven substrate deformations that degrade angular resolution. Coating deposition methods must be scalable for mass production.
Scientific, Engineering, and/or Programmatic Benefits		High X-ray reflectance and low surface roughness are needed to achieve high telescope collecting area. Without the development of effective methods to mitigate coating-stress-induced substrate deformations, sub-arcsecond telescope resolution will not be possible using thin-shell mirror substrates.
PCOS Applications and Potential Relevant Missions		Lynx
Time to Anticipated Need		**Named missions:** Lynx **Development needed for 2020 Decadal:** Yes **Other drivers:** Explorer, Probe, and MO opportunities.

Gap Name		Ultra-high-resolution focusing X-ray observatory telescope *Submitted by General Community*
Description		Very high angular resolution in the X-ray band is needed to study the structure surrounding and jets emanating from SMBHs at the cores of galaxies. However, the Chandra X-ray observatory's 0.5-arcsec resolution is already near the best that can be expected from grazing-incidence reflection. Simulations suggest that above 4 keV, a transmitting diffractive-refractive pair in direct contact in which the focal length of the refractive component is minus twice that of the diffractive element can achieve milliarcsec resolution by nullifying chromatic aberration over a 15% bandwidth. However, a 1-m-diameter system would have a focal length of the order of 1000 km. Optics and detector would be aboard separate spacecraft that engage in "formation flying." Only one spacecraft can be in a true orbit; the other has to be powered by an engine to overcome the gravity gradient to maintain alignment and to reposition for target changes. The center of the detector spacecraft has to be < 10 cm from the optical axis or a designated position in a raster scan. The position of the optical axis has to be known to < 5 mm for milliarcsec resolution. Pointing direction of the optics and the distance between the two spacecraft are not critical.
Current State-of-the-Art (SOTA)		This system requires new technology in two areas, X-ray optics and mission operations. Construction of the optics is not expected to be difficult; in fact, it should be much less demanding and much lower mass than a grazing-incidence optic. However, the very long focal length precludes laboratory tests of large-diameter optics. The principle but not the level of performance can be verified by testing miniature components at synchrotron radiation facilities with a very long vacuum pipe to accommodate the large distance between the optics and detector. Mission operations have to be studied analytically. No other high-energy mission or mission concept that this author knows of has had operational requirements comparable in difficulty to this, but there is no apparent reason why they cannot be satisfied.
TRL	**SOTA**	1
	Solution	
Performance Goals and Objectives		The mission should be considered only after the development of a successor to Chandra (Lynx) has begun. It would begin with a study of formation flying of two spacecraft separated by 1000 km to determine the feasibility and costs of maintaining the position of the detector within 10 cm of the optical axis, or a designated point on the focal surface of a raster scan, with a positional uncertainty < 5 mm for a period of several years, during which time there will be target changes. Propulsion, most likely by ion engines, is needed for both maintaining pointing and changing targets. The quantity of propellant that can be accommodated determines the lifetime of the mission. The presence of either two optics or detector spacecraft will result in more efficient utilization of propellant. One spacecraft navigates to the next target position while the other is observing.
Scientific, Engineering, and/or Programmatic Benefits		This X-ray telescope system offers in theory three orders-of-magnitude higher angular resolution than any current or future grazing-incidence X-ray telescope and any single-lens telescope in any wavelength band. The formation-flying capability that would be developed for this mission is applicable to an even more ambitious project, X-ray interferometry with multiple lenses. Development of formation-flying capability between two or more spacecraft should be useful in other space projects.
PCOS Applications and Potential Relevant Missions		A very-high-angular-resolution X-ray telescope would be enabled by the development of technology for long distance formation flying between two spacecraft with 5-cm pointing accuracy of the detector with respect to the optical axis or another direction of a raster scan, and changing targets. The principal objectives are observing the structure of the environment surrounding SMBH and the small clumps of material in their jets. The same would apply to the nebula surrounding neutron stars and the jets emanating from them.
Time to Anticipated Need		**Named missions:** **Development needed for 2020 Decadal:** No **Other drivers:** Applicability would be a decade after the next high-angular-resolution telescope, i.e. Lynx, has operated for several years, and has revealed specific targets that require higher-angular-resolution observations to probe more deeply.

Gap Name		Very-wide-field focusing instrument for time-domain X-ray astronomy *Submitted by General Community*
Description		There exists considerable support in the astronomical community for a Probe-type mission dedicated to Time-Domain X-ray Astronomy. Given the large number of X-ray sources across the sky that are variable, or transient, the key instrument would be a focusing telescope with an extremely large field of view, i.e. several steradians. The type of optics with the large field of view is known as a "lobster-eye." There are two types. One is based on an array of square pores slumped onto a spherical surface. Small units have been constructed and, in fact, such an optic is scheduled to be aboard the ESA mission to Mercury. The other type of lobster-eye is a hybrid consisting of an equally spaced array of flat mirrors that lie along the radii of a cylinder. Both faces of the mirrors are coated with a heavy metal with good X-ray reflectivity. It provides position information in one dimension. A circumferential cylindrical coded mask provides positions in the other dimension. Both types require similar detector systems, which would consist of an array of CCD, CMOS or other type of pixelated detectors. While the detector chips currently exist, there has not been an array of X-ray devices that covers efficiently a very large area (up to a square meter). Compared to the 2D channel-plate optic, the hybrid has an order of magnitude more effective area and much broader bandwidth but more background. For very short-lived transients, such as gravitational waves (GWs) and short gamma-ray bursts (GRBs), where little background accumulates, the larger area and broader bandwidth is desirable.
Current State-of-the-Art (SOTA)		Small prototype telescopes of both types have been constructed but are not close to the optics size required for the Transient X-ray Astrophysics Probe. Leicester University in the UK has been leading the thermally slumped channel-plate effort. So far, the angular resolution of small units has been ~5 arcmin, far short of the 20-arcsec theoretical value. Also, the coatings on the walls of the channel plate have not been optimal. Small versions of the cylindrical-geometry 1D focusing lobster-eye telescopes have been constructed at SAO and in the Czech Republic. However, the problem of a low-mass structure for the mirrors has not been addressed and no effort has been made to develop a circumferential cylindrical coded mask to go with the cylindrical 1D lobster-eye. While optical astronomers have successfully made large arrays of optical/infrared CCDs, there has not been the need so far for a comparable X-ray detector. Technologies for the channel plate version are ~TRL 4. Technologies for the hybrid exist in concept but insufficient support delays design of a prototype optic integrated with a coded mask. Optics are at ~TRL 2 and the 1D cylindrical coded mask at TRL 3 thanks to the success of Swift and XMM coded masks. The UK is supporting most channel-plate telescope development efforts. Support for the hybrid would have to be provided by NASA. The detector array for both 2D and 1D focusing systems is at TRL 3. Comparable-size arrays have been constructed for optical telescopes but with less need for continuous focal surface coverage. Kepler is an example of a large focal plane detector array in space.
TRL	**SOTA**	Channel-plate telescope 3–4; cylindrical hybrid 2–3
	Solution	4
Performance Goals and Objectives		With a 1-m focal length and 120° azimuth coverage, the lobster-eye focal plane would be a closely packed cylindrical array of pixelated X-ray detectors over a focal surface with ~1-m2 total area. Ideally, the detector active region would occupy a very large fraction of that area, efficient to at least 10 keV, with 50-μm pixels sufficient. Telescope technical goals are several arcmin or better angular resolution and sub-arcmin position determination (by finding image centroid) with a FOV ≥ 2 ster. Sensitivity for GRB detection at least ×10 better than Swift, capable of detecting and positioning all kinds of variable (and static) sources at least ×10 better than the scanning Rossi X-ray Timing Explorer (RXTE) All-Sky Monitor and Japan's Monitor of All-sky X-ray Image (MAXI) on the International Space Station (ISS). Many sources are nearly constantly in the FOV (except during Earth occultation in Low Earth Orbit, LEO) for both types of lobster-eye telescopes. The hybrid's larger exposure time and area ensure superior sensitivity to the scanning collimated monitors, with background reduction of focusing adding another level of superiority.

Scientific, Engineering, and/or Programmatic Benefits	Both types of lobster-eye telescopes are new types of X-ray optics that have not been in orbit. The channel-plate type will be very low mass. The FOV of both types is several ster whereas current and previous focusing telescopes, e.g. Chandra and XMM, have fields that are a fraction of a square degree. The difference in sky coverage is a factor of 104. Large non-focusing detectors with similar large FOVs, e.g. Swift, do not cover the same bandwidth, and have much less sensitivity and angular resolution. The lobster-eye telescopes enable an entire new class of measurements, detecting and positioning short-lived transient sources such as distant GRBs and likely transients with sub-second duration transients associated with GWs. They have much more sensitivity than the non-focusing scanning all-sky monitors for all types of temporal variations.
PCOS Applications and Potential Relevant Missions	The very-wide-field lobster-eye X-ray telescope enables the development of the Transient Astrophysics Probe, a candidate PCOS mission that carries out studies of multiple sources varying over a large range of time scales simultaneously from the same pointing position. By detecting and positioning very distant GRBs, Cosmic Origins (COR) objectives will be fulfilled because the distant GRBs' host galaxies will be the youngest galaxies in the universe. Lobster-eye telescopes can map X-ray emission from planets and asteroids in our solar system. Depending on the viewing distance and the size of the object, X rays from a large part or the entire front-facing surface of the planet can be mapped much more quickly with the lobster-eye telescope's large FOV.
Time to Anticipated Need	**Named missions:** **Development needed for 2020 Decadal:** No **Other drivers:** NASA is not likely to launch a Probe-type mission in less than five years. Meanwhile technology development of the optics and X-ray detector arrays can proceed via Astrophysics Research and Analysis (APRA) and SAT programs.

Gap Name		Advanced millimeter-wave focal-plane arrays for CMB polarimetry *Submitted by General Community*
Description		The Inflation Probe (IP) requires arrays of detectors with background-limited sensitivity, dual-polarization detection capability, and control of systematic errors at multiple frequencies between ~30 and ~600 GHz for foreground removal. Architectures must be scalable to large arrays for the requisite sensitivity. Simultaneous multiband operation, high multiplexing factors, and efficient detector and readout focal-plane packaging represent desirable design qualities. Detector systems must be compatible with the space environment. This includes low dielectric exposure to low-energy electrons and robust performance in the presence of cosmic rays. Continued deployment in ground-based and balloon-borne platforms will benefit development efforts.
Current State-of-the-Art (SOTA)		A great deal of progress has been made with a variety of approaches, including feedhorn and antenna-coupling waveguide probes, and filled absorber structures. TESs are currently the leading candidate technology for the detecting element in these integrated sensors. Arrays of several thousand detectors are operating in ground-based Cosmic-Microwave-Background (CMB) -polarization experiments. Balloon experiments E and B Experiment (EBEX) and Suborbital Polarimeter for Inflation Dust and the Epoch of Reionization (Spider) have demonstrated two TES architectures in the environment closest to space. Primordial Inflation Polarization Explorer (PIPER) will soon demonstrate a third. Fabrication of TES arrays on 150-mm diameter substrates, which addresses pixel-count scalability, is now maturing at multiple fabrication foundries. However, no fielded 150-mm arrays exist at this time.
TRL	**SOTA**	4
	Solution	3
Performance Goals and Objectives		The detectors must demonstrate high efficiency, background-limited sensitivity, and linearity over a wide spectral range (~30 to ~600 GHz), while at the same time controlling systematic errors to a level sub-dominant to the instrument statistical-noise floor. The technology must demonstrate extremely low levels of polarized-beam systematic errors to achieve this goal. The technology must be compatible with space-borne operation, and provide appropriate magnetic shielding, cosmic-ray immunity, vibration tolerance, and excellent noise stability. Process uniformity, high detector efficiency, and high yield are also important. One technical development that would have a large impact on instrument design is a reduction of the TES detector-to-readout interconnects at the milliKelvin stage. Current TES readout schemes demand a large number of additional hardware elements, which require interconnects and an associated mechanical support structure. Technical approaches that do away with additional readout hardware elements will reduce the mass, volume, and complexity of the entire instrument. Integrated fabrication of TES detectors and SQUID readouts represents one avenue to achieve this goal.
Scientific, Engineering, and/or Programmatic Benefits		Measurement of CMB polarization to search for evidence of, and characterize, Inflation is a top NASA priority. Polarization measurements on finer angular scales probe large-scale structure sensitive to neutrino mass and dark energy. Such detectors are a key enabling technology for a space-borne measurement that can probe for a polarization pattern imprinted by a background of GWs generated at the time of Inflation in the early universe.
PCOS Applications and Potential Relevant Missions		These are needed for measuring CMB polarization to search for and characterize the faint polarized signature of Inflation. The targeted mission is IP as recommended in the NWNH report. Other possibilities include Explorer and international CMB-polarization and absolute-spectrum experiments. Development also has technological overlaps with superconducting far-IR and X-ray detectors.
Time to Anticipated Need		**Named missions:** IP (2020s) **Development needed for 2020 Decadal:** Yes, IP **Other drivers:** IP technology development is a NWNH priority recently revisited by the mid-Decadal review. US contribution to the Japanese Aerospace eXploration Agency (JAXA) mission Lite (light) satellite for the study of B-mode polarization and Inflation from cosmic background Radiation Detection (LiteBIRD) is already in a phase A study through the Explorer's program. An additional Explorer proposal to contribute to a European Space Agency (ESA) mission is likely this year.

Gap Name		Polarization-Preserving Millimeter-wave optical elements *Submitted by General Community*
Description		High-throughput telescopes and optical elements with controlled polarization properties are required for the IP. These require development of cryogenic mm-wave filters and coatings. Measurement of CMB polarization on large scales may require rapid polarization modulation to separate sky-signal polarized intensity from instrumental effects. Employing modulators large enough to span the telescope primary aperture is an advantage in that sky polarization can be separated from instrumental effects.
Current State-of-the-Art (SOTA)		Single-layer anti-reflection (AR) coatings are in widespread use. Meta-material AR structures are in development and early use. Several experiments in the field are currently using rapidly spinning half-wave plates as the primary means of modulating the signal and separating it from longer time variations. More experiments are coming online using both half-wave plates and variable-delay polarization modulators that endeavor to measure larger areas of the sky.
TRL	**SOTA**	2–5
	Solution	
Performance Goals and Objectives		Develop robust multi-layer coatings for broadband applications for commonly used dielectrics (e.g., silicon, alumina, and sapphire). Develop thermal filtering technologies suitable for large Focal-Plane Arrays (FPAs) operating at sub-Kelvin temperatures. Develop space-compatible modulators, including work on frequency-selective surfaces and mechanisms compatible with the space radiation environment. Minimizing dielectric cross-section to low-energy electrons is a priority. Develop and compare strategies for instrument architectures with and without rapid modulators. A secondary goal is to ensure that the technology can be implemented in a cost-effective way for large optical elements. Large in this context is up to 100 cm in diameter.
Scientific, Engineering, and/or Programmatic Benefits		Broadband optics can reduce the necessary focal-plane mass and volume for CMB polarization measurements. This may open options for compact optical systems appropriate for lower-cost Explorer opportunities; an international mission concept using broadband refracting optics is in the planning stages. Modulators are potentially a key enabling technology.
PCOS Applications and Potential Relevant Missions		IP, Far-IR, Explorer, and international experiments to study CMB polarization and absolute spectrum.
Time to Anticipated Need		**Named missions:** IP (2020s) **Development needed for 2020 Decadal:** Yes, IP **Other drivers:** IP technology development is a NWNH priority that was recently revisited by the mid-Decadal review. International and Explorer implementations of the IP have proposed launch dates during the second half of the next decade.

Gap Name		High-power, narrow-line-width laser sources *Submitted by LISA Study Office*
Description		GW missions need lasers that are either intrinsically stable or can be stabilized to external references. The laser phase must also be modulated to allow exchange of clock-noise information, ranging tones, and potentially data.
Current State-of-the-Art (SOTA)		The laser system is usually envisioned as a master oscillator power amplifier (MOPA) system. The Tesat laser flying on LISA Pathfinder (LPF) meets most of the master laser requirements for Laser Interferometer Space Antenna (LISA). Lasers of a similar type Non-Planar Ring Oscillator (NPRO) exist commercially in the US. GSFC has partnered with LGS to develop an alternative master laser based on an External Cavity Laser (ECL), which is currently at TRL 3. Commercial amplifier products exist in the US and Europe but are typically intended for other applications and require integration into a laser system and subsequent testing. A 2-W laser amplifier was constructed by LGS, tested at GSFC, and is at TRL 4. An alternative to the MOPA approach is a single-stage laser. Commercial (not space-qualified) single-stage laser systems with 2-W output power exist that can be controlled to meet power and frequency noise requirements but lack capability to sufficiently modulate the laser field. This could be remedied with the inclusion of a high-power phase modulator, which would require some development.
TRL	**SOTA**	3
	Solution	3

Performance Goals and Objectives		The goal is to assemble and test a full space-qualified laser system meeting all requirements listed below. This includes laser power, frequency noise, intensity noise, and a possibility to modulate the laser with GHz sidebands, Pseudo-Random Noise (PRN) codes, and maintain phase fidelity throughout the laser system.
		
		The key performance parameters are:
		• Laser power ~ 2W;
		• Intrinsic Frequency noise: < 60 kHz/√Hz* (1Hz/f);
		• Relative intensity noise:
		  • 10^{-4}/√Hz in LISA band,
		  • 10^{-8}/√Hz above ~2 MHz;
		• Phase fidelity of GHz phase modulation < 6×10^{-4}/√Hz in LISA band; and
		• Lifetime: 4-10 years hot; 5 years cold redundancy.
		
		All parameters measured at output of single-mode polarization-maintaining fiber.

Scientific, Engineering, and/or Programmatic Benefits		The laser is a potential US contribution to an ESA-led LISA mission selected by ESA in 2017. It is also required for a potential future US-led laser-interferometric GW mission. Laser technology is in general a critical technology for a vast range of future applications. All formation-flying plans in the 30-year Astrophysics Roadmap require laser systems that meet at least some of these requirements. Having a space-qualified commercial-off-the-shelf (COTS) laser system meeting the GW mission requirements should be a general goal of NASA.
PCOS Applications and Potential Relevant Missions		Space-based laser-interferometric GW detectors such as LISA. Space-based geodesy missions, such as Gravity Recovery and Climate Experiment (GRACE) II, require low-power versions of these types of lasers. Future missions: Interferometry was named as one of the crosscutting, game-changing technologies in the Astrophysics Roadmap, and ultra-stable lasers are essential for this.
Time to Anticipated Need		**Named missions:** LISA (late 2020s / early 2030s) **Development needed for 2020 Decadal:** Yes, LISA **Other drivers:** ESA is considering accelerating the LISA schedule in response to the recent GW detections and the LPF results. The earliest expected date for mission adoption would be 2022. Targeting TRL 6 by 2022 would enable NASA to offer the laser as a contribution to LISA. The schedule for a US-led mission would likely lag by 2-3 years.

Gap Name		Highly stable low-stray-light telescope *Submitted by LISA Study Office*
Description		LISA-like missions need optical telescopes to expand and compress laser beams. A robust design is needed for small-scale manufacturability of functionally interchangeable units. A total of order 10 telescopes are required, including 6 flight units, 1-2 spares, and additional units for ground testing and test beds. The need for in-field guiding will depend on the orbits and progress in other areas, such as designs that allow correlating the two local lasers at the pm/√Hz level (back-link fiber or free-space link).
Current State-of-the-Art (SOTA)		The most unusual performance parameters are pm/√Hz stability and stray-light requirements. Telescopes that meet the phase-front quality, FOV, and diameter requirements are fairly standard. The long-term imaging requirement with a set-and-forget focus adjustment is probably also standard. However, this adjustment mechanism might introduce unacceptable dimensional noise beyond the pm/√Hz level and some realizations have shown increased scattered-light levels. Relying on the passive absolute stability of the secondary/primary distance (~μm) would eliminate the need for a focus adjustment. The pm/√Hz stability has been tested for several spacer materials but never for a realistic telescope that includes mirrors and mounts. Additional work on stable materials may be needed. The backscatter has been studied in small tabletop experiments for the secondary mirror for on-axis telescopes but not for a full telescope. On- and off-axis telescopes have been studied with ray-tracing programs, which are not ideal for laser interferometric applications. In-field guiding has not been integrated into any telescope test, and would require development of a mechanism. These tests and simulations put the telescope at TRL 4 without in-field guiding and below TRL 4 with it.
TRL	**SOTA**	4
	Solution	4
Performance Goals and Objectives		The key performance parameters are: pm/√Hz stability at $f > 1$ mHz $\sqrt{[1 + (3\text{ mHz}/f)4]}$; < 100 pW of stray light from the telescope back into the fundamental spatial mode on the optical bench (for up to 2-W input power); long-term imaging stability (set-and-forget focus adjustment or passive absolute stability) to generate small (5-mm) collimated beam on optical bench; aperture stop for transmitted beam; phase-front quality: λ/30; FOV: ±200 mrad; diameter: 20 - 40 cm. The goal is to build a prototype telescope (ideally two: one on-axis, one off-axis) and test for pm/√Hz stability and minimal backscatter while also evaluating the received and transmitted laser fields. Tests with a full telescope would lead to TRL 5 and allow a decision between a simple on-axis design and a more complex off-axis design. In-field guiding should be studied through design and simulation first, and the need should be evaluated against progress in other areas including mission design (orbits, lifetime). In-field guiding would require development of a mechanism that could change the direction of propagation of a beam without inducing any change in the optical path length.
Scientific, Engineering, and/or Programmatic Benefits		The telescope is one of the potential US contributions to an ESA-led LISA selected in 2017 or a potential US-led follow on.
PCOS Applications and Potential Relevant Missions		Space-based laser-interferometric GW detectors such as LISA. Potentially other precision interferometric measurement applications.
Time to Anticipated Need		**Named missions:** LISA (late 2020s / early 2030s) **Development needed for 2020 Decadal:** Yes, LISA **Other drivers:** ESA is considering accelerating the LISA schedule in response to the recent GW detections and the LPF results. The earliest expected date for mission adoption would be 2022. Targeting TRL 6 by 2022 would enable NASA to offer the telescope as a contribution to LISA. The schedule for a US-led mission would likely lag by 2-3 years.

Gap Name		Low-mass, long-term-stability optical bench *Submitted by LISA Study Office*
Description		Space-based laser-interferometric GW missions need optical benches to prepare, split, direct, and combine the different laser fields to form all required beat signals.
Current State-of-the-Art (SOTA)		Europe developed the optical bench for LPF using an all Zerodur®, hydroxide-bonded bench (TRL 8 now). Recent LPF results show that the optical bench greatly exceeds the stability requirement. However, the assembly of the bench took very long and was always on or near the critical path. This technology does not scale well for the 4× larger LISA bench, which also carries 4× more components, and LISA requires six flight units instead of one. The European team is exploring a robotic assembly technique to reduce assembly time. This technology is probably at TRL 2 or 3. Alternatively, or more likely in addition, the optical bench could be re-designed to trade some of the performance margin in stability for ease in manufacturing. This technology is probably at TRL 2 or 3.
TRL	**SOTA**	8
	Solution	2
Performance Goals and Objectives		At least two approaches should be considered. The first is to develop a manufacturing technique to robustly produce optical benches using the LPF-proven approach but with reduced assembly time and labor. This is the approach being taken in Europe. The second approach is to re-visit the optical bench design and look for trades to reduce the difficulty of assembly at the expense of the significant performance margin in dimensional stability demonstrated by the LPF bench. This might include replacing some (or most) of the bench with a classical mechanical structure and only applying the labor-intensive hydroxy catalysis techniques for the most critical components. Composite structure using other materials such as single-crystal silicon and non-carbon-fiber-based composites should be investigated, as should metals. Key performance parameters are: dimensional stability of $\sqrt{(1+(1\text{mHz}/f)^4)}$ pm/$\sqrt{\text{Hz}}$; long-term-alignment stability; low mass; and assembly procedures that allow for small-scale manufacturability, perhaps through automation, modular design, simplified bonding techniques, and/or optical fiber techniques (LISA-like missions will require of order 10 optical benches, including 6 flight units, 1-2 spares, and additional units for ground testing).
Scientific, Engineering, and/or Programmatic Benefits		A lighter and easier-to-assemble optical bench would significantly reduce cost and programmatic risks associated with any complex assembly process. In addition, the bench could be a deliverable for NASA in the ESA-led mission LISA, which was selected in 2017 or as part of a future US-led follow-on mission.
PCOS Applications and Potential Relevant Missions		NASA contribution to ESA's LISA mission. In principle, rapid (perhaps automated) construction of dimensionally stable optical structures could be generalized to other applications including telescopes.
Time to Anticipated Need		**Named missions:** LISA (late 2020s / early 2030s) **Development needed for 2020 Decadal:** Yes, LISA **Other drivers:** ESA is considering accelerating the LISA schedule in response to the recent GW detections and the LPF results. The earliest expected date for mission adoption would be 2022. Targeting TRL 6 by 2022 would enable NASA to offer the optical bench as a contribution to LISA. The schedule for a US-led mission would likely lag by 2-3 years.

Gap Name		Phase measurement system (PMS) *Submitted by LISA Study Office.*
Description		Space-based laser-interferometric GW missions measure the phase evolution of laser beat signals to monitor the minute length changes caused by GWs (~pm/√Hz level), extract the phase of the clock noise tones (~0.1 millicycle/√Hz), measure absolute spacecraft distances at the sub-meter level, and provide signals for phase-locking and arm-locking the lasers and for aligning the constellation. The PMS includes the analog front end, quadrant photo-receivers, anti-aliasing filters, and Analog to Digital Converters (ADCs). An ultra-stable oscillator (USO) and a frequency distribution system that includes frequency multipliers are also considered part of the PMS.
Current State-of-the-Art (SOTA)		A fully functional LISA Phasemeter has been developed to TRL 4. The system consists of many subcomponents at different TRLs. The most critical part is the analog front end of the measurement system, which is at TRL 4. Quadrant photo-receivers based on COTS detectors have been developed at ANU, and a custom-designed detector with much lower capacitance (and therefore lower noise) has been developed through the Small Business Innovation Research (SBIR) program. Both alternatives need further development or at least flight qualification. The frequency multipliers in the frequency distribution system are at TRL 5. The phasemeter core is at TRL 6, although general advances in digital signal processing should be used to simplify and advance the capabilities of the PMS over time. A phasemeter has been developed to flight maturity for NASA's GRACE Follow-On mission, for the Laser Ranging Interferometer (LRI) instrument. The LRI phasemeter represents relevant flight heritage for a LISA-like missions. While several phasemeter performance requirements on the LRI are relaxed compare to LISA requirements, the LRI phasemeter is expected to meet LISA requirement levels.
TRL	**SOTA**	4
	Solution	4
Performance Goals and Objectives		Advance the maturity of the LISA Phasemeter based on the flight Phasemeter developed for LRI. There are several clear ways to achieve this: 1. Test the LRI phasemeter to LISA performance requirements, thereby validating the technology for use in LISA. 2. Incorporate flight LRI phasemeter developments, such as automatic laser lock acquisition sequences, into the TRL 4 LISA PMS. 3. Study the best options for increasing channel count from the LRI to LISA phasemeters. Quadrant photo-receivers and ADCs should be developed to meet the original LISA requirements (which serve as benchmarks for all currently discussed mission designs) and reach TRL 5. These analog parts present the largest remaining risk for the PMS. Further development of the frequency multipliers requires a final mission design that includes a frequency distribution plan.
Scientific, Engineering, and/or Programmatic Benefits		The PMS, in the form discussed here, meeting the requirements presented here, is critical for all LISA-like missions. A working PMS with an adequate analog front end is also important for many tests for other subsystems in LISA-like missions such as the optical bench or the telescope. The PMS is a strategic technology with multiple uses in many areas; the initial phasemeter evolved out of the Blackjack receivers used in GPS. The analog front end would allow application to optical signals, which vastly improves the sensitivity compared to GPS.
PCOS Applications and Potential Relevant Missions		Space-based laser-interferometric GW detectors such as LISA or follow-ons. Advanced Geodesy missions such as GRACE-II. Other future interferometric missions; interferometry has been named as one of the crosscutting, game-changing technologies in the Astrophysics Roadmap.
Time to Anticipated Need		**Named missions:** LISA (late 2020s / early 2030s) **Development needed for 2020 Decadal:** Yes, LISA **Other drivers:** ESA is considering accelerating the LISA schedule in response to the recent GW detections and the LPF results. The earliest expected date for mission adoption would be 2022. Targeting TRL 6 by 2022 would enable NASA to offer the PMS as a contribution to LISA. The schedule for a US-led mission would likely lag by 2-3 years.

Gap Name		Non-contact charge control for Gravitational Reference Sensors (GRS) *Submitted by LISA Study Office*
Description		Space-based GW observatories like LISA use free-floating test masses (TMs) as references for measuring GWs The free-floating TMs can become electrically charged due to cosmic-ray impacts and during release from the TM caging system. This charge introduces a force on the TM due to stray electric fields associated with the spacecraft, limiting the sensitivity of the entire system to GWs. A charge control system is needed to control the TM with respect to its housing. A standard approach used on flight accelerometers is to use a thin metallic wire for charge control. However, the mechanical coupling produced by these wires would introduce disturbances that exceed the requirements for a GW mission. Non-contact charge control units use ultraviolet (UV) light to control charge via the photoelectric effect. The LPF charge control system, which uses ultraviolet (UV) light generated by Hg lamps, operates in a maintenance mode. This means that it requires a pause in science operations in order to provide charge control. A charge control system that could operate without disturbing the science measurement would be advantageous.
Current State-of-the-Art (SOTA)		In the current LPF charge management design, UV light generated by Hg lamps is directed via a UV fiber feedthrough toward the TM surface if the goal is to increase the TM potential, or toward the electrode housing surface if the goal is to decrease the potential. The Hg-lamp-based charge management system on LPF was successfully demonstrated in 2016. The TRL in Europe is high (8). Non-contact charge control using deep-UV LEDs operating at 240 - 255 nm are a promising new UV source for controlling TM charge. Compared to the Hg lamps, UV LEDs are smaller, lighter, consume less power, have a wider spectrum selection, and have a higher dynamic range, with at least an order-of-magnitude improvement in each performance area.
TRL	**SOTA**	8
	Solution	
Performance Goals and Objectives		Develop a non-contact charge management system that can be integrated seamlessly into the LPF GRS, with bi-directional charge control at an average rate of 50 e/s. For maintenance activity, the charge control rate of the device needs to be increased by the maintenance duty cycle (~2 hrs/week) or ~9 ke/s. Demonstrate AC charge control in a low-disturbance environment and assess whether the science measurement is disturbed (TM force < 1 fN/√Hz at modulation frequency).
Scientific, Engineering, and/or Programmatic Benefits		Non-contact charge control is an essential element of a space-based GW instrument and will enable the science that has been endorsed by the past two decadal surveys. A charge management system is a candidate NASA contribution to the ESA-led LISA GW mission.
PCOS Applications and Potential Relevant Missions		GW observatories such as a follow-on to LISA. Advanced Geodesy missions such as GRACE-II.
Time to Anticipated Need		**Named missions:** LISA (late 2020s / early 2030s) **Development needed for 2020 Decadal:** Yes, LISA **Other drivers:** ESA is considering accelerating the LISA schedule in response to the recent GW detections and the LPF results. The earliest expected date for mission adoption would be 2022. Targeting TRL 6 by 2022 would enable NASA to offer the charge control as a contribution to LISA. The schedule for a US-led mission would likely lag by 2-3 years.

Gap Name		Gravitational Reference Sensor (GRS) *Submitted by LISA Study Office*
Description		The ideal GRS is a free-falling TM subject only to the tidal forces caused by GWs. The GRS envisioned for LISA-like missions is a 2 kg gold/platinum cube surrounded by electrodes used to sense the position of the TM with respect to the spacecraft, and also apply forces to the TM in all non-sensitive directions. This GRS, as a technical unit, also includes the electrode housing, caging mechanisms, vacuum systems, and front-end electronics.
Current State-of-the-Art (SOTA)		The European GRS was successfully demonstrated on LPF, exceeding the LPF requirements and nearly meeting the LISA requirements. NASA has nothing comparable and it is difficult to assign a reasonable TRL for this specific case.
TRL	**SOTA**	8
	Solution	
Performance Goals and Objectives		The long-term target is to develop competency in the US in GRS technology. The immediate goals are to design and fabricate a TRL-3 electrode housing, to construct a torsion pendulum test facility to evaluate the performance of the GRS housing, and to develop capacitive readout and electrostatic actuation electronics, as well as an interferometric readout for calibration and high resolution measurements.
Scientific, Engineering, and/or Programmatic Benefits		GRS technology is absolutely critical for any GW detector mission. Having zero competency in the US puts us in a difficult position for a NASA-led mission that would address one of the leading science goals of the last two decadal surveys.
PCOS Applications and Potential Relevant Missions		LISA-like space-based GW missions and, with relaxed requirements, geodesy missions.
Time to Anticipated Need		**NASA-led:** TRL 3 by 2018 latest. TRL 5 by 2022. **ESA-led:** TRL 3 by 2018 to develop competency and the possibility of alternative vendors should the single vendor in Italy become unavailable.

Gap Name		Precision Microthrusters *Submitted by LISA Study Office*
Description		GW observatories, large exoplanet observatories including the star shade concept, and potentially any astronomy or astrophysics observatory currently planning to use reaction wheels, demand extraordinary fine pointing and precision attitude control. Especially for the drag-free platforms necessary to measure GWs, high-precision microthrusters are necessary to meet ~10 nm/√Hz position stability requirements. Microthrusters must have precise thrust steps (≤0.1 μN) with low noise (0.1 μN/√Hz) over a range of 5-50 μN for a primary application of a GW observatory. In all applications, higher specific impulse (>100 s) is also beneficial for low-mass systems. Studies have shown that using microthrusters instead of reaction wheels can actually be a net savings in terms of mass due to the elimination of heavy vibration isolation systems. Finally, a lifetime of ≥ 5 years is key for all major observatories. Currently, colloid microthrusters provide the most advanced microthruster technology, now being demonstrated on LPF, but still require a longer lifetime demonstration along with fully redundant architectures.
Current State-of-the-Art (SOTA)		Both cold-gas and colloid microthrusters are being demonstrated on LPF and other missions to reach TRL 7. Meeting once very challenging thrust-precision performance requirements is now absolutely feasible. However, many of these systems are single-string and only have space-based demonstrations on the order of 90 days of operation. To reach TRL 6 for flagship-class missions, additional developments and demonstrations of lifetime and reliability need to be addressed. PCOS SAT funding has already pushed a fully redundant colloid-thruster feed system to TRL 5 with enough capacity for a 5-year GW observatory mission. However, the fully redundant thruster system, including the thruster head itself, has not been tested, nor has lifetime been demonstrated greater than 1/3 of a year.
TRL	**SOTA**	7
	Solution	5
Performance Goals and Objectives		Performance targets have already been met by existing systems, such as the colloid microthruster. However, lifetimes of only ~3000 hours have been demonstrated on the ground. For flagship-class missions, additional development regarding reliability, maintaining performance while improving redundancy, and lifetime (≥ 5 year) demonstrations will be required prior to adoption and infusion.
Scientific, Engineering, and/or Programmatic Benefits		While the main application of precision microthrusters relates to drag-free GW observatories, further development of these systems would allow reaction wheel replacement on many future missions. Precision thrusters do not require the heavy vibration-isolation systems that current reaction wheel based systems (e.g., Hubble, Kepler, etc.) employ. Furthermore, if reliability and lifetime greater than current reaction-wheel technology can be proven, a leading cause to observatory failure (reaction-wheel failure) can be mitigated.
PCOS Applications and Potential Relevant Missions		The main application relates to GW observatory concepts that demand drag-free operation of the observing spacecraft. Other missions, such as exoplanet observatories or X-ray observatories that also require fine positioning and pointing, could also benefit. Eventually, precision microthrusters could be used to replace heavier and less-reliable reaction-wheel-based pointing systems on all future astronomy and astrophysics observatories.
Time to Anticipated Need		**Named missions:** LISA (late 2020s / early 2030s) **Development needed for 2020 Decadal:** Yes, LISA **Other drivers:** ESA is considering accelerating the LISA schedule in response to the recent GW detections and the LPF results. The earliest expected date for mission adoption would be 2022. Targeting TRL 6 by 2022 would enable NASA to offer the microthrusters as a contribution to LISA. The schedule for a US-led mission would likely lag by 2-3 years. The main lifetime demonstration necessary for infusion of this technology requires 6-8 years for a 1-to-1 operational hour test. Such was the case for the now successfully infused ion engines, first demonstrated on Deep Space 1 and now used on Dawn, which had a 30,000-hour ground-based lifetime test that lasted approximately 5 years. Significant investment in microthruster technology now would be required to meet normal NASA standards of a ≥ 1.5 × lifetime demonstration by mission PDR or Critical Design Review (CDR).

Gap Name		High-performance gamma-ray telescope *Submitted by General Community*
Description		Two technologies are needed to enable gaseous detectors, e.g., Time Projection Chambers (TPC), with large volumes, tens to hundreds of m^3, to be inflated on orbit: 1. The inflatable pressure shell must contain the detector gas at pressures up to ~3 Atm, be capable of self-sealing against micro-meteors, and have a surface density of < 1 g/cm^2. The TPC field-shaping electrodes are mounted on the inner surface of the inflatable shell, and deploy as the shell inflates to positions accurate to ~1 mm. 2. The TPC readout structure at the bottom of the TPC must unfold within the gas volume, be rigid, and have position accuracy of ~1 mm.
Current State-of-the-Art (SOTA)		Thin Red Line Aerospace developed and supplied 20 full-fidelity inflatable pressure shells of up to 320 m^3 volume for Bigelow Aerospace inflatable habitat Genesis spacecraft flight hardware. Thin Red Line designed, engineered, and manufactured the pressure-restraining hulls of Genesis 1 and 2 (launched 07/06 and 06/07, respectively), the first spacecraft on orbit successfully incorporating large-volume, high-stress inflatable architecture (other projects at http://www.thin-red-line.com/projects.html). Large deployable mirrors have been developed for JWST. This technology could be adapted for the deployable TPC readout.
TRL	**SOTA**	6
	Solution	
Performance Goals and Objectives		The goal is to enable construction of a ~100 m^3 gamma-ray pair telescope with arcmin angular resolution and continuum sensitivity of better than 5×10^{-7} between ~100 MeV and ~10 GeV. The objectives can be met by demonstrating an inflatable TPC gas shell with volume ~10 m^3 at ~1 Atm and deployable readout electrodes with area of ~2 m^2.
Scientific, Engineering, and/or Programmatic Benefits		Inflatable gaseous detectors would enable gamma-ray telescopes to achieve arcmin angular resolution. Deployable 2-D readout structures within a large gas volume would increase telescope sensitivity.
PCOS Applications and Potential Relevant Missions		Arcmin gamma-ray telescope.
Time to Anticipated Need		**Named missions:** **Development needed for 2020 Decadal:** No **Other drivers:** Applicability to Explorer opportunities.

Gap Name		Fast, few-photon UV detectors *Submitted by General Community*
Description		Near-UV (300 – 400 nm) single-photon detectors for measuring from space atmospheric fluorescence light produced by particle cascades induced by ultra-high-energy cosmic rays (UHECR).
Current State-of-the-Art (SOTA)		Current SOTA are multi-anode vacuum photomultipliers (PMTs). These are high TRL (quoted TRL applies only to these devices) and high performance, but are relatively costly per channel, heavy, sensitive to over-exposure, and delicate. Silicon photomultipliers (SiPM, also called multi-pixel photon counters or MPPC), based on arrays of avalanche-diode micro-pixels operating in quenched Geiger mode, are promising but current SOTA SiPM have unacceptable noise without cooling to < 20°C. In the large imaging arrays needed with $2\times10^5 - 1\times10^6$ pixels, uncooled noise produces high false-detection rate and cooling consumes unacceptable power. Also, most SiPM are not optimized for near-UV detection (although thinned, back-side-illuminated SiPM are possible).
TRL	**SOTA**	8
	Solution	
Performance Goals and Objectives		• Active area 8 mm^2 to 300 mm^2; • Active-area fraction > 85%; • Read out at > 10 MHz; • Suitable for use in ≥ 4 m^2 arrays with ≥ 2×10^5 detectors (pixels); • QE at 330 nm ≥ 30% (goal 60%); • Gain ≥ 10^4 to allow few-photon (single-photoelectron) detection; • Noise < 10^6 counts/(mm^2 sec) at half of single-photoelectron signal; • Signal duration < 10 ns; • Recovery from single-photoelectron pulse to 99.9% resolution of 10^3 photon pulse <10 ns; • Inactive area < 20% when in array (< 5% goal), and scalable detector (pixel) dimensions to match the imaging optics; • Minimum mass (goal < 2 g/cm^2); • Individual pixel readout is required; and • Active lifetime ≥ 5 years (goal 10 years) with integrated background exposure ≥ 3×10^{14} photons/mm^2.
Scientific, Engineering, and/or Programmatic Benefits		This technology would enable focal planes for UHECR (see below) instruments to be built at a small fraction of the cost, mass, and power that would be required for the current SOTA. This would in turn vastly increase the probability that a useful space-based UHECR instrument could be built. Coupled with lightweight, low-cost optics, this could enable a pathfinder instrument to be built as a MIDEX (possibly as a class-D SMEX, although this is ambitious).
PCOS Applications and Potential Relevant Missions		Focal planes for missions to measure UHECR by imaging, from LEO, the giant particle showers caused by UHECR (E ≥ 10^{18} eV) interacting in the Earth's atmosphere. This requires determining the time and spatial development of the UV light emitted by air fluorescence after excitation of atmospheric constituents, primarily N_2, by the particle cascade. A possible pathfinder mission, JEM-EUSO (Japanese Experiment Module Extreme Universe Space Observatory), is in the Astrophysics Roadmap but development would also be applicable to the more advanced OWL (Orbiting Wide-angle Light collectors) mission or other formulations. Detectors would also be important for ground Cherenkov arrays such as Cherenkov Telescope Array (CTA) and would have a variety of other astrophysics, accelerator, and medical imaging applications.
Time to Anticipated Need		**Named missions:** **Development needed for 2020 Decadal:** No **Other drivers:** Flight mission estimated no earlier than 2022 for JEM-EUSO or an OWL Pathfinder. Full balloon-flight prototype 2019.

Gap Name		Lightweight, large-area reflective optics *Submitted by General Community*
Description		Lightweight, easily deployable mirror as the primary of a Schmidt telescope (or similar) for measurements from space of atmospheric fluorescence light in the near UV (~330 - 390 nm) produced by particle cascades induced by UHECRs and also Cherenkov monitoring (in the 300 to 500 nm range) of the Earth's horizon to observe Earth-sourced tau neutrinos with astrophysical and cosmogenic origins.)
Current State-of-the-Art (SOTA)		SOTA is the optical system developed in NASA studies for the OWL mission concept, based on smaller mirrors that have flown. This was an f/1 Schmidt with 45° full FOV. The deployable primary mirror diameter was 7.1 m (Schmidt corrector diameter was 3.0 m, and focal plane was 2.3 m). This had eight petals, launching with the petals folded upward with four inner and four outer petals interleaved. After deployment, the outer ring of four petals unfolded and the inner ring unfolded and moved outward to form a uniform surface. The mass of the mirror and mechanisms was 581 kg. Publicly accessible SOTA in inflatable mirror technology is the Inflatable Antenna Experiment (IAE) which flew on STS 77 in 1996. It was a 14-m diameter microwave antenna in a convex-convex configuration with the reflective material on the inner surface of one of the sides. This requires highly UV-transparent material for the entrance surface.
TRL	**SOTA**	5
	Solution	
Performance Goals and Objectives		Spherical or piecewise-spherical surface when deployed with ≥ 50% (goal ≥ 90%) reflective area when compared to a complete spherical segment with the same solid angle. Reflector area ≥ 38 m^2 and full FOV ≥ 45°. Needed resolution is ~1 milliradian, ≥ 10^4 larger than the diffraction limit, so inflatable optics are one possible solution. Goal is for a ~7-m-diameter reflector to be compact enough when stowed for launch and light enough to facilitate a mission on a launch vehicle or a vehicle similar to the SpaceX Falcon 9 using a ≤ 4.6-m-diameter fairing. Goal for mass of solid 7-m mirror and mechanism (if any) is < 300 kg. Goal for mass of inflatable 7-m mirror is ≤ 5 kg. Long-term goal is 1,400 m^2 reflector area with mass ≤ 100 kg.
Scientific, Engineering, and/or Programmatic Benefits		This technology would enable reflective optics for a UHECR (see below) mission to be built at a small fraction of the mass of the OWL optics that represent the current SOTA. In turn, vastly increasing the probability that a useful space-based UHECR instrument could be built. Coupled with a lightweight, low-cost, high-performance focal plane and electronics, this could enable building a pathfinder instrument.
PCOS Applications and Potential Relevant Missions		Optics for missions to measure UHECR by imaging, from LEO, the giant particle showers caused by UHECR (E > 10^{18} eV) interacting in the Earth's atmosphere. This requires determining the time and spatial development of the UV light emitted by fluorescence after excitation of atmospheric constituents, primarily N_2, by the particle cascade. A possible pathfinder mission, JEM-EUSO, using refractive (Fresnel) optics is in the Astrophysics Roadmap. However, this has not been selected for flight by any space agency. It is generally agreed that a full UHECR mission would use reflective optics similar to the Schmidt telescope designed for the NASA OWL mission. Extending full measurement down to 10^{18} eV to enable measurements of neutrinos from UHECR interactions with the CMB would require a 42-m-diameter reflector, achievable only using a very light mirror such as an inflatable. If the lightweight technology could be applied to mirrors with better resolution, then a wide variety of missions would be enabled. Probe Of Extreme Multi-Messenger Astrophysics (POEMMA), currently selected for a NASA Probe Mission design study for the 2020 Decadal. POEMMA will combine the well-developed OWL concept with the recently proposed Cherenkov from Astrophysical Neutrinos Telescope (CHANT) concept to form a multi-messenger probe of the most extreme environments in the universe.
Time to Anticipated Need		**Named missions:** **Development needed for 2020 Decadal:** No **Other drivers:** Flight mission estimated no earlier than 2022 for JEM-EUSO or an OWL Pathfinder. Full balloon flight prototype 2019. Potential Super Pressure Balloon flight in 2019 with 100-day mission goal.

Gap Name		Low-power time-sampling readout *Submitted by General Community*
Description		Time-sampling low-power readout electronics to measure pulse amplitude and photon-arrival time for detection from space of atmospheric fluorescence light in the near UV (~330 - 390 nm) produced by particle cascades induced by UHECRs using fast photodetectors (e.g., multi-anode vacuum photomultiplier or silicon photomultiplier).
Current State-of-the-Art (SOTA)		SOTA are switched capacitor arrays with ~1024 sampling cells per channel and switching using a "domino" strobe that causes the input to be sampled continuously until stopped by an external signal. Some devices include onboard digitizer and others clock out charge to an external digitizer. Channels can be cascaded to increase depth. Effective resolution 9 to 11.5 bits. Reported power consumption at 200 MS/s (mega-samples per second) sampling (10× faster than needed) ~4 mW/channel. Development push is toward faster sampling rather than lower power consumption. Sample-to-sample timing is not constant, but can be calibrated. Most implementations require an external amplifier. A competing technology uses a series of delay lines acting as a circular analog memory. Sampling depth depends on the total delay that can be achieved. Depth of 1024 samples has been reported at 500 MS/s but same delay would have a depth of only 40 samples at 20 MS/s.
TRL	**SOTA**	6
	Solution	
Performance Goals and Objectives		• Sampling rate ≥ 20 MS/s for ~100 ns photon-arrival-time resolution (allowing photodetector pulse to overlap two samples); • Full time sampled 3×10^{-4} s so depth 6000 samples at 20 MS/s; • Usable dynamic range ≥ 11 bits per sample; • Charge resolution ~0.25 pC; • Readout clock speed ~10–33 MHz; • Operating power at 20 MS/s ≤0.5 mW/channel (goal 0.25 mW/channel) including any required amplification; • Area required including ancillary components ≤ 8 mm^2/channel; and • Channels/ASIC ≥ 9.
Scientific, Engineering, and/or Programmatic Benefits		This technology would enable readout electronics for UHECR (see below) instrument focal planes to be built with a small fraction of the cost and power that would be required for the current SOTA. In turn, this would vastly increase the probability that a useful space-based UHECR instrument could be built. Coupled with lightweight, low-cost, optics and high-performance photodetectors, this could enable building a pathfinder instrument as a MIDEX (or class-D SMEX, though this is ambitious).
PCOS Applications and Potential Relevant Missions		Readout electronics for the focal planes of missions to measure UHECR by imaging, from LEO, the giant particle showers caused by UHECR (E ≥ 10^{18} eV) interacting in the Earth's atmosphere. This requires determining the time and spatial development of the UV light emitted by air fluorescence after excitation of atmospheric constituents, primarily N_2, by the particle cascade. A possible pathfinder mission, JEM-EUSO, is in the Astrophysics Roadmap but development would also be applicable to the more advanced OWL mission or other formulations.
Time to Anticipated Need		**Named missions:** **Development needed for 2020 Decadal:** No **Other drivers:** Flight mission estimated no earlier than 2022 for JEM-EUSO or an OWL Pathfinder. Full balloon flight prototype 2019.

Gap Name		Low-power comparators and logic arrays *Submitted by General Community*
Description		Low-power space-qualified pulse comparators and logic arrays to implement the event trigger logic for detection from space of atmospheric fluorescence light in the near UV (~330 - 390 nm) produced by particle cascades induced by UHECRs using fast photodetectors (e.g., multi-anode vacuum PMT or SiPM).
Current State-of-the-Art (SOTA)		Comparators: SOTA for low-power space-qualified comparators are CMOS devices with 1.2 V output voltage. Many devices are available, but lowest power consumption is ~10 mW/channel. No low-voltage output (0.5 V) comparator development for mobile devices seems to be underway. Logic: General SOTA for low-power, space-qualified logic implementations are flash-based FPGAs using 1.2 V logic. It is difficult to define a specific SOTA because of the wide variation in numbers of logic cells and I/O lines. However, devices with 6×10^5 logic cells suitable for UHECR applications, and ≥ 100 MHz maximum clock speed (2.5× faster than needed), are available with power consumptions ≤ 100 mW. There is tremendous effort toward low-voltage (0.5-V) logic for mobile device applications, but to date this has not been fully realized in space-qualified versions.
TRL	**SOTA**	9
	Solution	
Performance Goals and Objectives		Comparator: • Voltage threshold range 2 mV to 0.5 V; • Nominal input voltage to 1 V, but overdrive tolerant to 5 V; • Response time ≤ 50 ns; • Output pulse 0.5 V; • Drive capability ≤ 600 Ohms; • Supply voltage ≤ ± 5V; and • Quiescent power consumption ≤ 0.7 mW/channel (goal 0.2 mW/channel). Logic: • FPGA or similar programmable logic with ≥ 6×10^5 cells per device; • Clock speed 40 MHz; • I/O lines ≥ 210; • Internal logic and I/O logic 0.5V; and • Power consumption ≤ 25 mW per unit at 40 Mhz (goal 10 mW per unit).
Scientific, Engineering, and/or Programmatic Benefits		This technology would enable trigger electronics for UHECR (see below) instrument focal planes to be built with a small fraction of the power required for current SOTA. In turn, this would vastly increase the probability that a useful space-based UHECR instrument could be built. Coupled with lightweight, low-cost, optics and high-performance photodetectors and readout electronics, this could enable building a pathfinder instrument as a MIDEX (or class-D SMEX, though this is ambitious).
PCOS Applications and Potential Relevant Missions		Event trigger components for missions to measure UHECR by imaging, from LEO, the giant particle showers caused by UHECR ($E \geq 10^{18}$ eV) interacting in the Earth's atmosphere. This requires determining the time and spatial development of the UV light emitted by air fluorescence after excitation of atmospheric constituents, primarily N_2, by the particle cascade. A possible pathfinder mission, JEM-EUSO, is in the Astrophysics Roadmap but development would also apply to the more advanced OWL mission or other formulations. The proposed technology developments would enable a wide variety of other missions from flagships down to nano-sats.
Time to Anticipated Need		**Named missions:** **Development needed for 2020 Decadal:** No **Other drivers:** Flight mission estimated no earlier than 2022 for JEM-EUSO or an OWL Pathfinder. Ground tests (in conjunction with Telescope Array) or limited balloon flight tests ~2017. Full balloon flight prototype 2019.

Gap Name		Lattice optical clock for Solar Time Delay mission and other applications *Submitted by General Community*
Description		There are a number of probable applications of optical clocks in future PCOS missions. However, a particularly attractive one is looking for a suspected breakdown in General Relativity [e.g., T. Damour and G. Esposito-Farese, Phys. Rev. D **53**, 5541-5578 (1996)]. Probably the most promising place to look for such a breakdown is in a possible small deviation of the space-curvature parameter gamma from unity, suggested by string theory or theories with additional dimensions. The present accuracy for gamma as determined by Doppler measurements of the solar time delay during the Cassini mission is 2.3e-5. A new determination with 3e-8 or better accuracy could be made with a high-performance optical clock on a spacecraft near the L-1 point of the Earth-Sun system.
Current State-of-the-Art (SOTA)		Both Sr-87 and Yb-131 optical clocks have reached accuracies in the lab of better than 5e-18 over periods of 104 s. This is better than precision of 1e-14/(√Hz) down to 1e-6 Hz needed for a high-accuracy Solar Time Delay mission, but has not yet been demonstrated at frequencies below 1e-4 Hz. Also, the Physikalisch-Technische Bundesanstalt (PTB, National Metrology Institute) in Germany and the Istituto Nazionale di Fizica Nucleare (INFN, National Institute for Nuclear Physics) in Italy have jointly developed a transportable Sr-88 optical clock with a short term noise level of 4e-15 at 1 second that is nearly ready for field use. Other groups in Europe are investigating other types of transportable optical clocks. Some components for cold-atom systems are being tested at a drop tower in Bremen, Germany, for future use in space.
TRL	**SOTA**	
	Solution	
Performance Goals and Objectives		A proposed Solar Time Delay mission was described by N. Ashby, P.L. Bender, J.L. Hall, et al. in "Measurement of gravitational time delay using drag-free spacecraft and an optical clock" [Relativity in Fundamental Astronomy, Proc. IAU Symp. No. **261**, 2009, P.K. Seidelman, S. Klioner, and M. Soffel, Eds., Int. Astron. Union]. Optical time delay measurements would be made from a drag-free spacecraft near the L-1 point to a small transponder satellite during a period of about 20 days when the optical path between the satellites passed by the Sun. The transponder satellite would be in a two-year period orbit with an eccentricity of 0.37. The clock performance required is a precision of 1e-14/(√Hz) down to 1e-6 Hz and an accuracy of 1e-17. Other versions of Solar Time Delay missions are expected to be proposed in response to future PCOS requests for proposals.
Scientific, Engineering, and/or Programmatic Benefits		The primary scientific benefit of a Solar Time Delay mission would be a very strong test of General Relativity (GR). Looking for a small offset of 1e-7 or less in the parameter gamma from solar time delay measurements is fairly widely believed to be the best candidate for detecting an effect on GR of its merger with quantum physics. Optical clocks are also expected to have high value in connection with spacecraft communications and navigation applications, and are listed under TA 5.4.1.3 in the May 2015 Draft NASA Technology Roadmaps. A Technology Candidate Snapshot for Cold Atom Lattice Optical Clocks is listed on page TA5-94. However, in view of the scientific benefits of a future PCOS Solar Time Delay Mission, technology development of optical clocks to the necessary TRL should also be listed under TA 8.1.

PCOS Applications and Potential Relevant Missions	Before the proposed Solar Time Delay mission can be fully evaluated, demonstration of the necessary optical clock performance on the ISS may be needed. This will require vibration isolation and some additional precautions because of the on-board noise level. In view of the problem of frequency comparison between the ISS and ground, two clocks on the ISS operating under somewhat different conditions will need to be compared. This demonstration will facilitate applications to other NASA missions, as well as to the expected future PCOS Solar Time Delay mission. The operation on the ISS of the Project d'Horloge Atomique par Refroidissement d'Atomes en Orbit (PHARAO) clock based on cooled Cs atoms with an accuracy of about 1e-16 and of a mercury trapped-ion clock will help provide experience on the requirements for optical clock operation.
Time to Anticipated Need	**Named missions:** **Development needed for 2020 Decadal:** No **Other drivers:** Discovery opportunities would benefit from TRL 6 by 2019.

Gap Name		Low-power, low-resolution continuous GSa/s direct RF digitizer *Submitted by General Community*
Description		A low-power (below 250 mW/channel total), low cost continuous multi-GSa/s digitizer and high bandwidth (3 dB point of ~1 GHz) is needed for continuous direct digitization of RF inputs for triggered readout, allowing for correlation-based triggers on power-limited multi-antenna radio astrophysics experiments designed to look for transient impulses from cosmic rays and neutrinos. For a triggering subsystem, high dynamic range is not needed, therefore the resolution of the digitizer (number of bits) can be traded for power, with as few as 4 bits. Time resolution, especially between antennas, is more important to allow antenna signals to be added in phase.
Current State-of-the-Art (SOTA)		Digitizer designs exist meeting design goals in laboratory conditions (Macpherson et al., http://doi.org/10.1109/CICC.2013.6658551 , Nishimura et al., https://doi.org/10.1109/RTC.2012.6418181), however neither have been deployed in a correlation-based trigger environment, and both were developed on a 0.13µm semiconductor process in prototype quantities. Commercial devices meeting goals do not exist for reasonable (below $1K/channel) costs and power.
TRL	**SOTA**	7–9
	Solution	4
Performance Goals and Objectives		The goal is to develop, on a low-cost semiconductor process, a 4+-bit digitizer with low noise (>3.5 ENOB, with <0.5 LSB digitization noise) which consumes below 250 mW/channel total while operating (including all static power dissipation and power consumption at the receiving device). Sample rate for the digitizer should be above 2.5 GSa/s with a 3 dB analog bandwidth beyond ~1 GHz. Synchronization of multiple digitizers must also be possible to allow for multiple antennas to be added in phase without degrading the combined ENOB of the sum of multiple antennas. This solution would hopefully be directly usable in a near-term NASA balloon flight to allow for TRL 9 validation of the technology.
Scientific, Engineering, and/or Programmatic Benefits		Correlation-based triggers have been shown to significantly improve triggering capability of multi-antenna experiments (Nishimura et al.), and in fact would be necessary for space-based cosmic ray detections (e.g. SWORD arXiv:1302.1263). Interferometric imaging of impulses is the reconstruction method used for existing multi-antenna radio astroparticle physics experiments (Romero-Wolf et al., https://doi.org/10.1016/j.astropartphys.2014.06.006) and this solution would allow a running trigger to use similar techniques during normal operation.
PCOS Applications and Potential Relevant Missions		An additional balloon flight of the ANITA experiment (ANITA-5) currently proposed would be able to utilize this digitizer immediately, if available in time, putting this solution up to TRL 9 if successful. Balloon programs were specifically mentioned in the Decadal Survey as being valuable testing grounds for future technologies. Future NASA experiments utilizing similar techniques have been proposed (The ExaVolt Antenna, https://doi.org/10.1016/j.astropartphys.2011.08.004, SWORD, or PRIDE https://doi.org/10.1016/j.icarus.2012.05.028), and this solution would allow future similar proposals to directly use this digitizer as proven and usable. In addition, interferometric techniques are directly mentioned in the Astrophysics Roadmap as a crosscutting, game-changing technology. A low-power, low-cost digitizer for use in balloon-borne or other power-limited, low cost missions will have broad application for novel ideas.
Time to Anticipated Need		The ANITA-5 mission is proposed for launch in the 2019-2020 Antarctic season. If the solution were available at that point, it would allow the technology to reach TRL 9, being flight-proven, for future missions. This could be a significant advantage for similar future experiments.

Gap Name		Optical-blocking filters (OBF) *Submitted by General Community*
Description		Future EUV and X-ray missions will have large effective area optics and silicon based detectors on the focal plane. These large X-ray optics will focus optical photons as well as the photons of interest, causing the silicon based detectors to be swamped by an optical photon background, deteriorating their signal-to-noise performance. Future missions will require a method of attenuating this optical background while optimizing the effective area of the instruments for the target photon energy. The method used to attenuate the optical photons needs to offer high transmission of the target photons, good optical photon attenuation, high throughput, and relative immunity to contamination issues. This will allow these future missions to realize their maximum effective area performance, which will lead to high scientific yield.
Current State-of-the-Art (SOTA)		Current state-of-the-art filters fall into two categories. Directly deposited OBFs are deposited onto the surface of the detector. They can be thin and don't require a support structure, but are as cold as the detectors. Contaminants in the payload are attracted the coldest surface, so a cold filter will not prevent detector contamination buildup. Directly deposited filters have been used on RGS on XMM-Newton (TRL 9) and examples suitable for future EUV and X-ray missions, are currently under development (TRL 5). • Ryu, K.K. et al. Development of CCDs for REXIS on OSIRIS-REx. Proc. SPIE 9144, 91440O (2014). • Bautz, M., et al. Directly-deposited blocking filters for high-performance silicon X-ray detectors. Proc. SPIE 9905, 99054C (2016). • Brinkman, A. C. et al. The Refection Grating Spectrometer on board XMM. in SPIE EUV, X-ray and Gamma Ray Instrumentation for Astronomy 2808, 463–480 (1996). • den Herder, J. et al. The reflection grating spectrometer on board XMM-Newton. Astron. Astrophys. 365, L7–L17 (2001). • Pollock, A. M. T. Status of the RGS Calibration. XMM-Newton Users Group, European Space Astronomy Centre, Villanueva de la Canada, Madrid, Spain (2008). doi:10.1002/hed.21900 • Chandra X-ray Observatory. HRC Calibration Information. HEX IPI Team, CXC Calibration Team, cfa Harvard (2014). At http://cxc.harvard.edu/cal/Hrc/detailed_info.html#uvis_trans Free-standing filters are held in-front of the detectors. This removes them from the detector so they can be warm (reducing contamination issues). However, they require a support structure, often have a polyimide structure to support the blocking material, and are thicker than directly deposited filters (>100 nm Al) which all affect instrument effective area. Free-standing filters have been used on Chandra, XMM-Newton, and Hitomi (TRL 9), but filters on highly transmissive frames are at TRL 4 or 5. • McCammon, D. et al. The X-ray quantum calorimeter sounding rocket experiment: Improvements for the next flight. J. Low Temp. Phys. 151, 715–720 (2008). • Takahashi, T. et al. The ASTRO-H Mission. in SPIE Space Telescopes and Instrumentation 7732, 18 (2010). • Koyama, K. et al. X-Ray Imaging Spectrometers (XIS) on Board Suzaku. Publ. Astron. Soc. Japan 59, 23–33 (2007). • Chandra X-ray Center. The Chandra Proposers' Observatory Guide. Chandra Project Science, MSFC Chandra IPI Teams, Version 14.0 (2011). http://cxc.harvard.edu/proposer/POG/html/chap6.html • Gastaldello, F. et al. Status of the EPIC thin and medium filters on-board XMM-Newton after more than 10 years of operation: II - analysis of in-flight data. in Proceedings of the SPIE 8859, 885914 (2013). The full solution technology is based around lithographic support meshes that have a high transparency (> 90%) and thin Al films (50 nm). They are a new technology that has had minimal testing and so has a TRL of 3.
TRL	**SOTA**	5
	Solution	2–3

Performance Goals and Objectives	Optical blocking filter technology needs to be advanced along both categories of filters. Direclty deposited OBFs have, to date, consisted entirely of a thin film of Al deposited on the back surface of a Si sensor. There are complex trade-offs between optical blocking and X-ray transmission for other filter materials, but these have not been fully explored because of the chemical and electrical effects that metal deposition has on the back-surface of pixellated Si sensors. Investigation of direct deposition of thin films of Ti, W, and other materials onto Si sensors needs to be undertaken to truly optimize soft X-ray sensitivity and minimize optical contamination. Alternatively, free-standing filters that can be thin enough to compete with directly deposited filters (50 nm or thinner), with a structure that supports the filter film that is better than 90% transparent also need to be explored. This structure would have to be strong enough to survive launch vibrational loads and the thermal cycling environment that would be expected in a space mission. The filters would have to have a high X-ray transmission over the 150 eV to 2 keV energy range, while maintaining a good optical attenuation performance. The requirement would be > 40 % X-ray transmission above 200 eV and >10% X-ray transmission below 200 eV. The optical attenuation at a thickness of 50 nm should be 10-3. It would also be advantageous to have the ability to control the temperature of the filters so that any contamination that did build-up on them could be removed through heating.
Scientific, Engineering, and/ or Programmatic Benefits	The potential benefit of advanced filter technology is significantly greater effective area of the instrument, below 2 keV through high X-ray transmission. This will increase the potential scientific yield of the spacecraft. The signal-to-noise performance of the instrument can be optimized by limiting the amount of optical photons that would be able to reach the detectors without affecting target photon energy throughput. Contamination build-up can be controlled by free-standing filters as they can be thermally isolated from the detectors and so can act as a warm barriers between the cold detectors and the hydrocarbon contamination within the payload. Free standing filters allow multiple filter foil thicknesses to be included in an instrument on a filter wheel, optimizing filter characteristics for a particular observation.
PCOS Applications and Potential Relevant Missions	Advances in OBF technology will be applicable to any missions that use detectors on the focal plane that are sensitive to optical photons but that target photons in the EUV to soft X-ray bandpass (50 eV to 2 keV). This would include missions such as Lynx that has a large effective area optic and an imaging camera on the focal plane that would be silicon based. Effective optical blocking filters will allow the signal-to-noise of the detected photons to be maximized by attenuating optical photons, while maximizing effective area with highly X-ray transparent filters.
Time to Anticipated Need	Filter technologies for Lynx will have to be identified in the early 2020s. Filters will also be required in any future X-ray spectrograph, either for grating readouts, imaging readouts, or calorimeter filters. Many future mission concepts (observatory class and probes) will emphasize high-redshift science where maximinzing the instrument response below 0.5 keV will optimize the sensitivity

Gap Name		Long-wavelength-blocking filters for X-ray micro-calorimeters *Submitted by Lynx STDT*
Description		A new generation of filters is needed to block undesirable photons being incident on an X-ray microcalorimeter array that has greater transmission in the soft X-ray energy band of 0.2-1.0 keV. A stack of these filters, located at various temperatures, need to be able to block optical, UV and infra-red photons from being absorbed in the X-ray microcalorimeter array. They need to be optimized to be as thin as possible in order to optimize the transmission at low energies, allowing the increase in transmission by more than an order of magnitude at 0.2 keV. The use of optimized micro-machined meshes will allow the mechanical support and high throughput.
Current State-of-the-Art (SOTA)		Blocking filters of the general type have successfully flown on Hitomi, and thus the SOTA is designated TRL-9. For Lynx, higher transmission is desired for soft X-rays requiring thinner aluminum and polyimide, thinner than has so far been developed or demonstrated. The filters also need to be significantly larger (> 6 cm). Thus for the full solution, the TRL is listed at TRL-3, with the principle having been demonstrated experimentally. The waveguide cut-off filter option has been demonstrated for 15 micron holes, but not at small enough holes for this application (~1-2 microns).
TRL	**SOTA**	9
	Solution	3
Performance Goals and Objectives		Large area (> 6 cm) films supported by fine meshes, as thin as 10 nm of aluminum, and 20 nm of polyimide. Another approach is the use of wave-guide cut-off filters that have no films between a support mesh, with extremely tiny holes (~1-2 microns across).
Scientific, Engineering, and/or Programmatic Benefits		Having more than an order of magnitude transmission available for the softest X-ray makes more of the collecting area of the X-ray optic available for science. The X-ray optic would have a corresponding order of magnitude more area for some scientific measurements. Measurements include observations of highly redshifted sources such AGN and baryons from distant groups of galaxy clusters.
PCOS Applications and Potential Relevant Missions		Lynx. The technology is also synergistic with an enabling technology for the US contribution to Athena.
Time to Anticipated Need		Need to demonstrate credibility before the 2020 Decadal Survey, and would require TRL 6 by mission PDR anticipated in the mid-2020s.

Gap Name		High-efficiency, low cost cooling systems for temperatures near 100 mK *Submitted by General Community*
Description		Sensor arrays cooled to temperatures near 100 mK are needed for the Inflation Probe, Athena, and planned X-ray and Far-IR missions. Refrigerators to reach 100 mK are needed, especially refrigerators that are stable, continuous, low mass, have long lifetimes, and are low cost. The cost of reaching 100 mK is an impediment to small or mid-size missions that incorporate sensors requiring such low operating temperatures.
Current State-of-the-Art (SOTA)		The Planck satellite demonstrated continuous cooling to 0.1 K for 2.5 years but vented ^{3}He to space. Adiabatic demagnetization refrigerators on Suzaku and Hitomi operated successfully but were not continuous. Various technologies are under development in the laboratory that can provide 100 mK or useful launching temperatures for subsequent 100 mK coolers. These include continuous dilution refrigerators, continuous adiabatic demagnetization refrigerators, solid-state tunnel junction refrigerators, and continuous ^{3}He refrigerators. Hence, there are a wide range of TRLs.
TRL	**SOTA**	
	Solution	
Performance Goals and Objectives		Stable, continuous, and long lifetime 100 mK refrigerator technology. Cooling powers matched to the full range of future mission concepts. Cost reductions of 3-5x compared to 100 mK refrigerators demonstrated to date. Mass reductions of 2-3× compared to 100 mK refrigerators demonstrated to date.
Scientific, Engineering, and/or Programmatic Benefits		Enables improved sensor performance in a variety of passbands. Enables 100 mK sensors on small or mid-size missions. Extends mission lifetimes.
PCOS Applications and Potential Relevant Missions		Inflation Probe, X-ray Surveyor (Lynx), future FIR observatories, and international missions with similar science goals.
Time to Anticipated Need		**2020s.** **Named missions:** Athena, IP, Lynx, possibly OST **Development needed for 2020 Decadal:** Yes **Other drivers:** IP technology development is a NWNH priority that was recently revisited by the mid-Decadal review. International and Explorer implementations of the IP have proposed launch dates during the second half of the next decade.

Gap Name		Tileable, 2-D Proportional Counter Arrays *Submitted by General Community*
Description		High-energy photon polarization is the missing element to complete the full description of the most prominent astrophysical messenger. At gamma-ray energies, above 1 MeV, detection of photon polarization requires low density, large volume detectors, with high spatial resolution for three-dimensional tracking of the electron pair. The MPPC readout for a large volume TPC would allow the electrons from pair production to be accurately measured resulting in a mission with high polarization sensitivity and angular resolution. The ability to tile the MWD readout would make a SMEX-scale pathfinder gamma-ray polarization mission possible. Demonstration of the scientific value of gamma-ray polarization would lead the way for a wide range of high sensitivity gamma-ray polarization missions. The gaseous time projection chamber (TPC) provides the high spatial resolution 3-D track imaging required for gamma-ray polarimetry above 1 MeV (pair production regime). Large area, 2-D micro-pattern proportional counter (MPPC) arrays for the TPC readout plane (the third coordinate is derived from the relative time of arrival of the signals) are required with sufficient gain to detect avalanches produced by single ionization charges produced along the tracks of the electron-positron pair traversing the gas. The MPPC structure is envisioned as a micro-well-detector (MWD) with orthogonal strip electrodes separated by an insulating layer. Holes in the upper (cathode) electrode are concentric with cylindrical wells in the insulating layer exposing the orthogonal (anode) electrodes at the bottom of the well.
Current State-of-the-Art (SOTA)		The MWD SOTA is laser micro-machined flexible printed circuits fabricated with polyimide insulator. Functional MWDs have been fabricated with areas up to 30 x 30 cm^2 area. These MWDs are tileable into square meter size areas, but their long-term lifetime is reduced by charge migration in the polyimide at the walls of the wells resulting in breakdown.
TRL	**SOTA**	5–6
	Solution	3
Performance Goals and Objectives		MWDs fabricated using photolithographic techniques (e.g. photosensitive glass) to pattern the electrodes and well structure of the MWD. The goal is to fabricate MWDs with active area at least 85 x 85 mm^2 with 50-100 µm diameter wells on a center-to-center pitch of twice the well diameter. The aspect ratio of wells for ideal performance is ~1:1, thus the insulating layer is 50-100 um thick. The strip electrodes are 100–200um wide with wire bond pads on both ends. Dead space around the edge of the MWD would be less than 1mm.
Scientific, Engineering, and/or Programmatic Benefits		This technology would enable large-volume, low-density, high-spatial-resolution TPC to be fabricated enabling a sensitive gamma-ray pair polarimetry mission.
PCOS Applications and Potential Relevant Missions		The Advance Energetic Pair Telescope (AdEPT) is currently being developed with APRA and IRAD support. The AdEPT concept will provide the complete picture of the gamma-ray universe, including photon time of arrival, direction, energy, and polarization.
Time to Anticipated Need		**Named missions:** **Development needed for 2020 Decadal:** No **Other drivers:** Flight mission estimated no earlier than 2022 an AdEPT Pathfinder. A full balloon flight prototype in 2019.

Appendix B
Program Technology Development Quad Charts

Gravitational Waves

Jordan Camp – "Demonstration of a TRL-5 Laser System for eLISA" 65

William Klipstein – "Gravitational-Wave-Mission Phasemeter Technology Development" . . . 66

Jeffrey Livas – "Telescopes for Space-Based Gravitational-Wave Observatories". 67

X Rays

Mark Bautz – "Directly Deposited Optical-Blocking Filters for Imaging X-ray Detectors". . . . 68

David Burrows – "Fast Event Recognition for the Athena Wide-Field Imager". 69

Caroline Kilbourne – "Providing Enabling and Enhancing Technologies for a Demonstration Model of the Athena X-IFU" 70

Randall McEntaffer – "Reflection Grating Modules: Alignment and Testing" 71

Paul Reid – "Development of 0.5-Arcsecond Adjustable Grazing-Incidence X-ray Mirrors for the SMART-X Mission Concept" 72

Mark Schattenburg – "Development of a Critical-Angle Transmission Grating Spectrometer" . . 73

Joel Ullom – "Technology Development for an AC-Multiplexed Calorimeter for Athena" 74

William Zhang – "Next-Generation X-ray Optics: High Angular Resolution, High Throughput, and Low Cost" 75

Cosmic Microwave Background

James J. Bock – "Planar Antenna-Coupled Superconducting Detectors for CMB Polarimetry" 76

Edward Wollack – "High-Efficiency Feedhorn-Coupled TES-based Detectors for Cosmic Microwave Background Polarization Measurements". 77

Demonstration of a TRL-5 Laser System for eLISA

PI: Jordan Camp / GSFC

Objectives and Key Challenges:

- Develop 2.5-W light source for the LISA gravitational wave (GW) mission using a Master Oscillator Power Amplifier (MOPA) design with a novel diode laser oscillator (External Cavity Laser, ECL) followed by a 2.5W Ytterbium fiber amplifier, providing a highly stable, compact, and reliable system
- Test the laser system for reliability, and for amplitude and frequency stability, achieving the required noise performance
- Demonstrate system TRL 5
- Development, with industrial partner (Redfern Integrated Optics, RIO) space qualified, ultra low-noise oscillator
- Demonstrate low-noise power amplifier with servo controls
- Noise and reliability tests of full laser system

Significance of Work:

- Required for LISA or any similar GW mission

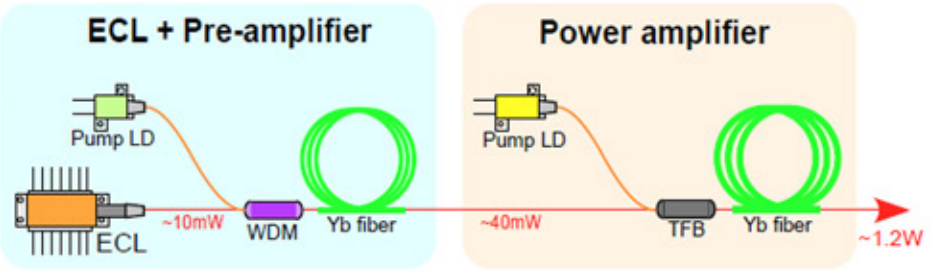

MOPA configuration of LISA laser, including ECL, preamp, and diode-pumped Ytterbium fiber amplifier

Approach:

- Noise optimization of 1064-nm ECL (RIO)
- Reliability study of ECL
- Implementation of amplitude and frequency servo controls on full laser system, achieving:
  - Relative Intensity Noise (RIN) = 10^{-4} at 10^{-3} Hz;
  - Frequency noise = 300 Hz / $Hz^{1/2}$ at 10^{-2} Hz; and
  - Differential phase noise = 6×10^{-4} rad/$Hz^{1/2}$ at 10^{-2} Hz

Key Collaborators:

- Kenj Numata, Mike Krainak (NASA/GSFC)
- Lew Stolpner (RIO)

Development Period:

April 2014 – Oct 2016

Accomplishments:

- ✓ Rebuilt and tested 2.5-W laser amplifier
- ✓ Conducted preliminary laser system test with NPRO
- ✓ Conducted preliminary laser system test with ECL
- ✓ Conducted ECL reliability tests
- ✓ Conducted preamplifier reliability testing
- ✓ Conducted full laser system noise testing

Next Milestones:

- Noise optimization of ECL (Oct 2018)
- Demonstration of NPRO oscillator (Oct 2018)
- Laser system lifetime testing (Oct 2019)

Applications:

- Laser source for LISA GW mission
- Oscillator for ground-based GW LIGO project
- Oscillator for GRACE-II mission

$TRL_{In} = 3$ $TRL_{Current} = 3$ $TRL_{Target} = 5$

Gravitational-Wave-Mission Phasemeter Technology Development

PI: William Klipstein / JPL

Objectives and Key Challenges:

- Advance our phase-measurement system from TRL 4 to 5 through significant system-level hardware fidelity increase and greater fidelity of signal test environment by adding low light levels
- Mature the TRL of phase readout with high strain sensitivity through micro-cycle/√Hz precision on a 4-16 MHz beat-note in the presence of laser frequency noise and local clock noise, already demonstrated in a lab test bed
- Develop demonstration unit with large number of channels for infusion into L3-LISA

Significance of Work:

- High-performance phase readout is an enabling technology for multi-spacecraft laser-interferometer-based missions such as LISA-like gravitational-wave missions

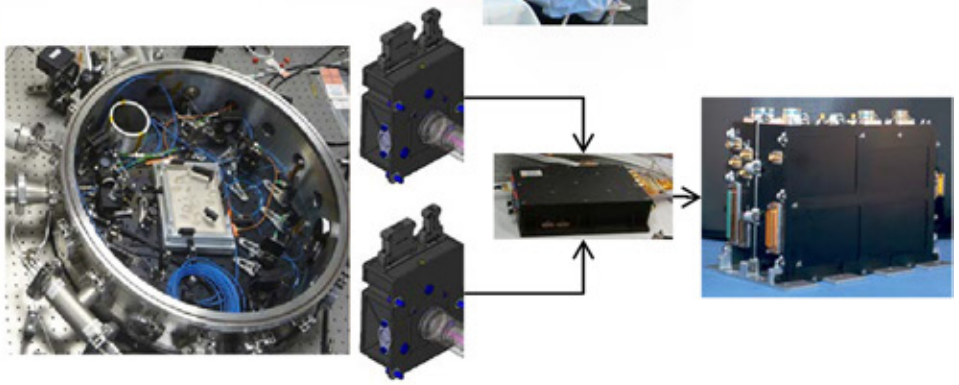

EM Hardware (QPD Photoreceivers, Pre-Amp, and Phasemeter) infused into the LISA Testbed

Approach:

- Advance component technologies
  - Infuse compatible EM hardware from GRACE Follow-On Laser-Ranging Interferometer (LRI)
  - Demonstrate wavefront sensing with quadrant photoreceivers
- System-level testing
  - Modify interferometer test bed to include low-light signals
  - Replace COTS components in interferometer test bed with LRI EM hardware and demonstrate performance

Key Collaborators:

- Jeff Dickson, Brent Ware, Bob Spero, Dmitry Strekalov, Kirk McKenzie, Brian Bachman-Okihiro, Jehhal Liu, and Chris Woodruff (JPL)

Current Funded Period of Performance:

Apr 2014 – Sep 2018 (SAT plus directed funding)

Recent Accomplishments:

- ✓ Demonstrated wavefront sensing
- ✓ Migrate additional photoreceiver algorithms from LabView phasemeter to EM from GRACE-FO
- ✓ Established infusion plan into L3-LISA with German partners
- ✓ Initiated TRL 6 phasemeter core demonstration path

Next Milestones:

- Initiate contract for TRL-6 daughter card development to implement large number of channels for L3-LISA (Oct 2017)
- Encode carrier-assisted tracking for low-visibility demonstration (Nov 2017)
- Demonstrate tracking of low-visibility signals with EM Phasemeter (May 2018)
- Incorporate EM photoreceivers and signal chain into test bed (Jul 2018)
- Demonstrate test bed performance at TRL 5 or better (Sep 2018)

Applications:

- Inter-spacecraft laser interferometry and pm-precision interferometer readout electronics for future missions, e.g., LISA
- Other interferometry concepts (e.g., planet searches)

Telescopes for Space-Based Gravitational-Wave Observatories

PI: Jeffrey Livas / GSFC

Objectives and Key Challenges:

- Design, fabricate, and test a lightweight LISA telescope design in a flight-like environment and demonstrate the ability to satisfy mission requirements for low scattered light and high dimensional stability in time for selection for the LISA L3 Mission Opportunity
  - Key Challenge 1: dimensional stability
  - Key Challenge 2: stray-light performance

Significance of Work:

- First demonstration of a validated scattered-light model combined with a previous demonstration of dimensional stability will provide a firm basis for a realistic engineering model design for a flight-qualifiable telescope
- Potential technology contribution to ESA L3 Cosmic Visions

Section View of Telescope Design

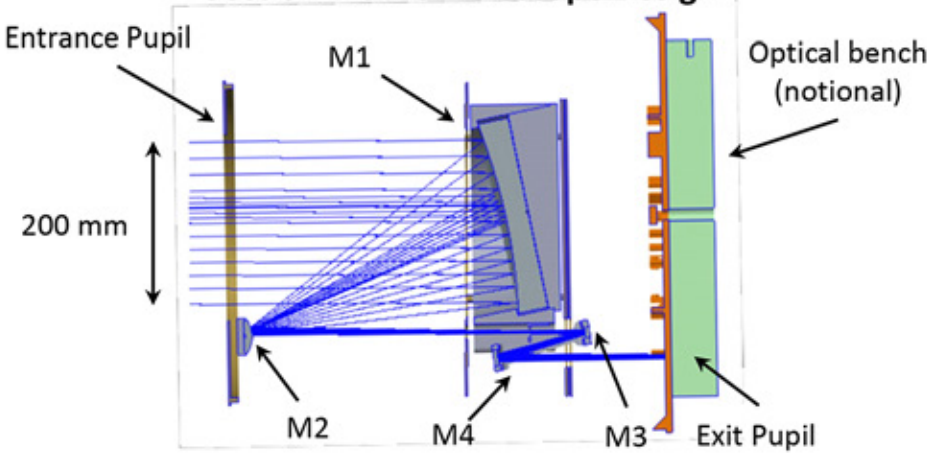

Approach:

- Use requirements developed for existing telescope
- Modify based on experience
- Merge a high-thermal-conductivity material in a simple symmetric mechanical configuration with a low-scatter optical design
- Fabricate and test for compliance with specifications

Key Collaborators:

- J. Howard, G. West, P. Blake, L. Seals, J. Ward , S. Sankar (NASA/GSFC)
- Prof. Guido Mueller (University of Florida)

Currently Funded Period of Performance:

Oct 2015 – Sep 2017

Recent Accomplishments:

- ✓ LISA Proposal submitted to ESA L3 AO
- ✓ LISA Proposal selected by SPC
- ✓ Transition to a directed funding program

Key Milestones:

- Award contract for telescope fabrication (Jul 2018)
- Telescope delivery; start stability testing (Dec 2020)
- Start T-VAC and performance testing (Jul 2021)
- Deliver EM to ESA (Jul 2022)

Applications:

- Flagship GW missions (e.g., LISA)
- Laser ranging and/or communications
- Precision metrology applications

$TRL_{In} = 3+\ TRL_{PI\text{-}Asserted} = 3+\ TRL_{Target} = 5/6\ (ISO)$

Directly Deposited Optical-Blocking Filters for Imaging X-ray Detectors

PI: Mark Bautz / MIT Kavli Institute

Objective and Key Challenges:

- Silicon imaging X-ray detectors require thin filters (< 300 nm) to block noise/background from UV and optical light
- State-of-the-art, free-standing filters use fragile, thin substrates
- Objective: deposit blocking filter directly on CCD X-ray detector, eliminating substrate
- Challenges:
  - — Deposit filter directly without compromising CCD performance
  - — Deposit sufficiently thin, uniform filters

Significance of Work:

- Filter deposited on detector requires no fragile substrate
- Allows cheaper, more robust sensors (no vacuum housing!)
- Improves crucial soft-X-ray QE and enables larger focal planes

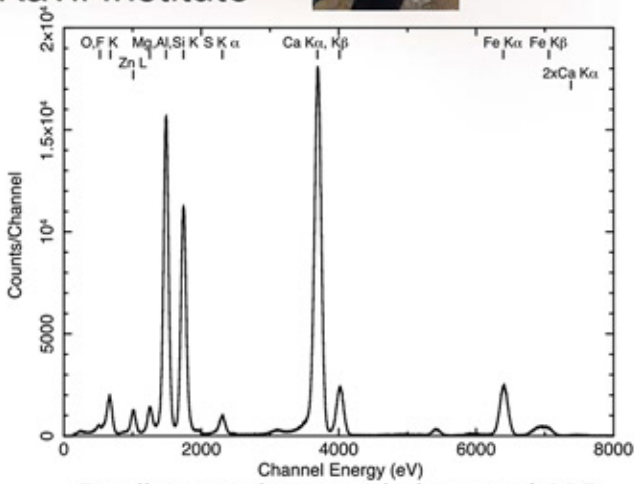

Excellent resolution with deposited OBF

Approach:

- Exploit existing stocks of (engineering grade/flight spare) X-ray CCD detectors at MIT Lincoln Laboratory
- Screen, thin, passivate, package, and apply filters to detectors
- Filter is Al with AlO_2 cap
- Start thick (220-nm Al), get progressively thinner
- Use existing MIT facilities for X-ray characterization
- Use existing and upgraded facilities for optical characterization

Key Collaborators:

- Bautz, Kissel et al. (MIT Kavli Institute)
- Suntharalingam, Ryu, Burke, and O'Brien (MIT Lincoln Laboratory)
- Masterson, Chodas, and Megerssa (MIT Dept. of Aero. and Astro.)

Current Funded Period of Performance:

Jul 2012 – Jun 2018

Recent Accomplishments:

- ✓ Reduced pinhole fraction to < 1% (OD < 7) for 220-nm OBF
- ✓ Tested devices with 70-nm and 100-nm-thick Al OBF; optical blocking as expected
- ✓ With REXIS, developed and qualified underside coating as effective countermeasure for near-IR leakage through package
- ✓ Supported environmental tests of REXIS flight CCDs/OBFs through launch
- ✓ Students developed, presented, and secured approval for TRL-6 demo plan from PCOS; test facilities completed

Next Milestone:

- Execute TRL 6 demo, surpassing project goals (2017/18 academic year)

Applications:

Every X-ray imaging or grating spectroscopy mission

- Explorers (Arcus, STAR-X, TAO-ISS, etc.)
- Probes (TAP, AXIS, etc.)
- Flagship (Athena, Lynx)

Fast Event Recognition for the Athena Wide-Field Imager

PI: David Burrows / PSU

Objectives and Key Challenges:

- High-speed event recognition and data compression

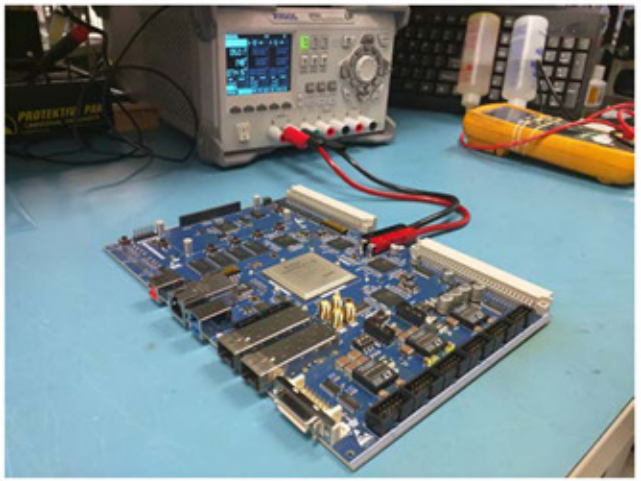

Lab testing using the PSU ERP prototype board

Significance of Work:

- Required for several proposed X-ray imagers, including Athena WFI (ESA L2), Arcus (MIDEX), Lynx/X-ray Surveyor

Approach:

- FPGA coding/simulation/testing
- Develop prototype board
- Test with fixed patterns up to 1GBps
- Test with real X-ray data up to 1GBps

Key Collaborators:

- Dr. Karl Reichard, Eli Hughes (PSU/ARL)
- Dr. Abe Falcone, Dr. Tyler Anderson (PSU/ECOS)
- Dr. Mark Bautz (MIT)
- Dr. Ralph Kraft (SAO)

Current Funded Period of Performance:

Jan 2015 – Dec 2016 (with no-cost extension to Dec 2017)

Recent Accomplishments:

- ✓ Completed development/testing of line processor
- ✓ Completed build of prototype board (photo above)
- ✓ Developed data ingest code

Next Milestones:

- Complete and test FPGA code (Jun 2017)
- TRL Review (Aug 2017)

Application:

- Athena WFI (ESA L2), Arcus (MIDEX), Lynx/X-ray Surveyor, etc.

$TRL_{In} = 3$ $TRL_{Current} = 3$ $TRL_{Target} = 4/5$

Providing Enabling and Enhancing Technologies for a Demonstration Model of the Athena X-IFU

PI: Caroline Kilbourne / GSFC

Objectives and Key Challenges:

- Develop large-format arrays of X-ray microcalorimeters and their readout for ESA's Athena X-IFU
- Support European-led primary technology demonstrations using GSFC arrays read out with frequency domain multiplexing (FDM)
- Advance TRL of time/code-division multiplexer (TDM/CDM) to maintain a viable backup readout scheme

Significance of Work:

- This solid demonstration of core technologies coupled with demonstrations of targeted enhancements will enable the best possible instrument for Athena
- This development has enabled NASA participation in the Athena mission

252-pixel TDM/CDM test package

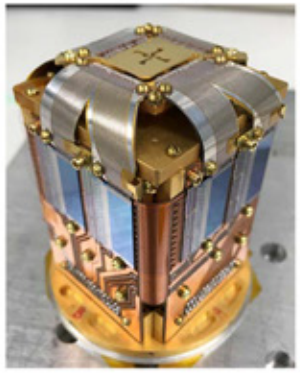

Combined spectrum for 143 pixels in a 6-column × 32-rowTDM measurement with 2.747 ±0.010 eV FWHM resolution

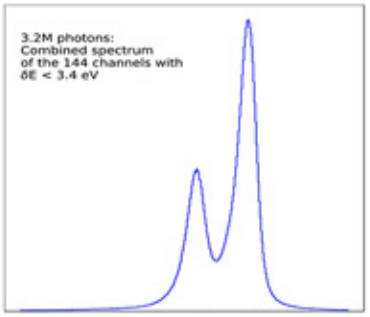

Reaching multiplexer speed and noise goals enabled breakthrough 6-column × 32-row TDM readout demonstration using Athena-like pixels

Approach:

- Develop large-scale testing infrastructure for Athena technology demonstrations and kilo-pixel array characterization
- Optimize SQUID TDM/CDM components and electronics
- Integrate full-Athena-scale TES arrays (Mo/Au TES with Au/Bi absorbers) with optimized multiplexed readout
- Provide arrays for European-led technology demonstrations using FDM
- Develop fabrication techniques for mission-enhancing 'hybrid' arrays

Key Collaborators:

- J. Adams, S. Bandler, R. Kelley, R.S. Porter, S. Smith, J. Chervenak (GSFC)
- J. Ullom, W. B. Doriese, C. Reintsema (NIST)
- K. Irwin (Stanford U.)

Current Funded Period of Performance:

September 2015 – October 2017

Recent Accomplishments:

- ✓ Provided first uniform 32×32 array to SRON for FDM testing
- ✓ Multiplexed 32 rows in single column with an average resolution at 6 keV of 2.55±0.01 eV using TDM and 2.77±0.02 eV using CDM
- ✓ Multiplexed 163 Athena-like pixels in a 6-column × 32-row TDM configuration with a median resolution of 2.75 eV

Next Milestone:

- Provide a uniform 32×32 array for Athena demonstration model (DM) with pixels optimized for new Athena baseline parameters (Dec 2017)

Applications:

- Contribution to the X-ray Integral Field Unit instrument on ESA's Athena mission
- Other potential missions needing high-resolution imaging X-ray spectroscopy

$TRL_{In} = 4$ $TRL_{PI\text{-}Asserted} = 4+$ $TRL_{Target} = 5$

Reflection Grating Modules: Alignment and Testing

PI: Randall L McEntaffer / PSU

Objectives and Key Challenges:

- Implement an alignment methodology specific to off-plane reflection gratings
- Populate a module with aligned gratings achieving spectral resolution > 3000 (λ/δλ) with high throughput over the 0.2-2.0-keV band
- Advance the OP-XGS technology to TRL 5

Significance of Work:

- Enables high throughput and high spectral resolving power below 2 keV, where the majority of X-ray spectral features reside
- This will be the first time that multiple off-plane gratings have been aligned at this tolerance level with associated performance testing

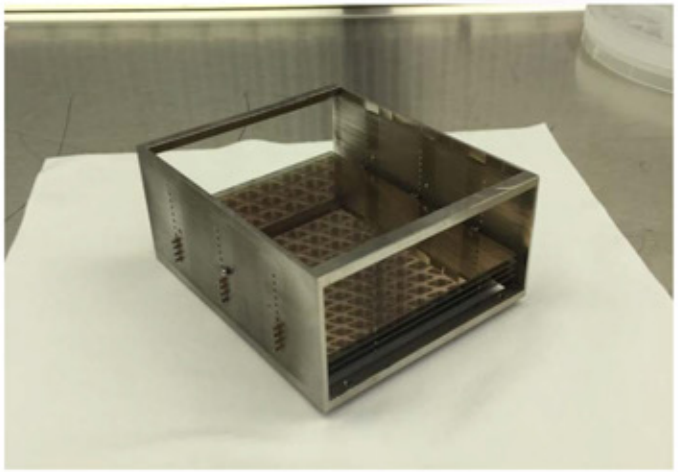

An Invar grating module with four aligned, large-format gratings

Approach:

- Quantify alignment tolerances
- Formulate alignment methodology
- Implement alignment methodology
- Performance- and environmental-test an aligned module
- Evaluate process and repeat in Year 2

Key Collaborators:

- Will Zhang (NASA/GSFC)
- Jessica Gaskin (NASA/MSFC)

Current Funded Period of Performance:

Jan 2015 – Dec 2016

Accomplishments:

- ✓ Quantified alignment tolerances for suborbital and Explorer spacecraft
- ✓ Initial alignment methodology and grating module were designed, constructed, and implemented
- ✓ Aligned and tested four gratings with slumped-glass optics at MSFC SLF
- ✓ Used results to design upgrades to alignment system
- ✓ Environmentally tested aligned module

Applications:

- Lynx
- Explorer class missions
- Suborbital rocket investigations

$TRL_{In} = 3$ $TRL_{Out} = 4$ ***(TMB vetted)***

Development of 0.5-Arcsecond Adjustable Grazing-Incidence X-ray Mirrors for the SMART-X Mission Concept

PI: Paul Reid / SAO

Objectives and Key Challenges:

- Develop an alignment and mounting scheme consistent with a large-area, high-resolution X-ray telescope (> 2m^2 and 0.5" HPD) that accommodates many (~100) closely packed mirror segments; align to 0.25" = Chandra alignment (mounting distortions < 1 µm P/V, correctable with adjusters)
- Approach must allow calibration of mirror surface figure as each segment is mounted, so that figure can be corrected before next segment is aligned
- Incorporate developments in high-connection-density flexible cabling and row-column addressing to minimize and simplify electrical connections for mirror-adjuster command and control

Significance of Work:

- Enables adjustable optics to correct mounting induced distortion and on-orbit thermal changes with LCD display electrical simplicity

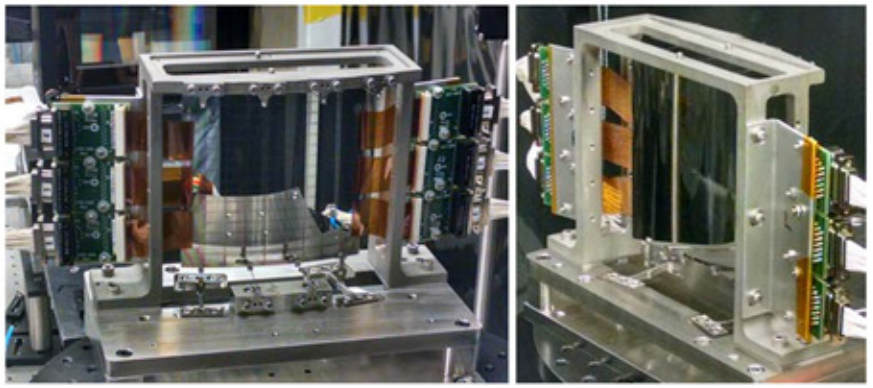

Single-shell mounting concept with a mounted adjustable mirror and ACF electrical connections to the mirror.

Approach:

- Investigate Anisotropic Conductive Films for high connection density (up to 100 contacts/mm)
- Develop ZnO thin film transistor over-layer with insulating top layer for row-column addressing and ease of electrical contact routing
- Through structural and thermal analysis and design, incorporate and extend alignment and mounting approach being developed for APRA TRL-4 X-ray test.

Key Collaborators:

- Susan Trolier-McKinstry, Tom Jackson, Julian Walker, Tianning Liu, Mohit Tendulkar (PSU)
- Brian Ramsey and Steve O'Dell (MSFC)

Current Funded Period of Performance:

Apr 2015 – Sep 2017

Recent Accomplishments:

- ✓ Demonstrated anisotropic conductive film connections (3/mm) on cylindrical test mirror.
- ✓ Mounted mirror with differential figure measurement at each mounting step

Next Milestones:

- High-fidelity deterministic figure control test 3 (Jul 2017)
- Measurement of correctibility as a function of frequency (Aug 2017)
- Single-mounted corrected mirror X-ray test (Mar 2018; (to be completed with internal SAO funding)

Application:

- Lynx (formerly SMART-X, then X-Ray Surveyor) mission concept

$TRL_{In} = 3$ $TRL_{PI\text{-}Asserted} = 3$ $TRL_{Target} = 4+$

Development of a Critical-Angle Transmission Grating Spectrometer

PI: Mark Schattenburg / MIT Kavli Institute

Objectives and Key Challenges:

- Develop key technology to enable a Critical-Angle X-ray Transmission Grating Spectrometer (CATXGS), advancing to TRL 6 in preparation for proposed mid- and large-size missions over the next decade
- Develop improved grating fabrication processes
- Develop frame mounting, alignment, and assembly techniques for CAT grating arrays

Significance of Work:

- Improved diffraction efficiency and resolving power for CATGS
- Ability to manufacture large-area, light-weight grating arrays

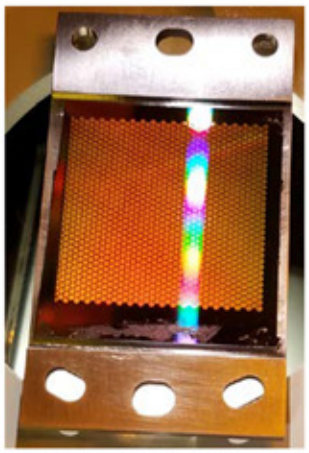

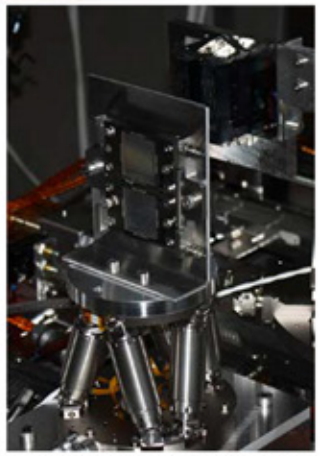

Left: Large frame-mounted grating. Right: Two pre-aligned gratings under simultaneous illumination by a single optic at the Panter X-ray facility

Approach:

- Integrated wafer front/back-side fabrication process using silicon-on-insulator (SOI) wafers
- Wafer front side: CAT grating and Level 1 support structure
- Wafer back side: Level 2 support mesh structure
- CAT grating fabricated by deep reactive-ion etching (DRIE) followed by KOH polishing
- Bonded to expansion-matched metal support frame (Level 3)
- X-ray tests of prototypes at synchrotron and MSFC/Panter facilities
- Environmental tests to advance TRL

Key Collaborators:

- William Zhang (GSFC)
- Steve O'Dell (MSFC)

Current Funded Period of Performance:

CY17-CY18

Recent Accomplishments:

- ✓ Successfully performed environmental tests on individual frame-mounted gratings with pre- and post-X-ray verification of efficiency and resolving power.
- ✓ Tripled grating size to > 30 mm × 30 mm; fabricated six samples.
- ✓ Developed improved laser-based alignment technique.
- ✓ Verified alignment with large grating pair using X rays.

Next Milestones:

- Demonstrate X-ray performance of aligned gratings with prototype frame assembly after environmental tests to achieve TRL 5 (fall 2018)

Applications:

- Flagship and Explorer X-ray missions
- Laboratory X-ray analysis (materials science, energy research)

*TRL in = **3*** *TRL current = **4*** *TRL target = **6***

Technology Development for an AC-Multiplexed Calorimeter for Athena

PI: Joel Ullom / NIST

Objectives and Key Challenges:

- Increase TRL of AC-biased Transition-Edge Sensor (TES) X-ray microcalorimeters from 3 to 4
- To achieve this, demonstrate that AC-biased TESs can meet the anticipated performance requirements of ESA's Athena mission, in particular, that AC-biased TESs can routinely achieve energy resolutions of 2.5 eV or better at 6 keV
- The key challenge is that, so far, TESs under AC bias do not have as good energy resolution as under DC bias

Significance of Work:

- AC-biased TESs and Frequency Division Multiplexing (FDM) are the baseline readout architecture for Athena; the performance of this approach strongly impacts mission design and success

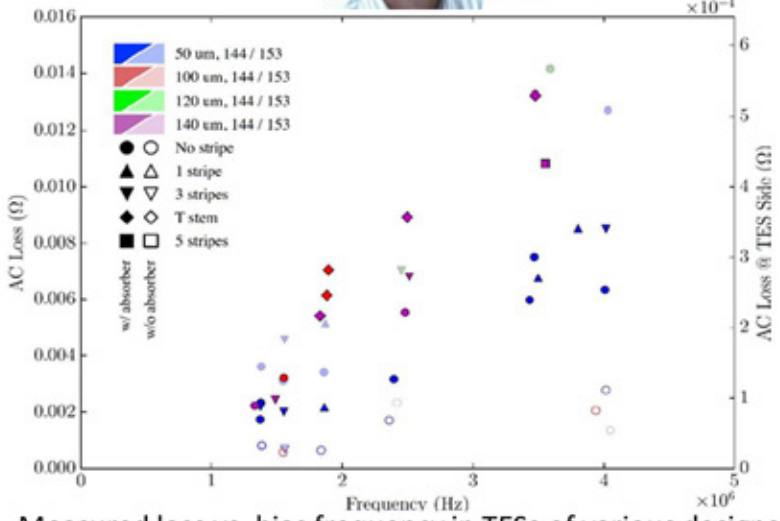

Measured loss vs. bias frequency in TESs of various designs

Approach:

- Study the behavior of single GSFC TESs under AC bias
- In one experiment, maximize the use of readout components from the European Athena team
- In a second experiment, separate the effects of the readout system from the TES by using a novel, open-loop readout architecture based on microwave SQUID amplifiers
- Study interactions among small numbers of AC-biased TES devices

Key Collaborators:

- Caroline Kilbourne, Simon Bandler, and Richard Kelley (GSFC)
- Kent Irwin (Stanford University)

Current Funded Period of Performance:

Oct 2015 – Sep 2017

Recent Accomplishments:

- ✓ Microwave SQUIDs demonstrated with 30-MHz input bandwidth suitable for AC-biased TESs
- ✓ Large number of TES designs measured under AC bias to understand how design affects AC losses

Next Milestones:

- Expand measurements of AC loss and compare to calculations based on classical theory of electricity and magnetism (Sep 2017)
- Measure response to X rays of AC-biased TESs using 30-MHz microwave SQUIDs (Sep 2017)

Applications:

- Athena and future X-ray missions based on TES microcalorimeters

$TRL_{In} = 3$ $TRL_{Current} = 3$ $TRL_{Target} = 4$

Next-Generation X-ray Optics: High Angular Resolution, High Throughput, and Low Cost

PI: William W. Zhang / GSFC

Objectives and Key Challenges:

- Develop an X-ray mirror technology that achieves better than Chandra's 0.5" Half-Power Diameter (HPD) angular resolution, while reducing mass and production cost by at least an order of magnitude on a per unit effective area basis.

Significance of Work:

- Enables major X-ray observatories such as ESA's Athena and NASA's Lynx
- Enables Probe missions such as NASA's AXIS, TAP, HEX-P and JAXA's FORCE
- Enables Explorer missions such as STAR-X and PolSTAR

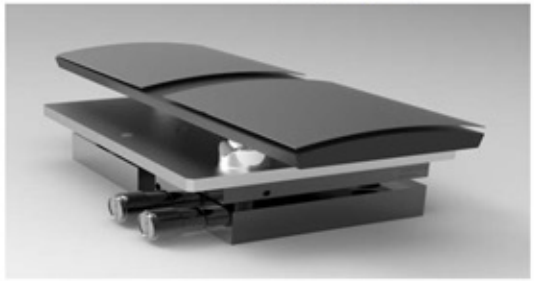

Technology Development Module (TDM) containing one pair of parabolic-hyperbolic mirror segments

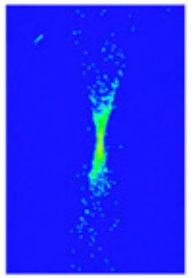

X-ray image with 4.5 -arcsec HPD

Approach:

- Precision-polish mono-crystalline silicon to fabricate lightweight mirror substrates
- Develop a coating process to maximize X-ray reflectance without introducing figure distortion
- Develop an alignment process to locate and orient mirror segments to optimize their image
- Develop attachment process to bond mirror segments without introducing alignment and/or figure errors

Key Collaborators:

- Kim Allgood, Michael Biskach, Kai-Wing Chan, Michal Hlinka, John Kearney, James Mazzarella, Ryan McClelland, Ai Numata, Raul Riveros, Timo Saha, and Peter Solly

Current Funded Period of Performance:

Oct 2016 – Sep 2018

Recent Accomplishments:

- ✓ Fabricated mono-crystalline silicon mirror substrates that are comparable to or better than Chandra's mirrors in figure quality
- ✓ Validated the meta-shell alignment and bonding approach by aligning, bonding, and X-ray testing a pair of silicon mirrors.

Next Milestones:

- Continue to refine mirror fabrication process to improve figure and roughness quality as well as to reduce production cost and time (Dec 2018)
- Refine mirror alignment bonding process to fully realize mirror segment potential of 0.2-arcsec HPD (Dec 2020)

Applications:

- Flagship and probe-class X-ray missions
- Explorer-type X-ray missions
- Medical research and diagnosis

$TRL_{In} = 3$ $TRL_{PI\text{-}Asserted} = 4$ $TRL_{Target} = 5$

Planar Antenna-Coupled Superconducting Detectors for CMB Polarimetry

PI: James Bock / JPL, Caltech

Objectives and Key Challenges:

Advance antenna-coupled superconducting detector technologies for space requirements:

- RF propagation properties
- Beam control and polarized matching
- Extended-frequency antennas
- Detector stability and cosmic-ray response
- Readout-noise stability
- Large-format, modular focal-plane units

Significance of Work:

- Antenna designs for bands required by the Inflation Probe
- Detector sensitivity, stability, and minimized particle susceptibility appropriate for space-borne observations

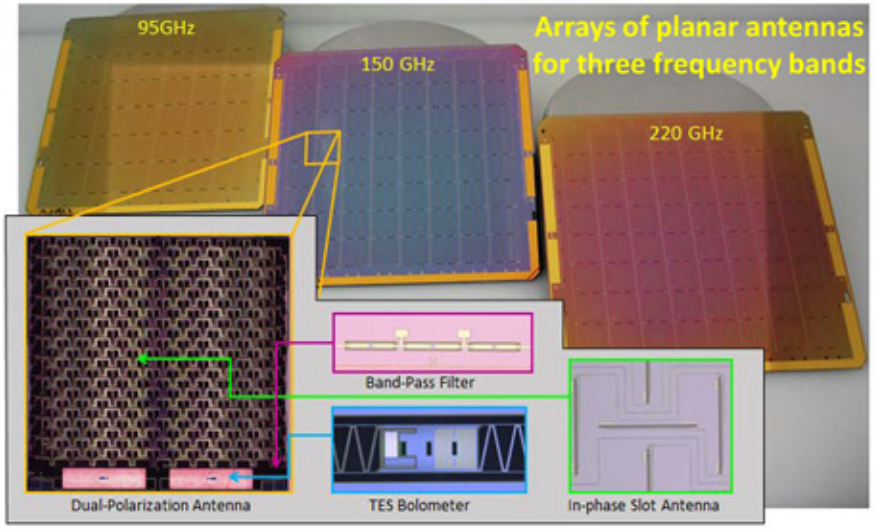

Approach:

- Planar antennas for entirely lithographed fabrication with no coupling optics
- Detectors provide photon-limited sensitivities in space
- Antennas provide excellent polarization and beam-matching properties
- Modular focal-plane unit for large focal-plane arrays

Key Collaborators:

- Koko Megerian, Hien Nguyen, Roger O'Brient, Anthony Turner, and Alexis Weber (JPL)
- Jon Hunacek, Howard Hui, Sinan Kefeli, and Bryan Steinbach (Caltech)
- Jeff Filippini (UIUC)

Current Funded Period of Performance:

Jan 2016 – Dec 2017

Recent Accomplishments:

- ✓ Wideband antennas tested
- ✓ 270-GHz science-capable Focal Plane Unit fielded
- ✓ Completed 150-mm diameter module design with dense Si board
- ✓ Radio Frequency Interference (RFI) mitigation filter tested at room temperature

Next Milestones:

- Test 150-mm diameter full-device wafer (Aug 2017)
- Fabricate prototype 150-mm diameter module (Nov 2017)
- Test loss from 300 to 600 GHz (Dec 2017)

Applications:

- NASA Inflation Probe mission
- Explorer and international CMB missions
- Technology commonalities with Far-IR and X-Ray missions

$TRL_{In} = 3\text{-}5$ $TRL_{PI\text{-}Asserted} = 3\text{-}6$ $TRL_{Target} = 4\text{-}6$

High-Efficiency Feedhorn-Coupled TES-based Detectors for CMB Polarization Measurements

PI: Edward J. Wollack / GSFC

Objectives and Key Challenges:

- Development of focal planes for characterization of CMB polarization with the following detector properties:
  - Background-limited millimeter-wave polarimetric sensor with high coupling efficiency and systematic error control
  - Inherently broadband design, scalable to large-format arrays over multiple frequencies of astrophysical interest

Significance of Work:

- Sub-orbital and space-borne operation of detectors, including:
  - Improved rejection of stray light by detector architecture
  - Improved broadband performance and coupling efficiency
  - Mitigation of space environmental concerns (surface/deep dielectric charging and cosmic rays)
  - Extend architecture to multiple frequencies

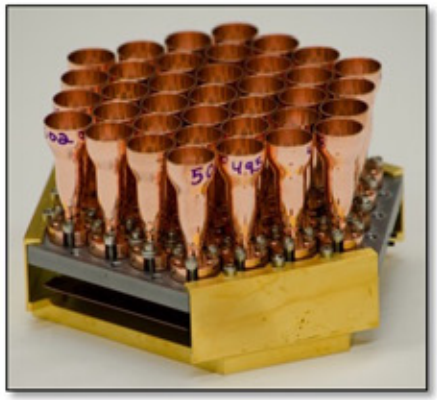

90-GHz Sensor Module

Detector Wafer

Approach:

- Multiple fabrication runs to integrate the new technologies into the detector architectures. Specifically, improved:
  - Stray-light mitigation and package thermalization
  - Implementation of air-bridge crossovers and ground-plane contacts for large-bandwidth/low-loss signal routing at higher frequencies

Key Collaborators:

- K. Denis, K. U-Yen, B. Bulcha, and S.H. Moseley (GSFC)
- K. Rostem (GSFC/JHU)
- D. Chuss (Villanova)
- T. Marriage and C. Bennett (JHU)

Current Funded Period of Performance:

Jan 2016 – Dec 2017

Recent Accomplishments:

- ✓ Air-bridge design and fabrication development
- ✓ Device bilayer development and validation
- ✓ CE7 package heat sink / plating validation

Next Milestones:

- Device run #2 testing (July 2017)
- Test facility commissioning (August 2017)
- High-frequency package validation (August 2017)

Application:

- CMB Polarimetry, suborbital

$TRL_{In} = 3\text{-}4$ $TRL_{PI\text{-}Asserted} = 3\text{-}5$ $TRL_{Target} = 4\text{-}6$

Appendix C
Program Technology Development Status

Gravitational Waves

Jordan Camp – "Demonstration of a TRL-5 Laser System for eLISA" 79

William Klipstein – "Gravitational-Wave-Mission Phasemeter Technology Development" . . . 89

Jeffrey Livas – "Telescopes for Space-Based Gravitational-Wave Observatories". 95

X Rays

Mark Bautz – "Directly Deposited Optical-Blocking Filters for Imaging X-ray Detectors". . . 106

David Burrows – "Fast Event Recognition for the Athena Wide-Field Imager". 121

Caroline Kilbourne – "Providing Enabling and Enhancing Technologies for a Demonstration Model of the Athena X-IFU" 126

Randall McEntaffer – "Reflection Grating Modules: Alignment and Testing" 136

Paul Reid – "Development of 0.5-Arcsecond Adjustable Grazing-Incidence X-ray Mirrors for the SMART-X Mission Concept" 145

Mark Schattenburg – "Development of a Critical-Angle Transmission Grating Spectrometer". . 157

Joel Ullom – "Technology Development for an AC-Multiplexed Calorimeter for Athena" . . . 165

William Zhang – "Next-Generation X-ray Optics: High Angular Resolution, High Throughput, and Low Cost" 174

Cosmic Microwave Background

James J. Bock – "Planar Antenna-Coupled Superconducting Detectors for CMB Polarimetry". . 181

Edward Wollack – "High-Efficiency Feedhorn-Coupled TES-based Detectors for Cosmic Microwave Background Polarization Measurements". 191

Abstracts of SAT Projects Starting in 2018

Mark Bautz – "High-Speed, Low-Noise, Radiation-Tolerant CCD Image Sensors for Strategic High-Energy Astrophysics Missions" 197

James J. Bock – "Superconducting Antenna-Coupled Detectors for CMB Polarimetry with the Inflation Probe" 198

Demonstration of a TRL-5 Laser System for eLISA

Prepared by: Jordan Camp (NASA/GSFC)

Summary

The gravitational-wave (GW) space mission Laser Interferometer Space Antenna (LISA) [1] was chosen for the European Space Agency (ESA) L3 GW astronomy opportunity, and NASA intends to contribute instruments to the mission. LISA's eventual flight will open a spectacular new window on the universe, using GWs to reveal the physics and astronomy associated with the merger of massive black hole systems. The backbone of LISA is a highly stable laser of ~2 W power, which enables the picometer interferometry necessary to record the passage of a GW; such a laser is listed as a top priority of the Physics of the Cosmos (PCOS) Program Analysis Group (PhysPAG) technology roadmap. LISA is now under technology development in Europe, and the Europeans have expressed interest in the laser system as a possible contribution from the US. To enable this contribution, we will provide the results described here to enable a Technology-Readiness-Level (TRL) 5 demonstration of the full LISA laser system by September 2019, allowing maximum flexibility for mission implementation. The laser system includes a state-of-the-art master-oscillator power-amplifier approach. The oscillator is a compact, low-mass, low-noise, semiconductor External Cavity Laser (ECL) that is robust for operation in space. In addition, our custom-designed fiber amplifier demonstrated the full range of LISA noise and power requirements.

The activity described here, funded through our Strategic Astrophysics Technology (SAT) grant, involved two steps. First, the understanding gained from our lab prototypes' noise and reliability testing was incorporated into a rebuilt oscillator and amplifier. Second, with the oscillator and amplifier development complete, we performed environmental testing on the ECL and preamp, and a full-system test of the laser, using control systems to achieve the required laser power, frequency, intensity, and differential phase noise. We estimate TRL 4 for the current laser system. With future work involving amplifier environmental testing, a redesign of the ECL to lower its frequency noise by a factor of ~5, and final laser reliability and lifetime testing, we will complete the laser development enabled here by the SAT grant, and demonstrate a TRL-5 LISA laser system in fall 2019 (assuming additional funding is secured).

Background

LISA will use laser interferometry to observe the disturbance of freely floating test masses, caused by the passage of a GW. The detection of these GWs will allow LISA to observe the mergers of supermassive black holes, giving unprecedented tests of General Relativity at high precision, as well as views of the astrophysics of merging galaxies back to very high redshift. Because gravity is a very weak force, the GW test-mass disturbance is expected to be very small, of the order of 10^{-21} in strain, or 10^{-12} m displacement over a 10^{9}-m arm length, with a timescale of ~10^{3} seconds. This displacement sensitivity and timescale flows through the LISA laser requirements [2], shown in Table 1.

Power (W)	λ (nm)	Intensity Noise (/Hz$^{1/2}$)	Frequency Noise (Hz/Hz$^{1/2}$)	Differential Phase Noise (rad/Hz$^{1/2}$)	Lifetime (Years)
2.0	1064	10^{-4} (at 10^{-3} Hz) 10^{-8} (at 10^{7} Hz)	300 (at 10^{-2} Hz) 5 (at 100 kHz)	6×10^{-4} (at 10^{-2} Hz)	5

Table 1. *Laser requirements for LISA.*

The design of the LISA laser system consists of a low-noise ECL oscillator and preamp, followed by a fiber power amplifier (Fig. 1).

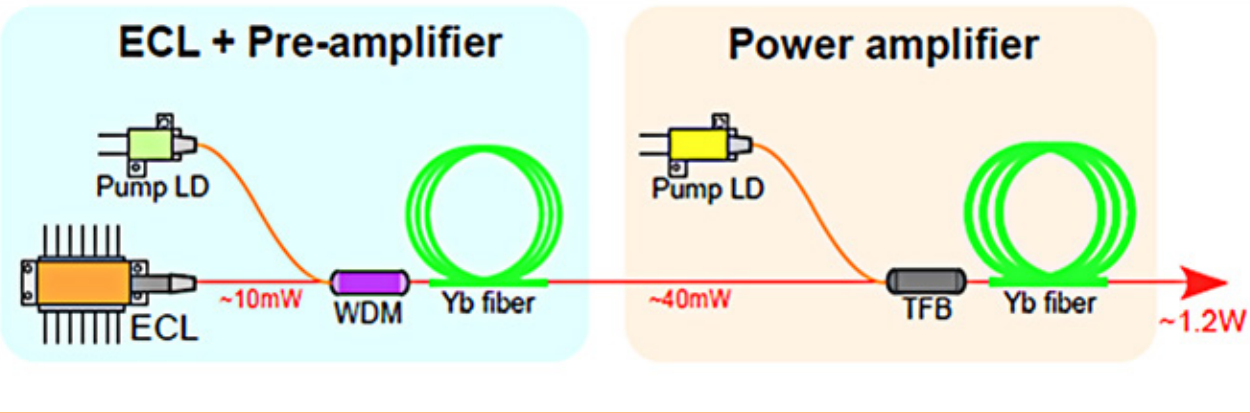

Fig. 1. *LISA laser system design (LD, Laser Diode; WDM, Wavelength Division Multiplexer; and TFB, Tapered Fiber Bundle).*

The ECL is a low-mass, low-cost, compact, simple, and highly reliable semiconductor laser, provided by a US vendor [3, 4]. These characteristics make it a compelling choice for the oscillator. The preamp is a simple and highly reliable subsystem that amplifies the ECL output by a factor of 4 to 20.

For the amplifier, a laser design utilizing optical fibers presents many advantages over solid-state bulk crystals, including:

- Insensitivity to contamination problems and ease of alignment, since the light is maintained within the fiber core and waveguide;
- Conveniently redundant design, since higher-risk components such as pump diodes are easily made redundant by splicing them into the gain fiber; and
- Ability to leverage the large resources of the telecommunications fiber industry.

The stringent noise requirements shown in Table 1 are achieved in the laser system design using well-known amplitude- and frequency-stabilization techniques described below, with which our group has had extensive experience. The power and wavelength requirements are compatible with the overall oscillator and power amplifier configuration.

Objectives and Milestones

The objectives involved three main aspects:

- Optimization of the oscillator (ECL);
- Construction of a preamp and laser amplifier; and
- Systems and environmental testing of the full laser system (oscillator, preamp, and amplifier).

Optimization of the ECL took place at the laser vendor (Redfern Integrated Optics, RIO). The first version of a 1064-nm-wavelength ECL in the preferred Butterfly package was produced in 2014, and allowed us to incorporate this low-mass, compact oscillator [5] into our laser design. The next step in the ECL development was optimizing its design to provide lower phase noise and high reliability. This was done by iterating the design of the planar Bragg grating which forms the reflector for the ECL

optical cavity, and by performing accelerated aging tests on the laser-gain chip. The final step involves a redesign of the laser-gain chip to lower the frequency noise, by September 2018. A space-qualified non-planar ring oscillator (NPRO) will also be built by September 2018, at which time the down-select for oscillator will be done.

The laser amplifier was constructed using a mechanically robust design to survive shake-testing and thermal cycling. It also included temperature stabilization, which is needed to limit amplitude noise. This construction involved use of a fiber splicer to combine fibers from the pump diode to the gain elements and a fiber coater to provide a coating layer with varying index of refraction to keep the light propagating through the fiber with low loss. The laser amplifier was tested for required output power, frequency noise, differential phase noise, and amplitude noise. By fall 2016, it will be environmentally tested for mechanical and thermal robustness.

Finally, the full laser system (oscillator and amplifier) will be monitored for noise and environmental robustness, as shown in Fig. 2. When TRL 5 is achieved individually for the oscillator and amplifier, we will demonstrate TRL 5 through a full-system-level test of the entire laser system, including lifetime testing, and power, frequency, intensity, and differential phase noise measurements. These studies will be complete in fall 2019 (see Path Forward section).

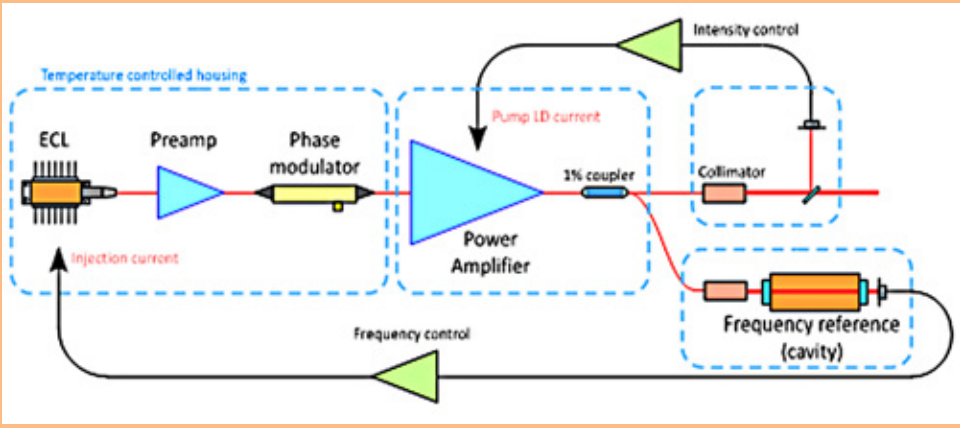

Fig. 2. *Laser system testing.*

The system test uses the fully fiber-coupled setup shown in Fig. 2 and incorporates the understanding gained in the measurements of the separate components. To simulate the stable space thermal environment, the oscillator and amplifier are located in a temperature-controlled housing, stabilized to 0.1°C over a one-hour timescale. The experimental arrangement of Fig. 2 presents the amplifier, preamp, phase modulator, and amplifier as a single integrated system.

The milestones for these activities are:

- Procurement of long-lead items (completed) . . . . . .Mar 2015
- Preliminary 1.5-W laser amplifier (completed) . . . . . .Apr 2015
- Preliminary laser amp test with non-optimized ECL (completed) . . . . . May 2015
- ECL optimization contract start (completed) . . . . . Jul 2015
- Optimized 2.5-W laser amplifier (completed) . . . . . .Sep 2015
- Noise tests of stabilized 2.5-W laser amplifier (completed) . . . . . Nov 2015

- Noise optimization of ECL (completed) . . . . . Jan 2016
- Reliability testing of ECL and preamp (completed). . . . . Feb 2016
- Laser system test with optimized ECL (completed). . . . . Feb 2016
- Full-laser-system noise testing (completed) . . . . . Mar 2016
- ECL gain-chip redesign to lower frequency noise. . . . . Sep 2018
- Space qualified NPRO build . . . . . Sep 2018
- Oscillator down-select. . . . . Sep 2018
- Full-laser-system reliability and lifetime testing . . . . . Sep 2019

By September 2019, assuming sufficient additional funding, we will have characterized the full-laser-system noise and demonstrated compliance with environmental and lifetime testing, establishing TRL 5 for this laser.

Progress and Accomplishments

We received notice of our SAT award in March 2014, and the funding arrived at GSFC in May 2014. Thus, all progress is measured against a start date of May 2014. We describe progress on the major activities of procurements, ECL optimization, preamp build, laser amplifier build, laser systems noise testing, and laser-system environmental testing.

Procurement of Long-Lead Items: We have prepared a temperature-stabilized enclosure for the laser systems testing. We have also procured all long-lead instruments necessary for the systems testing, including a frequency reference cavity, a fiber fusion splicer, two fiber coaters, and a mechanical shaker.

Preamp Build and Test: A counter-pumped preamp with a gain of 5 was constructed, using a gain fiber of 1-m length. A clean output spectrum was observed, with low Amplitude-Stimulated Emission (ASE) floor, no output leakage, and an efficiency of ~20%. The preamp is shown in the left panel of Fig. 3, along with the ECL oscillator mounted with its low-noise current driver. The right panel of Fig. 3 shows the preamp output power plotted against its pump diode power. The preamp enclosure houses two seed ECLs and two pump diodes for redundancy. Its fiber tray design was taken from the Lunar Atmosphere and Dust Environment Explorer (LADEE) flight mission.

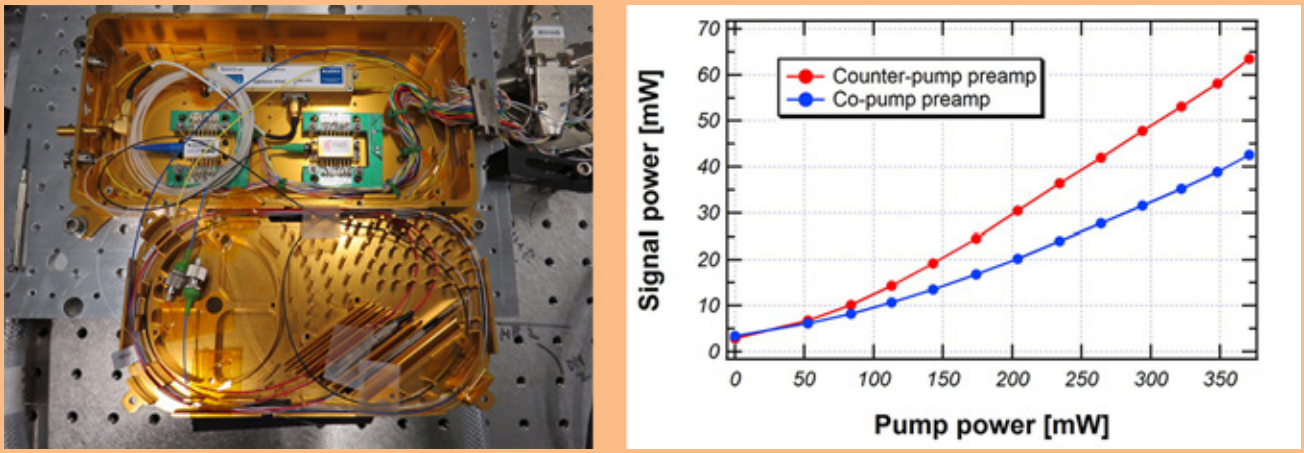

Fig. 3. Left: *Preamp and ECL oscillator.* Right: *Preamp output power vs. pump power.*

Amplifier Build and Test: the newly built 2.5-W fiber amplifier is shown in the left panel of Fig. 4. As shown schematically in Fig. 2, it includes a pump diode to provide power, a TFB to allow redundant power input, and a 2.3-m-length, 10-μm core, double-clad, large-mode-area gain fiber that converts the pump power to amplification gain. The forward-pumped design and optical isolator minimize potential sources of feedback. The amplifier uses a robust mechanical design and temperature stabilization to suppress fiber-length variations.

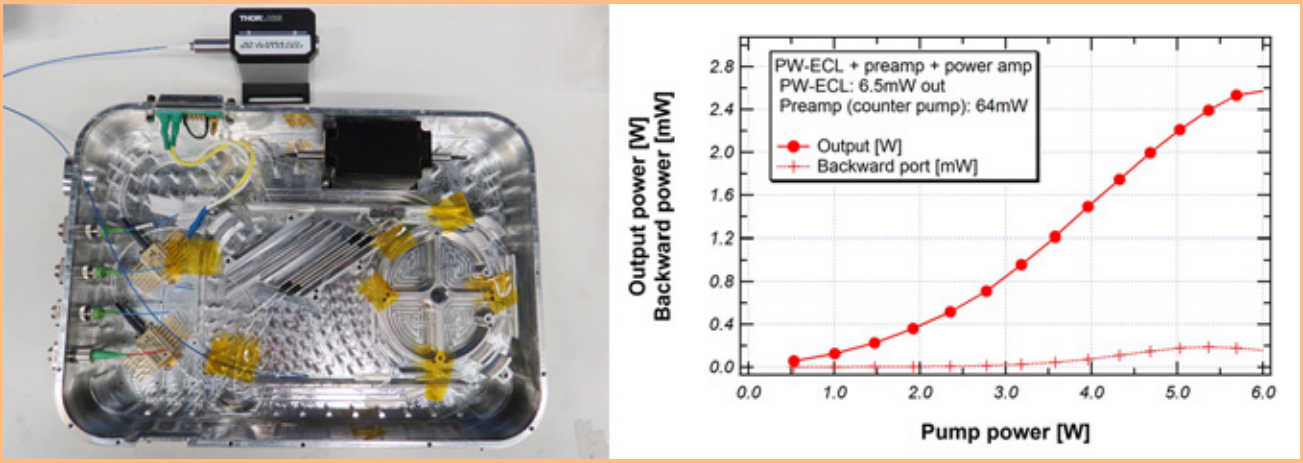

Fig. 4. Left: *Fiber-based laser amplifier.* Right: *Laser amplifier output power vs. backward port power.*

Testing of the amplifier has shown an unstabilized amplitude variation of about 1% root mean square (rms), and an output power of 2.5 W, significantly above the 1.5-W requirement, as shown in the right panel of Fig. 4. The constant backward-port power as a function of output power indicates that Stimulated Brillouin Scattering (SBS) is likely not a noise concern. Approximately 20 dB polarization extinction ratio (PER) was achieved at the output. A 1064-nm ECL with 6-mW output, followed by a preamplifier of gain ~10, was used as input to the amplifier.

Laser System Noise Testing: We have performed laser system noise tests by amplitude- and frequency-stabilizing the ECL and amplifier (Fig. 5). By stabilizing the amplifier pump-diode current, an amplitude noise attenuation of ~30 was achieved at a frequency of 0.1 mHz (a factor of ~10 above the LISA requirement, see red curve in right panel of Fig. 5). This noise will decrease significantly once temperature stabilization of the amplifier is applied. The laser system was also frequency-stabilized by locking a small fraction of the amplifier's output to the frequency reference cavity, using either the laser current or an Acousto-Optical Modulator (AOM) as frequency actuator. A control bandwidth of ~10 kHz was achieved; future work will increase this to order 1 MHz by optimizing the AOM driver. Finally, differential phase noise (or the stability of a 2-GHz sideband relative to the carrier frequency), observed in transmission through the amplifier, has been measured and found to meet the LISA requirement shown in Table 1.

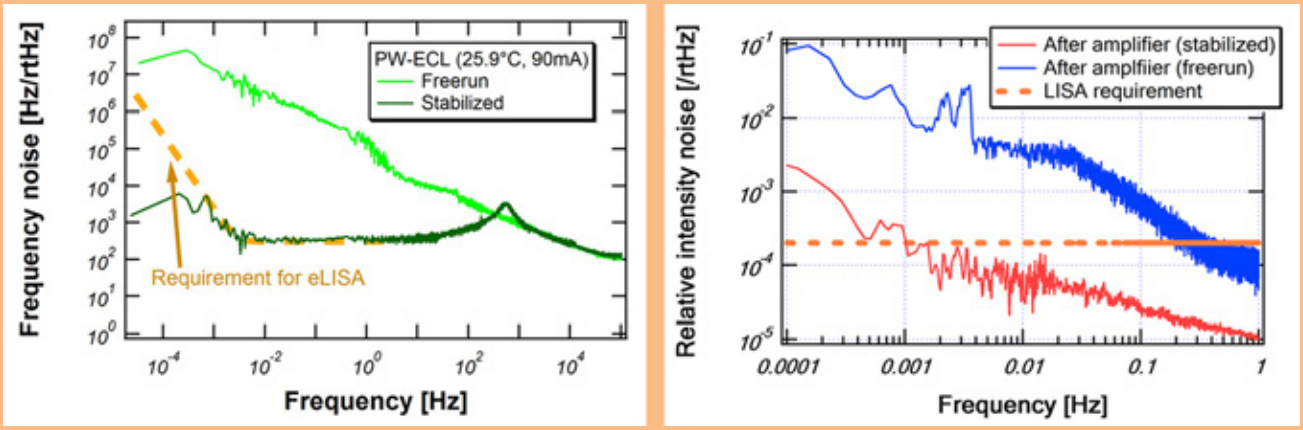

Fig. 5. *Frequency (left) and intensity (right) noise of laser system: ECL, preamp and amplifier.*

Design Optimization of ECL: This work was done at RIO, and involved modeling and analysis of the current-gain chip and Planar Linear Cavity (PLC) that comprise the ECL, and then modeling of the full oscillator. This fed a redesign of the PLC, which was followed by the manufacturing and integration of the new components, and then characterization to verify the improved phase-noise performance. The work also included final reliability testing of the laser-gain chip. Three designs of the ECL optical cavity are shown in Fig. 6 (black, red, and green curves), with the phase noise of each configuration plotted as a function of frequency. The purple and blue curves show for comparison the phase noise of the NPRO and the low-noise 1550-nm ECL, respectively. We chose the implementation providing the red curve, which had the lowest noise at 100 kHz (which has a strong effect on laser phase locking). The oscillator was delivered to GSFC in January 2016.

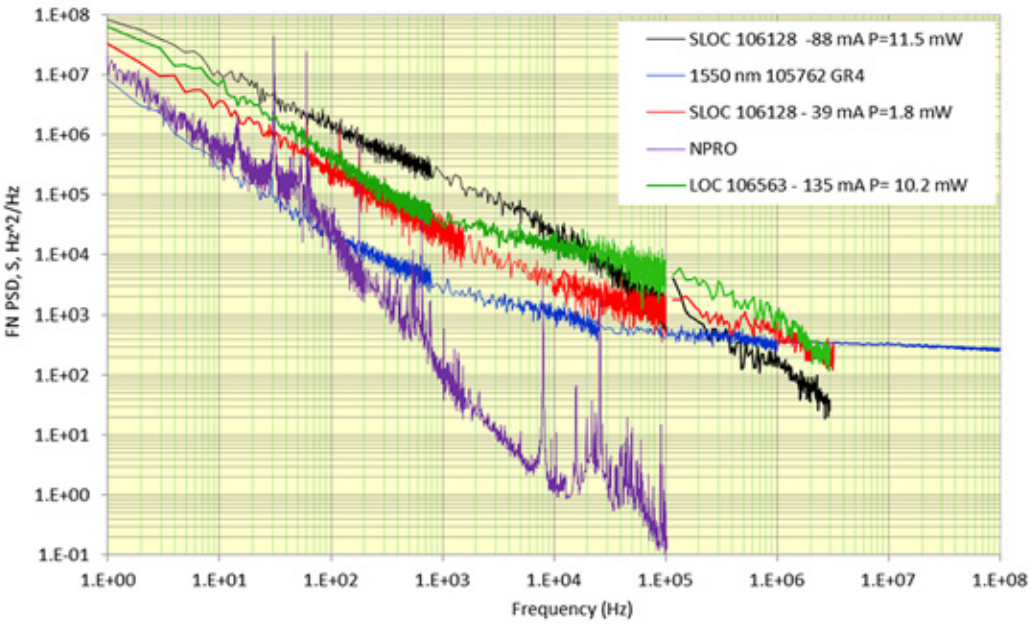

Fig. 6. *Power spectral density of phase noise of 1064 nm ECL with various optical cavity parameters. The noise at 100 kHz is most significant for phase locking separate lasers, so we chose the implementation providing the red curve. For comparison, the purple curve shows the phase noise of the NPRO.*

Oscillator and Preamp Environmental Testing: a critical aspect of this work is environmental testing, which involves thermal-vacuum cycling, vibration testing, and exposure to radiation levels that will be seen in the LISA space environment. These tests have been applied to the ECL oscillator and the preamp, as shown below. Figure 7 shows the vacuum cycling apparatus deployed in our laser lab, and Fig. 8 shows the thermal levels and duration used in the thermal cycling of the preamp.

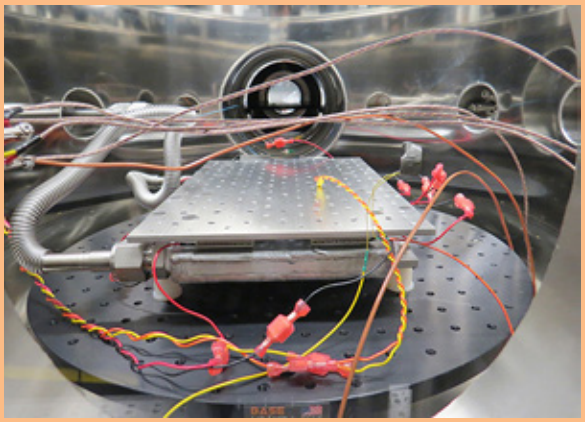

Fig. 7. *Thermal cycling apparatus in our lab.*

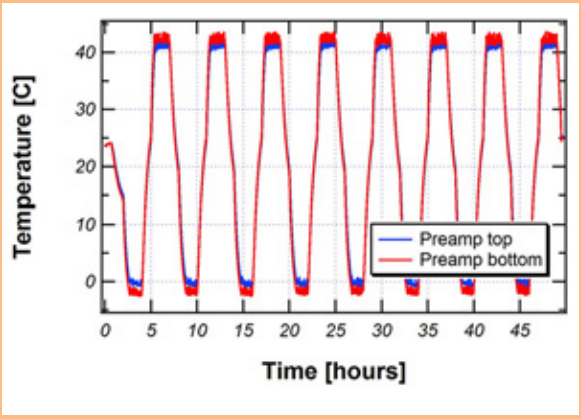

Fig. 8. *Thermal levels in preamp tests.*

Figure 9 shows the vibration ("shaker") apparatus used to vibrate the preamplifier and other components under test, while Fig. 10 shows the acceleration spectrum that the shaker provides.

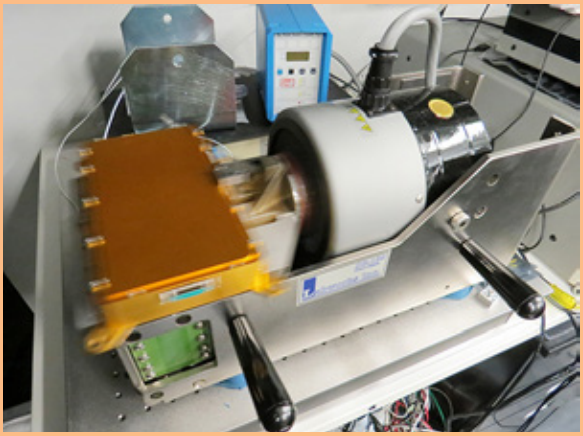

Fig. 9. *Vibration instrument shaking preamp/ECL.*

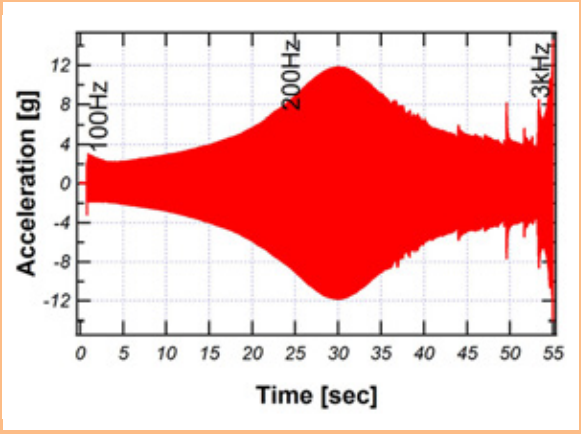

Fig. 10. *Acceleration from vibration apparatus.*

The results of the preamp environmental testing (Fig. 11) show no effect on the output power from thermal cycling or vibration, and ~30% drop in output power from gamma-ray radiation exposure, with exposure at the full LISA level of 45 krad in 8 hours, which represents a rate 10^4 times the LISA rate experienced during a 5-year orbit. Since radiation damage is related to both the exposure rate and total dose, further measurements are necessary to uncouple these two effects and determine whether radiation shielding may be necessary.

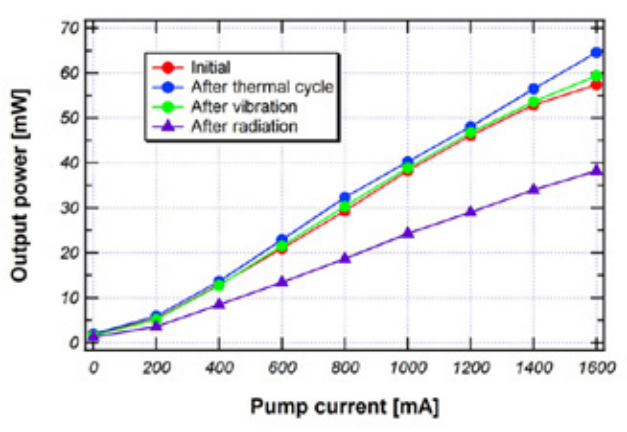

Fig. 11. *Results of environmental testing on ECL + preamp.*

Path Forward

Tests of the ECL noise performance done toward the end of the SAT grant period determined that its frequency noise is about a factor of 5 too high to allow robust phase locking of the lasers with the current design of the LISA phasemeter. This necessitates new activities for the laser oscillator. We are planning 1) a redesign of the ECL gain chip to further reduce the frequency noise, and 2) development of a space-qualified NPRO as a backup option in case the ECL redesign does not meet the noise requirements. We decided to delay the environmental testing of the laser system until the oscillator down-select between the ECL and NPRO is made, around September 2018. We have invested the remaining funds of the SAT grant in starting the NPRO build, and await further funding to start the ECL redesign and laser system reliability and lifetime testing described below.

ECL Gain Chip Redesign: Figure 12 shows the frequency noise of the 1064-nm (blue curve) and two grades of the 1550-nm ECL (black and red curves). To meet the LISA noise requirement at 100 kHz, the blue curve must be brought a factor of ~5 lower, below the red curve (whose associated 1550-nm ECL was able to phase lock using the LISA phasemeter in our lab). This will be done by a redesign of the 1064-nm laser gain chip, so that the thermal lensing is better controlled and the beam ellipticity, which causes high-order modes and excess frequency noise, is attenuated.

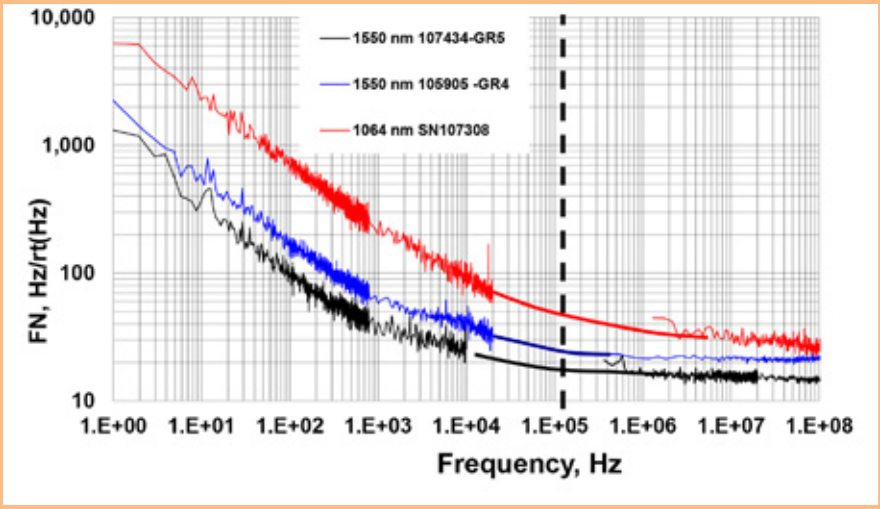

Fig. 12. *Frequency noise of 1064 nm and 1550 nm ECL.*

Space-Qualified NPRO build: as a backup option in case the ECL redesign does not meet LISA noise requirements, we will build and test a space-qualified NPRO oscillator. The NPRO has been space-qualified by a number of groups and this task will be straightforward. Figure 13 shows a layout of NPRO components in a design which is robust for space application.

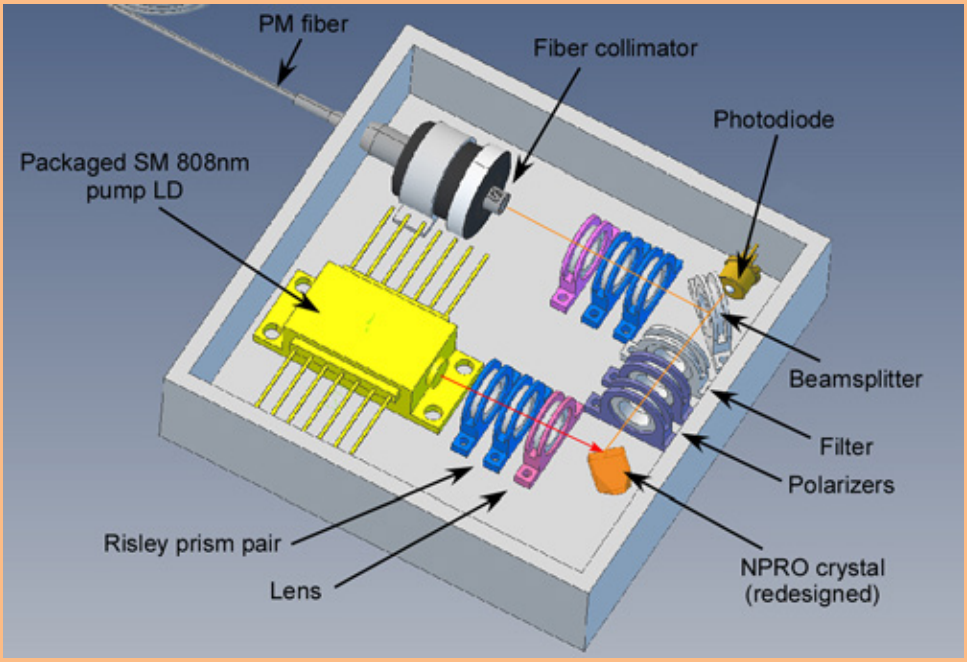

Fig. 13. *NPRO component layout.*

Amplifier Environmental Testing and Long-Term Reliability and Accelerated Aging: After the oscillator down-select in September 2018, the remaining LISA laser work involves reliability-testing of the individual laser components, followed by environmental testing of the full laser system, including thermal cycling, vibration, and radiation exposure. Finally, the full laser system will be operated at elevated temperatures to perform accelerated aging tests, to demonstrate the 5-year lifetime requirement. TRL 5 will be demonstrated with the conclusion of these tests in September 2019 (assuming sufficient additional funding).

Summary

We have made significant progress in our goal of delivering a TRL-5 laser to the LISA mission. Funded through the SAT award from April 2014–September 2016, we have built and tested a 2.5-W laser system consisting of an ECL oscillator, a fiber preamp, and a fiber amplifier. The ECL has very low frequency and intensity noise, and is robust for space application. The ECL and preamp has been environmentally tested in our lab, with thermal vacuum cycling, shaking, and radiation. The amplifier provides 2.5-W output with negligible SBS. The full laser system meets the LISA noise requirements, including differential phase noise. We estimate TRL 4 for the full laser system.

Towards the end of the program, we determined that the ECL frequency noise at 100 kHz was about a factor of 5 too high for phase locking with the LISA phasemeter. With this in mind, we initiated an effort to redesign the ECL laser-gain chip to reduce the noise, building a space-qualified NPRO as a

backup option in case the ECL noise remains too high. This new effort will require at least an additional two years, with the new oscillator down-select occurring as early as September 2018. Following the down-select, we will undertake the last step of verifying the laser system lifetime, by testing individual components and then performing accelerated aging tests on the full laser system. The completion of these tests will deliver a TRL-5 LISA laser system. This will require funding beyond the SAT award, and is currently under discussion with the PCOS Program Office.

References

[1] T. Prince et al., "*LISA: Probing the Universe with Gravitational Waves*," LISA-LIST-RP-436 Version 1.2 (2009)

[2] O. Jennrich and G. Heinzel, "*Laser requirements for a gravitational wave mission*" (2013)

[3] Redfern Integrated Optics Products Page

[4] K. Numata et al., "*Performance of planar-waveguide external cavity laser for precision measurements*," Optics Express **18** 22781 (2010)

[5] K. Numata et al., "*Characteristics of the single-longitudinal mode planar-waveguide external cavity diode laser at 1064 nm*," Optics Letters **39** No. 7, 2101 (2014)

For additional information, contact Jordan Camp: *jordan.b.camp@nasa.gov*

Gravitational-Wave-Mission Phasemeter Technology Development

Prepared by: William Klipstein (PI; JPL); Brian Bachman-Okihiro, Jeff Dickson, Jehhal Liu, Kirk McKenzie, Robert Spero, Dmitry Strekalov, Brent Ware, and Chris Woodruff (JPL)

Summary

The proposed work in the framework of this Strategic Astrophysics Technology (SAT) project will advance the Technology Readiness Level (TRL) of our phase-measurement electronics, and demonstrate their performance in an upgraded interferometer system-level test bed. The test bed will provide signals representative of gravitational-wave (GW) missions, such as the Laser Interferometer Space Antenna (LISA). Our technology-development effort starts with demonstrating the "photons-to-bits" phase-measurement system (interferometer readout electronics) as a system to TRL 4 in an interferometer test bed providing signals representative of a LISA-like mission. Some components, most notably the digital phasemeter board, have been developed beyond TRL 4, as assessed by NASA's Earth Science Program. We are pursuing an infusion path into L3-LISA with our German partners based on designs from the Gravity Recovery And Climate Experiment (GRACE) Follow-On Laser Ranging Interferometer (LRI), which was itself based on LISA technology development. First steps of the hardware development path for a TRL-6 LISA Phasemeter are described below.

Background

LISA-like GW mission concepts rely on heterodyne laser interferometry to measure picometer-level fluctuations in the separation between three widely separated spacecraft. The transmit and receive beams from a spacecraft pair are mixed optically (interfered) on a beam combiner, resulting in a detected signal varying sinusoidally at the frequency difference between the local transmit laser and the laser received from the distant spacecraft. Picometer-level displacement sensitivity requires microcycle-level precision in measuring the phase difference compared to the micron-scale wavelength of the laser light.

Since 2005, we have been developing phase-measurement systems to validate and support photons-to-bits interferometer-signal readout based on mission parameters described in the LISA Technology Development Plan. Future variants of GW missions all (except the less-mature atom interferometer concepts) involve laser interferometry between widely separated spacecraft. Thus, they will all rely on a LISA-like phasemeter and time-delay interferometry to mitigate the impact of laser frequency noise on mission performance.

Elements of our phase measurement system include quadrant photoreceivers, an analog signal chain, analog-to-digital converters (ADCs), and digital signal processing for the phase measurement. In addition to measuring the phase (distance) change in the interferometer, the phasemeter also controls laser frequency and provides an optical communication link between spacecraft. We recently used the phasemeter from GRACE Follow-On (GRACE-FO) to implement differential wavefront sensing using our LISA four-quadrant photoreceivers, and used that signal to maintain relative pointing of incoming and outgoing lasers by feeding back to a steering mirror in the transmitted light path.

Objectives and Milestones

The objective of this project is to advance our phase measurement system from TRL 4 to 5, through a significant system-level hardware-fidelity increase and greater fidelity of the signal-test environment by adding low light levels. With follow-on funding, we will also be developing the digital core of the phasemeter to TRL 6.

Key project milestones:

1. Incorporate quadrant photoreceivers into test bed.
2. Demonstrate wavefront sensing.
3. Migrate additional photoreceiver algorithms from LabView phasemeter to an Engineering Model (EM).
4. Demonstrate tracking of low-visibility signals with EM phasemeter.
5. Incorporate EM photoreceivers and signal chain.
6. Demonstrate test-bed performance at TRL 5 or better.
7. Develop an Engineering Development Unit that supports the large number of tracking channels.

Progress and Accomplishments

Work on this task was postponed in order to take advantage of synergistic developments on the Earth Science mission, GRACE-FO, which will carry an LRI based on technology development of the phasemeter for a GW mission. LRI will demonstrate inter-spacecraft interferometry with requirements quite similar to the former LISA mission by design. LRI is a partnership between the US and Germany, relying on partners from LISA formulation. The phasemeter team's share in LRI includes the phasemeter, laser, and laser stabilization cavity. LRI will fly LISA phasemeter algorithms implemented and advanced to flight maturity. The hardware complement is shown in Fig. 1.

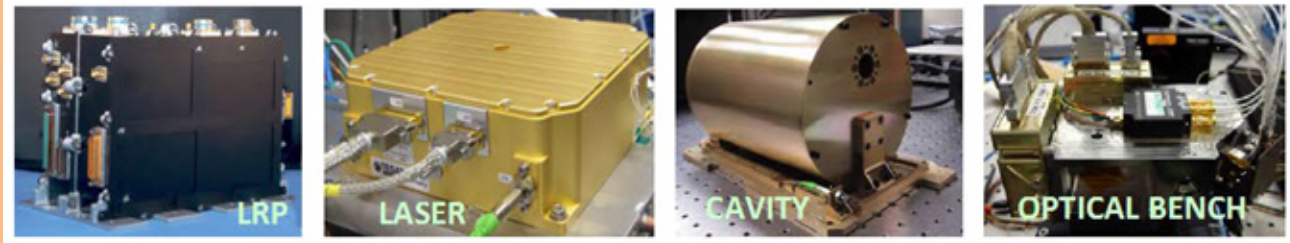

Fig. 1. *The LRI design requirements and designs came from US and German investments in GW technology as well as geodesy. LRI hardware shown (left to right): Laser Ranging Processor (LRP), Laser, Optical Cavity, and Optical Bench Assembly (OBA).*

An EM of the quadrant photoreceivers and signal chain has been delivered to the US to support testing and will be made available to support this task as a complement to the US-developed photoreceivers. A comparison of LRI requirements to LISA requirements is shown in Table 1.

Parameter	LRI	LISA
Measurement noise • Shot noise • Photoreceiver noise • Phasemeter noise • Optical pathlength noise • Laser frequency noise • Ultra-stable oscillator (USO) noise	0.08 μm/√Hz • 10 pm/√Hz • 1 nm/√Hz • 1 nm/√Hz • 30 nm/√Hz • 35 nm/√Hz • 1 nm/√Hz	2×10^{-5} μm/√Hz • 7 pm/√Hz
Satellite separation	170 – 270 km	5 million km
Satellite relative velocity	< ± 3 m/s	< ± 15 m/s
Wavelength	1064 nm	1064 nm
Phase precision	10 microcycle/√Hz	1 microcycle/√Hz
Nominal carrier-to-noise density (CNR)	>75 dB-Hz (single phasemeter channel)	>75 dB-Hz (single phasemeter channel)
Intermediate Frequency (IF) signal frequency	4 - 16 MHz	2 - 18 MHz
IF signal dynamics (@1Hz) • Before frequency stabilization • After frequency stabilization	 • 50 kHz/√Hz • 30 Hz/√Hz	 • 5 kHz/√Hz • 300 Hz/√Hz
Science bandwidth	2 mHz to 0.1 Hz	0.1 mHz to 1 Hz
Prescription optical power	80 pW	80 pW
Number of phasemeter channels	4	64
ADC clocking rate	38.656 MHz	50 MHz
Time coordination	GPS (laser ranging could be used)	Laser ranging code
Laser phase locking	Required	Required
Pointing information	Wavefront sensing	Wavefront sensing

Table 1. *LRI requirements are closely matched to LISA requirements. The primary differences are that LRI has tighter laser-frequency-noise requirements (demonstrated) and LISA requires more tracking channels, including multiple channels per signal stream. LRI will fly LISA phasemeter algorithms.*

The LRI phasemeter has demonstrated the following LISA-relevant requirements:

- Microcycle phase measurement of heterodyne signals with CNR of 66.5 dB-Hz from 4-16 MHz from quadrant photoreceivers (Fig. 2);
- Differential wavefront sensing and steering mirror control at ~60 dB-Hz;
- Phase locking of a flight non-planar ring oscillator (NPRO) laser at 66.5 dB-Hz;
- Laser stabilization of a flight NPRO laser to a flight cavity; and
- Automated inter-spacecraft optical link acquisition.

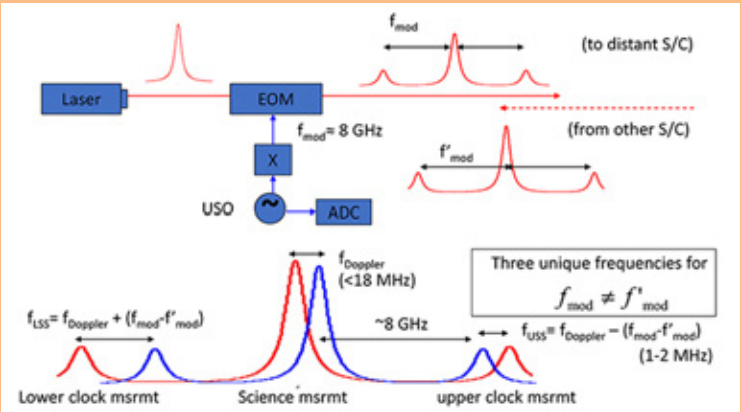

Fig. 2. *LISA puts microwave sidebands on the laser light using an ElectroOptic Phase Modulator (EOM) and then tracks the sideband-sideband beat-note to measure clock noise. This avoids the requirement to have super-stable clocks, but requires multi-toned tracking in the phasemeter (S/C, spacecraft; LSS, Lower Sideband-Sideband; USS, Upper Sideband-Sideband).*

As the first and most critical step to mapping remaining required functions from our TRL-4 Labview phasemeter to our flight platform, we have modified the GRACE-FO flight Field Programmable Gate Array (FPGA) code and software to include multi-tone tracking, to allow tracking of the sideband-sideband beat-note used to transfer and measure relative clock noise between distributed spacecraft (Fig. 2). This technique was used in our previous test bed work but was unnecessary in GRACE-FO, which has only two spacecraft, and so is limited by laser frequency noise, not sampling clock noise. As shown in Fig. 2, the sideband-sideband measurements are much lower amplitude than the carrier-carrier science signal. This requires some special attention, because one of the phasemeter design challenges is accurate tracking of laser frequency noise (as signal) in the presence of photon-counting noise. With the low signal amplitudes of the sideband-sideband beat-note, we cannot track typical laser frequency noise for a flight laser. Instead, we implement "carrier-assisted tracking" in which the carrier-carrier science signal is used to track in the presence of laser frequency noise, and a much-lower-bandwidth loop tracks the residual additional noise in the sideband-sideband beat-notes. As of this writing we have implemented a scheme for this carrier-assisted tracking but have not tested its performance or optimized the design.

The algorithm development has been demonstrated on a "system-on-a-chip" developed for GRACE-FO (Fig. 3). There are two FPGA evaluation boards, simulating two separate spacecraft, allowing us to synthesize laser frequency and shot noise and track it under different noise conditions. We use this same platform to simulate link acquisition and reacquisition, and generally to test software and firmware before putting it on the flight boxes. This allows us to get the design about right under certain assumptions about system behavior, and is far more efficient than starting with test-bed signals, which are harder to vary. We had similar test abilities with our Labview phasemeter, but this platform has been extremely useful for GRACE-FO and for the current LISA work.

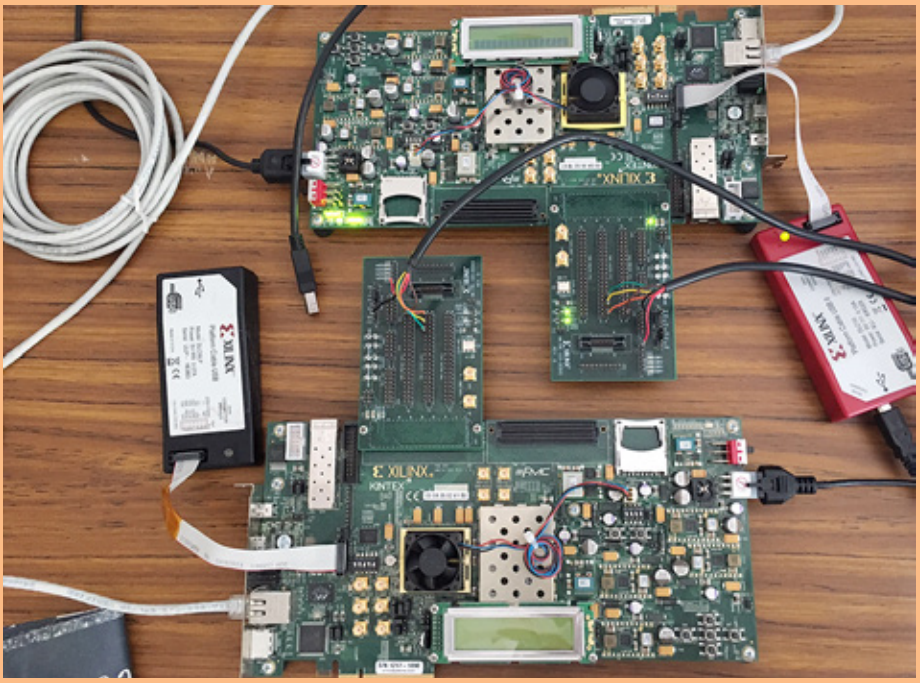

Fig. 3. *We have used the GRACE-FO "system-on-a-chip" test bed to test the clock-tone algorithms added to the GRACE-FO phasemeter firmware and software for this task. The test bed runs the actual firmware and flight code from the phasemeter with simulated signals; it represents an excellent development tool for the final lab test.*

Figure 4 (left) shows the frequency tracked, with three independent tones representing the carrier-carrier beat-note (at 10 MHz), and the upper and lower sideband-sideband beat-notes at 11 and 9 MHz, respectively.

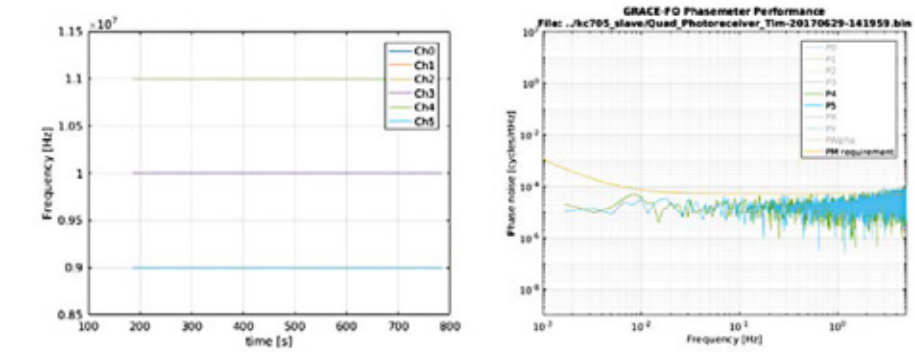

Fig. 4. *We have incorporated multi-tone tracking in the GRACE-FO LRP code and demonstrated its effectiveness in a "system-on-a-chip" digital test bed (Fig. 2).* Left: *Tracking of the three signals required for clock-noise transfer in LISA: the Carrier-Carrier science beat-note at 10 MHz, then the upper and lower sideband-sideband beat-notes at 11 MHz and 9 MHz, respectively.* Right: *Tracking channels demonstrating low-noise readout.*

While the system-on-a-chip platform is a powerful development tool, we still intend to demonstrate performance on our optical test bed. We have restored operation of the "single bench" test bed configuration (Fig. 5) after the substantial delays in completing GRACE-FO. This represents half of the "three-spacecraft" capability we demonstrated before, but adequately supports integration and test of new hardware including the LRP itself, quadrant photoreceivers, and multi-tone tracking. The second half of the test bed will be realigned in parallel with other work to support the full demonstration. The current setup relies on the commercial-off-the-shelf (COTS) hardware used in the past to verify and optimize the performance of the test bed with a "known-good" configuration before switching to the EM hardware. The optical configuration has been re-established, but some work remains in re-setting up the measurement chain, which just returned from Germany where it supported GRACE-FO.

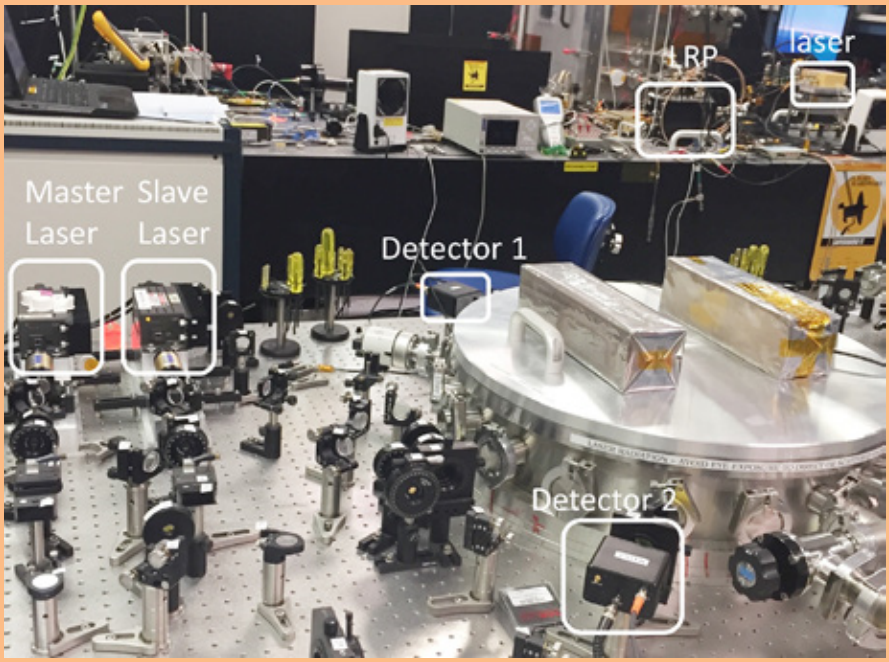

Fig. 5. *We have re-established our single-bench test bed in the same laboratory as the GRACE-FO hardware, seen in the distant table at the top.*

Path Forward

Incorporating these EMs into our LISA phase-measurement test bed, modified to provide low-visibility signals, will advance the GW technology development, just as it was instrumental in seeding the application to Earth Science. GRACE-FO will likely launch in early 2018. The LRI hardware has been integrated into both spacecraft, and used to demonstrate science operation in their integrated environment. The environmental test campaign has been completed for spacecraft 1 and nearly completed for spacecraft 2.

One capability we developed under GRACE-FO that will pay dividends to phasemeter development is the system-on-a-chip test bed, which allows high-fidelity simulations of phasemeter performance without access to the optical test bed. This is not a replacement for a "live" demonstration, but serves as a fantastic coding development tool.

Most of GRACE-FO was LISA-like, except for the mechanism for reacquiring the interferometer link, which on GRACE-FO uses a fast steering mirror, where on LISA it requires spacecraft attitude changes. Getting a stable, consistent acquisition that did not result in race conditions for different Doppler shifts turned out to be trickier than expected. This has led us to start thinking in more detail about how this will work for LISA, with its much longer light time and much slower spacecraft response. Earlier studies resolved the "57-degree-of-freedom" initial acquisition, so our thoughts have more to do with efficiency. For example, it might make sense to use the point-ahead mirror in a "look-behind" configuration to allow faster spatial scanning, with the determined offset removed slowly with spacecraft motion. The long light time makes the "spacecraft responding to its local environment" a bit tricky to optimize, but we are starting to think about this.

As the phasemeter task continues, we will be developing a TRL-6 version of the phasemeter core, and we are pursuing what we think will be an efficient path that leverages existing system architecture work by JPL's Radar Instruments section and the GRACE-FO hardware and firmware implementation. We intend to build a daughter card on an existing parallel FPGA development platform; the daughter card is anticipated to have ten samplers on it, which can be piped to an FPGA signal-processing board that will host the LISA Phasemeter algorithms. We think this is the most time- and money-efficient way to execute this work in the short time we have. The existing platform was designed in a technology program but with path-to-flight parts throughout.

Over the past year, we have made significant advances in the infusion plan of the NASA phasemeter into an ESA-led LISA mission. We have proposed to our German partners from GRACE-FO, formerly our LISA counterparts, that we continue our strong collaboration for the Phasemeter as a contribution to the German metrology system for LISA. The acceptability of this partnership on the phasemeter was enabled by the switch to Department of Commerce regulations that allow us to be far more transparent partners, so we will develop the phasemeter seamlessly together based on the capabilities developed and demonstrated by NASA with the expertise of both partners. We anticipate active collaboration to begin in 2018.

For additional information, contact William Klipstein: *bill.klipstein@jpl.nasa.gov*

Telescopes for Space-Based Gravitational-Wave Observatories

Prepared by: Jeffrey Livas (NASA/GSFC)

Summary

Telescope development for gravitational-wave (GW) detection began in Fiscal Year (FY) 2012 with a funding award from the Physics of the Cosmos (PCOS) Program. It was funded until FY 2015 with a two-year Strategic Astrophysics Technology (SAT) grant plus a no-cost extension. A follow-on SAT grant was awarded in FY 2015 to continue work through FY 2017.

The program status changed with the submission of a proposal [1] in January 2017 to the European Space Agency (ESA) call for proposals for the L3 launch opportunity, and the subsequent formal selection of that proposal by ESA's Science Program Committee (SPC) in June 2017. The proposal was written by the Laser Interferometer Space Antenna (LISA) Consortium in collaboration with the US GW scientific community, including NASA. Although a formal decision on the contributions to the mission from ESA and NASA, as well as ESA member states, awaits discussions between Agency representatives, the current plan calls for NASA to supply a telescope, a laser, and a charge management system. These technologies are described in more detail in the interim report of the L3 Study Team [2]. With the selection of the proposal and the tentative agreement to supply a telescope as part of the LISA mission, the telescope technology development program transitions from a research and development effort funded by the SAT program to a directed technology program under the direction of the L3 Study office. This report will summarize the status of the telescope effort and the expected plan forward.

The goal is to develop a telescope suitable for precision metrology for a space-based GW observatory [3-6], where the application is to measure the separation of two spacecraft with a precision of 10^{-11} m/√Hz (10 pm/√Hz) over several million kilometers. The telescope technology study effort has developed a set of suitable requirements for the GW metrology application and will investigate the two key design challenges, dimensional stability and scattered-light performance; with modeling, analysis, and experiments. We have adopted the mission described in the L3 Proposal [1] as the reference mission for work beginning in 2017. This is a departure from previous work, but the main impact on the telescope effort is that the primary mirror diameter is now 30 cm instead of 20 cm, and the pupil diameter on the optical bench is now 2.24 mm. These changes required a new optical model, which is still in progress at the time of this writing.

The work has been supported by a team of engineers from the NASA Goddard Space Flight Center (GSFC) Optics Branch; a mechanical engineer; and a postdoctoral fellow, Shannon Sankar, currently a scientist with the Center for Research and Exploration in Space Science & Technology/Universities Space Research Association (CRESST/USRA) (Table 1).

With the transition to a directed program under the direction of the L3 Study Office, the telescope project will be reorganized under the direction of a project manager (PM)/product design lead (PDL) with a slightly different team that includes more support from the Mechanical Engineering Division (Code 540). The precise makeup of the team has not yet been determined, but for continuity will include several of the people in Table 1 who have been involved to date.

Name	Expertise	NASA/GSFC Code
Jeff Livas	PI	663
Peter Blake	Mirror fabrication	551
Joseph Howard	Optical designer	551
Shannon Sankar	Stray light measurement	663
Lenward Seals	Stray light	551
Garrett West	Optical design	551
Justin Ward	Mechanical engineering	540/Newton

Table 1. *The LISA prototype telescope team.*

The most significant accomplishment of the past year is the preliminary testing of a prototype telescope that we plan to use to validate our scattered-light model. A summary of the telescope requirements, design, and results has been published [7].

Background

The telescope technology development targets the requirements for displacement measurement for space-based GW detection. GWs are generated by any mass distribution with a time-changing quadrupole moment [8]. The simplest example is a pair of gravitationally bound masses orbiting around a common center of mass. The efficient generation of GWs requires large compact objects moving at a large fraction of the speed of light. The canonical source is a pair of million-solar-mass black holes colliding. It is believed that black holes of this size are located at the centers of galaxies and co-evolve with them. Therefore, this type of source represents collisions of pairs of galaxies, one of the ways large-scale structure is formed in the universe. The estimated event rate is between 10 and 100 mergers per year, i.e., from once per month to twice per week.

In February 2016, the ground-based Laser Interferometer Gravitational-wave Observatory (LIGO) network of GW detectors announced the detection of a merging pair of 30-solar-mass black holes. In June 2016, LIGO announced detection of a pair of approximately 10-solar-mass black holes merging. These detections confirm in spectacular fashion the basic existence of these sources. The million-solar-mass black holes at the centers of galaxies move more slowly and their GW signals can only be detected from space.

LISA addresses a number of science goals [9-11] and was specifically endorsed by the 2010 Decadal Survey, "*New Worlds, New Horizons in Astronomy and Astrophysics*" (NWNH), as the second-priority large-scale space mission (third priority overall: NWNH, Table ES.5, p. 8) for three specific reasons:

- Measurements of black-hole mass and spin will be important for understanding the significance of mergers in the building of galaxies;
- Detection of signals from stellar-mass compact stellar remnants as they orbit and fall into massive black holes would provide exquisitely precise tests of Einstein's theory of gravity; and
- Potential for discovery of waves from unanticipated or exotic sources, such as backgrounds produced during the earliest moments of the universe or cusps associated with cosmic strings.

Examples of other expected science returns are the study of galactic populations of binary stars [12] and precision determination of cosmological distances in a manner independent from EM measurements [13].

The function of the telescope for the baseline LISA GW observatory is to serve as a precision beam expander to deliver optical power efficiently from one spacecraft to another [14]. The telescope design for a space-based GW mission is based on a near-diffraction-limited classical Cassegrain-style reflecting

optical system. However, since the application is precision-displacement measurement rather than image formation, the normal requirements for high-quality image formation must be augmented by two challenges not needed for typical imaging applications and that require development:

1. The requirement for picometer-level optical-path-length dimensional stability through the telescope in the presence of both axial and transverse temperature gradients.
2. The requirement for low scattered-light levels. Scattered-light levels must be extremely low because the distance measurement uses interferometric techniques that are very sensitive to low light levels and because the telescope must simultaneously transmit a 1W beam and receive a 100 pW beam.

The long-term goal of this telescope technology-development effort is to make a prototype telescope that meets the basic requirements for a space-based GW observatory and bring it to Technology Readiness Level (TRL) 5-6 in time to be a serious candidate for a mission within the ESA Cosmic Vision program L3 opportunity. As of 2017, the best indication we have from ESA is for the technology to be ready by 2022 (see next section), which requires sustained development for the telescope. The ground-based detections announced by LIGO have had the effect of renewed interest in the community. The immediate goal of the telescope development is to test dimensional stability with flight-like materials and mirror mounts and to bring the telescope to ISO TRL 5/6 level by 2022.

Objectives and Milestones

Overall Objectives in the Context of the International Community

Figure 1 shows one possible timeline for development activities for an ESA-led mission. Activities in Europe (top section) and the US (center section, gray background) are shown separately. Shown is the launch and mission of the LISA Pathfinder (LPF) technology demonstration mission, and development activities associated with ESA's Cosmic Vision program L2 opportunity. Not shown are activities associated with the Cosmic Vision L1 mission, JUpiter ICy moons Explorer (JUICE), scheduled for a 2022 launch.

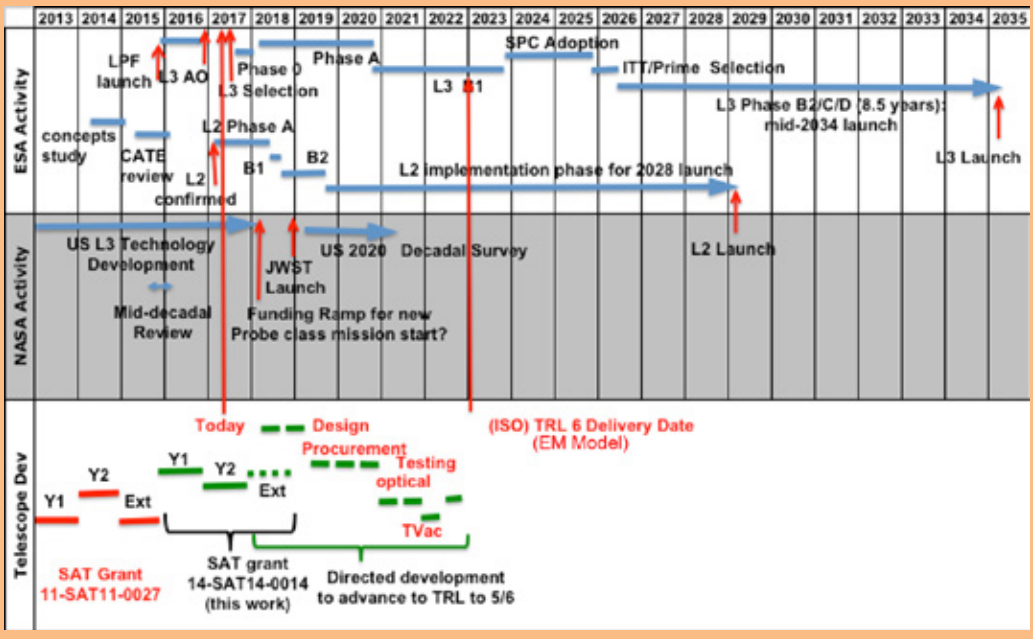

Fig. 1. *A possible timeline for an ESA-led mission as part of the Cosmic Vision L3 Opportunity showing work in the US (middle section) and Europe (top section). Preliminary results from LPF have been released and show that the gravitational reference system (GRS) meets LISA specifications.*

The "Gravitational Universe" was selected as the science theme for ESA's third large-class mission for the Cosmic Vision Program. With a nominal launch date in 2034, mission adoption would nominally occur in 2024. However, ESA also recently indicated it has technology-development funding available and that we may apply for adoption earlier if we are ready. Therefore, technologies to be considered for the engineering model need to be at TRL 5-6 by the end of 2022. We have adopted this timeline as a working schedule for now.

In this context, the objective of this work over the next few years is to advance the knowledge needed to build a telescope meeting the requirements, so that the US can be a credible international partner for an ESA-led mission, as well as providing a compelling candidate for consideration in the next US Decadal Survey.

Objectives and Milestones Specific to Telescope Technology Development

The original tasks and milestones specific to the telescope development are summarized in Fig. 2.

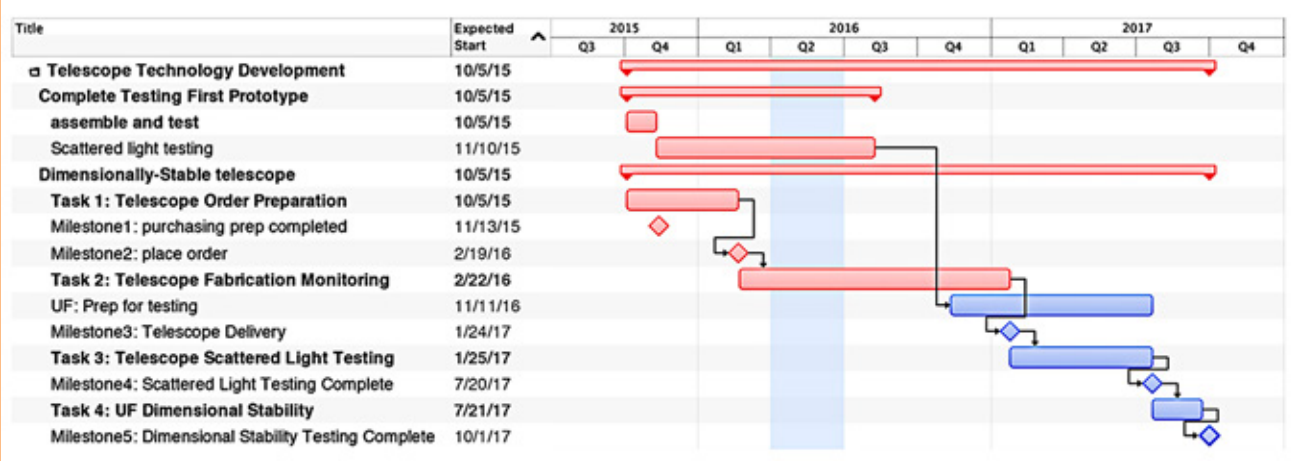

Fig. 2. *Key project tasks and milestones with an emphasis on procurement and testing of the second version of the telescope prototype.*

This original work plan is no longer in place due to the submission of a mission proposal for L3 in January 2017, and the selection of that proposal by ESA's SPC in June 2017. Replanning is in progress to develop a detailed schedule that implements the high-level directed development plan shown in the bottom row center of Fig. 1.

Progress and Accomplishments

Previous Accomplishments

The major accomplishment during 2012-2013 was to complete a study of the telescope design with an industrial contractor. The study included a complete thermal, optical, and a partial mechanical analysis of two implementations – an on-axis design and an off-axis design, and two material systems – carbon-fiber composite and silicon carbide. The study contractor was also required to develop plans for manufacturing and verification testing of these designs. The main results and recommendations are summarized below.

- An on-axis design does not meet the stray-light requirement, so use an off-axis design (on- vs. off-axis manufacturing complexity is similar);
- Use silicon carbide to avoid the unknown effects on dimensional stability from water absorption and subsequent out-gassing with composite materials; and
- The estimate for a ground prototype was a 16-month delivery with a cost of $2.5M, including:
  - $1.5M recurring engineering;
  - $0.26M non-recurring engineering;
  - $0.43M testing; and
  - $0.22M focus mechanism.

After the study concluded in April 2013, we chose to concentrate on developing and validating a scattered-light model due to limitations in time and funding. This amounts to a redefinition of Key Milestone #2 (Table 2). We chose to investigate scattering because we had previously investigated silicon carbide for the metering structure and showed it can be stable enough. We therefore fabricated the structure of the telescope out of conventional low coefficient-of-thermal-expansion (CTE) materials instead of the more expensive silicon carbide.

Year	Milestone	Date	Milestone Description	Redefinition	New Date
FY 2013	1	9/13	Stray-light measurement capability	No redefinition – achieved; demonstrated dynamic range of 10^{-10}	Achieved
FY 2014	2	3/14	Demonstration of scattered-light performance of $<10^{-10}$ of transmit power	Develop and validate a scattered-light model	9/16
FY 2014	3	9/14	Demonstration of optical-path-length stability	Not possible – materials and construction of prototype that could be environmentally tested too expensive	Projected 10/17

Table 2. *Key milestones as redefined. No change from 2014.*

We modified the telescope design from the one developed in the study, simplifying it while retaining its essential features. We then designed the mirrors for the simplified telescope design. We ordered a complete set of mirrors to build a prototype, as well as several pairs of M3 and M4, the two mirrors the model shows are the largest sources of scattered light. The idea is to try different combinations of surface roughness and coatings to better understand how to achieve the scattered-light requirement and demonstrate that we understand the physics.

We were able to find a vendor who agreed to build a complete prototype telescope to meet our requirements at room temperature, and held a kick-off meeting on June 19, 2014. We supplied a set of mirrors as Government-Furnished Equipment (GFE). The Critical Design Review (CDR) was held on October 30, 2014, and the telescope was delivered to GSFC on June 5, 2015.

Recent Accomplishments

Figure 3 shows the telescope, a 4-mirror afocal design with a 200-mm-diameter primary, and a 5-mm collimated output beam. The left panel shows the path of the central ray through the telescope. The right panel shows a photo of the telescope as it was finally aligned in the vendor's clean facility.

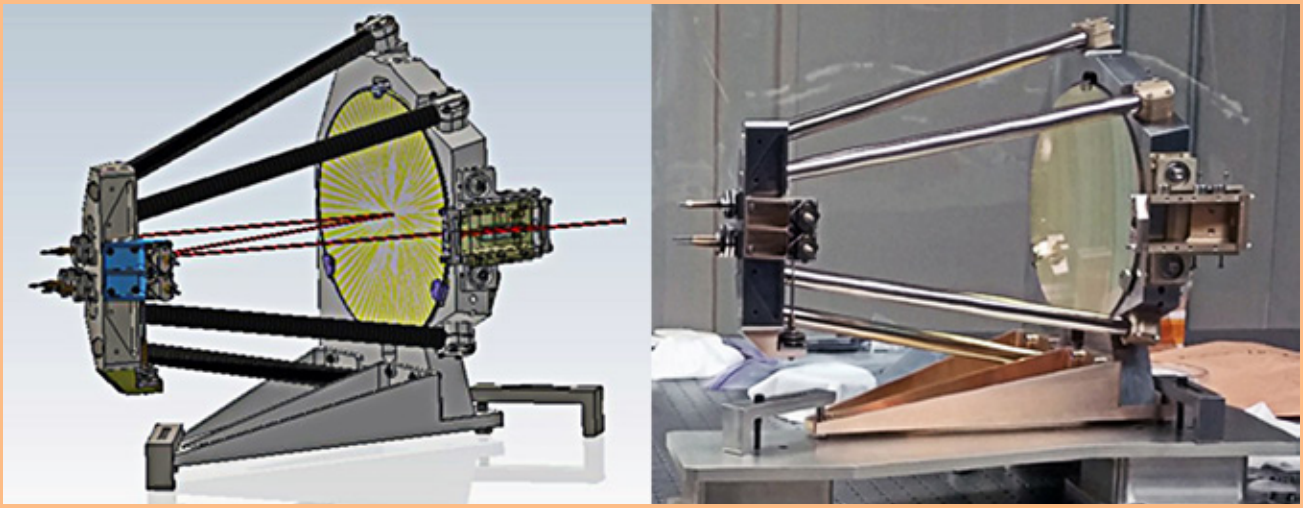

Fig. 3. *Prototype telescope.* Left: *Drawing of the telescope with the central, or "gut" ray's path through the telescope indicated by the solid brown line. The secondary mirror is in the blue mount to the left of the primary.* Right: *Photo of the telescope as aligned in the vendor's cleanroom.*

The telescope was installed in the Laser Communication Relay Demonstration (LCRD) cleanroom, where we arranged to share the space through the end of the calendar year. The immediate next step was to re-assemble and re-align the telescope. The M3/M4 assembly was relatively easy to align with the alignment jig supplied by the vendor, and we were able to recover the coarse alignment of the M1 and M2 pair using a Point-Source Microscope (PSM).

Final alignment was accomplished with a test setup based on a Laser Unequal Path-length Interferometer (LUPI) and a large auto-collimating flat in a double-pass configuration. Figure 4 shows the results. The telescope meets specifications at both wavelengths.

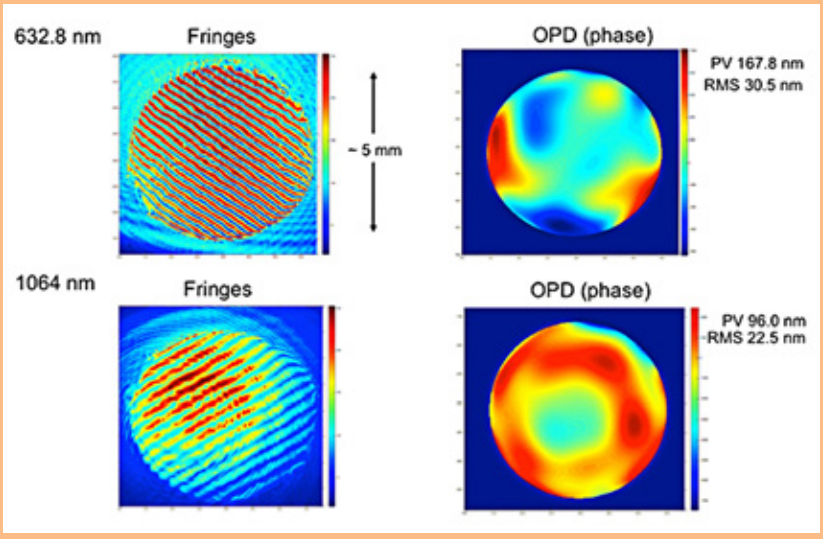

Fig. 4. *Measured wavefront error maps through the telescope at 632.8 nm (helium neon) and a1064 nm (Nd:Yag). The telescope operating wavelength is 1064 nm.*

Figure 5 shows the optical layout with the LUPI on the lower right hand side injecting a collimated beam into the 5-mm entrance pupil of the telescope. A 200-mm collimated beam is reflected from a 318-mm-diameter flat mirror (12.5") and re-enters the LUPI. Figure 6 shows a photograph of the test setup as installed in the cleanroom.

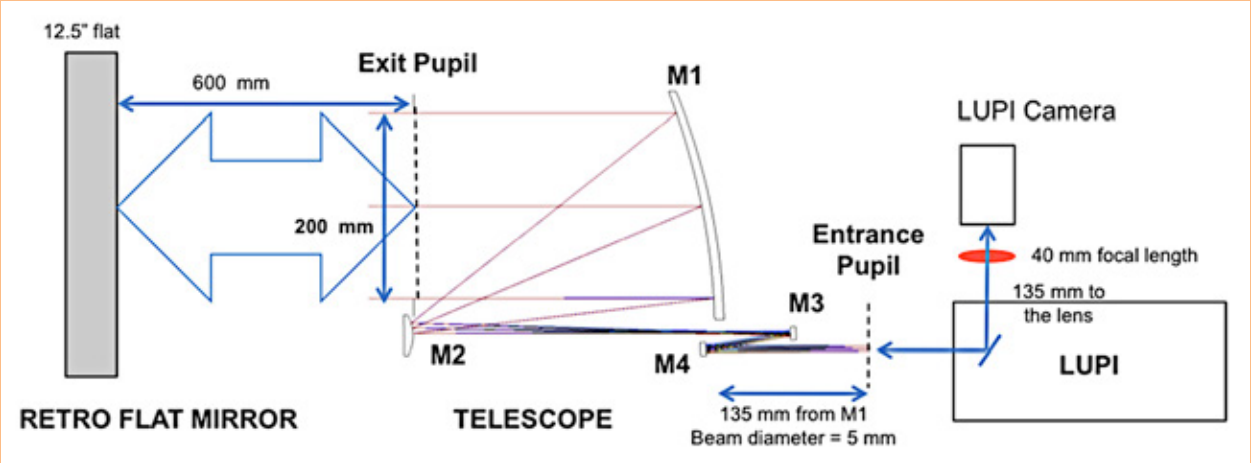

Fig. 5. *Layout of the alignment and test setup for the telescope. A double-pass test with an auto-collimating flat allows the use of a LUPI with a 5-mm beam to test the full 200-mm aperture telescope.*

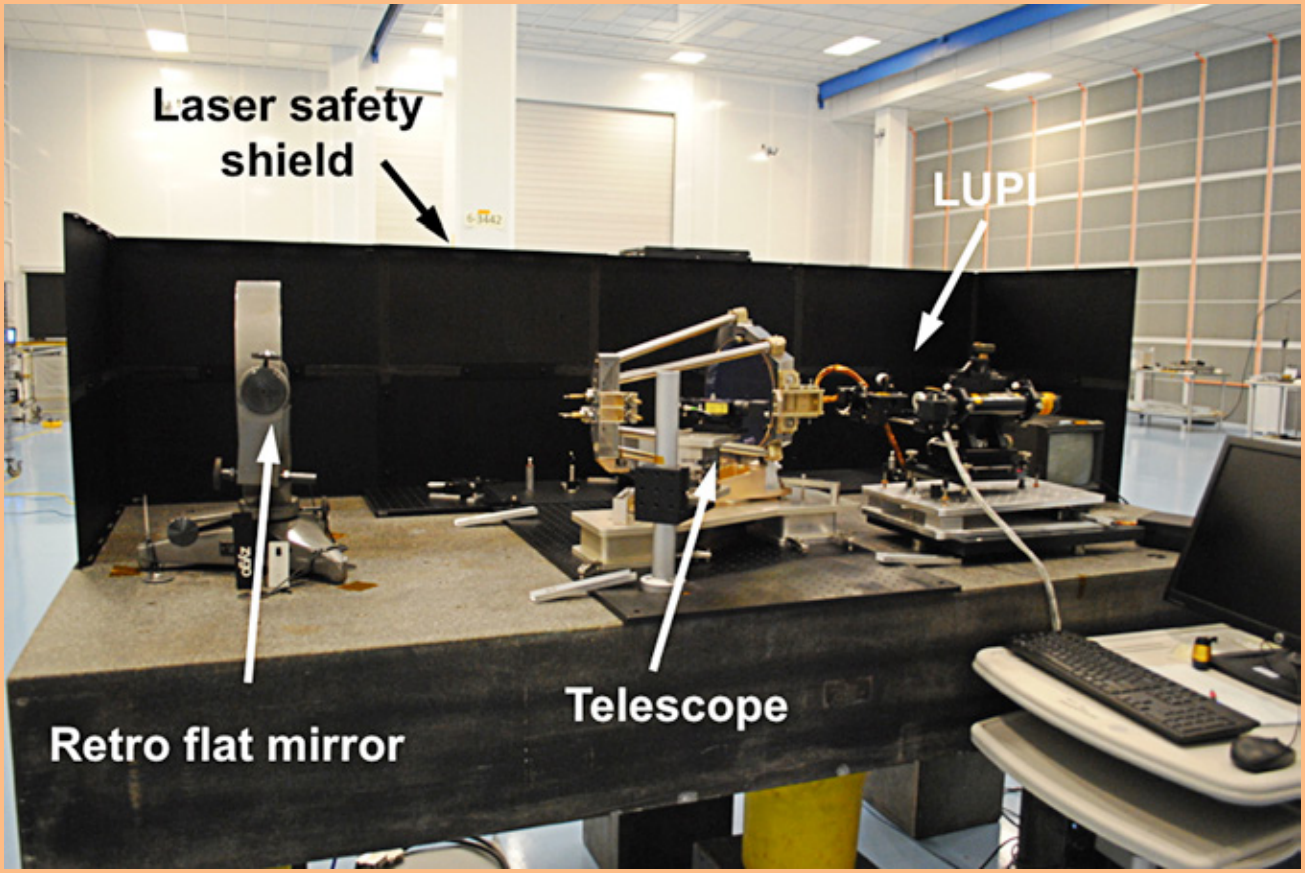

Fig. 6. *Photograph of the test setup in the LCRD cleanroom. Setup is shown schematically in Fig. 5.*

In April 2016, the LCRD project needed more space, and we were able to relocate to the Advanced Interferometry and Metrology (AIM) Laboratory cleanroom. We reassembled the test bed in the AIM laboratory, realigned the telescope, and modified the test setup slightly as shown in Fig. 7 to include a coherent receiver. A difference between the setup in Figs. 5 and 7 is that instead of auto-collimating the light transmitted through the telescope back on itself, we direct it off-axis to a beam dump. The only light coming back into the detector should be that scattered from the telescope.

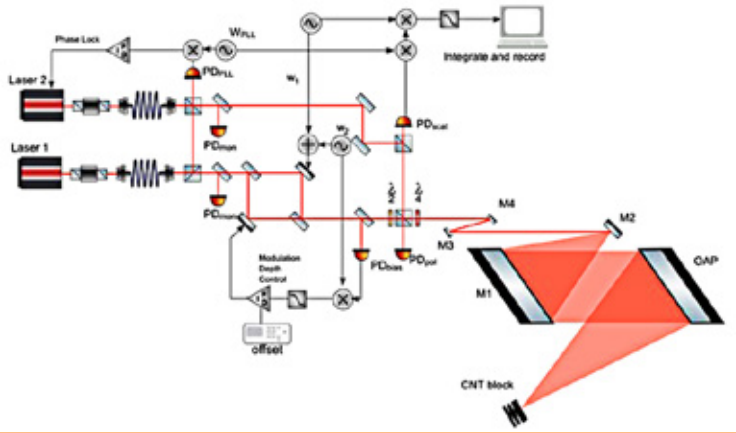

Fig. 7. *Coherent receiver for measuring scattered-light in the AIM Lab. Light transmitted through the telescope is directed to a carbon nanotube beam block with an off-axis parabolic mirror. Compare with Fig. 5 showing alignment setup (PD, Photodetector; PLL, Phase Locked Loop; CNT, carbon nanotube; OAP, off-axis parabola).*

Before moving to the AIM Lab, we found rough agreement between a scattered-light model and measurements of total integrated scatter. This is a good start, but we still need to verify scattering into the correct solid angle at the receiver, and the distribution of scattering among the different mirrors. Work is now proceeding to return to the same level of scattered-light sensitivity we had in the LCRD cleanroom.

As part of the scattered-light testing, we collaborated with Gari Billingsley and Liyuan Zhang from the LIGO project at Caltech to make some measurements of the scattered light from the M3 mirror. Their preliminary results are shown in Fig. 8, and appear to agree well with the standard models that are built into the FRED modeling software. We would like to be able to relate the system-level performance of the telescope to the individual mirror properties eventually.

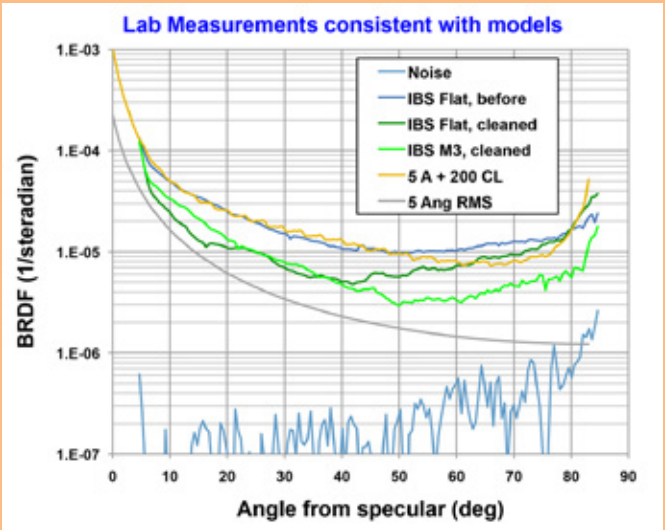

Fig. 8. *Scattered-light measurements from M3. Data courtesy of Gari Billingsley and Liyuan Zhang, LIGO Caltech (BRDF, Bidirectional Reflectance Distribution Function).*

Historically, we investigated scattered-light suppression work with petaled masks. This effort was augmented with funding received by Ron Shiri through the GSFC Internal Research and Development (IRAD) program for development of partially transparent petaled masks. This funding enabled Ron to engage with the University of Delaware for fabrication of partially transparent masks. Fabrication methods have been tested and a patent application filed [15, 16]. Additional work on masks has been done by our collaborators at the University of Florida [17]. In a separate application, US Patent 8,963,068 was granted for mask designs using carbon nanotubes: "*System and method for nanostructure apodization mask for transmitter signal suppression in a duplex telescope,*" with John Hagopian, Ron Shiri, Stephanie Getty, June Tveekram, and James Butler.

The purpose of this work with masks is risk reduction. Successful implementation of these masks may allow us to adopt an on-axis telescope design, which may be less expensive to build and better suited to the application's environmental requirements compared to an off-axis design. The same design techniques can be applied to coronagraph applications, which are currently proposed for exoplanet missions. At this point we are not actively pursuing this line of research, mainly due to lack of manpower.

Path Forward

Figure 9 shows the optical design that has been developed for the mission. The design is based on the earlier 20-cm-diameter prototype, but one of the key insights from the scattered-light modeling was that although the mirrors all scatter light into a hemisphere, the M3 and M4 mirrors contribute most of the scattered light on the detector because they focus the beam. The optical design for Prototype 2.0 makes M3 a flat so that it has no focusing properties at all. The optical correction for the loss of the M3 focusing power has been made on the primary mirror, where the added complexity is relatively easy to fabricate and does not contribute to stray light on the detector. A flat mirror can also be polished extremely flat, so in principle this design takes M3 out of the scattered light budget.

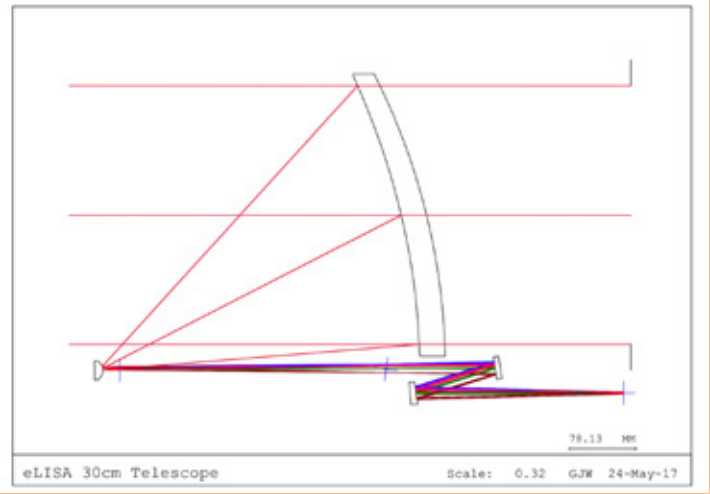

Fig. 9. *Prototype Telescope 2.0 optical design. This design is based on the previous prototype, but includes some insight from scattered-light modeling and testing. It has a 30-cm-diameter primary mirror per the LISA proposal to the L3 Announcement of Opportunity.*

With the formal selection of the LISA proposal by the ESA SPC on June 20, 2017, the path forward has changed. We are currently in the process of reformulating the telescope development plan to deliver a 30-cm-diameter telescope under the direction of the LISA Study office and funded through the PCOS program. The goal is to deliver an engineering-model-level prototype at ISO TRL 5/6 by 2022, if possible, and certainly before the nominal formal adoption date of 2024. A detailed schedule has not

yet been generated, but the nominal plan is shown at the bottom of Fig. 1. After approximately a year of design work; and 18-24 months for a vendor to fabricate, assemble, and align a telescope; there are two years of testing to demonstrate TRL 5/6. We are currently in the process of developing a schedule and budget and assembling a team, and expect to start the development program by mid-2017.

An important extension of this work is to examine the possibility of including a small moving mirror as part of the design. This design extension is referred to as "in-field pointing," which allows the telescope in principle to accommodate a large change (±1°) in the line-of-sight of the input beam without physically moving the telescope. The current baseline design has the telescope mounted as a complete assembly with the optical bench and the gravitational reference mass so the entire assembly can be moved on a pivot.

The choice between these two approaches is currently considered an open trade at the system level for the mission. Preliminary work indicates that the basic design with a small steerable mirror may be optically possible, but that it may have implications on scattered-light performance [18]. We plan to pursue the baseline design where the entire telescope assembly is moved as a unit on a pivot, and demonstrate a proof-of-concept design that can accomplish the motion and articulation of the optical assembly to reduce risk and mitigate concerns over this approach. As resources permit, we will evaluate the in-field pointing concept and its implications for scattered light to determine if it is feasible or not.

Acknowledgements

The author would like to thank P. Bender, G. Mueller, J. Sanjuan, A. Spector, and R. Stebbins, as well as the members of the GW Study Team and the eLISA Telescope Team for advice, support, and stimulating discussions.

References

[1] LISA Proposal for the L3 mission: *https://www.elisascience.org/files/publications/LISA_L3_20170120.pdf*

[2] L3 Study Team Interim Report: *https://pcos.gsfc.nasa.gov/studies/L3/L3ST_Interim_Report-Final.pdf*

[3] P. Bender, K. Danzmann, and LISA Study Team, "*LISA for the Detection and Observation of Gravitational Waves*," Max-Planck-Institut fur Quantenoptik, Garching Technical Report No. MPQ233 (1998)

[4] "*LISA Unveiling a Hidden Universe Assessment Study Report*," (Yellow Book), ESA/SRE 3 (2011)

[5] P. Amaro-Seoane et al., "*The Gravitational Universe*," eLISA L2 White Paper

[6] "*Gravitational-Wave Mission Concept Study Final Report*" (2012)

[7] J. Livas, P. Arsenovic, J. Crow, P. Hill, J. Howard, L. Seals, and R.S. Shiri, "*Telescopes for Space-based Gravitational Wave Missions,*" Opt. Eng. **53**, 9, 091811 (2013). doi: 10.1117/1.OE.52.9.091811

[8] B.F. Schutz, "*Gravitational waves on the back of an envelope*," Am. J. Phys. **52**, 412 (1984)

[9] P. Amaro-Seoane et al., "*Low-frequency gravitational-wave science with eLISA/NGO*," Class. Quantum Grav. **29**, 12, 124016 (2012)

[10] P. Amaro-Seoane et al., "*Intermediate and extreme mass-ratio inspiral astrophysics, science applications, and detection using LISA*," Class. Quantum Grav. **24**, 17 (2007)

[11] A. Stroeer and A. Vecchio, "*The LISA verification binaries*," Class. Quantum Grav. **23** S809-S817 (2006)

[12] S. Nissanke et al., "*Gravitational-wave emission from compact Galactic binaries*," Astrophys. J. **758**, 131 (2012)
[13] C. Cutler and D.E. Holz, "*Ultra-high precision cosmology from gravitational waves*," Phys. Rev. D **80**, 104009 (2009)
[14] O. Jennrich, "*LISA technology and instrumentation*," Class. Quantum Grav. **26**, 15, 153001 (2009)
[15] R.S. Shiri et al., "*Fabrication of petal-shaped masks for suppression of the on-axis Poisson spot in telescope systems*," Rev. Sci. Instrum. **87**, 043112 (2016)
[16] R.S. Shiri and J. Livas, "*Design and Fabrication of Partially Transparent Petaled Mask or Occulter Using Grayscale Lithography*," US Patent application GSC-17289-1, filed May 25, 2016
[17] A. Spector and G. Meuller, "*Back-reflection from a Cassegrain telescope for space-based interferometric garvitational-wave detectors*," Class. Quantum Grav. **29**, 205005 (2012)
[18] eLISA Telescope In-Field Pointing and Scattered Light Study *http://www.physik.uzh.ch/events/lisa2016/uploads/156/in-field_pointing_and_stray_light_LISA_Symp_final2.pdf*

For additional information, contact Jeffrey Livas: *Jeffrey.Livas@nasa.gov*

Directly Deposited Optical-Blocking Filters for Imaging X-ray Detectors

Prepared by: Mark Bautz (PI; MIT Kavli Institute for Astrophysics and Space Research, MKI); S. Kissel (MKI); K. Ryu and V. Suntharalingam (MIT Lincoln Laboratory); and M. Chodas and S. Megerssa (MIT Space Sciences Laboratory, SSL); with special thanks to R. Masterson and the SSL's REXIS team.

Summary

We aim to raise the Technology Readiness Level (TRL) of enhanced charge-coupled-device (CCD) detectors capable of meeting the requirements of X-ray grating spectrometers (XGS) and wide-field X-ray imaging instruments for small, medium, and large missions. Because they are made of silicon, all X-ray CCDs require blocking filters to prevent corruption of the X-ray signal by out-of-band, mainly optical and near-infrared (near-IR) radiation. We endeavor to replace the fragile, extremely thin, free-standing blocking filter that is current standard practice with a much more robust filter deposited directly on the detector surface.

High-performance, back-illuminated CCDs have flown with free-standing filters (e.g., one of our detectors on Suzaku), and other relatively low-performance CCDs with directly deposited filters have flown (e.g., on the X-ray Multi-mirror Mission-Newton, XMM-Newton; Reflection Grating Spectrometer, RGS). However, a high-performance, back-illuminated CCD with a directly deposited filter has not yet been demonstrated. Our effort will be the first to show such a filter can be deposited on an X-ray CCD that meets the requirements of a variety of contemplated future instruments.

This Strategic Astrophysics Technology (SAT) project, a collaboration between the MKI and MIT Lincoln Laboratory, began July 1, 2012 and is scheduled to end on June 30, 2018.

Background

The past two decades have brought extraordinary progress in X-ray astronomy, in large measure as a result of unprecedented improvements in X-ray imaging and grating spectroscopy. Beginning with the launch of the Advanced Satellite for Cosmology and Astrophysics (ASCA) in 1993, and continuing to the present, concurrent operation of Chandra, XMM-Newton, and Swift, much of this success has been enabled by X-ray photon-counting CCDs. Advanced CCDs and emerging silicon detectors such as active pixel sensors (APS) will likely remain essential to X-ray astronomy for decades. In the relatively near term, the extended ROentgen Survey with an Imaging Telescope Array (e-ROSITA) and the X-ray Astronomy Recovery Mission (XARM), will feature silicon CCDs. Instruments using CCDs or APS X-ray detectors are also baselined for both Athena and Lynx, the only two strategic high-energy astrophysics missions now in development or under study by NASA. These instruments address a broad range of important scientific objectives. For example, as noted in the X-ray Mission Concepts Study Report commissioned by NASA's Program Office for the Physics of the Cosmos (PCOS) [1], several high-priority scientific questions identified by the 2010 Decadal Survey, "*New Worlds, New Horizons in Astronomy and Astrophysics*" (NWNH) [2] are best addressed by an XGS, which requires large-format X-ray imaging detectors. Specific science goals for XGS and wide-field imaging instruments are also identified in NASA's Astrophysics Roadmap "*Enduring Quests, Daring Visions*" [3], with examples listed in Table 1. As a result, both an XGS and a silicon-based, high-definition X-ray imager (HDXI) are key

instruments for Lynx* [4]. For these reasons, technology development for XGS (in 2012) and HDXI (in 2016) has been ranked as a Priority 1 (highest priority) need in recent PCOS Program Annual Technology Reports (PATRs) [5].

Science Question	Measurement	Instrument
How did the first supermassive black holes form?	Find and characterize the seeds of supermassive black holes at very high redshift, and trace their growth	HDXI
How did large-scale structure and baryons co-evolve in the local universe?	Find and characterize the missing baryons in hot galaxy halos and the Warm-hot Intergalactic Medium (WHIM) via absorption spectroscopy	XGS
	Characterize the diffuse baryons in the first virialized galaxy groups	HDXI
How do black hole feedback processes affect galaxy structure and evolution?	Understand black hole accretion physics and quantify energy and mass content in Active Galactic Nuclei (AGN) outflows	XGS

Table 1. *High-priority science drivers for future instruments featuring large-format, imaging X-ray detectors (adapted from the PCOS X-ray Mission Concepts Study Report [1] and the Astrophysics Roadmap [3]). Directly deposited optical blocking filters (OBF) will improve detection efficiency, especially in the soft-X-ray band, while reducing cost and risk of instruments addressing these questions.*

Large-format, X-ray imaging detectors are also required for many missions envisaged for the Explorer program, which NWNH deemed "*a crown jewel of NASA space science*." For example, an Explorer XGS has been proposed for a focused study of the cycles of baryons in and out of galaxies, and their role in galaxy evolution [6]. Other future Explorers will exploit the power of rapid-response X-ray imaging, so clearly demonstrated by Swift, but with much wider fields of view. As noted in [7], a wide-field X-ray imaging instrument on an agile spacecraft can address with unprecedented sensitivity a variety of important science objectives ranging from the nature of the first galaxies to high-energy, time-domain astrophysics. An especially exciting prospect is identification of sources that may be detected by ground-based gravitational-wave observatories later in this decade [8, 9].

Our program aims to raise the TRL of advanced OBF technology required for these instruments. If successful, our effort will improve instrument sensitivity, robustness, and reliability. At the same time, it will reduce mass, complexity, risk, and cost. Our approach is to replace the fragile, free-standing, optical-blocking membrane of current practice with a filter deposited directly on the detector surface. A directly deposited filter can be thinner than a free-standing one, improving instrument sensitivity. Moreover, directly deposited filters do not require the heavy, complex, and expensive vacuum housings used in current instruments, and are of course much more robust than free-standing filters. The key challenge for our program is to demonstrate that blocking filters can be applied directly to the sensitive entrance surfaces of modern CCD detectors without compromising spectroscopic resolution.

To minimize cost, our program uses existing stocks of engineering-grade detectors produced for past programs at MIT Lincoln Laboratory. We apply so-called 'back-illumination' (BI) processing to these detectors, and then use coating facilities at Lincoln to apply blocking filters. X-ray and optical performance-testing is then conducted at MKI. We have also joined forces with REgolith X-Ray Imaging Spectrometer (REXIS), an MIT student instrument for NASA's Origins Spectral Interpretation Resource Identification Security – Regolith Explorer (OSIRIS-REx) mission, to incorporate directly deposited blocking-filter technology into a flight program.

* Lynx scientific objectives in particular, require maximum detection efficiency in the soft-X-ray band (E <0.5 keV) and, as explained below, directly deposited optical blocking filter technology offers substantial improvements in this critical instrument capability.

Objectives and Milestones

Silicon X-ray imaging detectors require blocking filters to prevent ambient visible and ultraviolet (UV) background light from adding noise and degrading X-ray spectral resolution. As noted above, most such detectors flown to date have used fragile, free-standing filters comprised of thin plastic substrates coated with aluminum. Free-standing filters usually must be protected from ground-handling and launch acoustic loads using heavy vacuum enclosures equipped with complex door mechanisms. This project aims to show that adequate OBFs can be deposited directly on a detector, eliminating the need for fragile, freestanding filters. To the extent that they eliminate plastic films, such filters could also improve soft-X-ray (E <1 keV) detection efficiency.

A key challenge in this project is to demonstrate that directly deposited OBFs provide the requisite optical blocking performance without compromising the spectral resolution of the detectors in the soft band. The latter depends critically on the electric fields present just inside the entrance surface of the detector, and these fields in turn require precisely controlled implant-density profiles. Our aim is to deposit blocking filters in such a way that the surface fields are unaffected by the deposition process or the filter itself. A secondary objective is to demonstrate that such filters are sufficiently robust to survive the repeated thermal cycling any such detector is likely to experience.

Originally, we planned to complete the following four tasks:

Task 1: Select and thin existing CCID41 wafers and apply backside treatment

The target detectors for this project (Lincoln Laboratory model CCID41, now in use in Suzaku) were stored in wafer form as front-illuminated (FI) devices (typically four to a wafer). We identify functional devices using wafer-probe equipment. We then subject selected wafers to a custom, backside treatment process, involving wafer thinning and molecular-beam-epitaxy (MBE) passivation, which has already been shown to provide good X-ray results. Selected BI devices are packaged (removed from the wafer and installed in suitable test packages) for subsequent test at MKI.

Task 2: Establish baseline X-ray performance

We use established X-ray characterization facilities and procedures at MKI to verify suitable X-ray performance of the BI (but uncoated) devices.

Task 3: Apply filters and characterize filter-equipped devices

We deposit aluminum blocking layers using established thin-film deposition facilities at MIT Lincoln Laboratory, and then package and test the filter-equipped devices. Filters are applied at the wafer level, with control areas masked to allow direct comparison of filtered and unfiltered areas of each device. We contemplate three cycles of filter deposition and test (one wafer per cycle), applying a relatively thick filter in the first cycle, and then continuing, after successful test, to progressively thinner filters. In so doing, we span the range of filter thicknesses required by future instruments. All filters will be capped with a 10-nm Al_2O_3 layer to improve robustness and provide UV blocking. Both optical rejection and X-ray spectral resolution will be measured in the characterization protocol.

Task 4: Test robustness and stability

To verify coating temporal stability and robustness to the repeated thermal cycling experienced by CCD detectors during instrument development and test, we will perform thermal cycling and long-term (6-8 months) stability measurements.

Soon after program start, we decided to alter the sequence of the program for two reasons. First, we discovered that a number of BI devices were already available at MIT Lincoln. To make best use of these, we needed to develop a filter deposition process that would accommodate individual chips as well as full wafers. Second, we learned that the MIT team developing REXIS wished to fly X-ray CCDs with directly deposited blocking filters. We decided to collaborate with REXIS because by doing so we gain the opportunity to demonstrate much higher TRL for our process than we could achieve in our original program. Indeed, as discussed below, through this collaboration, and with the support of the PCOS Program Office, we have defined a clear path to demonstrating that this technology has achieved TRL 6.

Major milestones and our progress in achieving them are summarized in Table 2. We describe our progress in more detail in the following section.

Milestone at completion of:	Success Criteria	Status as of June 2017
1. BI processing	Wafer-probe testing of BI wafers shows: • ≥3 wafers with functional devices • ≥10 functional devices total	• Twelve FI wafers processed, yielding 33 devices with at least some functionality, of which eight are allocated to REXIS • Ten other functional BI devices identified as single chips
2. X-ray test of baseline BI device	X-ray performance demonstrated per protocol specified in proposal	• Complete; X-ray performance supports program objectives
3. 1st device with thickest directly deposited filter	Packaged device delivered to MKI	• Complete (220-nm-Al OBF)
4. X-ray and optical testing of device with thickest filter	X-ray and optical tests done per protocol specified in proposal	• Complete; three devices with 220-nm OBF characterized
5. X-ray and optical testing of device with thinnest filter	X-ray and optical tests done per protocol specified in proposal	• Complete; one device with 100-nm OBF and two with 70-nm OBF characterized
6. Long-term stability test	X-ray and optical tests done per protocol specified in proposal	• Eight-month test completed
7. Thermal cycle test	X-ray and optical tests done per protocol specified in proposal	• Thermal vacuum (TVAC) X-ray testing of REXIS flight unit completed; X-ray performance of OBF unaffected; optical performance of OBF not measured • Detailed test plan completed and approved by PCOS for TRL-6 demonstration with REXIS flight spare detector; includes TVAC and vibration; test facilities assembled and calibrated

Table 2. *Project milestones and status.*

Progress and Accomplishments

We have developed an OBF deposition process and thoroughly characterized X-ray and optical performance of BI CCDs with OBFs of a range of thicknesses (220-, 100-, and 70-nm Al) as specified in Milestones 1-7 in Table 2. Details of our process and principal results have been presented in the literature [10, 11] and may be summarized as follows.

1. We demonstrated that it is feasible to deposit effective aluminum OBFs directly on high-performance BI CCDs with at most modest effect on X-ray spectral resolution.
2. The measured X-ray transmission of these OBFs is consistent with theoretical expectations.
3. The measured visible/near-IR transmission of these OBFs is consistent with the expected level of attenuation over most of the filter area, but higher than expected transmission is observed in a small fraction of pixels. The pixels exhibiting these so-called "pinholes" can have sensitivity to visible light that is 10× to 1000× theoretical expectations. We find evidence that these pinholes are produced by irregularities on the detector surface. These irregularities, each extending over at most a few

hundredths of a square micron of detector surface, seem to cause small breaks in the aluminum blocking layer. The irregularities in turn may be caused either by intrinsic roughness of the CCD surface or by sub-micron particulate contamination. The fraction of pixels exhibiting pinholes can be reduced to 1% or less by (i) minimizing the density of sub-micron particles on the detector surface before aluminization, and (ii) suitably orienting the detectors relative to the aluminum source during OBF deposition.

4. For very demanding optical-blocking applications, requiring visible/IR-band attenuation factors greater than 10^6, we found that it may be necessary to take additional steps to prevent light from entering the detector through its sidewalls and through the adhesive layer that affixes the detector to its package. We developed methods for doing this for the REXIS instrument.
5. Results from our long-term stability tests show no change in visible/IR blocking performance of a directly deposited OBF after eight months of storage in a laboratory environment.
6. In collaboration with the OSIRIS-REx/REXIS instrument team, and with the support of the PCOS Program Office, we have extended our project goals from the originally proposed thermal testing (Milestone 7 in Table 2 above) to include a demonstration that our OBF technology has achieved TRL 6. Although REXIS is now aboard OSIRIS-REx and cruising toward its asteroid rendezvous, the flight instrument's OBF will not be tested until early 2019 when the REXIS door is to be opened. Before launch, the flight instrument completed environmental testing with successful X-ray performance, but it was not possible to verify the post-test visible-band performance of its OBFs. Therefore, to demonstrate TRL 6, we have engaged MIT graduate and undergraduate students to plan, develop facilities for, and execute an environmental test program with the REXIS flight spare detector assembly mount (DAM). This plan has been presented to and approved by PCOS technology managers as acceptable for a TRL-6 demonstration. As of this writing, we have just begun to execute this plan. In this way, our technology development program is also providing a valuable educational opportunity for MIT students.

We discuss each of these results in turn.

1. Soft-X-ray spectral resolution with directly deposited blocking filters

Soft X rays (with energies below 1 keV) are photo-electrically absorbed within ~1 μm of the entrance surface of a silicon detector, so good X-ray spectral resolution requires efficient collection of photoelectrons generated in this region. Precise doping of the entrance ('back') surface of the detector is necessary to produce the internal electric fields required to achieve this. We aimed to determine whether a metal OBF layer deposited directly on this surface would affect the spectral resolution of an X-ray CCD detector. Figure 1 shows a broadband, multi-line pulse-height spectrum obtained from a back-illuminated CCD with a directly deposited, 220-nm-thick OBF. The spectrum shows that such a detector (similar to those installed on REXIS) can readily resolve characteristic lines of elements ranging from oxygen to iron.

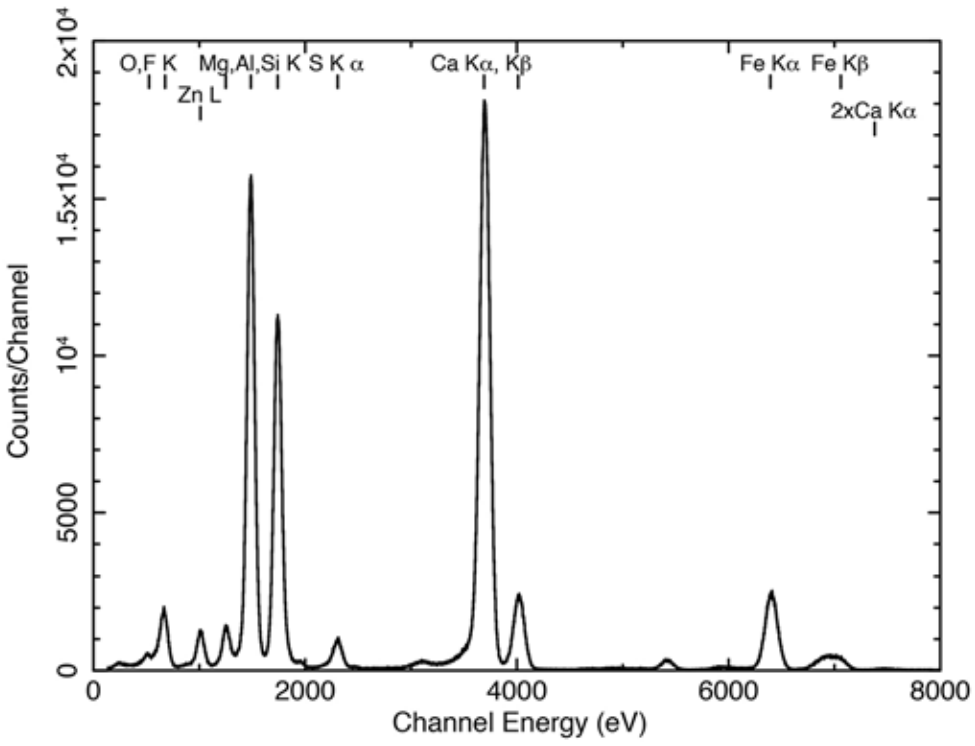

Fig. 1. *Broadband, composite pulse-height spectrum from a BI CCD equipped with a directly deposited 220-nm-thick aluminum OBF [device 53-1-7-1]. Characteristic lines of elements ranging from oxygen to iron are readily resolved.*

How does a directly deposited OBF affect CCD spectral resolution at very soft (E <1 keV) energies? Figure 2 addresses this question by comparing pulse-height spectra from three representative devices. The back surfaces of all of these detectors were treated with MIT Lincoln Laboratory's MBE process. One device has no OBF, and the other two have directly deposited aluminum OBFs with thicknesses of 70 nm and 220 nm, respectively. Identical exposure times to the same radioactive X-ray source were used to obtain the spectra. The source produces characteristic lines of C-K, V-L, O-K, and F-K, with energies ranging from 277 eV to 677 eV. As expected, X-ray absorption in the filters reduces the amplitudes of the lower-energy peaks. Figure 3 compares peak widths (full-width at half-maximum, or FWHM) measured for different spatial regions, called quadrants, on each device. Each device quadrant has a dedicated on-chip amplifier. These are engineering-grade devices, so the noise levels, and thus the expected peak widths, differ from quadrant to quadrant. The points in Fig. 3 for the unfiltered ('No-OBF') and '220-nm-OBF' cases show the mean, minimum, and maximum of three device quadrants in each configuration. The 70-nm-OBF points show results for a single quadrant. The means of the unfiltered and 220-nm configurations are closer than the quadrant-to-quadrant scatter within each configuration, and the single-quadrant measurements available from the device with the 70-nm OBF are marginally better than any of the quadrants on the other two devices at all three energies. Thus, we find no evidence that the directly deposited OBF compromises the soft-X-ray FWHM of these detectors.

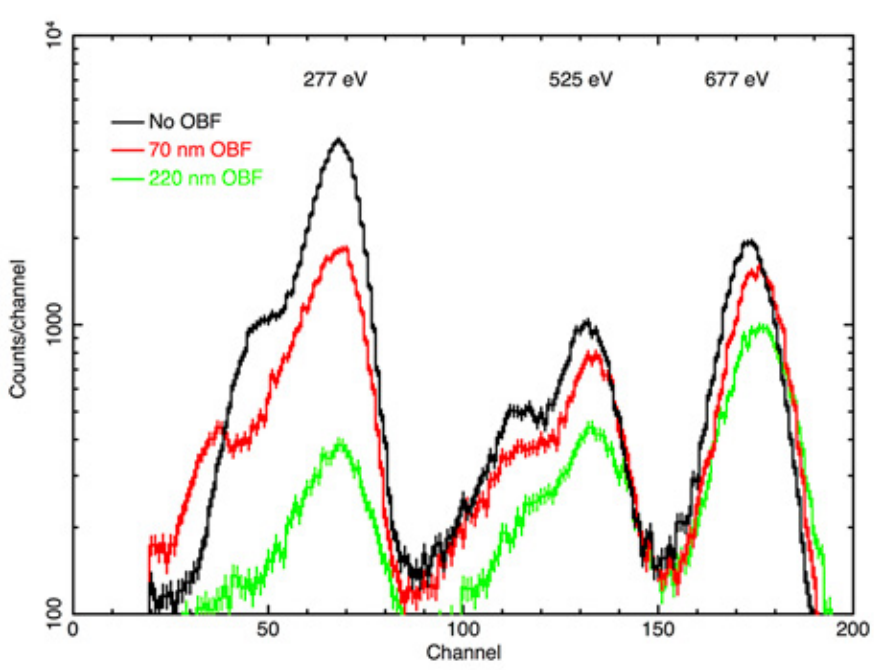

Fig. 2. *Soft-X-ray response of a device with no OBF (black) and with 70-nm- and 200-nm-thick directly deposited aluminum filters (red and green, respectively). The filters have very little effect on spectral resolution.*

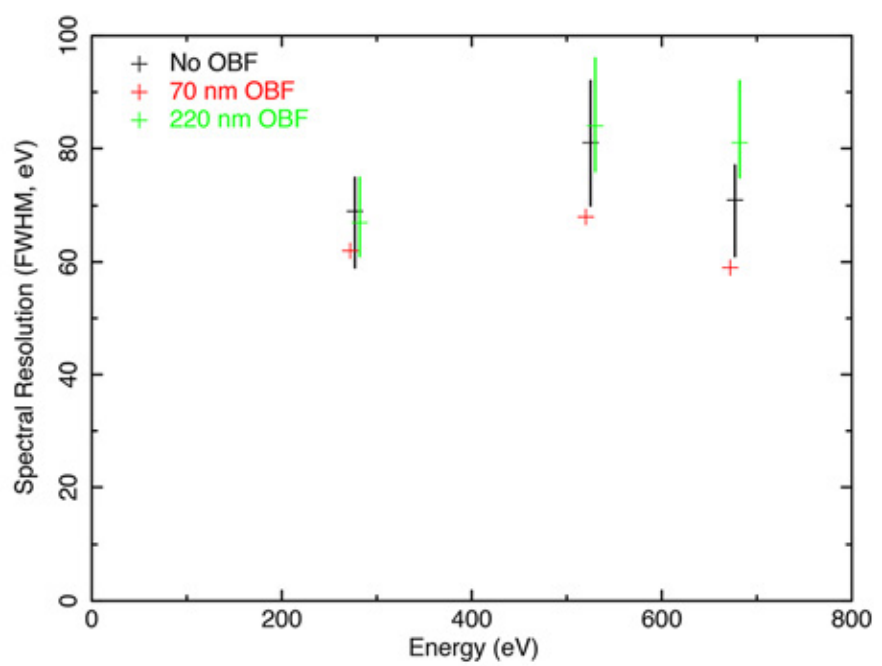

Fig. 3. *Spectral resolution (FWHM) of devices with no OBF (black), 70-nm-aluminum OBF (red), and 220-nm-aluminum OBF (green). "No-OBF" and "220-nm-OBF" points show mean, minimum, and maximum FWHM measured for three independent CCD quadrants in each configuration; 70-nm points show measurements for a single CCD quadrant. The OBFs have no clear effect on spectral resolution. Energy coordinates have been displaced slightly to show the ranges in FWHM clearly.*

Returning to Fig. 2, it is clear that shape of the spectral redistribution function of all devices degrades to some extent at the lowest energies. At 677 eV, the response function is quite symmetrical for all three devices. Near 500 eV, the blend of vanadium-L and oxygen-K lines produced by the source is evident, and this blend makes it difficult to assess the shape of the response function there. The responses of all three devices at 277 eV show a clear low-energy shoulder. The ratio of main-peak to shoulder amplitudes (about 5:1) is about the same for all devices, suggesting that the shoulder is due neither to the source spectrum nor to the presence of the OBF. We hypothesize the tail is a consequence of the relatively thick (20 nm) p^+ MBE layer applied in fabricating these devices. About 15% of the incident photons at this energy will be absorbed in the MBE layer. A thinner MBE layer might thus be expected to provide better charge collection for very-soft-X-ray photons. We find no evidence that the shape of the response function is affected by the presence of the OBF.

2. X-ray transmission of directly deposited OBFs

Measured X-ray transmission of a 70-nm-thick OBF is compared to expectations in Fig. 4, with generally good agreement. The data were obtained from a device (53-1-4-2) on which only part of the detector was covered by the OBF. Both covered and uncovered regions were exposed to a multi-line source like the one used to produce the spectra in Fig. 1, and transmission was determined from the line fluxes measured in the two regions. The red circles show measurements obtained by fitting Gaussian profiles to the data. Green crosses show fluxes obtained by summing over a spectral region within ±3 standard deviations of line centers. The two methods agree reasonably well, except at the very lowest energy measured (183 eV) where the line profiles are distinctly non-Gaussian. Similarly, good agreement between measurements and expectations is obtained with 200-nm OBFs (see [10] for details).

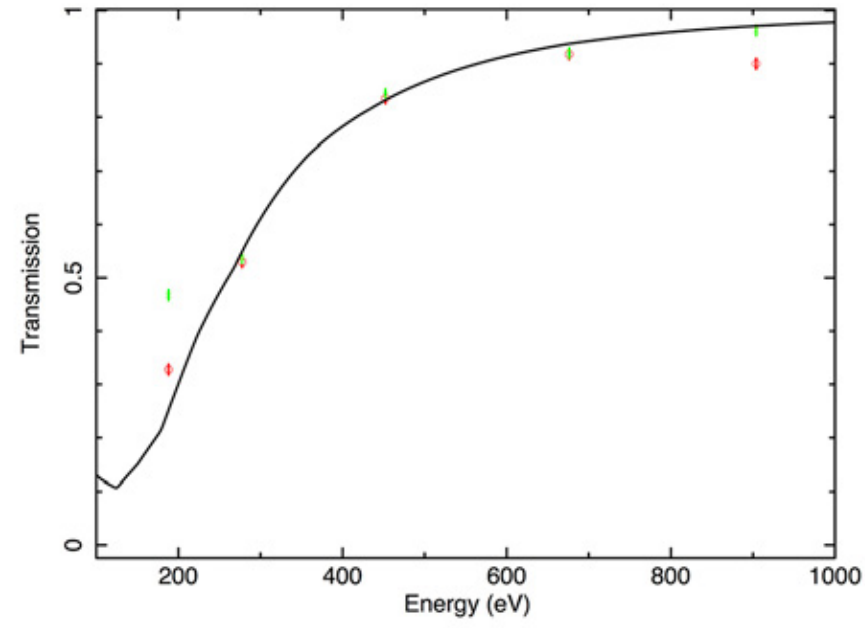

Fig. 4. *Measured (points) and modeled (curve) X-ray transmission of 70-nm-thick aluminum OBF. Red and green points obtained with different X-ray measurement methods discussed in the text.*

3. Visible/near-IR transmission of directly deposited OBFs

Figure 5 shows the measured visible-band quantum efficiency (QE) of a device with a directly deposited blocking filter with a nominal thickness of 70 nm. The measurements agree reasonably well with a simple model of an aluminum layer over a thick silicon substrate. The aluminum thickness in the model has been adjusted to 63 nm to fit the data. The model assumes perfect internal CCD QE, which is certainly an overestimate redward of 600 nm, as the (thinned) detector's sensitive volume (depletion region) is nominally 45 microns thick. A more sophisticated model, incorporating an accurate treatment of the internal detector efficiency, is clearly required to represent the data in the near-IR spectral band. The present results may indicate the OBF is somewhat more transparent in this spectral band than the simple model predicts.

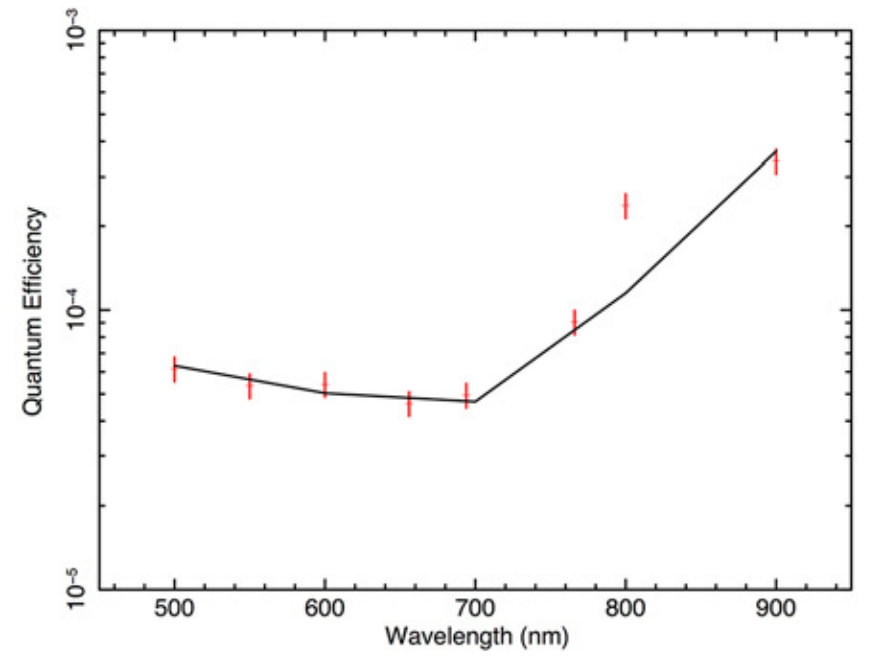

Fig. 5. *Visible/near-IR QE of a CCD with a directly deposited blocking filter. Nominal filter thickness is 70 nm. The points are measured values; the line is a simple model of a 63-nm-thick OBF. Note: data from device 53-1-4-2.*

Visible-band, flat-field exposures with both 220-nm-thick and 70-nm-thick OBFs show "pinhole-like" regions of relatively high transmission, as shown in Fig. 6. The image on the left shows pinholes in a 220-nm-thick OBF. The device was exposed to a fluence of 1.3×10^{6} photons/pixel at 800 nm. A histogram of the 440,000 pixel amplitudes in the image is shown in the right panel. The theoretically expected transmission of this OBF at this wavelength is less than 10^{-9}, so if the OBF was perfect, all pixels would have zero amplitude, modulo the readout noise with root-mean-square (rms) width of a few electrons. The histogram shows that 99% of pixels are in fact consistent with zero amplitude, and about 1% of pixels are affected by pinholes with transmission ranging from about 10^{-6} to as high as 5×10^{-4}.

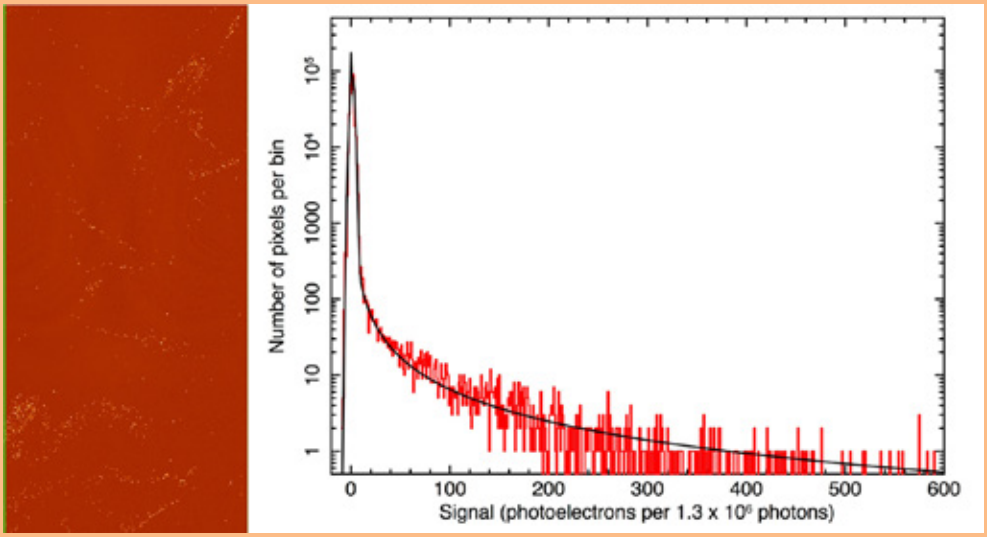

Fig. 6. Left: *Image obtained using CCD with a 220-nm-thick OBF illuminated with 1.3×10^6 photons/pixel of 800-nm light. Pinholes (white spots) are evident.* Right: *Histogram of amplitudes of the 440,000 pixels in the image on the left. While 99% of pixels are in the peak, consistent with zero amplitude, about 1% show transmission greater than 10^{-6}.*

Wafer-level measurements at MIT Lincoln Laboratory of other devices equipped with 220-nm-thick OBFs show an extinction ratio of 10^{13} at 633 nm, except in the small fraction of pixels affected by pinholes [11]. The inferred absorption coefficient is 1.3×10^6 cm^{-1}, close to the expected value of 1.5×10^6 cm^{-1} [12], confirming the high quality of the OBF film as a whole.

As discussed in detail in [10] and [11], we believe the pinholes are caused by surface irregularities present on the detector surface before the OBF is deposited. Several lines of evidence support this explanation. First, test coatings on quartz substrates do not show pinholes. Second, as shown in Fig. 7, scanning electron micrographs of deposited OBFs show texture with sizes (<100 nm) and spatial density consistent with the observed number and transmission of pinholes. Third, the number of pinholes is dramatically reduced if an optically transparent, 1-μm-thick layer of photoresist is deposited on the detector surface before the aluminum OBF layer is deposited. Although such an interlayer is opaque to soft X rays and so could not be used on an X-ray sensor, this result does suggest there are no fundamental limitations to fabrication of a pinhole-free, directly deposited OBF.

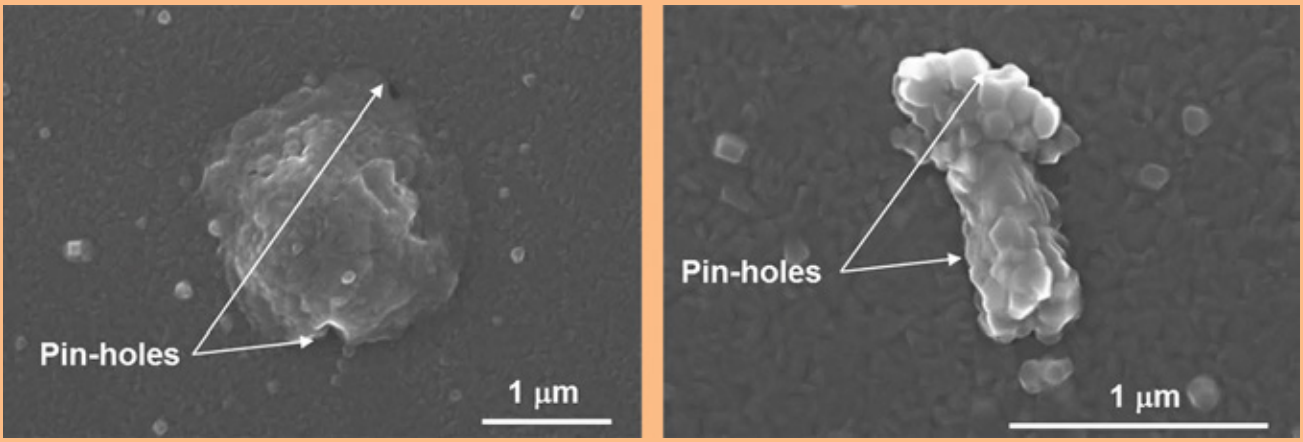

Fig. 7. *Scanning electron micrograph images of an OBF directly deposited on the surface of a CCD.*

Indeed, our success in reducing the pinhole fraction to less than 1%[†] for REXIS OBFs is further evidence in favor of this explanation for the origin of pinholes. Two measures in particular have proven effective. First, the interior surfaces of the coating chamber were aluminized after cleaning, to minimize particulate contamination originating in the chamber walls. Second, the deposition geometry was changed so that the incident aluminum atoms approach the detector surface at about 45° to the surface normal. The detector rotates about its surface normal during this process. This 'angled-deposition' allows the aluminum to cover the vertical sides as well as the tops of residual surface irregularities, and thus reduces the number of pinholes.

4. Detector sidewall and bond-line leakage paths

The thickest OBF layers we tested, with 220 nm of aluminum, have a theoretical attenuation well in excess of a factor of 10^9. The REXIS instrument, which will map fluorescent X-ray emission from the sunlit surface of asteroid RQ36, requires substantial optical blocking and is equipped with filters of this thickness. Our evaluation of directly deposited OBFs of this thickness revealed that to achieve very large attenuation (greater than a factor of ~10^6), one must block not only the light entering the entrance surface of the detector, but also light entering its thin side walls and even its mounting surface.

The effect and location of these leakage paths are illustrated in Fig. 8. The left panel shows a grayscale image obtained by illuminating a CCD with a 220-nm-thick OBF. The white areas around the edges of the device have an attenuation factor of 10^7 or less. The right panel shows two leakage paths responsible for this effect. Light can enter the photosensitive regions of the device through its thin (45-µm-thick) sidewalls. Light can also penetrate the thin (~10-µm-thick) epoxy bond-line that attaches the CCD to the (photo-insensitive) silicon support wafer. A third leakage path, similar to the second but not shown in the figure, runs through a second, thicker epoxy bond-line that attaches the support wafer to the detector package, through the support wafer and into the detector from below. This third leakage path transmits mainly near-IR radiation to which the support wafer is relatively transparent.

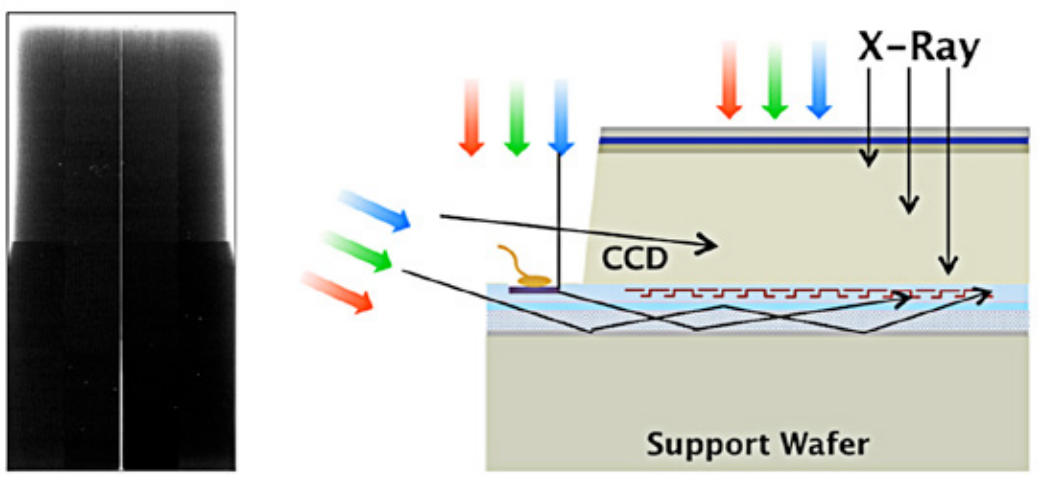

Fig. 8. *Edge and 'bond-line' leakage.* Left: *A CCID-41 with a directly deposited blocking filter under flood illumination. White areas around edges have attenuation < 10 [7], and are due to light entering the sides and back of the detector.* Right: *Illustration of two leakage paths.*

[†] Specifically, the mean fraction of pixels with optical density less than 7 (i.e., with pinholes) in 220-nm-thick OBFs in the 12 best REXIS flight devices is 0.76%; the rms pinhole fraction in this sample is 0.45%. An anomalous 13th device showed a pinhole fraction of 4.1%. See [11] for details.

Leakage through the two paths shown in Fig. 8 was reduced to levels acceptable to REXIS by depositing an additional 100 nm of aluminum using the angled-deposition geometry described in the previous section. This coating covers the detector sidewalls and the bond-line between the detector and the support wafer. In addition, the REXIS team qualified two effective countermeasures against bond-line leakage at the bottom of the support wafer. One method was to coat the bottom of the support wafer with black paint, using a suitable adhesion promoter. The other method was to deposit a 300-nm-thick aluminum layer on the bottom surface of the support wafer. REXIS has adopted the latter approach because it permits a flatter surface coating that can be applied more quickly.

5. Long-term stability of directly deposited OBFs

The final task in our original program is to evaluate the long-term stability of directly deposited OBFs. We began this process in September 2014 with a baseline evaluation of device 53-1-17-2, which is equipped with a 100-nm-thick OBF. We monitored this device over a period of eight months and did not detect any significant change in OBF performance. In particular, Fig. 9 compares pinhole maps obtained for this device before and after eight months of laboratory storage. The images have been scaled to correct for light-source-intensity differences so that the mean of the amplitudes of a set of randomly selected pinhole pixels is the same in both images. To date, we find no evidence for change over time in the optical blocking properties of this OBF.

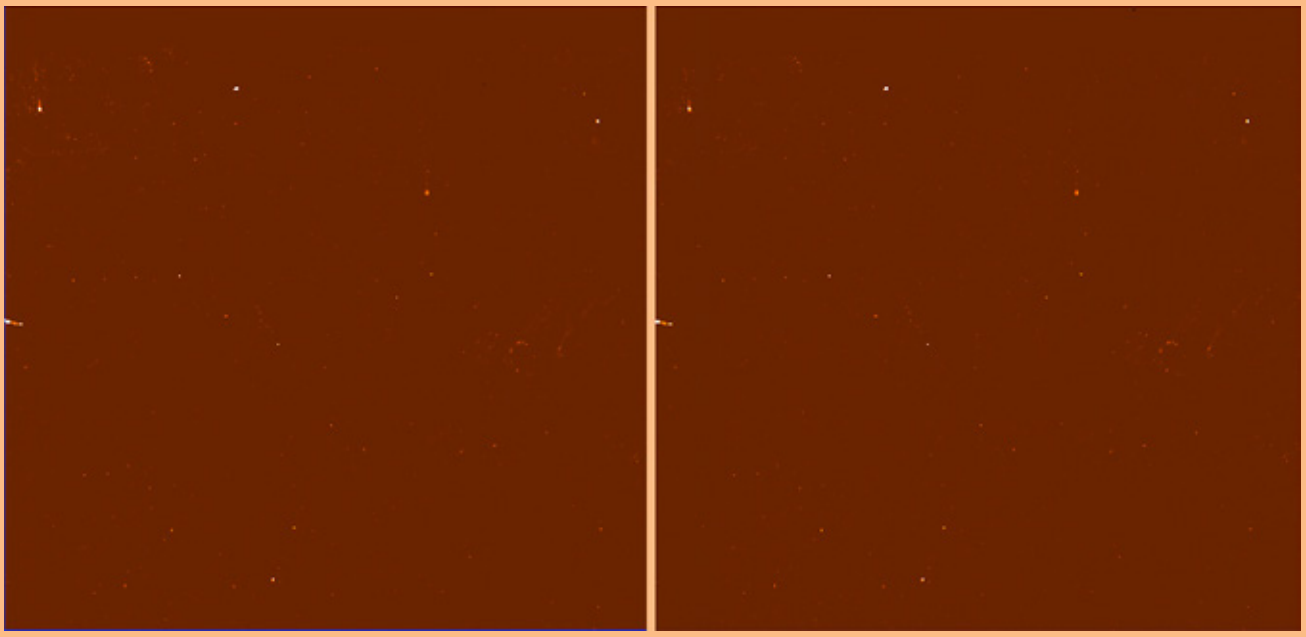

Fig. 9. *Pinhole maps of a randomly chosen 400×400 pixel section of CCD 53-1-17-2 equipped with a 100-nm-thick directly deposited aluminum OBF, obtained in September 2014 (left) and June 2015 (right). These images demonstrate the stability of the OBF over an eight-month period of laboratory storage.*

6. Plan for TRL-6 demonstration with the REXIS flight spare DAM

Graduate and undergraduate students in MIT's Department of Aeronautics and Astronautics on the REXIS team, supervised by the REXIS project manager, developed a plan to demonstrate that our OBF technology is at TRL 6. The students presented this plan to PCOS Program Office technology managers who judged it suitable, after some modification, for this purpose. Here we summarize the key elements of the plan and our progress toward its execution.

Objectives and environments: The principal goal of the demonstration is to characterize the effect of environmental stresses on the performance of directly deposited OBFs in the REXIS flight spare DAM (Fig. 10), with particular emphasis on environmental effects on the number and characteristics of pinholes in the OBFs. Given our finding that these pinholes are caused by surface irregularities on the detector surface, the team decided that thermal cycling and vibration tests are relevant, but that electromagnetic environments are not. The relevance of atomic oxygen was discussed with PCOS technologists, and it was concluded that for sufficiently high-altitude ("interplanetary") mission trajectories like that of OSIRIS-REx, atomic oxygen is not relevant. The effects of atomic oxygen on directly deposited OBFs may be relevant for low-Earth-orbit missions.

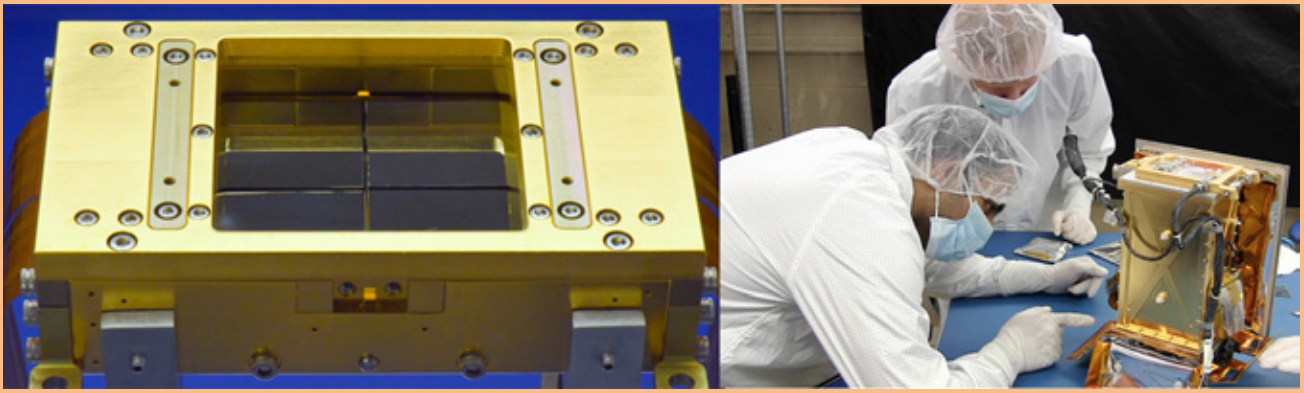

Fig. 10. Left: *The REXIS DAM features four MIT/Lincoln CCDs, each with a directly deposited OBF. The total active area of the detectors is about 5 cm × 5 cm.* Right: *Students preparing the REXIS instrument for environmental testing. We plan an Undergraduate Research Opportunities Program (UROP) project using REXIS engineering-model hardware to demonstrate that directly deposited OBF technology is at TRL 6. Images courtesy of MIT Lincoln Laboratory and MIT Space Sciences Laboratory.*

Performance characterization: The set of OBF performance measurements made at each phase of the test is referred to as the 'light-leak test.' Two datasets ('X ray only' and 'X ray plus optical flood') are taken in each light-leak test. A radioactive ^{55}Fe X-ray source (producing 5.9-keV and 6.4-keV photons) and a calibrated 633-nm laser source (nominal flux of 10^{15} photons s^{-1} cm^{-2}, or ~6×10^{9} photons $pixel^{-1}$) illuminate one quarter of the focal plane during data acquisition. Three different performance metrics are to be extracted from these data. Large-area optical performance (LAOP) is simply the number of pinholes detected above a threshold within the illuminated region, as determined by comparing the two datasets. Pinholes can be discriminated from X-ray events based on amplitude, and, if necessary by exploiting the random, frame-to-frame variation of X-ray event locations. Pixel optical density (POD) is to be computed for each identified pinhole from the ratio of detected signal to incident (optical) photon flux. A decrease in POD after environmental exposure would indicate that a pinhole had grown. Finally, pinhole density (PD), the fraction of illuminated pixels that have pinhole of a particular density, is to be computed as a function of pinhole optical density. In addition to these optical performance metrics, the X-ray spectral resolution of the detectors will be monitored.

Test levels and sequence: Test levels were chosen in accordance with the NASA General Environmental Verification Standards (GEVS). REXIS is expected to operate at temperatures between -60°C and -90°C, so the thermal cycle test will consist of eight cycles between -50°C and -100°C. Integrated vibration levels of 14.1 g rms over 20-2000 Hz, with a spectrum specified in GEVS, will be applied consecutively on each of three axes. The test sequence is shown in Fig. 11.

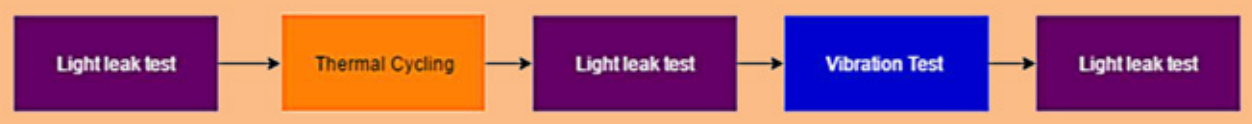

Fig. 11. *TRL-6 demonstration test flow.*

Status: As of this writing, all facilities required for the test, including the thermal vacuum chamber and optical light source and associated calibration equipment, are operational. Existing facilities at MIT Lincoln Laboratory have been identified for use in the vibration test. The flight-spare REXIS DAM has been successfully operated at temperature in the thermal vacuum chamber, and the calibrated light source has been used to obtain baseline pinhole maps (Fig. 12). We expect to complete the TRL-6 demonstration in the coming academic year.

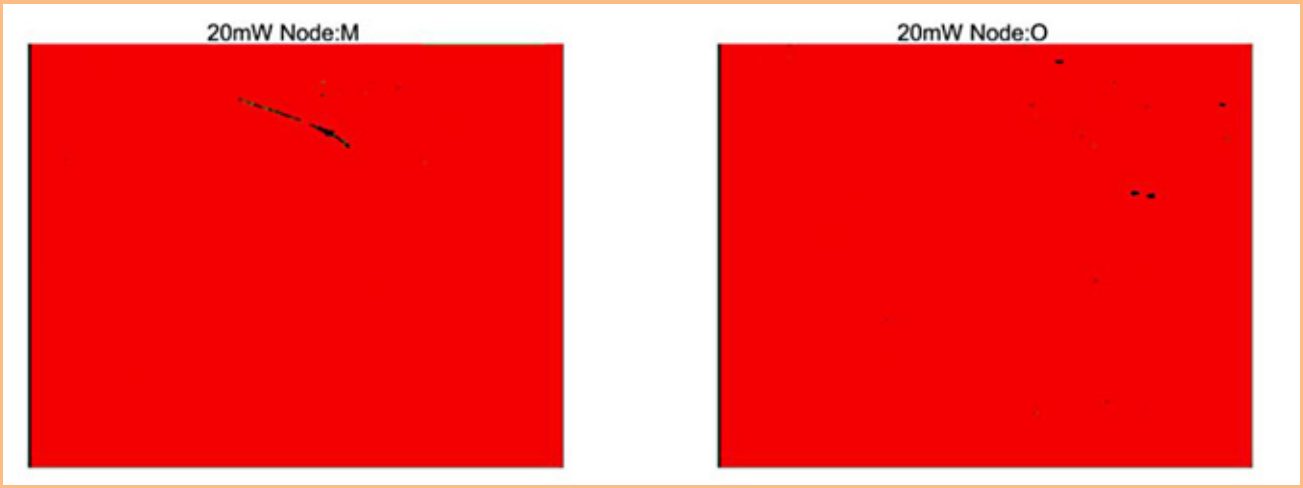

Fig. 12. *Baseline (pre-environmental) pinhole maps obtained from the REXIS flight spare detector mount with our TRL-6 test set. The images were obtained from two of the 16 independent sectors ('nodes') of the focal plane, and are shown here in high contrast with the pinholes in black. Illumination is from a 633-nm laser operating at 20 mW, fed via a fiber-optic link into the thermal vacuum chamber.*

Summary

We have demonstrated that directly deposited aluminum OBFs are compatible with high-performance BI X-ray CCD detectors. The techniques we developed may be used to deposit OBFs directly on other BI silicon X-ray detectors as well. We have developed deposition methods that minimize the number of pinholes in such filters, and demonstrated high-quality filters ranging from 70 nm to 220 nm in thickness. We have also developed effective countermeasures against light leakage through the sidewalls and packages of such detectors, having found these to be necessary for applications requiring filters with optical density greater than ~6. We have published our findings in the refereed literature [11].

The OBF technology we developed has been incorporated in the flight model of the REXIS instrument on OSIRIS-REx. In collaboration with the REXIS team and the PCOS Program Office, we have extended our program goals to include a demonstration that directly deposited OBFs have achieved TRL 6. We have enlisted MIT engineering students who have planned and begun to execute this demonstration, and expect it to be completed in the coming academic year.

References

[1] X-ray Community Science Team, X-ray Science Support Team, and X-ray Engineering Support Team, "*X-ray Mission Concepts Study Report*" (2012)

[2] National Academy of Science, Board on Physics and Astronomy, "*New Worlds, New Horizons in Astronomy and Astrophysics*" (2010)

[3] NASA Astrophysics Roadmap Team, C. Kouveliutou, Chair, "*Enduring Quests, Daring Visions: NASA Astrophysics in the Next Three Decades*" (2013)

[4] M. Weisskopf et al., "*Beyond Chandra – The X-ray Surveyor*," Proc. SPIE 1505.00814 (2015)

[5] NASA Physics of the Cosmos Program Office, "*NASA Physics of the Cosmos Program Annual Technology Report*" (2012, 2016)

[6] R. Smith et al., "*Arcus: an ISS-attached high-resolution X-ray grating spectrometer*," Proc. SPIE **9144**, id. 9144Y, (2014)

[7] N. Gehrels, S. Barthelmy, and J. Cannizzo, "*Time-Domain Astronomy with Swift, Fermi and Lobster*," Proc. IAU, **Vol. 285**, pp. 41-46, (2012)

[8] Laser Interferometer Gravitational-wave Observatory (LIGO) Scientific Collaboration, "*Predictions for the rates of compact binary coalescences observable by ground-based gravitational-wave detectors*," Classical and Quantum Gravity, **Vol. 27**, p. 173001, (2010)

[9] B.D. Metzger and E. Berger, "*What is the Most Promising Electromagnetic Counterpart of a Neutron Star Binary Merger?*" Astrophysical Journal, **Vol. 746**, p. 48, (2012)

[10] K. Ryu et al., "*Development of CCDs for REXIS on OSIRIS-REx*," Proc. SPIE **9144**, 91444O-1 (2014)

[11] K. Ryu, M. Bautz, S. Kissel, P. O'Brien, and V. Suntharalingam, "*Directly Deposited Optical-Blocking Filters for Single-Photon X-ray Imaging Spectroscopy*," JATIS 2017 (in press).

[12] A. Rakic, A. Djurvic, J. Elazar, and M. Majewski, "*Optical Properties of Metallic Films for Vertical-Cavity Optoelectronic Devices*," Applied Optics **Vol. 37**, p 5271 (1998)

For additional information, contact Mark Bautz: *mwb@space.mit.edu*

Fast Event Recognition for the Athena Wide-Field Imager

Prepared by: David N. Burrows (PSU)

Summary

High-throughput X-ray missions of the future, including the Arcus Medium-class Explorer (MIDEX) mission proposed last year, the European Space Agency (ESA) Advanced Telescope for High ENergy Astrophysics (Athena) mission, the Lynx mission concept being studied in preparation for the 2020 Decadal Survey, and several Probe missions currently being studied, will use detectors with very high readout speeds that are too fast for software event recognition. Under this Strategic Astrophysics Technology (SAT) program, we are developing a high-speed Event Recognition Processor (ERP) running on a field-programmable gate array (FPGA). The purpose of this project is to advance the ERP from Technology Readiness Level (TRL) 3 to at least 4.

Background

For the past two decades, the state-of-the-art detector for X-ray astronomy missions has been the CCD detector. X-ray CCD instruments use a technique of "event recognition" to read images, scan them for X-ray events, and telemeter only X-ray events; compressing the data rate from these instruments by more than a factor of 500. These algorithms are well-proven in flight, and have been shown to produce data quality indistinguishable from laboratory analysis of full CCD images [1, 2].

Objectives and Milestones

Technical Approach and Methodology

The primary objectives of this proposal are to design and build a prototype breadboard version of a high-speed ERP, and to advance the design to TRL 4. This board must extract X-ray events from the high-speed data stream from a CCD or Active Pixel Sensor (APS); in other words, it performs event recognition and data compression. The existence of high-speed, radiation-tolerant FPGAs makes this feasible. During Phase A of our Joint Astrophysics Nascent Universe Satellite (JANUS) proposal, we developed a preliminary design concept for this circuitry that is at TRL 3. Over the past year, we developed a high-fidelity prototype board and implemented our event-recognition algorithms on this board.

Event Recognition

Most pixel data obtained with a CCD or APS are "empty," containing only read noise (Fig. 1). Reducing the data to fit satellite telemetry bandwidth requires extracting candidate X-ray signals from this data stream, a process we refer to as "event recognition," and passing them to the flight software for characterization and transmission to the ground. The spatial distribution of charge generated by X-ray interactions has characteristic features: charge is usually deposited in 1–4 pixels, depending on exactly where the photon lands within the pixel [3]. For example, if a photon hits near a pixel boundary, the charge cloud produced in the detector will be split between the adjacent pixels (Fig. 1). By contrast, background events due to charged-particle interactions in the detector tend to deposit large amounts of charge across many adjacent pixels (Fig. 2). Thus, classifying the "morphology" of an event allows it to be interpreted with high confidence as either an X-ray or background event [4]. Amplitude windows provide a second

powerful discriminator, since charged particles deposit charge packets in the deep depletion region of an active-pixel detector that are much larger than those produced by X rays in the instrument bandpass. These techniques have been used for several decades, achieving charged-particle rejection efficiencies of order 99.9% in X-ray CCD data [4–8]. Because they depend primarily on photoelectric absorption in pixelated silicon detectors, the same techniques apply to active pixel detectors.

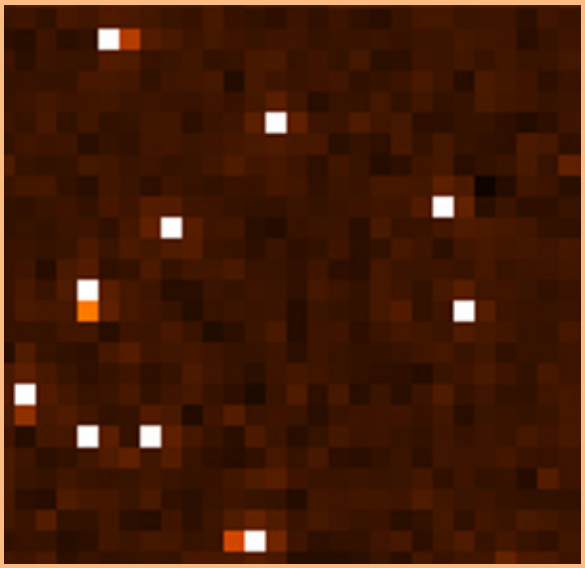

Fig. 1. *Small portion of a single frame of ground-test data from hybrid CMOS detectors developed by PSU, where color indicates the signal in each pixel. Most pixels show read noise (dark red/black). A few isolated bright pixels (white) represent X-ray events depositing their energy into single pixels. Several events are also seen in which the charge is spread into adjacent pixels, indicating the photon was absorbed near a pixel boundary [3].*

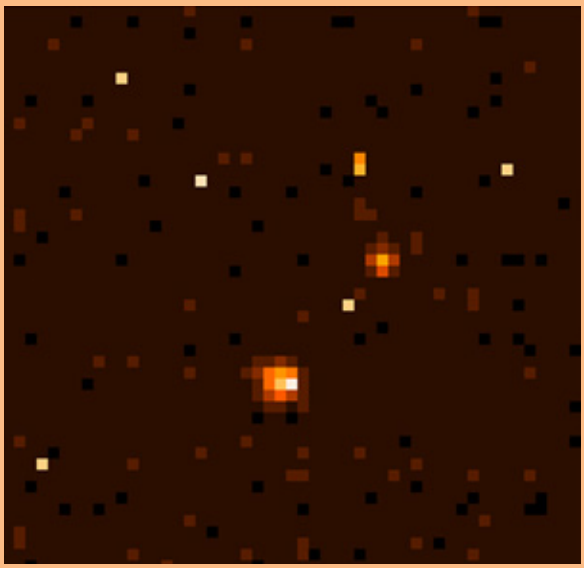

Fig. 2. *Small portion of a single frame of flight data from the Swift X-Ray Telescope (XRT) CCD. Most pixels show read noise. A few isolated bright pixels (white/yellow) represent X-ray events depositing their energy into one or two pixels. Two broad, "blobby" events are from cosmic-ray interactions in the detector, which produce wide charge clouds, easily distinguished from X rays.*

ERP Concept

The ERP is an FPGA-based board that performs high-speed processing of CCD or active-pixel frames and identifies candidate X-ray events. A block diagram of the main functions of the ERP is shown in Fig. 3. The ERP consists of a high-speed data capture and demultiplexing block, masking of bad pixels, event detection and grading (event recognition), and an output buffer (not shown). A full-scale ERP must be able to combine data from multiple readout channels. The required logic is very similar to that which we designed for JANUS and updated for the International X-ray Observatory (IXO) Wide-Field Imager (WFI). Under this grant, we have implemented a single-channel version of the ERP to test our ability to process data accurately at speeds approaching those required by future instruments, including the Athena WFI.

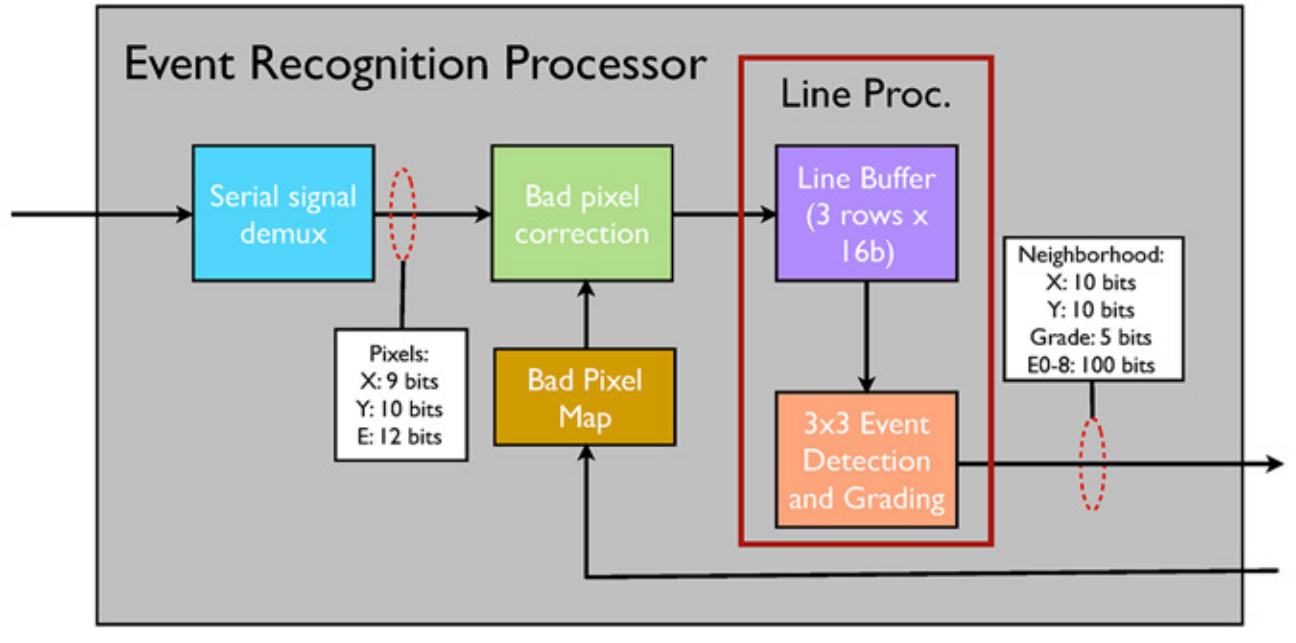

Fig. 3. *A simplified block diagram of the ERP. High-speed serial digital data are demultiplexed and bad pixels are zeroed as needed. The data are then inserted into a three-line buffer in the Line Processor (LP) and scanned for valid X-ray events using a sliding 3×3 pixel window. Event grades are encoded based on a simple comparator with a settable threshold. Output data are 3×3 "neighborhoods" centered on candidate X-ray events. Bit assignments shown are nominal.*

Implementation of a Single-Channel ERP

The heart of the ERP is the LP, as shown in Fig. 3. The LP accomplishes the event-recognition task through signal processing and pattern matching. The input data have already had any necessary bias and gain corrections applied and have been demultiplexed to determine the (X, Y) location and signal value of each pixel. The data are temporarily stored in high-speed FPGA memory. A sliding 3×3 pixel window is then virtually scanned across the three-row pixel buffer and each 3×3 "neighborhood" is searched for a local maximum (that exceeds an adjustable threshold) in the central pixel. When one is found, this pixel is identified as a possible X-ray event, and the event is graded using an uploadable lookup table to assign event grades. The event is then formatted and passed to the output telemetry stream as a 3×3 "neighborhood" or as an X ray with position, energy (E), and grade (depending on the instrument telemetry mode).

The basic processing implied in the previous sentence has been implemented in software by all three of our groups (PSU in our laboratory CCD and CMOS cameras on the Satelite de Aplicaciones Cientificas-B, SAC-B, and the Swift X-ray Telescope; MIT on the Advanced Satellite for Cosmology and Astrophysics, ASCA, Chandra, and Suzaku; and SAO in their laboratory CMOS cameras). Various event-grading schemes have been used in previous missions, ranging from the ASCA grades (0-7) to the Chandra Advanced CCD Imaging Spectrometer (ACIS) system, in which a bit is assigned to each of the eight surrounding pixels in a 3×3 neighborhood, resulting in grades from 0 to 255. We use the ACIS system internally, optionally converting to the Swift system for output data.

Progress and Accomplishments

For this project, we implemented the single-channel ERP shown in Fig. 4. This provided a proof-of-concept for hardware implementation of the critical function of this board, identification and grading of X-ray events in a data stream.

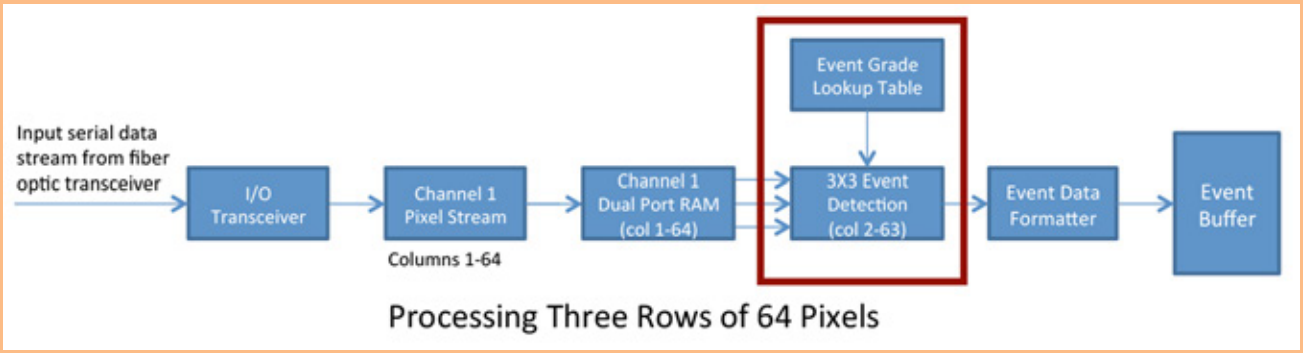

Fig. 4. *A single-channel implementation of the ERP, capable of handling a string of events from a 64-row-wide strip of an APS or CCD (figure shows processing schematic for three rows of 64 pixels). We will test this using fixed data patterns. The architecture allows row widths up to 1024 columns. Events from rows 1 and 64 cannot be fully processed in this breadboard implementation because they do not have a full 3×3 pixel "neighborhood" available to classify the event grade (I/O, Input/Output;.RAM, Random Access Memory).*

The ERP has been implemented on a Xilinx Virtex-5 (V5) FPGA. Following testing of the basic event recognition core on a Virtex-5 OpenSPARC Evaluation Platform, we designed, built, and tested a high-fidelity prototype board. This was necessary for full implementation of the ERP, because the prototype board had insufficient memory for applications requiring bias map subtraction or digital Correlated Double Sampling (CDS). Our prototype board is shown in Fig. 5. Further details are given in [9].

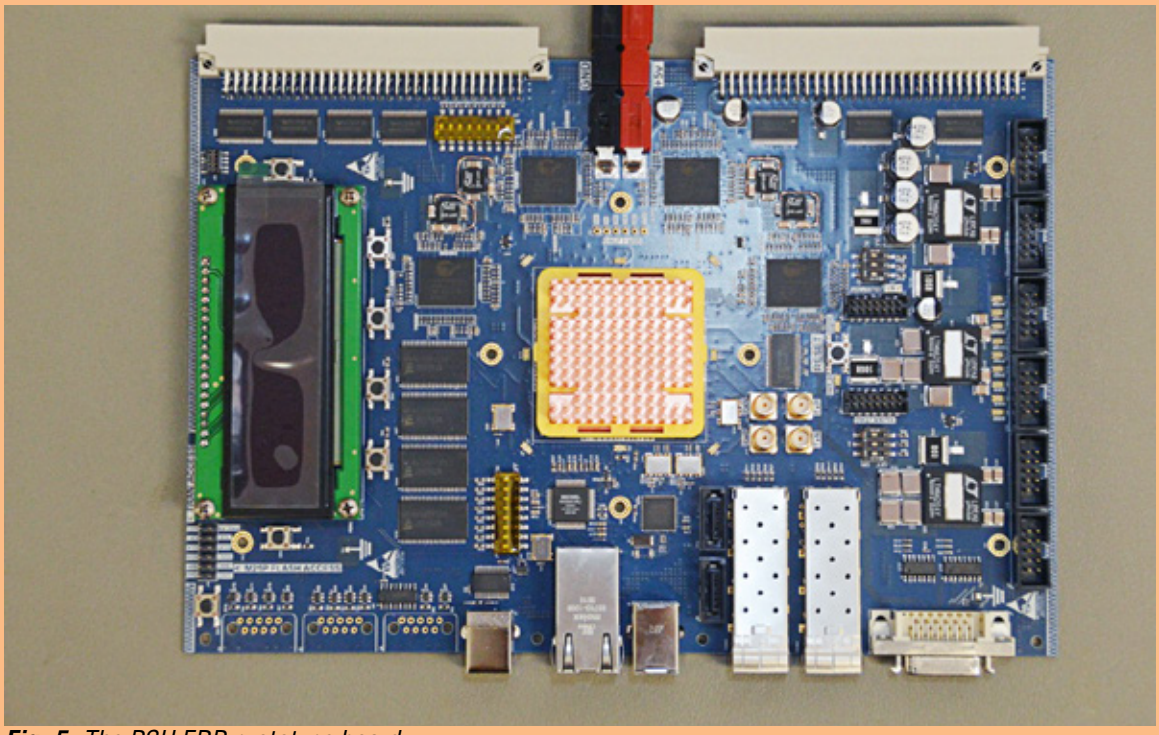

Fig. 5. *The PSU ERP prototype board.*

Laboratory tests using the LP, which processes individual detector rows, show that speeds of > 1 GBps can be achieved by this board. We are now finalizing the firmware to include the capability of loading complete detector images. Testing of the completed version should advance technical readiness to TRL 5, which we expect to achieve in August 2017.

Path Forward

We expect to have the prototype board tested by mid-2017, and to hold a TRL review with the Physics of the Cosmos (PCOS) Program Office in the coming months, to verify that TRL.

References

[1] L.J. Cawley et al., "*CCD x-ray detectors: on-board data processing*," in O.H.W. Siegmund and J.V. Vallerga (eds.), EUV, X-Ray, and Gamma-Ray Instr. for Astr. VI, **2518** SPIE Conf. Series, 179–187 (1995)

[2] J.E. Hill et al., "*Readout modes and automated operation of the Swift X-ray Telescope*," in K.A. Flanagan and O.H.W. Siegmund (eds.), X-Ray and Gamma-Ray Instr. for Astr. XIII, **5165** SPIE Conf. Series, 217–231 (2004)

[3] J. Hiraga et al., "*Subpixel Spatial Resolution of the X-Ray Charge-Coupled Device Based on the Charge Cloud Shape*," Japanese Journal of Applied Physics, **40**, 1493 (2001)

[4] D.H. Lumb and A.D. Holland, "*Event recognition techniques in CCD X-ray detectors for astronomy*," Nuclear Instruments and Methods in Physics Research A, **273**, 696 (1988)

[5] D.H. Lumb and A.D. Holland, "*Background rejection techniques in CCD X-ray detectors for astronomy*," IEEE Transactions on Nuclear Science, **35**, 534 (1988)

[6] D.H. Lumb, "*Particle background in CCD detectors*," in O.H.W. Siegmund (ed.), EUV, X-Ray, and Gamma-Ray Instr. for Astr. IV, 2006 SPIE Conf. Series, 300–306 (1993)

[7] A. Owens and K.J. McCarthy, "*Energy deposition in X-ray CCDs and charged particle discrimination*," Nuclear Instruments and Methods in Physics Research A, **366**, 148 (1995)

[8] J.A. Mendenhall and D.N. Burrows, "*CCD Sounding Rocket Observation of the High-Latitude Soft X-Ray Background*," Astrophys. J., **563**, 716 (2001)

[9] D.N. Burrows et al., "*Fast event recognition for X-ray silicon imagers*," SPIE Conf. Series, **9905**, 99050L (2016)

For additional information, contact David Burrows: *burrows@astro.psu.edu*

Providing Enabling and Enhancing Technologies for a Demonstration Model of the Athena X-IFU

Prepared by: Caroline Kilbourne (PI; NASA/GSFC); Simon Bandler, James Chervenak, and Stephen Smith (NASA/GSFC); Joel Ullom and W. Bertrand Doriese (NIST); and Kent Irwin (Stanford University)

Summary

On June 27, 2014, the European Space Agency (ESA) announced its selection of the Advanced Telescope for High-ENergy Astrophysics (Athena) mission concept to study the science theme the "Hot and Energetic Universe." The theme aims to address two important astrophysical questions [1]:

1. How does ordinary matter assemble into large-scale structures?
2. How do black holes grow and shape the universe?

One of the two instruments for this mission, the X-ray Integral Field Unit (X-IFU), is a high-resolution imaging X-ray spectrometer. The use of Transition-Edge-Sensor (TES) microcalorimeters, originally pioneered by our collaboration and under development in our Strategic Astrophysics Technology (SAT) program, is currently assumed for this instrument [2]. Both NASA and the X-IFU Principal Investigator (PI), Dr. Didier Barret, had previously communicated interest in designating the X-IFU microcalorimeter array as one of NASA's principal contributions to Athena, with ESA's concurrence. As a consequence, this collaboration submitted a new SAT proposal to cover our contribution to X-IFU technology development in fiscal years (FYs) 2016 and 2017. Our US collaboration is recognized as part of the Athena proto-consortium and is responsible for providing the baseline TES array technology, and our time-division-multiplexed (TDM) [3] readout technology is currently viewed as a backup to the European-developed frequency-domain multiplexing (FDM) [4]. The current program has been supported by the SAT program since 2013, and is the work of a collaboration between our research groups at GSFC (PI C. Kilbourne); National Institute of Standards and Technology (NIST), Boulder (Lead J. Ullom); and Stanford University (Lead K. Irwin). These groups have been collaborating on microcalorimeter-spectrometer technology development since 1998, with the primary goal of advancing the integrated detector-TDM system to a strong demonstration of Technology Readiness Level (TRL) 5. The goal of the current project is to support critical technology development for the X-IFU instrument. Since the reference design for the X-IFU is based on FDM of the signals from the nearly 4000 TES pixels of the focal-plane array, primary demonstration models will incorporate this scheme. In addition to fully supporting these primary demonstrations, we are also developing a parallel demonstration model using TDM. TDM is more advanced than FDM, so developing it as a backup option provides important risk reduction for the X-IFU development schedule. We are also developing code-division multiplexing (CDM) [5], which promises better performance while making use of most of the same readout architecture as TDM.

The project also includes development of critical technologies needed for the thermal, electrical, and mechanical integration of the detector and readout components into the focal-plane assembly (FPA). We are also developing large-scale testing platforms and assemblies that are essential for screening full-scale arrays and for large-scale multiplexed demonstrations.

Background

The X-IFU [1, 2] will be an extremely powerful instrument that will capitalize on four decades of technology development to create an instrument that simultaneously provides high spatial and spectral resolution. The instrument is very similar to the X-ray Microcalorimeter Spectrometer (XMS) envisioned for the International X-ray Observatory (IXO) mission, which was highly endorsed scientifically in the 2010 National Research Council Decadal Survey, "*New Worlds, New Horizons in Astronomy and Astrophysics*" (NWNH). For the first time, astrophysicists will have a spectral resolving power of ~2500 over the most diagnostically rich part of the X-ray band with up to 5-arcsec spatial resolution. With the very high collecting area of 2 m^2 and 2.5-eV energy resolution projected for the X-IFU, a wide range of celestial high-energy sources will be available for detailed analysis out to a redshift of 2.

The reference detector technology we have been developing consists of Mo/Au TES thermometers (operated at < 0.1 K) with close-packed Bi/Au thermalizing X-ray absorbers on a 0.25-0.3-mm pitch. In our baseline TDM concept [3], outputs from the dedicated input Superconducting QUantum Interference Devices (SQUIDs) of individual TES pixels are coupled to a single amplifier, and multiplexing is achieved by sequential switching of these input SQUIDs. Under the previous program, we made substantial progress that is relevant for X-IFU. The integrated detector-TDM system reached TRL 4 in March 2008 with the successful demonstration [6] of multiplexed (2 columns × 8 rows) readout of 16 different pixels. We then defined the following milestone as necessary for achieving TRL 5: "*Demonstrate multiplexed (3 columns × 16 rows) readout of 48 different flight-like pixels. The pixels shall be placed on a 0.25-mm pitch in a 32×32 (or greater) array, and more than 95% of pixels must achieve better than 3-eV resolution at 6 keV, using an analysis method consistent with the requirement of 80% live-time at an X-ray rate of 50/s/pixel.*"

Fulfilling this milestone is consistent with the requirements for TRL 5 because the full detector requirements (as previously defined) would be demonstrated at the detector/readout subsystem level though on a smaller scale. Note that the multiplexing factor is not a performance requirement, but rather an accommodation requirement that comes out of the system design. For Athena-L1 it was 16 channels per multiplexer, for Constellation-X it was 32, and now for Athena-L2 it is 40.

The other related technology we are developing is CDM, a switched-multiplexing system like TDM. In TDM, only one TES channel is on at a time, whereas in CDM all channels are always on, but switched in polarity according to a matrix of combinations, thus avoiding the aliased noise of TDM. CDM is compatible with the TDM infrastructure, but provides increased design margin. In FDM, the TESs are biased with AC signals of different frequencies, acting as carriers for the slower thermal signals.

The X-IFU requirements are currently being refined, and ESA has yet to define the formal X-IFU TRL-5/6 requirement. The X-IFU project managers intend that the team produce a very-high-fidelity demonstration model (DM). The primary goal of the DM instrument is to provide a system-level demonstration of critical technologies, and in particular to characterize a prototype X-IFU FPA in a prototype X-IFU cryostat. DM development is thus expected to contribute to the demonstration of maturity (at TRL 5) and instrument development, but will not demonstrate the instrument design. Within the FPA development program, the DM FPA is also the first system demonstration in which the parallel development programs for the detector and its readout, the anti-coincidence detector and its readout, and the FPA shielding and suspension technologies are integrated; and the only such system demonstration before the instrument's TRL-5 demonstration.

The baseline instrument design concept is being defined in Phase A (2016-2017) and further developed in Phase B1 (2018-2020), with the design of the next instrument model, the engineering model (EM), a product of Phase B. In support of this instrument development, the FPA DM program includes technology development in parallel with the DM FPA to demonstrate critical components and sub-assemblies required for an EM FPA in Phase B, and as part of the FPA TRL-5 demonstration.

The X-IFU DM requires a detector array in a preliminary flight design, meeting the requirements determined by the noise budget. The baseline is a standard GSFC kilo-pixel array with Space Research Organization Netherlands (SRON) FDM readout. Though the full requirements are still being finalized, the detector array and readout would be expected to achieve performance commensurate with an energy resolution of 3 eV in a 2-column by 40-row FDM configuration.

As envisaged at the start of our program, the X-IFU flight array would be a uniform array of ~4000 pixels on a 0.26-mm pitch. This was referred to as the uniform Large-Pixel-Array-1 (LPA-1) configuration, and is the simplest array implementation scheme. However this configuration would not allow the highly desired count-rate goal of 10 mCrab for point-source observations. The use of identical pixels also represents an inefficient use of readout resources. This is because all pixels are optimized for the point-source count-rate requirement, even though the telescope point-spread function (PSF) only spreads the beam over a relatively small region of the array. Consequently, alternative options were also under consideration. For example, the project examined the feasibility of including the ability to adjust the distance between the mirror assembly and the focal-plane (by tens of mm), thus defocusing the telescope PSF and spreading the photons over a larger fraction of the array. Alternatively, different parts of the focal-plane array could incorporate pixels optimized for different energy resolution, angular resolution, or count-rate goals, whilst making more optimal use of available readout resources. At that point, we were studying the feasibility of developing these enhanced 'hybrid-array' configurations and supporting X-IFU trade studies between different proposed designs. In late 2016, we contributed to the recommendation of a new baseline configuration that was adopted by the project. This would combine the telescope-defocusing option with a new uniform Large Pixel Array 2 (LPA-2), with pixels optimized for approximately a ×2 reduction in speed. Thus, we are now pivoting the focus of our detector-research efforts toward this slower LPA-2 design, with reduced emphasis on demonstrating the hybrid-array technology.

Progress and Accomplishments

Multiplexed Readout of Large-Format Arrays

A standard GSFC 32×32 TES array [7] with pixels on a 0.25-mm pitch is shown in Fig. 1. All pixels are wired out to the edge of the array, but on these test devices only 252 of the pixels (25%) are wired to bond pads around the circumference of the silicon carrier wafer. This array format is also the baseline DM array configuration.

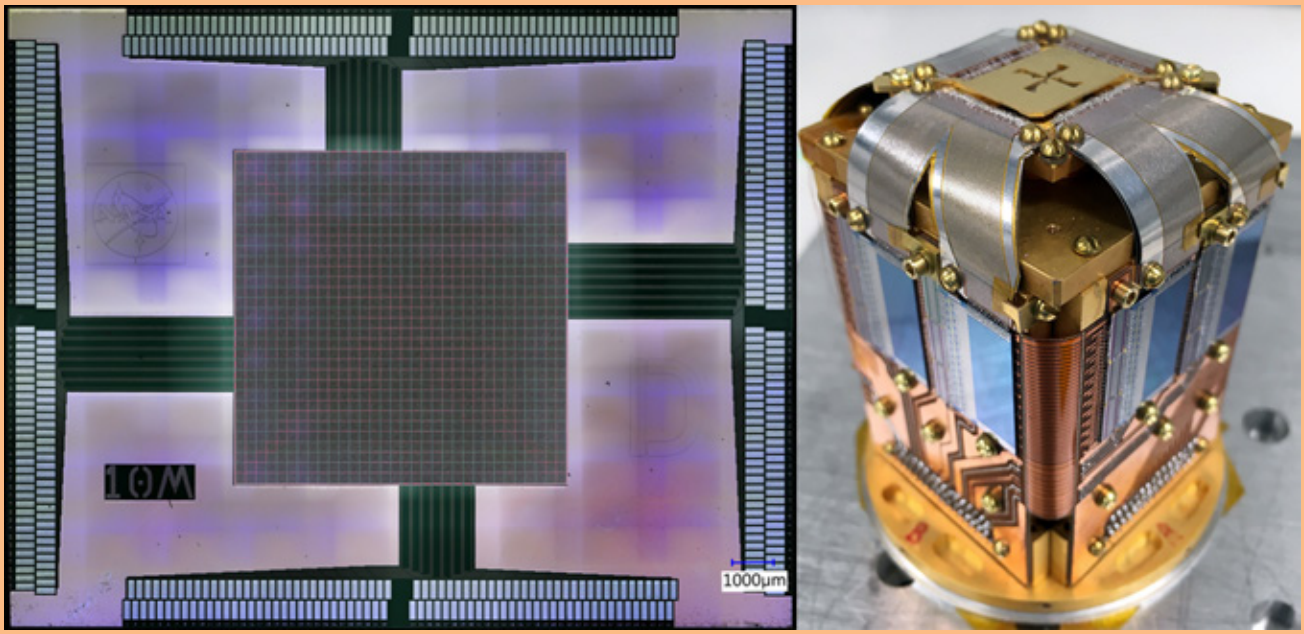

Fig. 1. Left: *A mosaicked image of a 32×32 array of close-packed X-ray microcalorimeters. Only the X-ray absorbers are visible; they are composed of a 1.5-µm-thick layer of gold and a 3.0-µm-thick layer of bismuth. The absorbers are 0.242 mm × 0.242 mm in size, on a 0.25-mm pitch.* Right: *Photograph of an 8-column-by-32-row TDM 'Snout' package with a GSFC array installed atop. Visible above the detector is an X-ray mask that exposes only those pixels that are physically connected to the bond pads.*

The main goals of the TDM development have been to lower the row-switching time and system readout noise. Significant improvements have already been made throughout the multiplexer system, which in combination more than satisfy the requirements for row-switching time and noise, and have been used in a breakthrough 32-row TDM demonstration at NIST achieving 2.55±0.01 eV average energy resolution at 6 keV in a single column [8]. The detector used was a NIST development array with 2.4-eV intrinsic resolution and a maximum slew rate of 0.21 A/s, but the readout is suitable for the target array design of <2 eV intrinsic resolution and twice the slew rate. Similar demonstrations were achieved using a GSFC detector. Of particular note is a 32-row TDM demonstration at 1.5 keV, in which we achieved 2.34±0.1 eV. For the same system and detector, the resolution at 6 keV was 3.3 eV, consistent with the non-linearity of that particular detector [9]. A successful 32-channel CDM demonstration with a NIST detector array, using the same flux-activated switching architecture that is used in the TDM, had a combined resolution of 2.77±0.02 eV full width at half maximum (FWHM) at 6 keV from the 30 TESs connected to the readout [10].

The test platform at GSFC used an eight-column FPA configured with TDM multiplexer chips and second-stage SQUID amplifiers of different designs. This mixed configuration enabled direct comparison of important performance metrics such as noise, crosstalk, and bandwidth for the different SQUID multiplexing architectures under consideration. Having now determined the most promising choice of system architecture, we have reconfigured this demonstration platform to have all eight columns of the same 1st-stage multiplexer chip, 2nd-stage SQUID amplifier, and room-temperature amplifier. We have recently begun testing this system and have now demonstrated the ability to multiplex eight columns by 32 rows with an array that is close to the target LPA-1 Athena detector specifications. This array had a very uniform transition temperature of 91.05±0.11 mK on 110 pixels that were measured

spanning the full extent of the array. This array is significantly faster than previously demonstrated, with a slew-rate of 0.36 A/s for 6 keV photons. We are currently evaluating the integrated system noise and energy-resolution performance. In an initial six-column-by-32-row demonstration, we already achieved a median FWHM energy resolution of 2.75 eV. The two columns that were not operating in this preliminary demonstration were found to have higher-than-anticipated total system noise, the origin of which is still being investigated. The histogram of achieved resolutions for all six multiplexed columns is shown in Fig. 2. Also shown is the combined spectrum for the 144 pixels, achieving a FWHM resolution of <3.5 eV. In this multiplexed configuration, we had access to 190 of the 252 total TES pixels in the array connected to bond pads. Of those 190 possible pixels, 27 pixels were not physically wire-bonded to the readout because of known pixel yield issues on this particular array. On this preliminary data run, 13 pixels had non-optimal flux-lock-loop (FLL) feedback parameters and were unstable, therefore those few pixels did not generate high-resolution spectra. By fine adjustment of the FLL feedback parameters, we have since shown we can improve the stability, which should eliminate these outliers on future acquisitions. This particular array had a known absorber-thermalization issue that resulted in long secondary decay time constants and degraded spectra performance in some of the pixels. Although all pixels are believed to suffer at some level, this effect is variable over the array and in this demonstration we identified seven pixels as especially affected. This effect has been eliminated on later wafers, which should enable more uniform array performance with ~2.5-eV FWHM energy resolution in future TDM demonstrations.

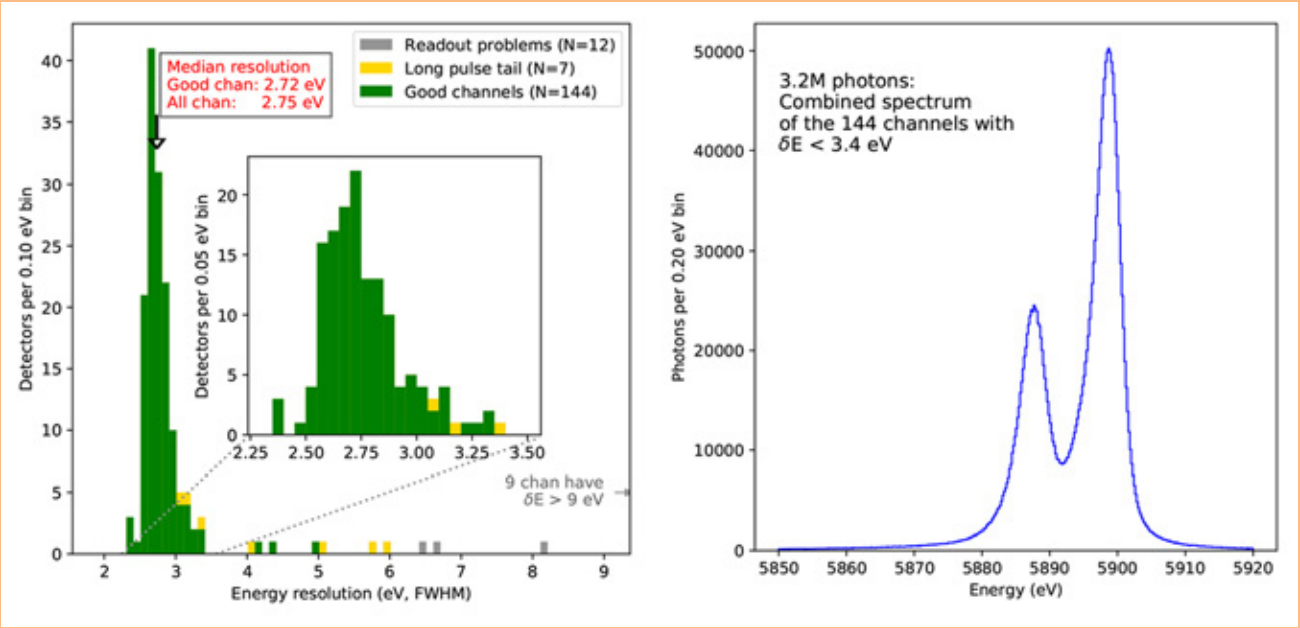

Fig. 2. Left: *Histogram of measured FWHM energy resolution for a six-column-by-32-row TDM demonstration at an energy of 6 keV. Of the 163 active pixels connected to the readout, 12 (grey) were not read out stably and seven (yellow) were determined to have significant secondary decay times in the measured pulses due to absorber thermalization issues.* Right: *Combined Mn-Kα spectrum for the 143 channels that attained an energy resolution <3.4 eV. The spectrum has a resolution of 2.747±0.010 eV. Using a targeted cross-talk cut to remove events that had simultaneous X-ray events in the same row or the same column, we improved the median resolution by ~ 0.06 eV and only removed 5.9% of the total acquired photons.*

Further Design Optimizations for TDM

We are developing the next generation of multiplexer and second-stage SQUID amplifier circuit targeted at reduction of multiplexed crosstalk and total readout noise. In the existing TDM multiplexer architecture, the FLL feedback is applied to all 1st-stage SQUIDs simultaneously, even though only one SQUID is actively biased at a time. This results in small but measurable crosstalk across all SQUIDs in a multiplexed column. We have developed new 'TDM+' chips that are designed to avoid this crosstalk mechanism by diverting the feedback current from the 'off' SQUIDs entirely using a bypass switch. These bypass switches are based on the same flux-actuated switch architecture used in the existing TDM designs to switch 1st-stage SQUIDs on and off. Our new TDM+ chips, with four different implementation schemes for the new feedback-bypass switches, have now been fabricated and are being tested.

In addition to the new TDM designs, we are also incorporating small design optimizations to the 2nd-stage series-array amplifier. We are increasing the total number of SQUIDs in the array by 50%; these will be arranged in four parallel banks for 76 series-connected SQUIDs. This design modification is intended to reduce the series-array-noise contribution to the total system noise and improve impedance matching of the series array with the readout wiring and room-temperature readout amplifier. We will also include new damping structures to help reduce the effect of SQUID resonances.

TES Pixel Designs for LPA-2

A uniform 32×32 array of the type shown in Fig. 1 has been screened at GSFC and sent to SRON for integrating into their new kilo-pixel FDM test platform. Our DC-biased measurements showed the array had excellent uniformity of transition temperature (T_C) and transition shape. The average T_C was 90.3±0.2 mK on 37 pixels spanning the full extent of the array. Spectral measurements on nine representative pixels showed an average energy resolution of 2.2±0.24 eV at 6 keV. This array will soon be operated at SRON using the baseline Athena readout technology, with an AC-bias excitation and FDM. The array is also a potential candidate to be used in the Athena DM. This array is designed to have characteristics very similar to the original LPA-1 X-IFU configuration. However, given the new X-IFU baseline configuration we have begun focusing efforts on achieving pixel designs optimized for the newly reduced per-pixel count-rate requirements. The target LPA-2 TES design parameters are essentially the same as those proposed for the original LPA-1, except that the thermal conductance to the heat bath (G_b) is reduced by approximately ×2. The value of G_b at a given temperature is determined by the perimeter of the TES and the thickness of the SiN membrane. We are exploring TESs with lateral size in the range L=50-140 μm, combined with SiN membranes with thickness in the range 0.25-1 μm. We have shown that a 140-μm TES, when deposited on 0.5-μm SiN, will achieve the necessary TES properties for LPA-1. Recent results on thinner, 0.25-μm SiN suggest we can achieve the desired LPA-2 properties with a 120-μm TES. Alternatively, results suggest that smaller, 50-μm TESs should yield the desired G_b on the thicker, 1-μm SiN. The first tests of the 50-μm devices showed very clean transition shapes with no evidence of the fine structure that often degrades performance, and excellent energy resolution of 1.6±0.1 eV. An example of Mn-Kα spectrum is shown in Fig. 3. Also plotted is a measured resistance vs. temperature curve and the unit-less transition sensitivity parameter $\alpha = T/R\ dR/dT$, which shows a very smooth transition shape.

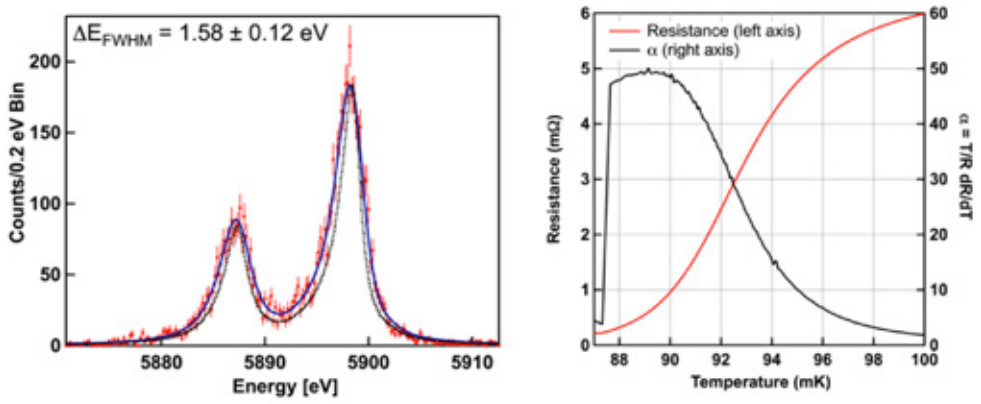

Fig. 3. Left: *Example of achieved Mn-Kα spectrum for slower pixels being developed for the LPA-2.* Right: *Measured resistance-temperature transition shape and the transition sensitivity parameter α for the same device.*

Since the smaller TES sizes only exist in diagnostic arrays of mixed pixel geometries, we are currently drawing a new mask set, which includes the first uniform 32×32 arrays of the reduced-size TESs. This will allow us to continue evaluating the best candidate LPA-2 pixel size and membrane thickness in arrays that can be used for the Athena DM.

Because the baseline X-IFU FDM readout applies an AC bias to the TES thermometers, we also need to characterize and optimize TES performance under AC bias. The optimal pixel design is not necessarily the same for AC- and DC-biased TESs, and generally AC performance has lagged that routinely seen in DC TESs. We have now delivered to SRON two different 8×8 diagnostic test arrays with different pixel geometries for testing. We have also started our own AC-biased pixel tests at GSFC and NIST. This single-pixel AC-bias research was the main component of the related program in which our collaboration is engaged (PI J. Ullom, "*Technology Development for an AC-Multiplexed Calorimeter for Athena*"). That effort has now merged with our overall effort to support these early technology demonstrations for the X-IFU. This effort is already bearing fruit and we have identified several geometric optimizations that suggest improvements in AC-pixel performance may be possible.

Development of Large-Scale Array and Readout Capability

We are developing two identical ^{3}He-backed Adiabatic Demagnetization Refrigerator (ADR) demonstration platforms to instrument a full kilo-pixel-scale TDM/CDM array for technology demonstration and device characterization. One of these systems will be at NIST and one at GSFC. Two systems are essential because we will be testing multiple array types (uniform arrays and hybrid arrays) with multiple readouts (TDM and CDM). These ADRs have been procured and will be received this year. Figure 4 shows a computer-aided-design (CAD) schematic of the new ADR and a close-up of the new 50-mK 'Snout' FPA. This system is a scaled-up version of the successful 256-pixel Snout shown in Fig. 1. This architecture is being dimensioned for a 40-row×24-column TDM/CDM, enabling 960-pixel characterization and multiplexed-technology demonstrations. The detector chip will sit atop the Snout, with flexible interconnects to the two sets of 80-pixel multiplexer and Nyquist chips (four columns) on each of the six side panels.

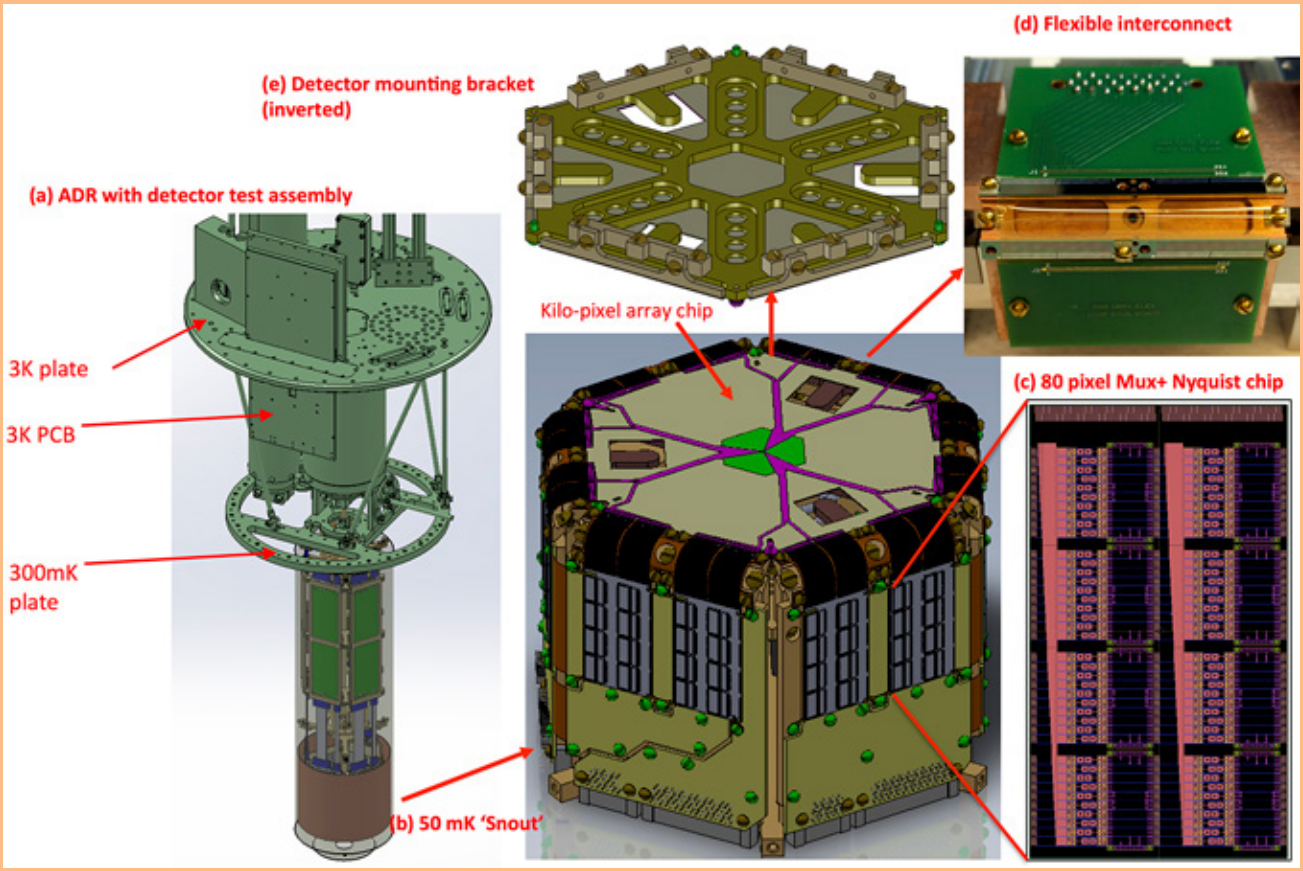

Fig. 4. *(a) CAD of new laboratory test platform for kilo-pixel array characterization and TDM/CDM demonstrations (PCB, printed circuit board). (b) CAD sketch of new 40-row × 24-column 50-mK 'Snout.' (c) New 2 × 80-pixel Nyquist and multiplexer chips that will populate the six panels. (d) Photograph of prototype around-the-corner flexible interconnect in a test set-up. (e) CAD sketch of detector array mounting bracket (as viewed from underneath).*

The TDM/CDM interface between detector and readout/bias circuit component is very different from that of FDM. Any large, Athena-scale, demonstration array will need to be characterized using both DC-biased (TDM/CDM) measurements, which will be wire-bonded to flexible interconnects, and AC-biased (FDM) measurements, which will be inductively coil-coupled to the readout components. We are developing wafers of the size, shape, and layout required for future kilo-pixel testing of the X-IFU arrays. We have a wafer-layout solution that will incorporate DC-biased pixels in three sectors of a hexagonal wafer, and AC-biased pixels in the other three sectors. We have completed a prototype wiring layout for a full-sized X-IFU array, and begun the first fabrication runs. Figure 5 shows a recently deposited test wafer with just the Nb bias leads and the Mo/Au TES layer deposited. The fully wired array consists of 3580 pixels on a 0.26-mm pitch. To wire all pixels to the edge of the array, there are up to 20 wire pairs (on a 4-μm pitch) per 92-μm-wide muntin between pixel pairs, with 960 pixels routed to the bond pads on the six sides of the hexagonal wafer. These will be DC tested.

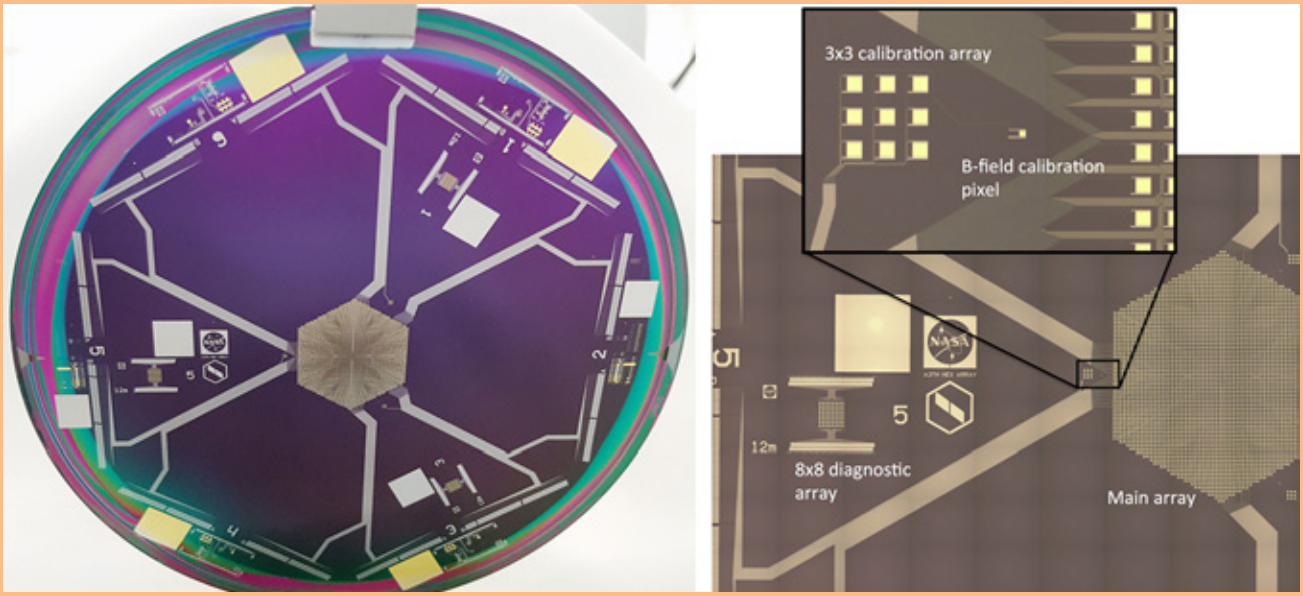

Fig. 5. Left: *Photograph of the full-scale Athena wafer in the early stages of fabrication. Only the lead layer and TES bilayer have been deposited so far. The 4000-pixel hexagonal TES array is at the center of the image. All pixels in the array are wired out to the edge of the array and 960 pixels are routed to bond-pads on the six sides that will form the perimeter of the hexagonal wafer once completed. The wafer also includes nine diagnostic test arrays (three on the interior and six on the exterior of the wafer) that will be etched out of the final wafer for independent tests.* Right: *Close-up photograph of section 5 of the full wafer shown at left. The inset shows a zoom-in of the 3×3 calibration array that will be used to track gain variations independently, and a single 50-μm pixel that will be used for calibration of the magnetic field coil. There are three identical sets of calibration pixels around the perimeter of the main array.*

Other ongoing supporting activities taking place include development of "around-the-corner" flexible interconnects and investigation of bump-bonded connections to the TES wafer. We are developing a process for $Nb/SiO_2/Nb$ micro-stripe wiring that is sandwiched between two layers of flexible polyimide. Figure 4 (e) shows a photograph of this flexible interconnect layer in a test jig. We have successfully demonstrated superconducting transitions on both wiring layers with a critical current of >4 mA and transition temperature of >4 K. We plan to use this flexible interconnect on the new 960-pixel Snout system.

The use of indium bump bonds between the flexible interconnects and the detector wafer would enable very high yield and high density of superconducting connections compared to conventional Al wire bonds. We are developing arrays of indium bumps deposited on molybdenum nitride. In initial test bumps using our proposed X-IFU geometry (10 microns of In mated to a 1 micron In pad), we measured a transition temperature of 3.1 K at a bias current of 3 mA and a normal resistance of 0.55 mΩ per interconnect. We have developed a hex-to-flex bump-bonding solution whereby an array of ~600 bumps in each of the six sections will be mated to the around-the-corner flex. Such a configuration would allow all pixels to be connected to the six side panels of the Snout.

We have begun depositions in the newly installed electron-beam evaporation tool that will be used for dedicated TES Mo/Au depositions. Due to the specific design of the system, variations of important process parameters such as film thickness and wafer temperature across each wafer and from wafer to wafer are set to be less than 2%. Initial depositions suggest we can achieve the target of <2-mK bilayer T_C uniformity over a full Athena-scale array. This new custom tool will produce seven-device bilayer wafers and a witness wafer (used for diagnostic T_C checks) in a single deposition run without

breaking vacuum, and is essential for achieving the required array-scale uniformity and wafer-to-wafer reproducibility. Over the past several months, we have been refining the critical deposition processes and have now begun producing the first product devices. We anticipate testing the first fully optimized detector arrays from this system later in FY 2017.

Path Forward

Having already delivered a 32×32 array to SRON for FDM testing, with characteristics close to the original reference design, we are now focused on producing DM arrays that more closely match the new LPA-2 pixel requirements. We plan to test and deliver a suitable DM array by the end of calendar year 2017.

With numerous improvements in system bandwidth and noise, we are now routinely achieving ~3 eV or better in various multiplexed demonstrations of 32 rows in single columns and more recently in multiple columns, now using fast TES arrays being developed for Athena. Thus, with respect to the original milestone, we are close to achieving TRL 5. This remains a highly relevant metric for demonstrating the feasibility of TDM as backup technology, and is commensurate with the main DM objectives using the baseline FDM readout. As the Athena baseline configuration continues to evolve, we will evaluate and refine our own TRL milestones. Beyond these demonstrations, our focus is on developing full-scale Athena arrays and designing the testing infrastructure to characterize these arrays and provide additional large-scale technology demonstrations.

References

[1] K. Nandra et al., "*Athena, the Advanced Telescope for High ENergy Astrophysics*," a mission proposal submitted to ESA's L2 large mission opportunity, recently accepted (2014)

[2] D. Barret et al., "*The Hot and Energetic Universe: The X-ray Integral Field Unit (X-IFU) for Athena+*," astro-ph arXiv:1308.6784 (2013)

[3] J.A. Chervenak et al., "*Superconducting multiplexer for arrays of transition edge sensors*," Appl. Phys. Lett., **74**, 4043-4045 (1999)

[4] R. den Hartog et al., "*Baseband Feedback for Frequency-Domain-Multiplexed Readout of TES X-ray Detectors*," AIP Conf. Proc. **1185**, 261-264 (2009)

[5] K.D. Irwin et al., "*Code-division multiplexing of superconducting transition-edge sensor arrays*," Supercon. Sci. Technol. **23**, 034004 (2010)

[6] C.A. Kilbourne et al., "*Multiplexed readout of uniform arrays of TES X-ray microcalorimeters suitable for Constellation-X*," Proc. SPIE **7011**, 701104 (2008)

[7] S.J. Smith et al., "*Uniformity of Kilo-Pixel Arrays of Transition-Edge Sensors for X-ray Astronomy*," IEEE Trans. Appl. Supercon., **25**, 2100505 (2015)

[8] W.B. Doriese et al., "*Developments in Time-Division Multiplexing of X-ray Transition-Edge Sensors*," J. Low Temp. Phys., **184**, 389-395, (2016)

[9] S.J. Smith et al., "*Transition-edge sensor pixel parameter design of the microcalorimeter array for the X-ray Integral Field Unit on Athena,*" Proc. SPIE **9905**, Space Telescopes and Instrumentation 2016: Ultraviolet to Gamma Ray, 99052H (20 July 2016)

[10] K.M. Morgan et al., "*Code-division-multiplexed readout of large arrays of TES microcalorimeters*," Appl. Phys. Lett., **109**, 112604 (2016)

For additional information, contact Caroline Kilbourne: caroline.a.kilbourne@nasa.gov

Reflection Grating Modules: Alignment and Testing

Prepared by: Randall L. McEntaffer (PSU)

Summary

The science requirements for future soft-X-ray spectroscopy missions drive the instrumentation requirements for spectral resolving power and spectrograph effective area. Key science goals that address the physical properties and distribution of hot matter in the universe can be realized with diffraction-grating-based spectrographs in a range of platforms from Explorers to Probes to Lynx. The majority of spectral features from astrophysical plasmas at temperatures >10^6 K occur in the soft-X-ray regime, below 2 keV, where diffraction gratings can provide the instrument performance required for these science goals. A sustained program of grating technology development is necessary to qualify these spectrographs for future flight opportunities.

This document details the results from a Strategic Astrophysics Technology (SAT) program with a period of performance spanning calendar years 2015 and 2016. These developments leverage heavily from associated NASA programs including:

1. A previous SAT program, "Off-plane Grating Arrays for Future Missions," that performed the initial trade studies necessary to identify grating fabrication, alignment, and testing techniques.
2. An ongoing Roman Technology Fellowship (RTF) dedicated to developing fabrication methodologies for reflection gratings.
3. A current Astrophysics Research and Analysis (APRA) grant for suborbital flight of a reflection-grating-based spectrograph.

The progress made during these programs [1–9] has enabled the current SAT to concentrate on the developments needed in the areas of grating alignment and performance testing. Collaborations with NASA's MSFC and GSFC provided critical support for this SAT. Colleagues at GSFC provided an X-ray telescope for use during grating performance testing, while MSFC is providing testing facilities and support at their Stray Light Facility (SLF) X-ray beamline. The ultimate goal of this project is to populate and qualify a flight-like grating module with several large-format, high-fidelity gratings to create a spectrograph subsystem that is ready for incorporation into the next spectroscopic X-ray observatory.

This is the third report during this project and therefore shares the same Background and Objectives and Milestones as the one in the 2016 Physics of the Cosmos (PCOS) Program Annual Technology Report (PATR) [10]. Subsequently, a description of the most recent developments in grating alignment and testing is given.

Background

The purpose of this study is to advance high-throughput, high-spectral-resolving-power, X-ray spectroscopy and its application in future NASA missions. Specifically, the project will concentrate on improving the Technology Readiness Level (TRL) of off-plane reflection-grating spectroscopy for soft X rays (0.2–2.0 keV). This technology has applications in a variety of NASA missions from suborbital rockets to Explorer-class missions to large observatories. An Off-Plane X-ray Grating Spectrograph (OP-XGS) was included in the instrument suite for the International X-ray Observatory (IXO) during the last Decadal Survey, which spurred many follow-on studies [11] including mission concepts such

as the Advanced X-ray Spectroscopic Imaging Observatory (AXSIO), the Notional X-ray Grating Spectrometer (N-XGS), and the Square Meter Arcsecond Resolution Telescope for X rays (SMART-X). An OP-XGS configuration has been studied extensively for an Explorer mission concept, Arcus [12], and is included as a spectrometer concept for the Lynx large-mission concept [13]. Progress made during the development of the OP-XGS was detailed in the five previous PATRs of the PCOS Program. The PCOS Program identified X-ray reflection gratings as a critical technology for development in this decade to address X-ray science goals. In this role, we also contributed a development roadmap detailing the efforts and milestones needed to advance the OP-XGS to flight readiness, incorporated into the most recent X-ray Technology Development Roadmap (TDR).

Soft-X-ray grating spectrometers with high throughput and high spectral resolving power can address many top science questions such as:

- What controls the mass-energy-chemical cycles within galaxies?
- How do baryons cycle in and out of galaxies, and what do they do while they are there?
- What are the flows of matter and energy in the circumgalactic medium?
- How do black holes work and influence their surroundings?
- How do massive stars end their lives?
- What controls the masses, spins, and radii of compact stellar remnants?

These science questions can be addressed with high-quality X-ray spectra as specifically stated in the 2010 Decadal Survey, "*New Worlds, New Horizons in Astronomy and Astrophysics*" (NWNH). At the lowest energies, the most efficient method of obtaining high spectral resolving power is grating spectrometers.

To achieve these science goals, a grating spectrograph must be capable of producing spectral resolving powers ($\lambda/\delta\lambda$) better than 1500, with high throughput over the soft-X-ray energy band. The major limiting factor is meeting the spectral-resolving-power requirement. In the context of off-plane reflection gratings, this requires customization of the groove profile to obtain blazed facets with high groove density that varies along the groove direction. In a parallel RTF effort, we are developing a new fabrication method using common lithographic techniques borrowed from the semiconductor industry. Electron-beam (e-beam) lithography enables tight control over the groove profile during recording, while various etching steps can be used to shape the facets to the desired blaze. An optimal groove profile will limit any grating-induced aberrations to the telescope focus while maximizing throughput and resolving power over our wavelength band-of-interest. We have used gratings fabricated during the RTF in the current SAT study to populate our grating modules. The design of the grating module has gone through several iterations during the previous SAT program. This design has been refined through testing and analysis leveraged from the APRA program and concept mission studies. In the course of our current SAT, we have implemented this design to house our gratings. During module population, alignment tolerances must be met so that every spectrum from every grating overlaps at the focal plane with limited alignment-induced distortion. We have previously analyzed our alignment tolerances, assessed required metrology, and developed a concept alignment methodology. Over the past year, we implemented these techniques to produce an aligned module of gratings, and undertook associated performance testing. Therefore, we are well on our way to achieving the two main paths of our development plan:

- Implementation of our alignment methodology; and
- Performance testing of aligned modules.

Objectives and Milestones

High diffraction efficiency and high spectral resolving power have been demonstrated for off-plane reflection gratings. Prototype gratings have been shown to place > 40% of incident light into diffracted orders [1, 14] while also achieving spectral resolving powers > 3000 in the soft-X-ray band. These demonstrations place off-plane gratings at TRL 4, as recently vetted by the PCOS Program. The Program has also agreed with our proposed path toward TRL 5.

While single prototype gratings have proven the capability of the off-plane design, aligned arrays of large-format, blazed gratings need to be fabricated and tested to prove the technology for flight missions. A program of grating fabrication, alignment, and performance/environmental testing is necessary to bridge the current technology gap and achieve flight readiness.

Several milestones needed to achieve our goals for this SAT were accomplished this past year. Here we outline some of the major ones achieved, as well as those remaining for the calendar year:

1. Install alignment fixtures and metrology in the lab – completed 3rd quarter of 2015.
2. Align multiple grating substrates into mount – completed 4th quarter of 2015.
3. Improve grating mounting and alignment methodology, informed by initial alignment results – completed 4th quarter 2015/1st quarter of 2016.
4. Design and fabricate high-fidelity grating mount – completed 1st quarter of 2016.
5. Implement alignment improvements – completed 1st quarter of 2016.
6. Receive large-format gratings from RTF program – completed 2nd quarter of 2016.
7. Align multiple large-format gratings into mount – completed 2nd quarter of 2016.
8. Carry out performance and environmental testing of a high-fidelity module of aligned, large-format gratings – completed 2nd quarter of 2016.
9. Analyze results – completed 4th quarter of 2016.
10. Publish results – planned for 3rd quarter of 2017.

Highlights of the results accomplished in the completion of these milestones are summarized below.

Progress and Accomplishments

The progress made during this SAT was enabled by advancements in the grating fabrication studies of the RTF program, as well as the system-level studies of the associated APRA program and Arcus Explorer mission concept. Our grating fabrication method, developed over the course of this SAT, resulted in our ability to fabricate large-format, flight-like gratings (Fig. 1). The first generation of these gratings were large format (75 mm × 96 mm × 0.5 mm), blazed (29.5° or 54.7° facet angle), variable line spaced (8× periods from 158.25 nm to 160 nm in 0.25-nm steps), coated (15-nm Au with 5-nm Cr binding layer), and replicated onto flat (< 5 μm peak-to-valley flatness over 80-mm diameter) fused-silica substrates. Large-format gratings such as these are necessary to address the issues of scale that are met during alignment, and are thus necessary to prove TRL 5.

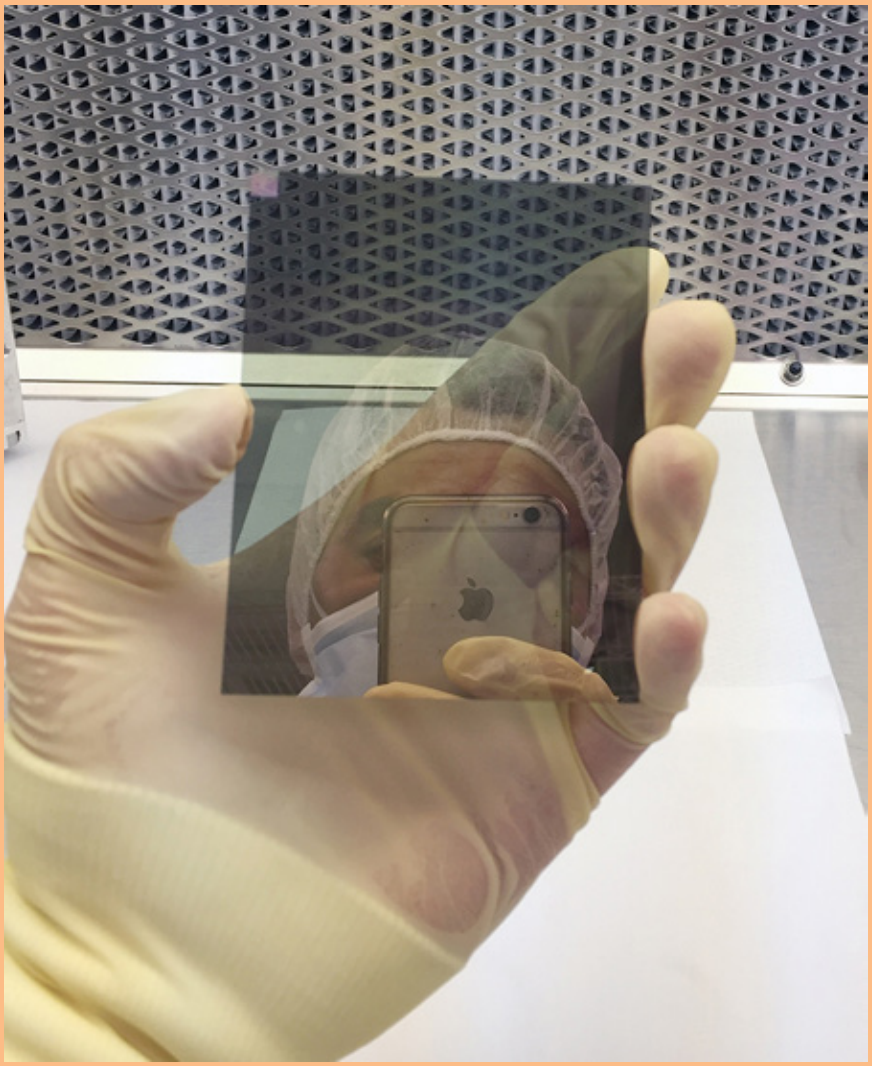

Fig. 1. *A full-format, off-plane, X-ray reflection grating. The grating measures 75 mm×96 mm in grooved area and is replicated onto a fused-silica substrate. The coating is 5-nm Cr under 15-nm Au. A 5 mm×5 mm area in the top left, with a noticeable optical diffraction grating, is used for alignment purposes.*

While addressing the issue of scale for alignment, our initial production processes require further development to create the continuously variable groove density that is optimal for spectral resolving power. Variables in the fabrication process can lead to period error, and hence reduced resolving power. Therefore, future off-plane grating development is required to perform the process development necessary to create a continuously variable groove period. Previous prototype gratings were capable of achieving high spectral resolving power, but these gratings are small in scale and only partially illuminated during testing. Large-format, optimized gratings continue to be a critical technology for development as future fabrication improvements and subsequent performance testing is required.

During our grating fabrication efforts, we also performance-tested the blazed profile for diffraction efficiency. These tests were carried out at the Advanced Light Source at Lawrence Berkeley National Laboratory (LBNL) in collaboration with Eric Gullikson. A 29.5° blazed grating from the initial batch of large-format gratings described above underwent testing and produced the diffraction efficiencies displayed in Fig. 2.

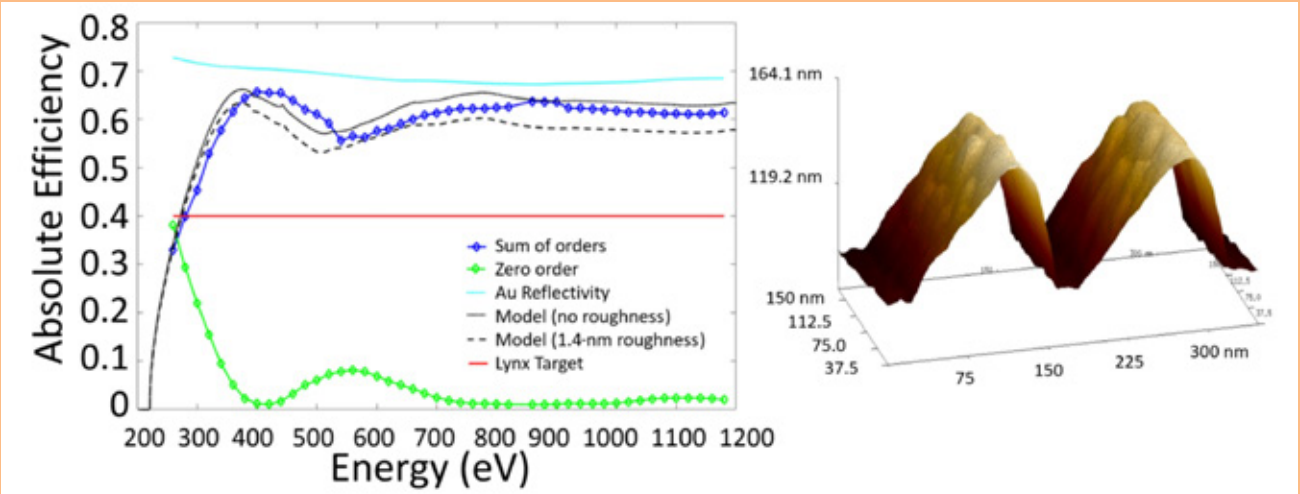

Fig. 2. Left: *The measured (blue data points) absolute diffraction efficiency (includes Au reflectivity, cyan line) is compared to theoretical models generated using PCGrate with (dashed black line) and without (solid black line) the measured roughness of the Au coating. The red line shows the Lynx requirement for reference.* Right: *atomic-force-microscopy (AFM) image of a small section of the grating used to produce these data and theoretical curves.*

The diffraction efficiencies of the blazed off-plane grating are shown in Fig. 2 for orders measured between 0.3 keV and 1.2 keV. The sum of absolute efficiencies (includes Au reflectivity) in diffracted orders 1-4 is shown and measured to be greater than ~60% over the band. This is the highest diffraction efficiency measured to date for a blazed grating and is an important result, as it shows that gratings such as these can achieve performance goals necessary for future spectrographs. A few-percent gain can still be realized by reducing roughness in the imprint resist and metal coating. Methods for achieving this gain have been formulated but require a future technology development study.

Our alignment developments paralleled our large-format grating production. We fabricated and aligned a high-fidelity, flight-like grating module. The alignment system is shown in Fig. 3 along with a table of the alignment tolerance goals we were trying to meet for this initial test. The module is made from Invar and holds onto the gratings with a clip-and-pin system [15]. The assembly with four aligned, large-format gratings is shown in Fig. 4 inside the SLF test chamber, along with the single shell of slumped-glass optics provided by Will Zhang's group at GSFC. These gratings are aligned to be parallel to one another, given that our X-ray test setup consists of a single mirror shell [16]. In this way, we can scan the individual gratings across the single telescope beam and watch the position of the spectrum at the focal plane to assess the alignment achieved. X-ray alignment tests were carried out at the SLF, including a vibration test between X-ray verification tests. The module was vibrated at the NASA General Environmental Verification Standard (GEVS) levels and survived qualification at 14.1g root mean square (rms) in three axes.

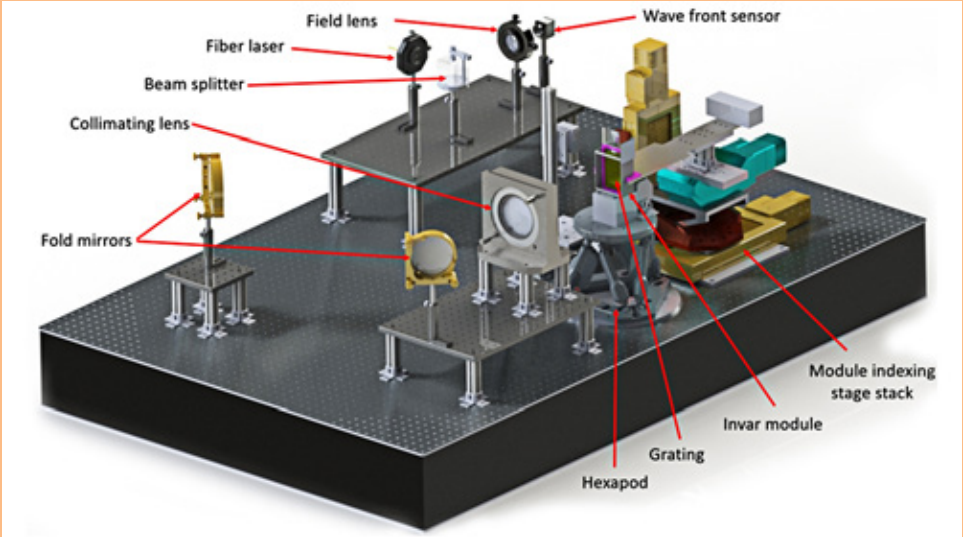

Fig. 3. *The off-plane reflection grating alignment setup. A spherically diverging laser is passed off the grating surface and back through the system to a wavefront sensor (WFS) to measure pitch and roll on the grating. The position of the grating is controlled by a hexapod. The grating module is indexed using an independent stage stack, and the module is referenced using a theodolite.*

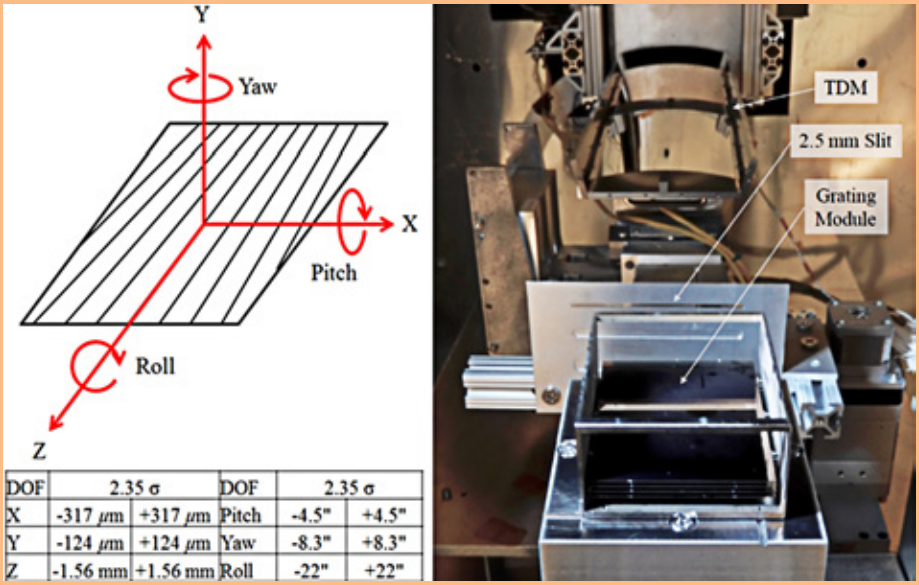

DOF	2.35 σ		DOF	2.35 σ	
X	-317 μm	+317 μm	Pitch	-4.5"	+4.5"
Y	-124 μm	+124 μm	Yaw	-8.3"	+8.3"
Z	-1.56 mm	+1.56 mm	Roll	-22"	+22"

Fig. 4. Left: *A definition of the grating axes and the alignment tolerances as full-width-half-maximum variance within the module (DOF, Degree of Freedom).* Right: *The aligned module being tested with a slumped-glass optic at the SLF. The grating module measures 83 mm × 99 mm × 45 mm and contains four large-format gratings (TDM, technology development module).*

Analysis of the achieved alignment has been completed [17]. Positions for the telescope focus, zero-order grating image, and orders up to ±3rd were used to construct a circle at the focal plane that defines the arc of diffraction and therefore the grating attitude. The projection of the grating surface is the diameter of the circle that is a perpendicular bisector to a line drawn between the telescope focus and the zero-order image, thus giving pitch and roll, while the center of the grating is the projection of the gratings' central groove onto the focal plane, thus giving yaw. Calculating the three rotational DOFs for each grating shows the variance of these factors within the module, which then qualifies our alignment. These measurements were repeated following the vibration test. The achieved alignment tolerances are shown in Table 1. These numbers signify the 1σ variation between gratings in the stack. For instance, a pre-vibe pitch measurement of 9.8" means that the four gratings vary about the average pitch angle by 9.8", 1σ, and that this number has a 13.5" error. In these calculations we have accounted for the translational constraints of our module and alignment metrology (σ_x = 130 μm, σ_y = 26 μm, σ_z = 15 μm) as well as the anticipated 1 g gravity sag (~1 μm over the 0.25×2.0 mm illuminated grating area) as calculated using a finite element analysis of the gratings in the module.

DOF	Goal 1σ	Pre-vibe 1σ	Post-vibe 1σ
Pitch	3.8"	9.80±13.5"	6.2±12.3"
Yaw	7.1"	97.8±8.20"	125±14.2"
Roll	19"	35.9±39.4"	36.6±37.8"

Table 1. *Goal and measured alignment tolerances from MSFC test.*

There are two main takeaways from these numbers. First, the measured values for the rotational DOFs are larger than the goal tolerances. Second, the measurement errors are substantial and often larger than the measured values. These takeaways demonstrate that our optical alignment setup is currently not constraining or measuring the grating's rotational DOFs sufficiently to achieve the alignment goals. The yaw measurement is the only one larger than its own uncertainty. The poor control of yaw was due to poor constraint of the yaw laser and camera positions during alignment. Inspection of the mounts uncovered that their positions drift over time and with temperature. Furthermore, the yaw laser is unstable with a shape that changes over the time it takes to mount a grating, thus affecting the calculation for the spot centroid and hence yaw. Future alignment setups must account for this and implement a stable yaw solution. Next, the values for pitch and roll need to be better constrained. The WFS likely under-samples the grating surface given only 29×37 measurement points over 72 cm^2. Also, WFS calibration to an external reference flat has comparable error to grating measurements, thus contributing to system uncertainty. The WFS system also includes several optical components with temperature-sensitive stability. We measured pitch and roll stability on a reference grating as a function of temperature over four days and found strong correlations. The pitch and roll varied by >5" and >2.5", respectively, given a 0.8° C temperature fluctuation. Therefore, upgrades to the pitch and roll measurement technique should sample the grating better, require fewer components, and be stable with temperature. The next factor to consider from Table 1 is the uncertainty in the roll measurement, which is large while also being larger than the measured value. This error is dominated by uncertainties associated with the detector stages. These are large, 1-m translation stages, mounted in an orthogonal configuration. The knowledge on the orthogonality is only 0.2° and the translations have errors of 0.1 mm. Therefore, future grating-module alignment verification using X-ray performance testing must incorporate metrology to verify detector-stage position to higher accuracy. Finally, while the errors in pitch are smaller than those for roll, they are still larger than the measured values. The pitch errors

are dominated by uncertainty in the circle fits to the measured order and focus positions. The circles are poorly constrained, not only due to detector-stage uncertainty, but also because the spectral-line lengths in the cross-dispersion direction increase with increasing order. This effect occurs because even though the grating is a variable-line-spaced grating, the grooves are still parallel to one another. When placed in the converging beam of a telescope, the incident light on one side of the grating has a much different α in the grating equation than light incident on the other side, thus resulting in spread along the cross-dispersion direction. This could be remedied using a true radial groove profile, but this effort simply used the first batch of large-format gratings, which were not optimized for this study.

In summary, we have measured alignment tolerances that are larger than our goals, with measurement uncertainties that poorly constrain these values. We have identified reasons for these shortcomings, and once they are addressed, we will be capable of assessing our achieved tolerances at the level required to verify our alignment. However, to overcome these shortcomings, we require 1) better radial approximations on the gratings; 2) more robust constraint and stability for pitch, roll, and yaw; and 3) better accuracy in detector staging. Once alignments are verified with X rays before and after environmental testing, the aligned modules will have achieved TRL 5 for off-plane reflection-grating spectrographs. These efforts will require a future development program.

Path Forward

SAT targeted development of reflection gratings has led to many successes while also elucidating several areas for future study. First, our grating fabrication process requires further development to create the continuously variable groove density that is optimal for spectral resolving power. The process needs to be tested on large-format gratings, as issues of scale arise when moving from process development pieces to flight-like structures. Once the process is in place, optimization studies could maximize grating performance through minimizing surface roughness, minimizing coating stress, and optimizing groove density. A series of performance-verification tests is necessary to verify diffraction efficiency and spectral resolving power at each step.

In addition to grating fabrication improvements, our alignment procedure requires upgrading the metrology system. Using our current system, we have measured alignment tolerances that are too large and poorly constrained. Fortunately, the reasons for the lack of accuracy are straightforward and can be remedied with a new alignment system that has been designed and is ready for implementation. Following the improved grating fabrication study, improved alignment results can be achieved with more-robust constraints on pitch, roll, and yaw, combined with better detector-staging and test-setup-metrology accuracy. Once alignments of newly fabricated gratings are X-ray-verified before and after environmental testing, the aligned modules will have achieved TRL 5 for off-plane reflection-grating spectrographs.

References

[1] R.L. McEntaffer, C. DeRoo, T. Schultz, B. Gantner, J. Tutt, A. Holland, S. O'Dell, J. Gaskin, J. Kolodziejczak, W.W. Zhang, K.-W. Chan, M. Biskach, R. McClelland, D. Iazikov, X. Wang, and L. Koecher, "*First results from a next-generation off-plane X-ray diffraction grating*," Experimental Astronomy, **36**, 389 (2013)

[2] R. Allured and R.L. McEntaffer, "*Analytical Alignment Tolerances for Off-Plane Reflection Grating Spectroscopy*," Experimental Astronomy, **36**, 661 (2013)

[3] R. Allured, B.D. Donovan, and R.L. McEntaffer, "*Alignment Tolerances for Off-Plane Reflection Grating Spectrometry: Theoretical Calculations and Laboratory Techniques*," Proc. SPIE, **8861**, 88611C (2013)

[4] C. DeRoo, R.L. McEntaffer, T. Schultz, W.W. Zhang, N.J. Murray, S.L. O'Dell, and W. Cash, "*Pushing the boundaries of X-ray grating spectroscopy in a suborbital rocket*," Proc. SPIE, **8861**, 88611B (2013)

[5] H. Marlowe et al., "*Performance Testing of an Off-plane Reflection Grating and Silicon Pore Optic Spectrograph at PANTER*," J. Astro. Tele., Inst., and Sys., **1**, 045004 (2015)

[6] R. Allured, B. Donovan, C. DeRoo, H. Marlowe, R.L. McEntaffer, J. Tutt, P. Cheimets, E. Hertz, R.K. Smith, V. Burwitz, G. Hartner, and B. Menz, "*Optical and x-ray alignment approaches for off-plane reflection gratings*," Proc. SPIE, **9603**, 960315 (2015)

[7] C. DeRoo et al., "*Line Spread Functions of Blazed Off-Plane Gratings Operated in the Littrow Mounting*," J. Astro. Tele., Inst., and Sys., **2**, 025001 (2016)

[8] J.H. Tutt, R.L. McEntaffer, H. Marlowe, D.M. Miles, T.J. Peterson, C. DeRoo, F. Scholze, and C. Laubis, "*Diffraction Efficiency Testing of Sinusoidal and Blazed Off-Plane Reflection Gratings*," Journal of Astronomical Instrumentation, **5**, 1650009 (2016)

[9] H. Marlowe, R.L. McEntaffer, J.H. Tutt, C.T. DeRoo, D.M. Miles, L.I. Goray, L.I. Soltwisch, F. Scholze, A. Fernandez Herrero, and C. Laubis, "*Modeling and Empirical Characterization of the Polarization Response of Off-plane Reflection Gratings*," Applied Optics, **55**, 5548 (2016)

[10] National Aeronautics and Space Administration, Physics of the Cosmos Program Annual Technology Report, REP. NO. 440-RPT-0019 (2016)

[11] M.W. Bautz, W.C. Cash, J.E. Davis, R.K. Heilmann, D.P. Huenemoerder, M.L. Schattenburg, R.L. McEntaffer, R.K. Smith, S.J. Wolk, W.W. Zhang, S.P. Jordan, and C.F. Lillie, "*Concepts for high-performance soft X-ray grating spectroscopy in a moderate-scale mission*," Proc. SPIE, **8443**, 844315 (2012)

[12] R.K. Smith et al., "*Arcus: an ISS-attached high-resolution X-ray grating spectrometer*," Proc. SPIE, **9144**, 91444Y (2014)

[13] J.A. Gaskin et al., "*The X-ray Surveyor Mission: a concept study*," Proc. SPIE, **9601**, 96010J (2015)

[14] C. DeRoo et al., "*Diffraction efficiencies of Blazed Off-Plane Gratings Operated in the Littrow Mounting*," Applied Optics, in preparation (2016)

[15] K.-W. Chan et al., "*Aligning, bonding, and testing mirrors for lightweight X-ray telescopes*," Proc. SPIE, **9603**, 96030Z (2015)

[16] J.H. Tutt et al., "*Alignment of off-plane reflection gratings using optical light*," J. Astro. Instr., in preparation (2016)

[17] B. Donovan et al., "*X-ray and environmental testing of an aligned off-plane grating module*," in preparation (2017)

For additional information, contact Randall McEntaffer: *rlm90@psu.edu*

Development of 0.5-Arcsecond Adjustable Grazing-Incidence X-ray Mirrors for the SMART-X Mission Concept

Prepared by: Paul B. Reid (PI; SAO) and Eric Schwartz (SAO)

Summary

"*Development of 0.5-Arcsecond Adjustable Grazing Incidence X-ray Mirrors for the SMART-X Mission Concept*," NASA Contract NNX15AC44G, is a Strategic Astrophysics Technology (SAT) program that began in February 2015 and is scheduled to run through the end of fiscal year (FY) 2017. This program follows an earlier Astrophysics Research and Analysis (APRA) project on the development of adjustable X-ray optics. The program seeks to develop a modular, highly nested grazing-incidence X-ray mirror assembly composed of bimorph adjustable X-ray mirror segments to achieve 0.5-arcsec imaging while also achieving extremely lightweight mirror assembly mass-per-unit-effective-area (e.g., <500 kg/m^2 effective area, compared to ~16,000 kg/m^2 for Chandra). Also included in this report is our new SAT program "*Hybrid lightweight X-ray optics for half arc second imaging*," NASA Contract NNX17AG77G. This program is for the development of the hybrid X-ray mirror segments that combine the two technologies of adjustable X-ray optics to correct low spatial-error frequencies and differential deposition to correct mid-spatial-error frequencies. Funding for this SAT has only recently been received at SAO through the Smithsonian Institution, so there is no work yet on which to report. Our technology will enable large-area, high-resolution, imaging X-ray telescope mission concepts such as the Square Meter Arc-second Resolution Telescope for X rays (SMART-X) [1], or equivalently, the 2013 NASA Astrophysics Roadmap committee-recommended X-ray Surveyor (XRS) [2] mission concept, now under NASA study as the Lynx mission concept. Lynx will study the early universe (growth of structure, and merger history of black holes), as well as the feedback and evolution of matter and energy.

Our adjustable-optics technology eliminates the figure errors and unwanted distortions usually inherent in thin lightweight mirrors. We use a thin (nominally 1.5-μm) film of the piezoelectric material, lead zirconate titanate (PZT), sputtered as a continuous film on the back of thin (0.4-mm) thermally formed glass Wolter-I mirror segments (a continuous ground electrode is first applied to the back surface). A pattern of independently addressable platinum (Pt) electrodes is deposited on top of the PZT layer, forming individual piezo cells. Applying a low (<10-V) DC voltage between a cell's top electrode and the ground electrode creates an electric field that produces a local strain in the piezo material parallel to the mirror surface. This strain causes localized bending in the mirror, called an influence function. By supplying an optimally chosen voltage to each of the individual cells, one can change the amplitude of each influence function to minimize figure errors in the mirror, thereby improving imaging performance. This allows us to correct mirror figure errors from fabrication, distortions introduced during mounting, and any gravity-release errors. Figure correction is implemented once on the ground during a calibration step after mirror alignment and mounting. Adjusting and correcting the figure of thin mirror segments increases their performance from the 10-arcsec resolution level to 0.5 arcsec. We have shown through simulations improvements from ~7 arcsec half-power diameter (HPD) to less than 0.5-arcsec HPD using exemplar-mirror figure data and modeled influence functions [3].

Besides the adjustable optics and Lynx teams at the Smithsonian Astrophysical Observatory (SAO), significant contributors to the adjustable optics team are our colleagues at Penn State University (PSU) Materials Research Institute. Prof. Susan Trolier-McKinstry and Prof. Tom Jackson; supported by Tianning Liu, Mohit Tendulkar, and Dr. Julian Walker; develop the PZT processes, compensating film stress layer, Anisotropic Conductive Film (ACF), and ZnO thin-film transistor.

The SAT project began at SAO in April 2015. Progress to date includes performing structural thermal and optical performance (STOP) analyses to examine the performance sensitivity of mirror-assembly temperature control, developing adjustable-mirror-segment technology, developing alignment and mounting technology, reducing mirror complexity via row-column addressing and developing the application of microelectronics industry electrical connectivity, and developing adjustable-mirror-performance monitoring technology that could be used for on-orbit figure correction.

Background

Lynx will be able to address a plethora of important science goals: studies of the growth of supermassive black holes (SMBH) and strong gravity effects, evolution of large-scale structure and detection of the warm-hot interstellar medium (WHIM), and active galactic nuclei (AGN) feedback and cycles of matter and energy. It will be able to carry out surveys to the Chandra deep-field depth over 10 deg^2; study galaxy assembly processes to z=2.5; track the evolution of group-sized objects, including those hosting the first quasars, to z=6; and open new opportunities in the time domain and high-resolution spectroscopy.

Over the past few years, we have developed the concept of the adjustable-optic X-ray telescope. The challenge is to develop a mirror assembly, equivalent to the Chandra High-Resolution Mirror Assembly (HRMA), to a high level of technical readiness over the next several years to provide Chandra-like 0.5-arcsec HPD angular resolution with large effective area. The goal is 2.3 m^2 at 1 keV, or ~30 times that of Chandra, which would be a tremendous increase (a factor-of-four increase in area from Palomar to Keck was considered a breakthrough at the time).

Lynx, formerly the XRS, was specifically mentioned in the 2013 Astrophysics Roadmap [2], and survives to the current date with its name changed but its science goals and telescope requirements unchanged. It is currently under study by a MSFC/SAO-led team as part of the 2020 Decadal Survey preparations authorized and funded by NASA HQ. The three other mission concepts being studied are the Large UV/Optical/IR (LUVOIR) Surveyor; the Habitable Exoplanet (HabEx) Imaging Mission; and the Origins Space Telescope (OST), formerly known as the Far-IR Surveyor.

Our baseline plan for Lynx optics uses slumped-glass mirror segments with deposited piezoelectric actuators energized to correct mirror figure errors from 10-arcsec HPD (achieved for the International X-ray Observatory, IXO; and Advanced X-ray Spectroscopic Imaging Observatory, AXSIO) [4] to better than 0.5-arcsec HPD. The slumped-glass mirror segments developed for IXO/AXSIO represent the current state of the art in lightweight optics. Another approach to develop adjustable X-ray optics, in parallel to our work, relied on gluing individual, thick (0.2-mm) ceramic piezoelectric actuators to thin mirrors. This resulted in large 'print-thru' errors in the mirror figure [5]. Our approach builds on the mirror development for IXO/AXSIO, in terms of the thermally formed substrates, as well as mirror alignment and mounting. The addition of the piezoelectric layer is essentially just a single process step in the mirror-fabrication process. Our approach resolves the two main problems with lightweight

slumped-glass mirrors: (1) it corrects for the low-frequency figure errors that result from a combination of mandrel and thermal-forming errors, and (2) it corrects after the fact for deformations introduced in coating and mounting thin flexible mirrors. In addition, the ability to make an on-orbit correction of mirror figure is critical for telescopes with apertures larger than can be tested with full aperture on the ground (i.e., larger than Chandra).

Our development plan contains several major activities:

1. Development of thin, lightweight slumped-glass, adjustable optics with corrected figure better than 1 arcsec, as demonstrated by X-ray testing of an aligned mounted pair of segments.
2. Flight-like mounting of aligned mirrors in a modular housing that maintains sub-arcsec alignment through the application of launch loads, and after (spacecraft) thermal survival temperature cycling.
3. Connection of control signals and power to the adjustable optics in their flight-like housing, without introducing loads into the mirrors and without losing connection after launch.

We will generate requirements for an adjustable-optic mirror assembly capable of achieving 0.5-arcsec HPD. This includes iterative error-budgeting as well as thermal and structural modeling, balancing the difficulty of achieving multiple mirror-assembly requirements.

We will develop, design, and model a flight-like mounting able to support multiple, closely spaced shells of adjustable mirror segments. This will entail structural and thermal modeling to ensure compatibility with system requirements. Subsequently, we will develop hardware to implement and test the designs.

We will explore the use of ACFs for connecting control and power lines to the mirror segment. ACFs are film adhesives with uniformly dispersed conductive particles, several micrometers in diameter, in a low-temperature thermo-setting resin [6-9]. They are used routinely in connecting to LCD and organic LED (OLED) displays and connecting bare chips directly onto glass, because they are extremely thin and allow a high connection density without difficult alignments. They are standard products manufactured by companies such as Hitachi and 3M, among others. We will investigate the deformations introduced into the mirrors by ACFs by measuring the figure of mounted mirrors before and after bonding ACF connections onto the mirror. We will also investigate thermal effects on ACF-induced stresses under temperature changes resulting from the differing coefficients of thermal expansion (CTEs) of the ACF and the mirror segment, and explore the best location structurally to make the connections without degrading mirror effective area, while mitigating attachment-related stresses. Lastly, the ACF connections will be in place before vibro-acoustic and thermal-cycling tests, and we will test for functionality after these environmental tests. This effort comprises about 10% of our budgeted work and will be performed at PSU. Performance testing will be carried out at SAO, and environmental testing at MSFC.

Objectives and Milestones

SAO began the project in April 2015 and has made good progress against the baseline plan. Figure 1 shows the annotated baseline schedule from our proposal. Thermal modeling and structural analysis have proved to be far more work than originally envisioned. Assembly, test, and alignment activities have also gone more slowly, as we have learned much and modified our approaches accordingly.

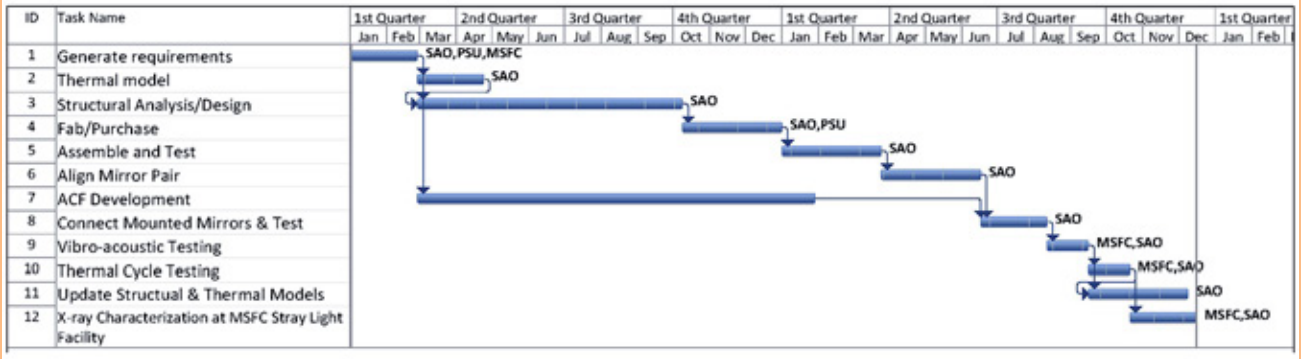

Fig. 1. *Project schedule (SLF, Stray Light Facility).*

At present, given that we expect to exhaust program funds by the end of FY 2017 or Calendar Year (CY) 2017, we will not accomplish work on Tasks 9 through 12. We continue working on Tasks 3, 5, 7, and 8 – structural analysis/design, assembly and testing, ACF development, and testing mounted mirrors, respectively – and will report in the next section on progress on those tasks, along with progress on Task 6, mirror alignment.

Progress and Accomplishments

We believe significant progress was achieved in the areas of design and analysis of the mirror mounting (Task 3), assembling the mirror into its mount and measuring impact on mirror figure (Task 5), development of ACF electrical connectivity to the mirror (Task 7), and testing the mounted connected mirror (Task 8). In addition, we gained significant additional understanding with respect to mirror alignment methodology and have modified our planned approach (Task 6). All these are discussed below.

ACF electrical connectivity: ACF development has progressed significantly over the past year. During that period, we first determined that the mirror deformations introduced by the ACF bonding process are both small and well localized to the vicinity of the bond – the distortions do not intrude into what would be mirror clear aperture. We developed the capability to apply the ACF bonds to conical mirrors (previously they were applied to flat mirrors). We increased our electrical contact density from 1 contact/mm to 3/mm (note that in a micro-electronics fabrication facility, ACF connections are used for contact densities as high as 100/mm, but we are doing this in a university lab). We fabricated a cylindrical mirror with 112 piezoelectric actuators and, for test purposes, six separate ACF bonded-ribbon cables, shown in Fig. 2. For purposes of assembling the mirror into its housing and also connecting it to the control electronics, we actually employ multiple connections and a small electrical interface board between the mirror and the control electronics, but these are just an artefact of trying to test out the ACF in a straightforward way and not reproduce already-manufactured cables and connections. An additional point to make is that this still complex-appearing mirror is not what is envisioned as the final version of adjustable X-ray optics. In our current versions, each actuator must be individually addressed by a wire – 112 wires and contacts for 112 adjusters, plus an extra for the ground electrode. That is what is shown in Fig. 2. In final form, ZnO thin film transistors, being developed by PSU, will be integrated directly with the mirror electrodes, enabling the same row-column addressing that exists in all LCDs. There, one only requires as many wires as the sum of the number of rows and columns, plus the ground. As an example, were we ready to use row-column addressing on this test mirror with

112 actuator cells, we would require only 24 wires (for 16 rows, 7 columns, and 1 ground), compared to 113 wires (for 112 cells and 1 ground) presently necessary. That would mean we would need only one ACF connection and one ribbon cable. We are just not ready to incorporate the ZnO Thin-film Transistors (TFTs) at this time. Continuity-testing of the ACF connections and the electrical cables indicate good electrical contact.

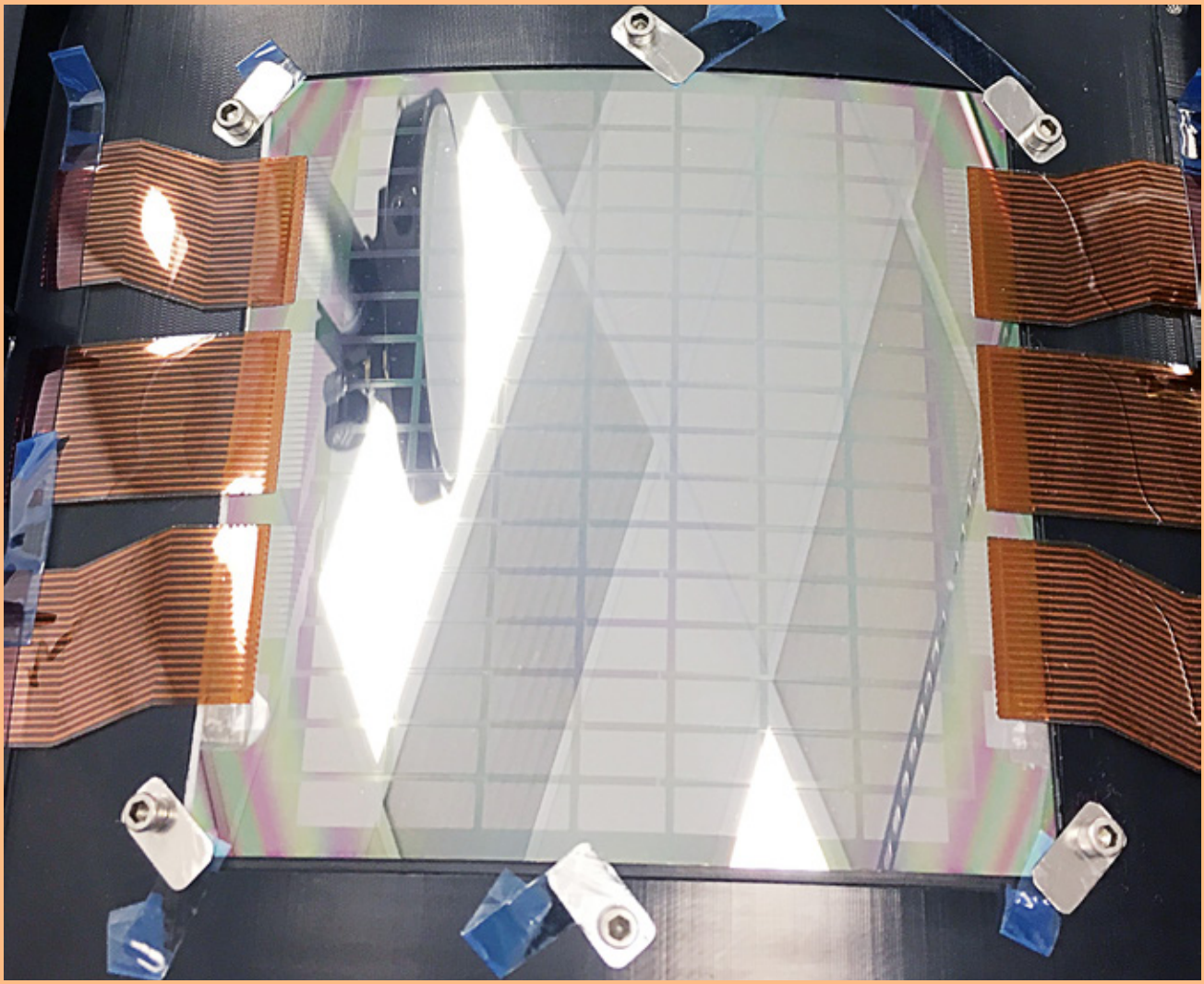

Fig. 2. *Adjustable mirror with six ribbon cables ACF-bonded to the mirror.*

Assembling mirror into mount and measuring mount-related distortions: We conducted mirror-mounting tests, wherein we go through all the steps to mount a mirror into the mirror housing, employing our wavefront sensor (WFS) optical metrology to monitor mirror figure during the assembly and bonding process. In the first test, we used a lower-quality cylindrical mirror without any piezoelectric film; and for the second test, we used a fully functional adjustable mirror including six ACF bonded-ribbon cables. A figure of the "dummy" mirror being mounted during an intermediate step is shown in Fig. 3. The mirror front surface is coated with 40 nm of evaporated gold to serve as a low (coating) stress reflective film for the WFS in-process figure metrology. During the first test assembly, we discovered an interfacing error that resulted in more bending than desired for our 5-degree-of-freedom (dof) radial

wire flexures. This introduced significant mirror distortions. For our second test, using a functional adjustable mirror complete with ACF-bonded flex cables, we addressed this issue by shimming to eliminate the wire flexure bending. A photograph of the mounted mirror (front and back) is shown in Fig. 4. Figure 5 shows the in-situ metrology setup with the WFS and a suitably sized diffractive cylindrical null corrector, also known as a computer-generated hologram (CGH). The cylindrical null converts a plane wave to a cylindrical wave for testing cylindrical or conical mirrors. Results of this test still reveal a large sensitivity to any loads introduced in the radial wire flexures, producing relatively large distortions, as shown in Fig. 6. The figure represents a contour plot of the change in mirror figure as a result of bonding and curing the radial wire flexures to the mirror. We do observe that the peak-to-valley change in shape is relatively large (>1 μm), greater than our targeted maximum figure change. The extremes of the changes, though, do mostly occur near the mirror edges which will in some cases be shadowed by mirror housing structure. We are still analyzing these data to determine how much of the distortion can be corrected in the mirror clear aperture via the adjusters.

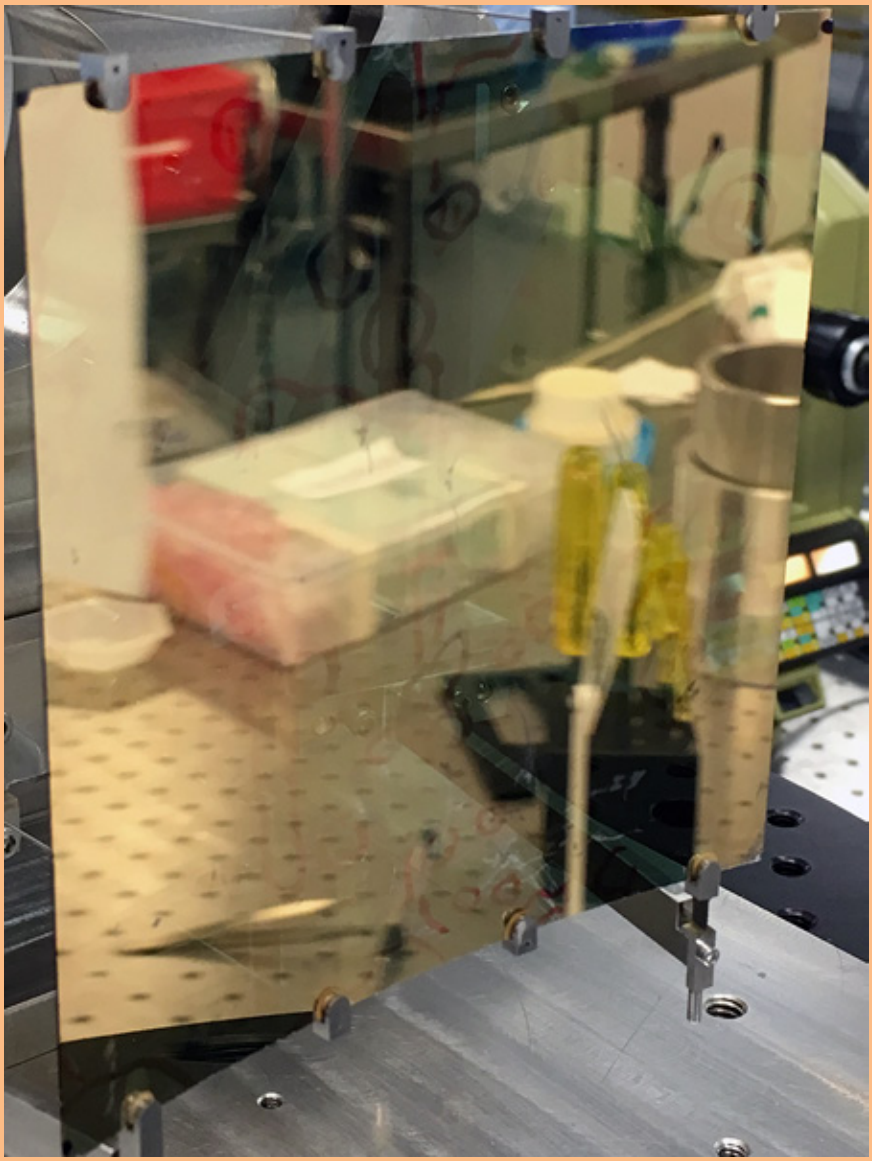

Fig. 3. *Intermediate assembly step of dummy mirror. The gold-coated concave side faces the reader.*

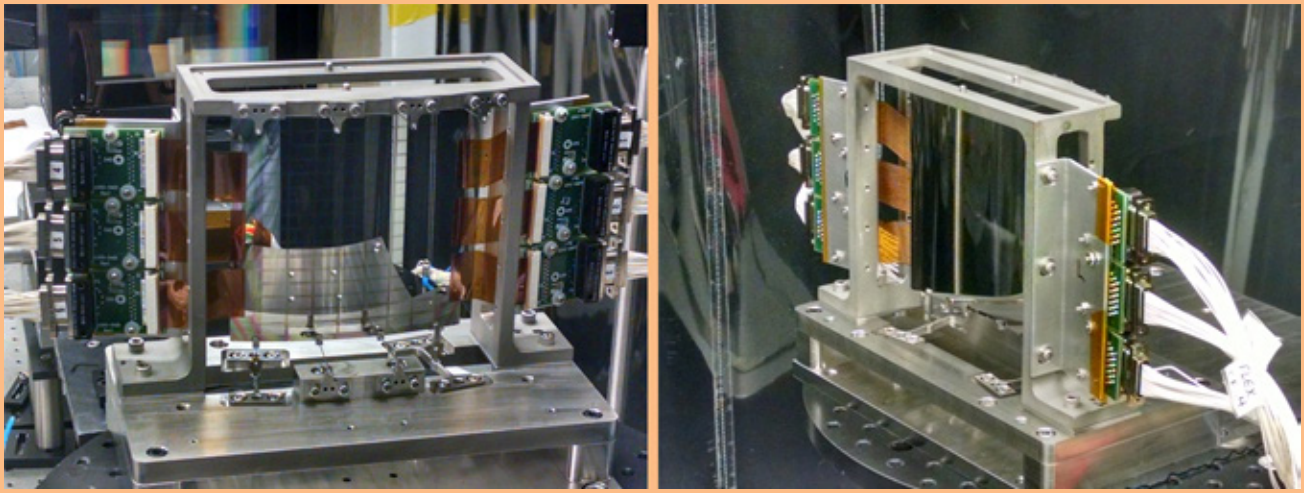

Fig. 4. Left: *Front (concave side) view of a functional adjustable mirror mounted in its housing with electrical cables.* Right: *Back (convex side) view of the adjustable mirror in its housing. The ACF connections and the adapter boards can be seen.*

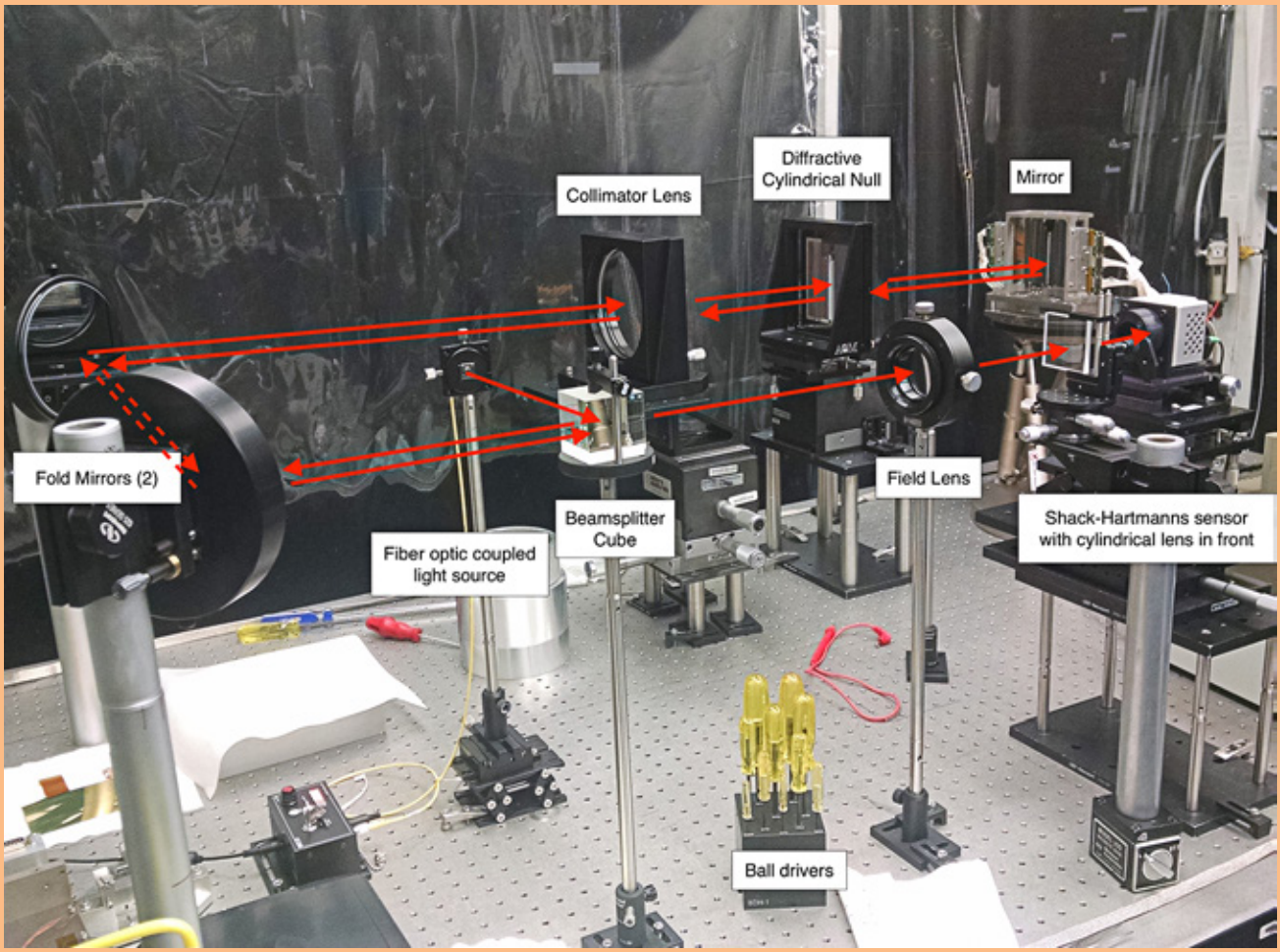

Fig. 5. *Metrology setup utilizing a diffractive cylindrical null corrector and a Shack-Hartmann WFS.*

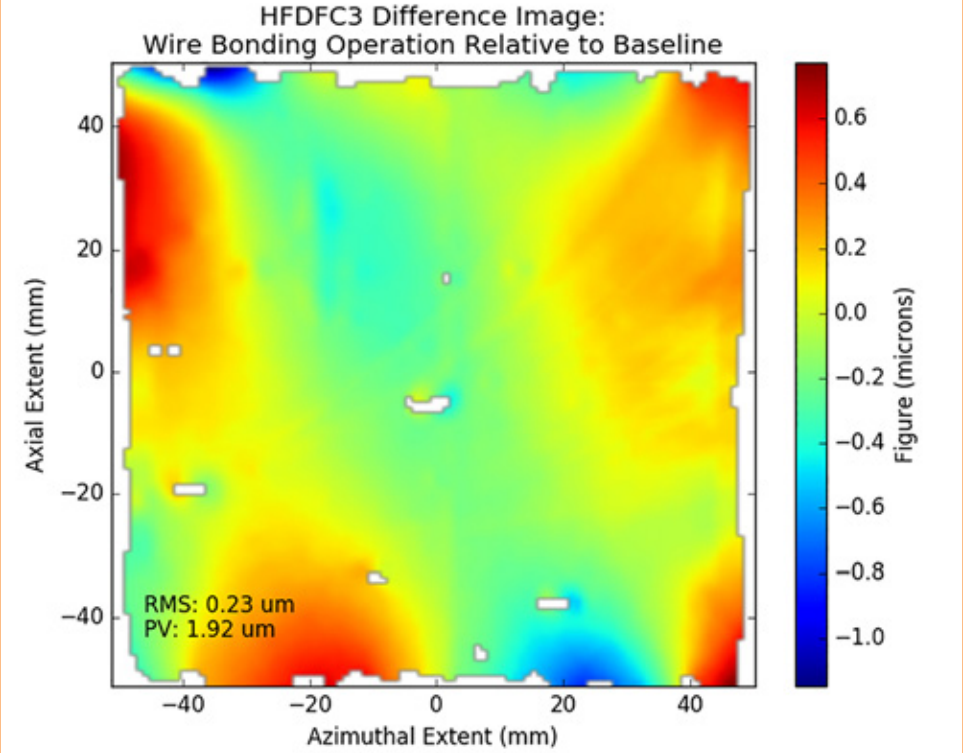

Fig. 6. *Contour map of figure change during the mounting process. This map shows the change from the baseline (pre-mounted) metrology to after the bonding (including curing) of the wire flexures to the mirror (HFDFC3, High-Fidelity Deterministic-Figure-Control experiment, 3rd version).*

Design and structural analysis of mirror mount: As a result of the larger-than-expected mount-related distortions introduced, we are taking another look to determine if a more optimal set of real-world constraints can be achieved. To do this, we are carrying out additional finite element analyses (FEAs), including comparing the sensitivity of designs where the support points are located on the axial ends (as is the case at present) vs. locating support points on the azimuthal sides. Our initial selection of the axial ends for the supports was intended to reduce stress on the glass during launch, when supports are located in the (launch) thrust axis. However, given that we believe results of much earlier (IXO) glass-strength testing show sufficient strength to support azimuthal side constraints, we will re-examine that possibility to see if it offers reduced sensitivity to random stray support loads during assembly. This analysis will all be done with finite element modeling, and will be described in our final report.

Mounted-mirror testing: Photographs of the mounted mirror are shown in Fig. 4, with mirror metrology shown in Fig. 5. We are in the process of testing this mirror as of this writing, so results are incomplete. At present, we are still in the characterization and calibration phase of our test plan, wherein we are measuring the influence functions for each of the 112 piezo cells as a function of voltage. An example of an influence function measurement is shown in Fig. 7. In the figure, a nice, well-defined influence function is observed at 5 volts. Voltage to each cell is controlled via the control electronics and PC-based control software. Calibration of the piezo cells includes calibrating the hysteresis curve for each cell. Following that activity, we will verify that the piezoelectric material is fully polarized ("poled")

by "re-poling"–applying the polarization voltage to all mirror cells for a fixed period of time–and then recalibrating to see if the calibration changes. At that point we will be ready to begin figure-correction testing. There will be several phases to that testing, including: (1) attempted correction of actual mirror-figure errors, (2) examining the use of different filtering methods to reduce the impact of metrology noise on the adjuster-voltage optimization algorithms, and (3) imparting deformations of various amplitudes and frequency content in order to characterize the error-correction transfer function. The second test, while not actually correcting the mirror, will give us more information as it will tell us what the correction efficiency is for a mirror with a different set of errors and a different error-power-spectrum density. This kind of test will provide an experimental verification of our computer-simulation tool, which does the same kind of thing, but of course, only in the virtual world.

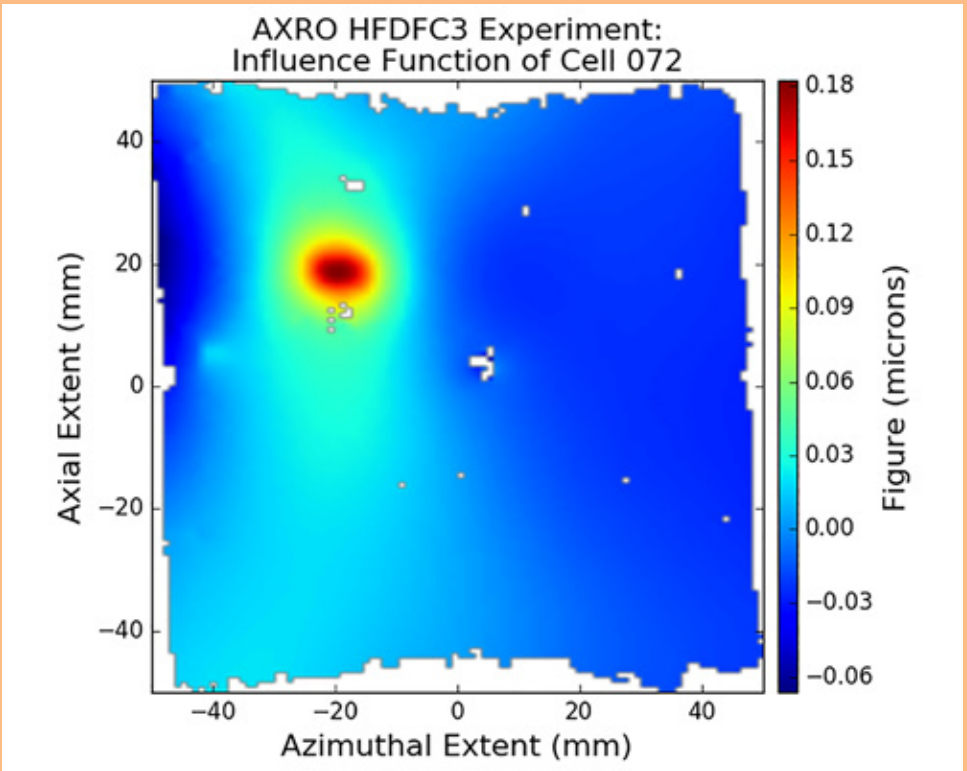

Fig. 7. *Sample influence-function measurement at 5 V (AXRO, Adjustable X-Ray Optics).*

Mirror-pair alignment: Over the past year, we performed extensive ray-trace modeling of our intended alignment approach, which was to apply the Chandra methodology of a double-pass-scanning Hartmann test. A Hartmann test is basically a physical implementation of ray-tracing, in that a pencil-beam of light is passed through an optical system, and the location where that pencil beam intersects the focal plane is determined. By using a sufficient number of pencil beams in predetermined "important" locations of the entrance aperture, one can reconstruct the optical aberrations present in the optical system. For grazing-incidence optics, one arrays the pencil beams about the annular aperture of the mirror. The method is well-suited for determining focus error and coma, which result from spacing error between the primary and secondary mirror, and relative tilts and decenters between the primary and secondary, respectively. For Chandra, a metrology instrument called the Centroid Detector Assembly (CDA) was used. This device both produced the pencil beams to interrogate the optics, and used a

position-sensitive quad cell to determine the return position of the pencil beams on the focal plane. The pencil beam source was positioned at the focus of the optical system, and the beams incident upon the aft end of the mirror or mirror pair, nominally collimated on the output of the mirror system, and then retro-reflected by a plane mirror back through the grazing incidence mirror system, to be focused on or near the original focus. This system worked well with Chandra, resulting in ~0.25-arcsec root mean square (rms) diameter image contribution from residual coma and focus alignment errors (this is nominally the error budget allocation for Lynx mirror pair alignment). For our alignment, we used an improved 2nd-generation version of the CDA.

Our ray-trace modeling revealed a significant problem with this approach for adjustable X-ray optics. A double-pass system was desirable for Chandra in order to improve metrology sensitivity (the impact of alignment errors are doubled in such a double-pass system). But the Chandra mirrors were at final figure requirements at the time of alignment; i.e., the mirror-pair figure errors were consistent with 0.5-arcsec imaging performance. The adjustable X-ray optics are aligned and mounted (like Chandra) as part of the same operation. The uncorrected adjustable mirrors would nominally form an ~10-arcsec mirror pair, or ~20 times larger errors than Chandra. We found via ray-tracing that the problem of retrace error would make the double-pass Hartmann test results basically uninterpretable. Retrace error is what happens in a double-pass system when the rays intersect one part of the optical system on the first pass through the system, but intersect a very different part on the second pass. This a result of the figure errors encountered the first time through the system–the rays are deviated enough from the first pass that they see different errors on the second pass and get further deviated by those–the rays *do not retrace* their path through the optical system. Rather than the wavefront errors measured being twice those in the optical system, the measured errors are the sum of two spatially uncorrelated errors in the system. In essence, the problem of determining the alignment errors migrates from solving a single equation with a single unknown to solving a single equation with two unknowns. With the ~20-times-better performance of Chandra at the time of alignment and mounting, impact from the figure errors was negligible. But simulations with 10-arcsec mirrors revealed large-enough errors that we would not be able to determine the relative misalignment of the mirrors.

This recognition has forced us to modify our alignment approach to a single pass system, which by its nature doesn't suffer from retrace error. We submitted an APRA proposal in March 2017 to develop a single-pass Hartmann test system using an off-axis parabolic reflector to collimate light from a single-mode fiber (which serves as a point source). There are several reasons for this approach, instead of, e.g., attempting to use an Original Equipment Manufacturer (OEM) interferometer as a collimated light source including more control over getting sufficient source intensity; control over the source wavelength (shorter wavelengths will suffer less diffraction in producing the small pencil beams); and most importantly, better ability to control, test, and calibrate the collimation of the output beam of the off-axis parabola – the beam that will serve as the input light to our grazing incidence mirror system.

Path Forward

Moving forward specifically on this SAT, we expect to finish our testing of the mounted mirror, and complete FEAs of revised mounting approaches. Both of these activities tie into Task 3 (structural analysis/design for the mirror mounting and mirror assembly), Task 7 (ACF development), Task 8 (test mounted mirrors), and Task 11 (update structural and thermal models). Successful results from testing (i.e., the things we test work as we expect) will achieve the ACF-development milestone and mounted-

mirror testing milestone. Successful testing (i.e., the results might not be what we desire, but the test runs successfully) will add data to the structural analyses and design tasks for mirror mounting and assembly. Whether we can truly say we have achieved the milestones for those tasks without achieving our goals is another question, although results of testing may indicate our concerns about the amplitude of the mounting distortions are overblown (although I do not feel that to be a likely outcome).

With respect to future development, we have several avenues besides the obvious one of re-proposing for the next Research Opportunities in Earth and Space Science (ROSES) SAT (which we fully expect to do).

1. Our newest SAT teamed with MSFC and PSU to explore hybrid adjustable/differential-deposition mirrors, giving us the opportunity to continue building and testing mirrors. Since the mirrors must be mounted/constrained in some way to produce influence functions, we will have the opportunity to incorporate what we learn in our tests and FEA, and determine if those results match expectations.
2. SAO continues to provide Internal Research and Development (IR&D) funding along with more generalized Research Equipment funding. We fully plan to continue with our IR&D activities in FY 2018. We expect to run an X-ray test of a mounted corrected mirror at the MSFC SLF sometime in FY 2018, and that test seems like an excellent candidate for future IR&D funds.
3. PSU has a fully awarded APRA for developing row-column addressing and on-orbit monitoring of the piezo cells, on which we are co-Investigators, responsible for mirror testing and determining realistic operational requirements and scenarios. Beside the development of row-column addressing, this work in total will also include higher-contact-density ACF, development of row-column control electronics, and improvement of testing by allowing more opportunity to try various noise-filtering approaches.
4. With respect to all three development avenues above, under a just-completed APRA, we procured a matched pair of high-precision Wolter-I slumping mandrels, which will enable us to demonstrate sub-arcsec performance should our technologies prove successful. We envision incorporating those mandrels into the program before the end of the summer, so we will have a chance to assess the improvement with mandrel, if any, improving our chances of success further downstream with the other planned testing.
5. We have an active APRA proposal, in response to the last ROSES APRA call, to develop mirror-alignment technology that can achieve the quarter-arcsec performance level necessary to meet the Lynx imaging specifications – such development should be applicable to any Lynx mirror technology.

Thus, we fully expect to continue with a robust development effort to demonstrate the capability of adjustable X-ray optics to meet the challenging Lynx telescope requirements.

References

[1] A. Vikhlinin et al., "*SMART-X: Square Meter Arcsecond Resolution X-ray Telescope*," SPIE Proc. **8443**, 844316 (2012)

[2] "*Enduring Quests, Daring Visions*," 2013 NASA Astrophysics Roadmap (Dec. 2013)

[3] T. Aldcroft et al., "*Simulating correction of adjustable optics for an X-ray telescope*," SPIE Proc. **8503**, 85030F (2012)

[4] W.W. Zhang et al., "*Lightweight and high angular resolution X-ray optics for astronomical missions*," SPIE Proc. **8147**, 81470K (2011)

[5] C. Feldman et al., "*The performance of thin shell adaptive optics for high angular resolution X-ray telescopes*," SPIE Proc. **7803**, 78030N (2010)

[6] J. Liu, "*Conductive Adhesives for Electronics Packaging*," Electrochemical, Port Erin, p. 12 (1999)
[7] S. Ganesan and M. Pecht, "*Lead-free Electronics*," Wiley, New Jersey, p. 437 (2006)
[8] W.S. Kwon and K.W. Paik, "*Experimental Analysis of Mechanical and Electrical Characteristics of Metal-Coated Conductive Spheres for Anisotropic Conductive Adhesives (ACAs) Interconnection*," IEEE Trans. Compon. Packag. Technol. **29**, 3, 528 (2006)
[9] K.W. Jang et al., "*Material properties of anisotropic conductive films (ACFs) and their flip chip assembly reliability in NAND flash memory applications*," Microelectron. Reliab. **48**, 1052 (2008)

For additional information, contact Paul Reid: *preid@cfa.harvard.edu*

Development of a Critical-Angle Transmission Grating Spectrometer

Prepared by: Mark L. Schattenburg (PI; MIT Kavli Institute, MKI), Ralf K. Heilmann (MKI), and Alex R. Bruccoleri (Izentis, LLC)

Summary

Critical-Angle Transmission (CAT) gratings combine the advantages of traditional phase-shifting transmission gratings–e.g., relaxed alignment and figure tolerances, low mass, and transparency at high energies; with the advantages of blazed reflection gratings–e.g., high diffraction efficiency and high resolving power due to utilization of higher diffraction orders. In combination with grazing-incidence X-ray mirrors and CCD detectors, they promise a five- to 10-fold increase in efficiency and a three- to 10-fold improvement in resolving power over existing X-ray grating spectrographs [1]. Development of CAT-grating fabrication technology has been supported by NASA under the Strategic Astrophysics Technology (SAT) program since January 2012.

Under a previous award, we achieved three major breakthroughs: the fabrication of several CAT gratings with record absolute diffraction efficiency, >30%; the extension of the CAT-grating bandpass through metal-coating the silicon grating bars; and experimental demonstration of a CAT-grating spectrometer with a spectral resolving power $R = \lambda/\Delta\lambda > 10{,}000$, exceeding requirements for all currently posed mission concepts. As a result, CAT-grating technology has been vetted at Technology Readiness Level (TRL) 4. We have since successfully performed environmental testing on frame-mounted gratings, and scaled up grating size by a factor of three.

This year, our SAT support was renewed, enabling us to develop an improved laser-based alignment technique for multiple gratings. X-ray tests with simultaneous illumination of two large gratings confirmed alignment within required tolerances.

Background

Absorption- and emission-line spectroscopy, with the performance made possible by a well-designed CAT X-ray grating spectrometer (CATXGS), will target science objectives concerning the large-scale structure of the universe, cosmic feedback, interstellar and intergalactic media, and stellar accretion. A CATXGS-carrying mission can address the kinematics of galactic outflows, hot gas in galactic halos, black-hole growth, the missing baryons in galaxies and the Warm-Hot Intergalactic Medium, and the effect of X-ray radiation on protoplanetary disks. All of these are high-priority International X-ray Observatory (IXO) science questions described in the 2010 Decadal Survey, "*New Worlds, New Horizons in Astronomy and Astrophysics*" (NWNH) [2], and are addressed further in the NASA "*X-ray Mission Concepts Study Report*" [3]. A number of mission concepts submitted in response to NASA Request for Information (RFI) NNH11ZDA018L could be enabled by a CATXGS; these include Advanced X-ray Spectroscopic Imaging Observatory (AXSIO), Astrophysics Experiment for Grating and Imaging Spectroscopy (AEGIS), and Square Meter Arcsecond Resolution Telescope for X rays (SMART-X), as well as the Notional X-ray Grating Spectrometer (N-XGS) studied by the X-ray Community Science Team (CST) [4-6] for future Explorers. Also, Lynx (formerly known as X-ray Surveyor), a mission described

in the 2013 "*Enduring Quests, Daring Visions*" Astrophysics Roadmap [7], is on a short list of mission concepts being studied in preparation for the 2020 Decadal Survey [8]. A core instrument for Lynx would be a grating spectrometer, for example one similar to the CATXGS design for SMART-X.

The soft-X-ray band contains many important diagnostic lines (C, N, O, Ne, and Fe ions). Imaging spectroscopy with spectral resolution better than 2 eV has been demonstrated with small transition-edge-sensor-based microcalorimeter arrays, providing resolving power over 3000 above 6 keV. However, toward longer wavelengths, energy-dispersive detectors cannot provide the spectral resolution required to address several of the NWNH high-priority science objectives. The only known technology providing high spectral-resolving power in this band is wavelength-dispersive, diffraction-grating-based spectroscopy.

The technology currently used for grating-based soft-X-ray spectroscopy was developed in the 1980s. The Chandra High-Energy Transmission-Grating Spectrometer (HETGS) carries polyimide-supported gold gratings with no more than 10% diffraction efficiency in the 1-5-nm band, but the whole moveable grating array only weighs about 10 kg. The X-ray Multi-mirror Mission–Newton (XMM-Newton) Reflection Grating Spectrometer (RGS) has more efficient grazing-incidence reflection gratings, but its mass is high (>100 kg) and it has low spectral-resolving power (~300). CAT gratings combine the advantages of the HETGS and RGS gratings, and promise higher diffraction efficiency over a broad band, with a resolving power greater than 3000 for a 10-arcsec Point-Spread-Function (PSF) telescope, and greater than 10,000 for a 0.5-arcsec-PSF telescope. These gratings also offer near-ideal synergy with a calorimeter-based imager, since CAT gratings become increasingly transparent at higher energies. Thus, high-resolution spectroscopy could be performed with a CATXGS in tandem with a calorimeter over the range of ~0.2 to tens of keV on a larger mission such as Lynx. Figures-of-merit for many types of observations, such as the accuracy of line-centroid measurement in absorption-line spectroscopy, could be improved by more than an order of magnitude over Chandra and XMM-Newton. The new, patented CAT-grating design relies on the reflection (blazing) of X-rays from the sidewalls of free-standing, ultra-high-aspect-ratio, sub-micron-period grating bars at grazing angles below the critical angle for total external reflection. Fabrication combines advanced novel methods and tools from the semiconductor and Micro-Electro-Mechanical Systems (MEMS) industries with patterning and fabrication methods developed at MIT over several decades.

We plan to bring CAT-grating technology to TRL 5 by the end of 2018 to reduce technology risk and cost for future CATXGS-bearing missions before they enter Phase A. We therefore want to demonstrate efficient, large-area (over 30 mm × 30 mm) CAT-grating facets with minimal blockage from support structures. Facets will be mounted onto thin and stiff frames, which can then be assembled into grating arrays sized on the order of 1 m^2.

Objectives and Milestones

The objective of this project is to demonstrate an aligned array of large-area, high-efficiency CAT gratings with minimal support-structure blockage, providing resolution higher than 3000 in the soft-X-ray band, and maintaining its performance after appropriate vibration, shock, and thermal testing. The array will consist of so-called grating facets mounted to a Grating-Array Structure (GAS). Facets are comprised of a grating membrane, etched from a silicon-on-insulator (SOI) wafer, and a facet frame that holds the membrane.

Key project milestones:

1. Develop silicon lattice-independent anisotropic etch capable of achieving the required aspect ratios for 200-nm-period gratings (Deep Reactive Ion Etch, DRIE, with a University of Michigan tool, completed in 2011).
2. Develop process for free-standing, large-area gratings with hierarchy of low-blockage supports (completed in 2012).
3. Combine (completed in 2013) and optimize (ongoing) dry- and wet-etch processes to obtain smooth grating-bar sidewalls and narrow Level 1 (L1) supports; produce free-standing, large-area gratings with hierarchy of low-blockage supports (demonstrated, improving yield); and test X-ray efficiency (ongoing).
4. Select, acquire, install, and test advanced DRIE tool at MIT (completed in 2014).
5. Demonstrate CAT-grating resolving power in an X-ray imaging system (completed in 2016); repeat with more than one grating or small array (Calendar Year, CY, 2017/18, first test with two gratings completed, data being analyzed).
6. Develop grating facet/frame design, process for integration of CAT grating membrane and frame, and alignment of facets on a breadboard GAS (ongoing, CY 2017/18).
7. Environmental and X-ray tests of aligned array of grating facets mounted to GAS (CY 2017/18).

Progress and Accomplishments

The key challenges in the fabrication of CAT gratings lie in their structure – small grating period (200 nm), small grating duty cycle (~40-nm-wide grating bars with 160-nm spaces between), and large depth (4-6 μm) result in ultra-high aspect ratios (100 - 150), with nm-smooth sidewalls. In addition, the gratings should not be supported by a membrane, but rather be freestanding. Structures with such an extreme combination of geometrical parameters, or anything similar, have never been made before.

Prior to SAT support, we fabricated small KOH-wet-etched CAT-grating prototypes that met all these requirements, and measured their efficiency at a synchrotron source, demonstrating good agreement with theoretical predictions [9, 10]. Due to their extreme dimensions and the requirement to be freestanding, CAT gratings must be supported by slightly "bulkier" structures. We use a so-called L1 cross-support mesh (period ~5 - 20 μm), integrated into the SOI device layer, and etched at the same time as the CAT gratings. Unfortunately, the wet-etch that provides the nm-smooth CAT grating sidewalls leads to widening L1 supports with trapezoidal cross sections and unacceptable X-ray blockage.

DRIE is an alternate process that can provide the required etch anisotropy for CAT grating bars and L1 supports simultaneously. To make large-area, freestanding gratings, we also use this process to fabricate a high-throughput hexagonal Level 2 (L2) mesh, etched out of the much thicker (~0.5 mm) SOI handle layer (Fig. 1). We developed a process that allows us to DRIE the CAT grating bars and the L1 supports out of the thin SOI device layer (front side), stopping on the buried-oxide (BOX) layer; and to subsequently etch the L2 mesh with a high-power DRIE into the back side, again stopping on the BOX layer. The BOX layer is removed with a hydrofluoric acid etch, and the whole structure is critical-point-dried in liquid CO_2. We fabricated several 31 mm × 31 mm samples with acceptable yield [11].

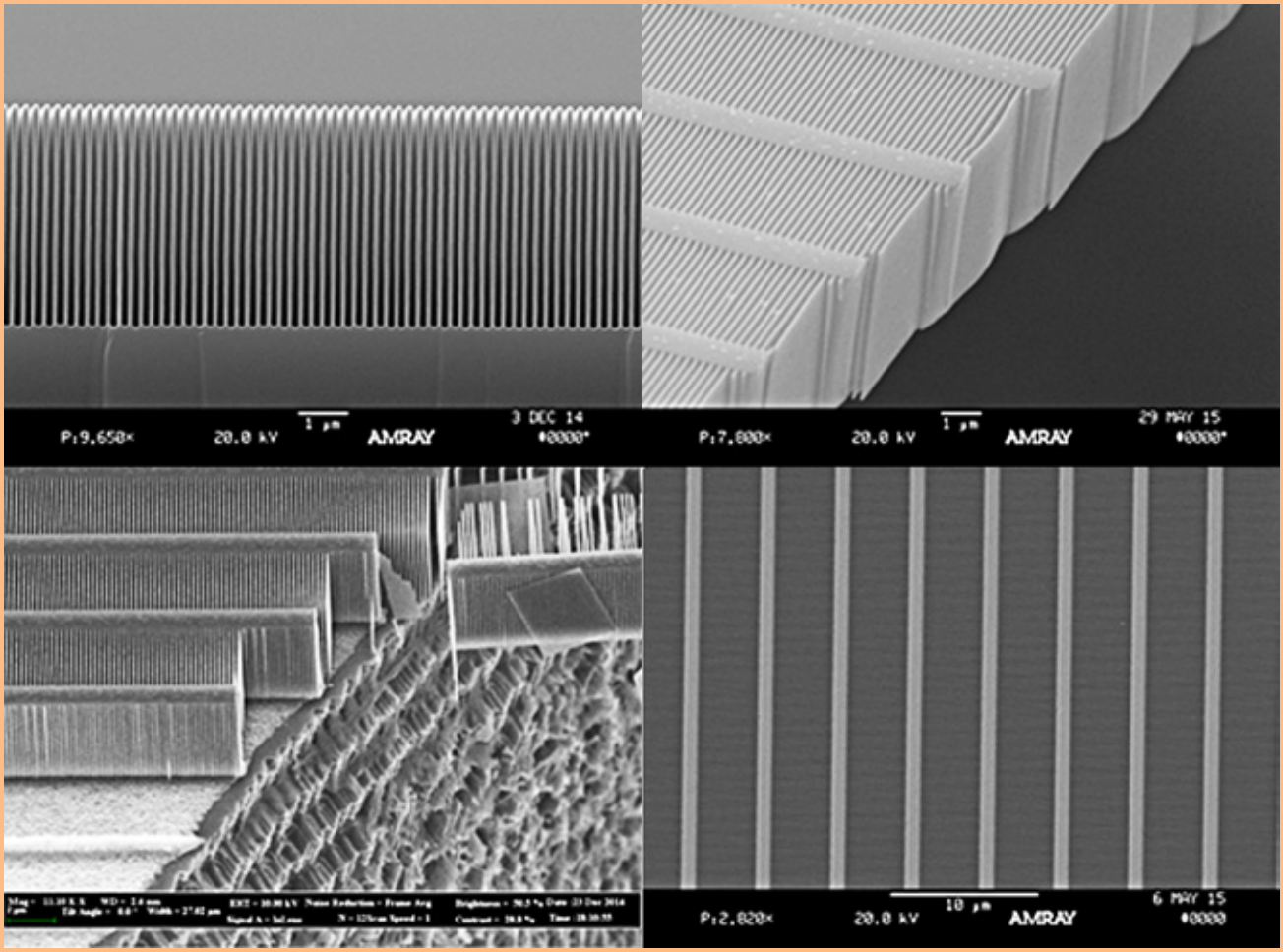

Fig. 1. Top left: *Cross-sectional scanning electron micrographs (SEMs) of CAT-grating DRIE, showing a high-quality, straight grating-bar profile before KOH etch.* Top right: *Cleaved free-standing CAT-grating membrane.* Bottom left: *Detail of cleaved CAT-grating membrane where back-side (very rough L2 mesh sidewalls from back-side DRIE) and front-side (much finer L1 and CAT grating structures) etches meet at the BOX layer.* Bottom right: *Top view of free-standing CAT-grating membrane, showing defect-free CAT grating bars suspended between L1 support mesh bars.*

Unfortunately, DRIE leaves the sidewalls of etched structures with several nm of roughness, detrimental to CAT grating efficiency. In 2012-13, we developed a combined DRIE/KOH approach on bulk silicon that follows DRIE with a relatively short KOH "polishing" step that reduces sidewall roughness, and straightens and thins the grating bar profile [12]. In 2014, we transferred and modified our new process to be compatible with the more delicate double-sided processing on SOI wafers for large-area, freestanding gratings (Fig. 1).

During 2014-15, our process development accelerated significantly, thanks to a newly acquired dedicated DRIE tool in our lab at MIT, funded through a previous SAT award. We greatly improved DRIE grating-bar profile control, and we now routinely achieve constant-thickness or slightly retrograde bar profiles (Fig. 1). These improved grating bars survive vastly longer wet-etch (sidewall polishing) times in concentrated KOH, presumably leading to smoother sidewalls and thus higher reflectivity and diffraction efficiency. In 2015, we produced several ~ 10 mm × 30 mm gratings with very similar record-high X-ray performance, a tribute to our improved and matured fabrication process [13–15].

The resolving power of an X-ray-objective transmission-grating spectrometer is usually limited by the optical design, the focusing optics PSF, and the angle of diffraction, but not by the alignment-insensitive transmission gratings. To verify the last point, last year we performed a measurement of resolving power at the NASA MSFC Stray Light Facility (SLF), using the Al $K\alpha_{1,2}$ lines from an electron bombardment source, and a segmented slumped-glass mirror pair from the Zhang X-ray optics group at NASA GSFC as the focusing optic. In order to resolve the line shape of the Al $K\alpha_{1,2}$ pair, we coated a 32-mm-wide CAT grating with a thin layer of platinum, using Atomic Layer Deposition (ALD). The metal coating increased the critical angle and allowed us to measure the Al $K\alpha_{1,2}$ line shape in 18th order, where the lines are much broader than the optic PSF. Data analysis demonstrated that our CAT gratings are compatible with a resolving power significantly in excess of R=10,000 (Fig. 2). Thus, CAT gratings will not degrade the resolving power of spectrometers designed for R on the order of 5000, such as a CATXGS for Lynx [16].

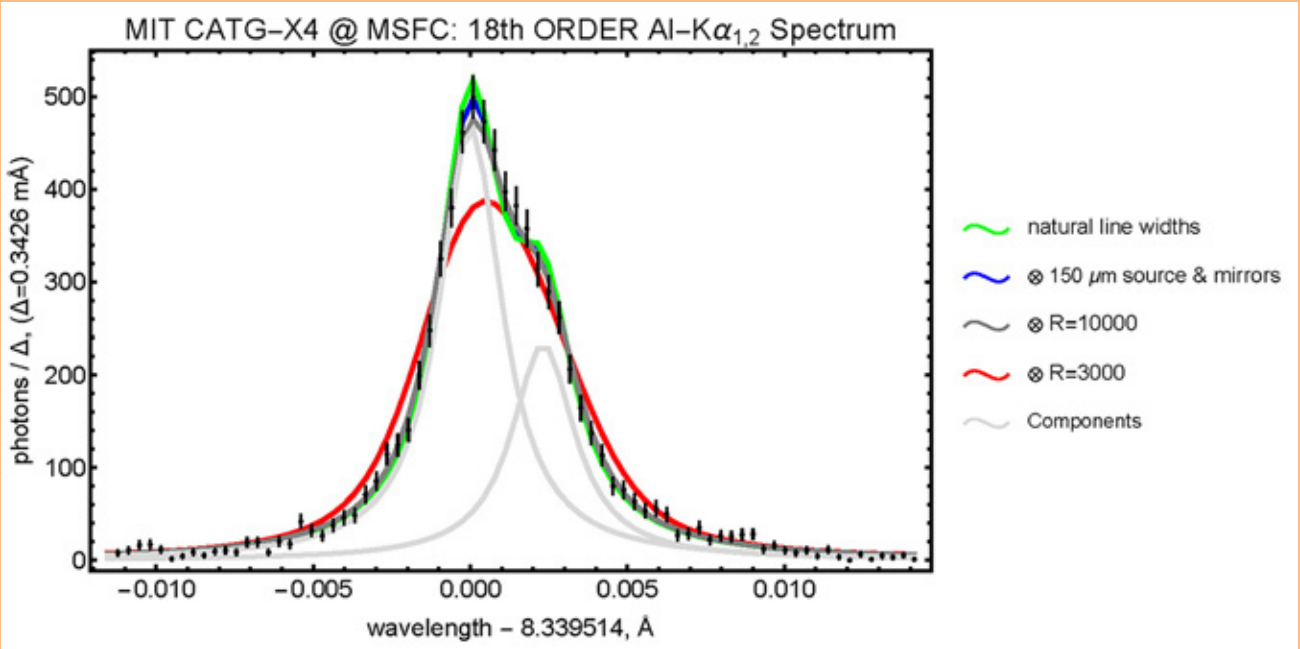

Fig. 2. *Measured Al $K\alpha_{1,2}$ spectrum in 18th order with 0.15-mm slit. Vertical lines are the error bars around the number of photons in a given bin. Light gray are the two Kα components with their natural Lorentzian widths and green is their sum. Blue is the convolution with the measured source/mirror 1-D line spread function, LSF. Dark gray is the blue curve convolved with broadening due to a Gaussian Δp/p distribution that would limit R to 10,000. It still falls short at the peak. The red curve also assumes a Gaussian Δp/p distribution, but corresponding to R=3000.*

Furthermore, the demonstrated ability to conformal-coat the ultra-high-aspect-ratio CAT grating bars with high-electron-density materials using ALD opens up a new design space for CAT gratings, extending their utility to shorter wavelengths and/or to larger blaze angles and thus higher spectrometer resolving power.

Since last year's report, we have been selected for continued SAT support, enabling us to make significant progress on several fronts. We measured the resolving power of an uncoated CAT grating, bonded to a frame and illuminated by a silicon pore optic (SPO) at the SLF and found R=3000 in 9th order (Al K_α), which was limited by the optic/source PSF and not by the grating. This performance exceeds the requirements of the proposed Arcus Explorer mission [17]. The frame-mounted grating was measured

again after vibration testing and thermal cycling and showed no degradation in resolving power or diffraction efficiency. As a result, CAT gratings in combination with SPOs were chosen as the core technologies for the Arcus Explorer proposal submitted in December 2016. We have since overcome a size-limiting fabrication obstacle and produced a significantly larger grating (~32 mm × 32 mm), with narrower L1 supports and slightly improved efficiency compared to our previous record, followed by five more gratings of the same size. As a first step towards a larger grating array, we have aligned two of these large, frame-mounted gratings to each other in the roll degree of freedom, which has the most stringent requirements, using an improved ultraviolet (UV) laser alignment technique in air. Illuminating both aligned gratings simultaneously with a single SPO at the Panter X-ray facility in Germany (Fig. 3), we confirmed that we exceeded our alignment requirements. The combined spectrum from the two gratings is currently being analyzed to determine resolving power. We are therefore well on our way toward achieving TRL 5.

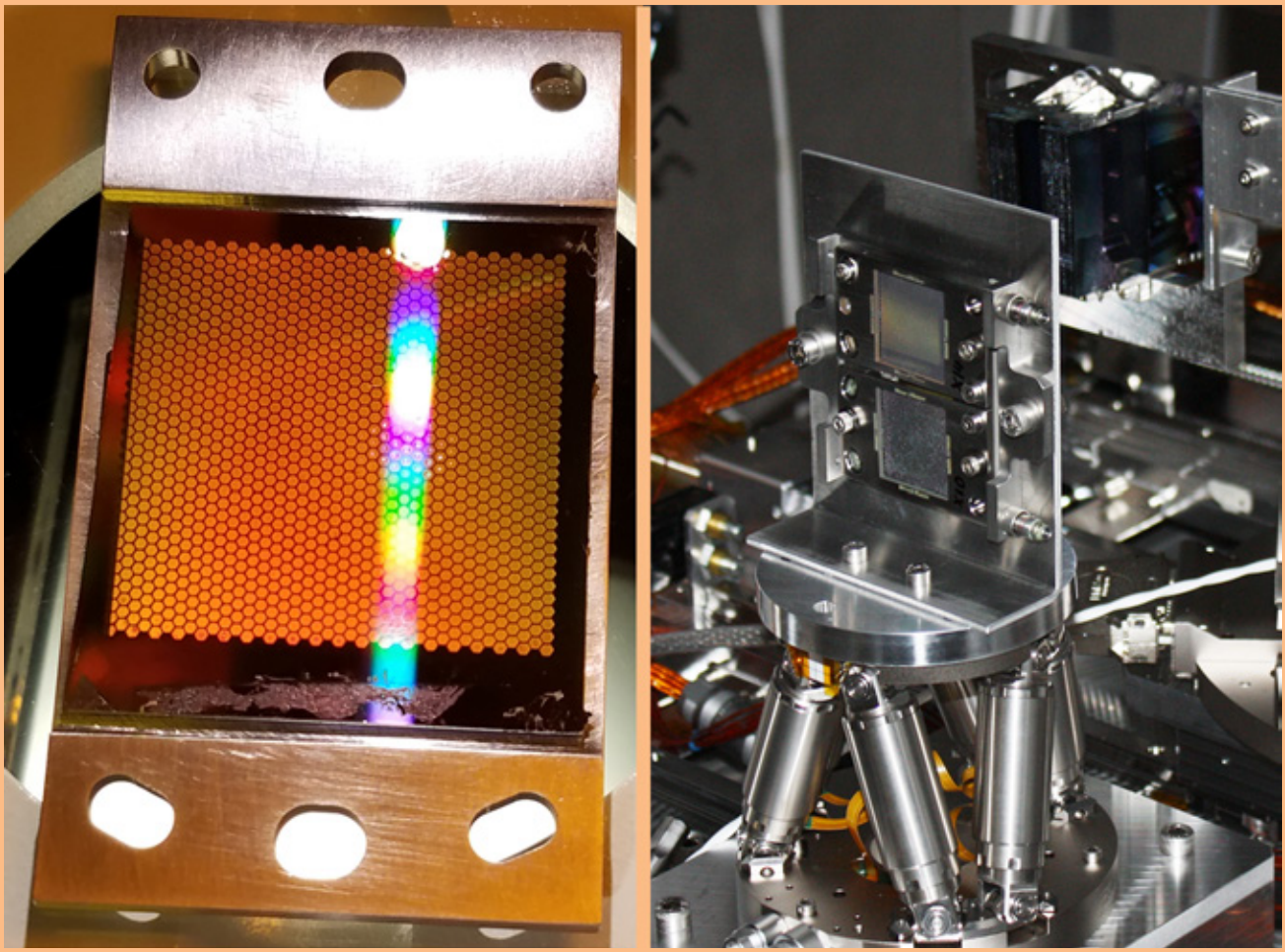

Fig. 3. Left: *One of several ~ 32 mm × 32 mm CAT gratings mounted to an alignment frame. Visible light diffraction is due to the L1 support mesh.* Right: *Two large gratings mounted to a hexapod stage and simultaneously illuminated by a single SPO at the Panter X-ray facility. The gratings were previously aligned in air using an improved laser-based technique.*

Path Forward

We are working toward the next TRL, which involves integrating facets and frames, mounting and alignment of a grating array, increasing diffraction efficiency, and environmental and X-ray tests to verify performance:

1. Develop grating facet/frame design, integration process of CAT-grating membrane and frame, and alignment of facets on a breadboard GAS (ongoing, Fiscal Year, FY, 2017/18).
2. Conduct environmental and X-ray tests of aligned array of grating facets mounted to GAS (CY 2017/18).
3. Increase grating efficiency further.
4. Scale up grating fabrication, frame design, and membrane/frame integration to full size (mission-dependent).

References

[1] R.K. Heilmann, J.E. Davis, D. Dewey, M.W. Bautz, R. Foster, A. Bruccoleri, P. Mukherjee, D. Robinson, D.P. Huenemoerder, H.L. Marshall, M.L. Schattenburg, N.S. Schulz, L.J. Guo, A.F. Kaplan, and R.B. Schweickart, "*Critical-Angle Transmission Grating Spectrometer for High-Resolution Soft X-Ray Spectroscopy on the International X-Ray Observatory*," Space Telescopes and Instrumentation 2010: Ultraviolet to Gamma Ray, M. Arnaud, S.S. Murray, T. Takahashi (eds.), Proc. SPIE **7732**, 77321J (2010)

[2] Blandford et al., "*New Worlds, New Horizons in Astronomy and Astrophysics*," National Academy of Sciences, (2010)

[3] "*X-ray Mission Concepts Study Report*" (2012)

[4] J.A. Bookbinder, R.K. Smith, S. Bandler, M. Garcia, A. Hornschemeier, R. Petre, and A. Ptak, "*The Advanced X-ray Spectroscopic Imaging Observatory (AXSIO)*," Proc. SPIE **8443**, Space Telescopes and Instrumentation 2012: Ultraviolet to Gamma Ray, 844317 (2012)

[5] M.W. Bautz, W.C. Cash, J.E. Davis, R.K. Heilmann, D.P. Huenemoerder, M.L. Schattenburg, R. McEntaffer, R. Smith, S.J. Wolk, W.W. Zhang, S.P. Jordan, and C.F. Lillie, "*Concepts for High-Performance Soft X-Ray Grating Spectroscopy in a Moderate-Scale Mission*," Space Telescopes and Instrumentation 2012: Ultraviolet to Gamma Ray, T. Takahashi, S.S. Murray, and J.-W. A. den Herder (eds.), Proc. SPIE **8443**, 844315 (2012)

[6] A. Vikhlinin, P. Reid, H. Tananbaum, D.A. Schwartz, W.R. Forman, C. Jones, J. Bookbinder, V. Cotroneo, S. Trolier-McKinstry, D. Burrows, M.W. Bautz, R.K. Heilmann, J. Davis, S.R. Bandler, M.C. Weisskopf, and S.S. Murray, "*SMART-X: Square Meter Arcsecond Resolution X-Ray Telescope*," Space Telescopes and Instrumentation 2012: Ultraviolet to Gamma Ray, T. Takahashi, S.S. Murray, and J.-W. A. den Herder (eds.), Proc. SPIE **8443**, 844316 (2012)

[7] "*Enduring Quests, Daring Visions*," Astrophysics Roadmap (2013)

[8] P. Hertz, "*Planning for the 2020 Decadal Survey: An Astrophysics Division White Paper*" (2015)

[9] R.K. Heilmann, M. Ahn, E.M. Gullikson, and M.L. Schattenburg, "*Blazed High-Efficiency X-Ray Diffraction via Transmission through Arrays of Nanometer-Scale Mirrors*," Opt. Express **16**, 8658 (2008)

[10] R.K. Heilmann, M. Ahn, A. Bruccoleri, C.-H. Chang, E.M. Gullikson, P. Mukherjee, and M.L. Schattenburg, "*Diffraction Efficiency of 200 nm Period Critical-Angle Transmission Gratings in the Soft X-Ray and Extreme Ultraviolet Wavelength Bands*," Appl. Opt. **50**, 1364-1373 (2011)

[11] A. Bruccoleri, P. Mukherjee, R.K. Heilmann, J. Yam, M.L. Schattenburg, and F. DiPiazza, "*Fabrication of Nanoscale, High Throughput, High Aspect Ratio Freestanding Gratings*," J. Vac. Sci. Technol. B **30**, 06FF03 (2012)

[12] A.R. Bruccoleri, D. Guan, P. Mukherjee, R.K. Heilmann, and M.L. Schattenburg, "*Potassium Hydroxide Polishing of Nanoscale Deep Reactive-Ion Etched Ultrahigh Aspect Ratio Gratings*," J. Vac. Sci. Technol. B **31**, 06FF02 (2013)

[13] R.K. Heilmann, A.R. Bruccoleri, D. Guan, and M.L. Schattenburg, "*Fabrication of Large-Area and Low Mass Critical-Angle X-ray Transmission Gratings*," Proc. SPIE **9144**, Space Telescopes and Instrumentation 2014: Ultraviolet to Gamma Ray, 91441A (2014)

[14] R.K. Heilmann, A.R. Bruccoleri, and M.L. Schattenburg, "*High-Efficiency Blazed Transmission Gratings for High-Resolution Soft X-ray Spectroscopy*," Proc. SPIE **9603**, Optics for EUV, X-Ray, and Gamma-Ray Astronomy VII, 960314 (2015)

[15] A.R. Bruccoleri, R.K. Heilmann, and M.L. Schattenburg, "*Fabrication Process for 200 nm-Pitch Polished Freestanding Ultra-High Aspect-Ratio Gratings*," submitted to J. Vac. Soc. Technol. B (2016)

[16] R.K. Heilmann, A.R. Bruccoleri, J. Kolodziejczak, J.A. Gaskin, S.L. O'Dell, R. Bhatia, and M.L. Schattenburg, "*Critical-Angle X-ray Transmission Grating Spectrometer with Extended Bandpass and Resolving Power >10,000*," Space Telescopes and Instrumentation 2016: Ultraviolet to Gamma Ray, Proc. SPIE **9905**, 99051X (2016)

[17] R.K. Smith et al., "*Arcus: The X-ray Grating Spectrometer Explorer*," Space Telescopes and Instrumentation 2016: Ultraviolet to Gamma Ray, Proc. SPIE **9905**, 99054M (2016)

For additional information, contact Mark Schattenburg: *marks@space.mit.edu*

Technology Development for an AC-Multiplexed Calorimeter for Athena

Prepared by: Joel Ullom (PI; NIST/Boulder), Simon Bandler and Caroline Kilbourne (NASA/GSFC), and Kent Irwin (Stanford)

Summary

We are developing large-format arrays of X-ray microcalorimeters and the associated readout that will enable the next generation of high-resolution X-ray imaging spectrometers for astrophysics. These sensors have very high spectral resolution, quantum efficiency, focal-plane coverage, and count-rate capability, combined with the ability to observe extended sources without spectral degradation. The goal of this program is to advance a readout architecture for an X-ray microcalorimeter imaging spectrometer from Technology Readiness Level (TRL) 3 to 4. The key components are (1) the use of an alternating current (AC) bias for microcalorimeter sensors, and (2) frequency-division-multiplexed (FDM) readout. This work is a collaboration between the National Institute of Standards and Technology (NIST), Boulder (PI J. Ullom); NASA/GSFC (lead C. Kilbourne); and Stanford University (lead K. Irwin). The work is supported by the Strategic Astrophysics Technology (SAT) program. It began in Fiscal Year (FY) 2015, and is supported through FY 2017. The scientists in our groups have been collaborating on technology development for an imaging X-ray microcalorimeter spectrometer since 1998. This heritage has focused on Transition-Edge-Sensor (TES) microcalorimeter arrays with a different readout architecture: direct current (DC) bias and time division multiplexing (TDM).

The landscape for future missions based on microcalorimeter sensors has recently changed with the choice of the Advanced Telescope for High ENergy Astrophysics (Athena) [1] for the European L2 large mission slot. One of the two key instruments for this mission is called the X-ray Integral Field Unit (X-IFU). X-IFU is based on the use of a large array of X-ray microcalorimeters as a high-resolution imaging spectrometer. The use of TES for the X-ray microcalorimeters, originally pioneered by our collaboration, is currently assumed for this instrument [2]. With this choice, the possibility for a near-term US-led or jointly led mission such as the International X-ray Observatory (IXO) has now ended. Thus, the aim of our program has shifted toward our collaboration trying to make a significant contribution to Athena's X-IFU.

The primary goal of the current project is to advance the technical readiness of the AC-biased readout of X-ray microcalorimeters from TRL 3 to 4. This advance requires work on both single TES devices and on small numbers of devices operating together. For single devices, we will compare sensor resolution under AC and DC bias; as well as properties that affect the energy resolution, such as transition shape and noise. Studies of small numbers of devices operating together will allow interaction pathways within the AC readout architecture to be identified and characterized. Interactions between sensors are a potential source of energy-resolution degradation.

Background

The ability to perform broadband imaging X-ray spectroscopy with high spectral and spatial resolution has been a core capability of recent X-ray satellite mission concepts. Multiplexed microcalorimeter

arrays provide this capability. The technology development program we are pursuing is a response to this need and is now directed toward Athena. The science case for developing microcalorimeter technology is that of the universe of extremes, from black holes to large-scale structure. The main goals are structured around three main topics–"black holes and accretion physics," "cosmic feedback," and "large-scale structure of the universe." Underpinning these topics is the study of hot astrophysical plasmas, which broadens the scope of this science to virtually all corners of astronomy.

The baseline readout architecture for the X-IFU on Athena is FDM [3], in which the TESs are biased with AC signals of different frequencies, which act as carriers for the slower thermal signals. The AC signals from different TESs are measured by a shared Superconducting-QUantum-Interference-Device (SQUID) current amplifier.

To date, the resolutions achieved using DC-biased TESs have not been reproduced in AC-biased TESs. When this work began, the best results with AC bias were from the Space Research Organization Netherlands (SRON) group, which reported a full-width-at-half-maximum (FWHM) resolution of 3.6 eV at 5.9 keV using transformer coupling to low resistance Mo/Au NASA/GSFC devices [4, 5]. Under DC bias, these same devices yielded 2.3 eV FWHM at 5.9 keV. Since the essential principle of AC bias has been demonstrated, its current TRL is 3. If we succeed in improving AC-biased performance to levels that meet the Athena mission specifications, then we will have increased the TRL of AC bias to 4. Thus, we will initially attempt to advance the TRL for reading out single pixels in large arrays of TESs with AC bias. We will attempt to demonstrate a FWHM energy-resolution performance of less than 2.5 eV at 6 keV, and be capable of achieving this energy resolution at an input X-ray count-rate of 50 counts per second, with 80% throughput for the high-resolution events. These results will likely meet the Athena mission requirements.

The behavior of a TES is more complicated than that of a temperature-dependent resistor because of the role of superconductivity. Noise and responsivity depend on both the current and the temperature in the device. Under AC bias, the current is constantly changing even though the temperature is very close to fixed. This current variation is one possible reason why results under AC bias are not as mature as those under DC bias. We will study how the properties of TES devices under AC bias compare to those under DC bias. We will focus on Mo/Au TES thermometers developed at GSFC that are currently the baseline sensor technology for the X-IFU, but will also study other TES designs insofar as these can provide insight into the details of AC bias. This work encompasses both the fundamental physics of TES devices and the role of the readout SQUID and feedback system in determining performance levels.

Progress and Accomplishments

In order to complete the goals of this program, new measurement setups were needed at both NIST Boulder and GSFC, capable of studying and evaluating the effects of AC bias on the performance of TESs. To broaden the impact and maximize the chances of success, different approaches were pursued at each institution. GSFC pursued an approach that allowed the maximum use of components from European institutes collaborating on the Athena mission. This approach provides the most straightforward path to boosting the collaboration's ability to characterize AC-biased TES. In contrast, the NIST AC-bias measurement setup is designed to maximally separate the contribution of the readout system from that of the TES microcalorimeter in assessments of detector performance, as described below. These two approaches for increasing the measurement capability for AC-biased TESs within the US are augmented by joint FDM measurements with European collaborators that are being carried out at SRON.

All the necessary components for the GSFC measurement platform have been installed. Some of the major components have been supplied by SRON, including the specialized LC filter chip; the transformer chip; and room-temperature electronics, which include an analog amplifier and digital base-band feedback electronics. The FDM setup at GSFC utilizes the same two-stage SQUIDs used by SRON that are provided by VTT Finland. The integrated setup (Fig. 1) has been used to characterize a large variety of TES designs.

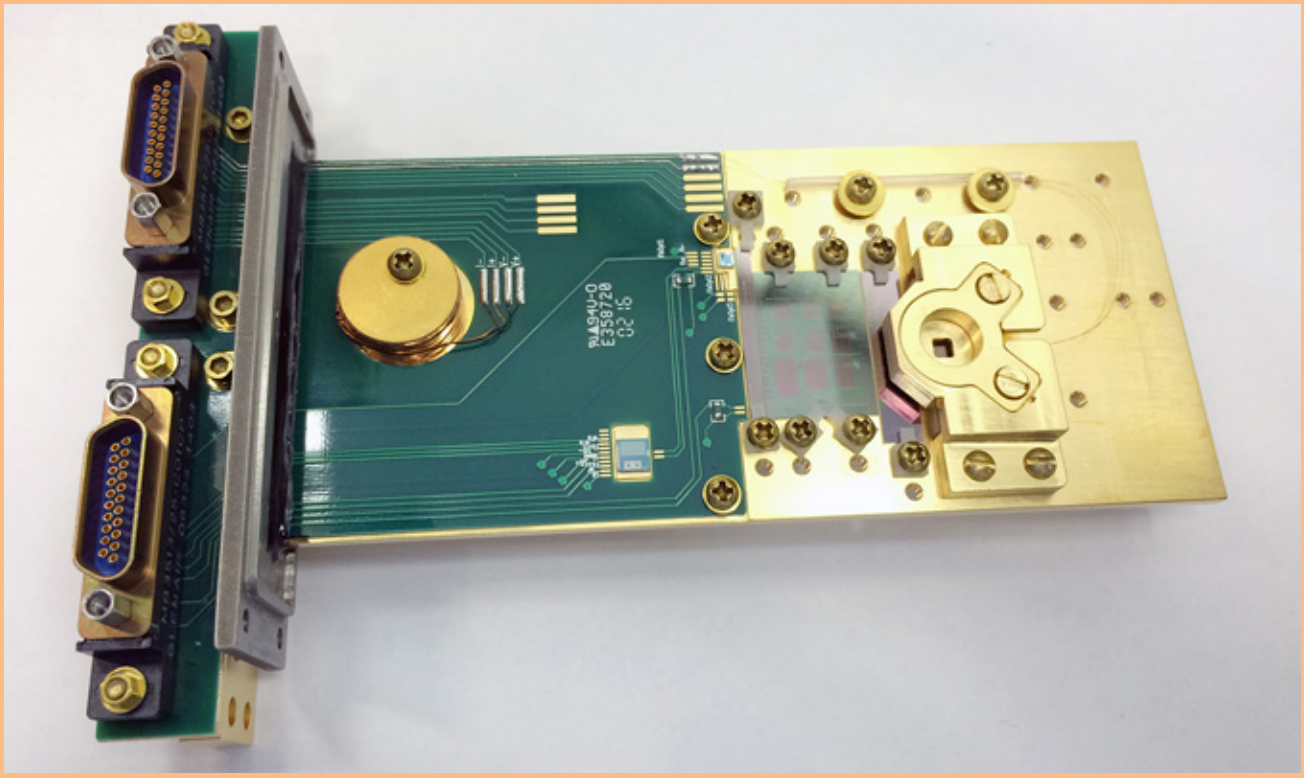

Fig. 1. *Assembled cryogenic mount for AC-bias test showing routing PC board, SQUIDs, LC filter chip, and transformer chip. The chip with the TES detectors is barely visible through the square photon access hole.*

All existing multiplexing architectures for TESs exploit the favorable properties of SQUID amplifiers. The non-linear response of SQUID amplifiers is typically mitigated by magnetic flux or current feedback. Feedback is particularly important in FDM because of the large amplitude of the fast carrier signals and the requirement that one SQUID simultaneously measure signals from many sensors. As a result, FDM system performance can depend strongly on the particular feedback implementation, and feedback systems with additional capability will likely be needed [3].

The motivation for the NIST AC-bias measurement platform is to measure AC-biased TESs without the use of feedback, by using microwave SQUIDs. In this setup, the microwave SQUID can be operated open-loop, allowing the TESs to be characterized independent of the complications of a fixed-bandwidth feedback loop. The microwave SQUID has the option of linearizing the SQUID response using flux ramp modulation [6]. The effect of this modulation on the measured response of the TES is directly calculable and can be separated from the response of the TES to AC bias. In this setup, the SQUID is

embedded in a passive microwave resonator and probed using microwave tones. This approach, shown schematically in Fig. 2 left panel, has the potential to provide very large readout bandwidths and high dynamic range without the use of feedback.

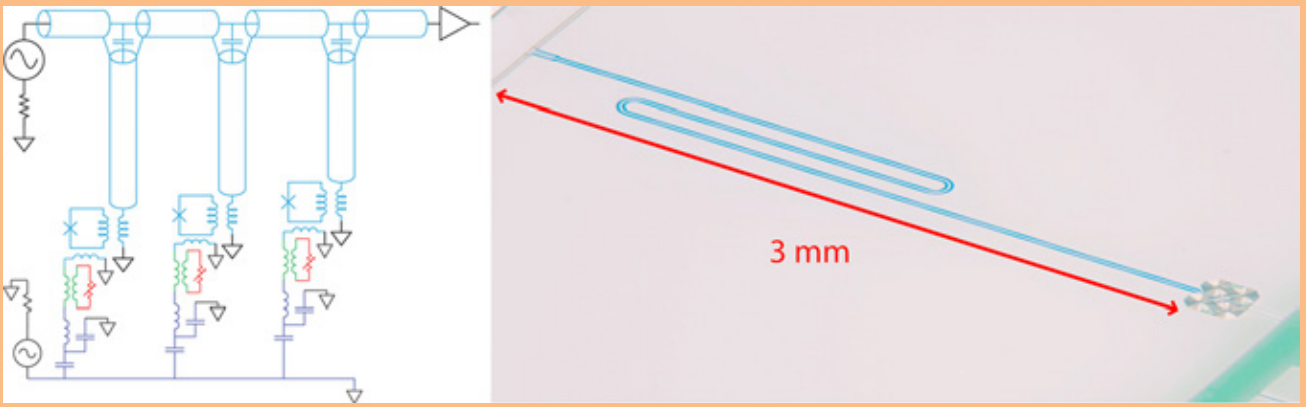

Fig. 2. *Circuit schematic (left) depicting a microwave SQUID multiplexer to read out AC-biased TESs, and micrograph (right) of a microwave SQUID multiplexing element showing the superconducting resonator coupled to the shared feedline in the top left corner and the SQUID coupling coils in bottom right corner.*

To meet the bandwidth requirements of the 1-5 MHz range for the Athena AC bias, microwave SQUIDs with 15 MHz of open-loop bandwidth were designed and fabricated (Fig. 2, right panel). These designs were tested with direct current inputs. The shift of the resonance frequency of one of the microwave SQUIDS as a function of input flux is shown in Fig. 3. After testing the microwave SQUIDs separately, they were integrated into the sample box with the AC-bias circuit using the SRON LC-filter and transformer chips. Four microwave SQUIDs are fabricated on the same chip, sharing a common microwave feedline. These four SQUIDs can be probed independently, and act as four independent readout channels. Each of the four channels can measure either an AC- or DC-biased TES. Initial tests demonstrated the functionality of the microwave SQUID readout. The open-loop bandwidth was confirmed to be 15 MHz, and a flux-ramp-modulated sampling rate of 8 MHz was achieved.

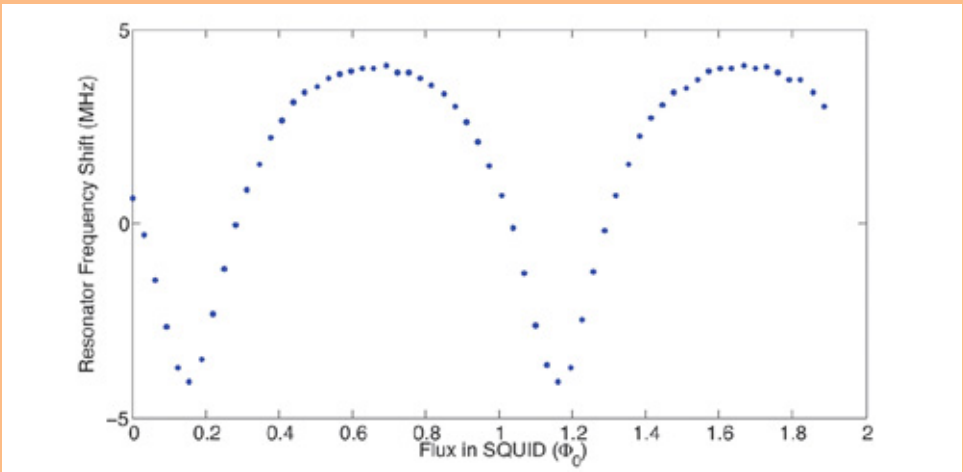

Fig. 3. *Modulation of the resonant frequency as a function of input flux for a microwave SQUID readout optimized to measure AC-biased TESs at the frequencies targeted for the Athena X-IFU instrument.*

When these SQUIDs were integrated with TESs in the AC-bias circuit, we discovered that the sampling rate of 8 MHz was not sufficient to track the slew rate of the TESs chosen for the AC-bias studies. For these TESs, the current amplitude of AC modulation was greater than expected, making the slew rate too fast for the first generation of high-bandwidth microwave SQUIDs. Measurements could still be performed without modulation but the data acquisition and analysis were undesirably slow. Recently, updated microwave SQUIDs were designed that increased the open-loop bandwidth to 30 MHz and halved the input coupling to the SQUID. Both of these modifications increase the maximum slew rate that can be tracked under flux-ramp modulation. Initial testing of the new devices confirmed the doubling of the maximum sampling rate, and they are currently being integrated into the AC-biased TES setup at NIST (Fig. 4).

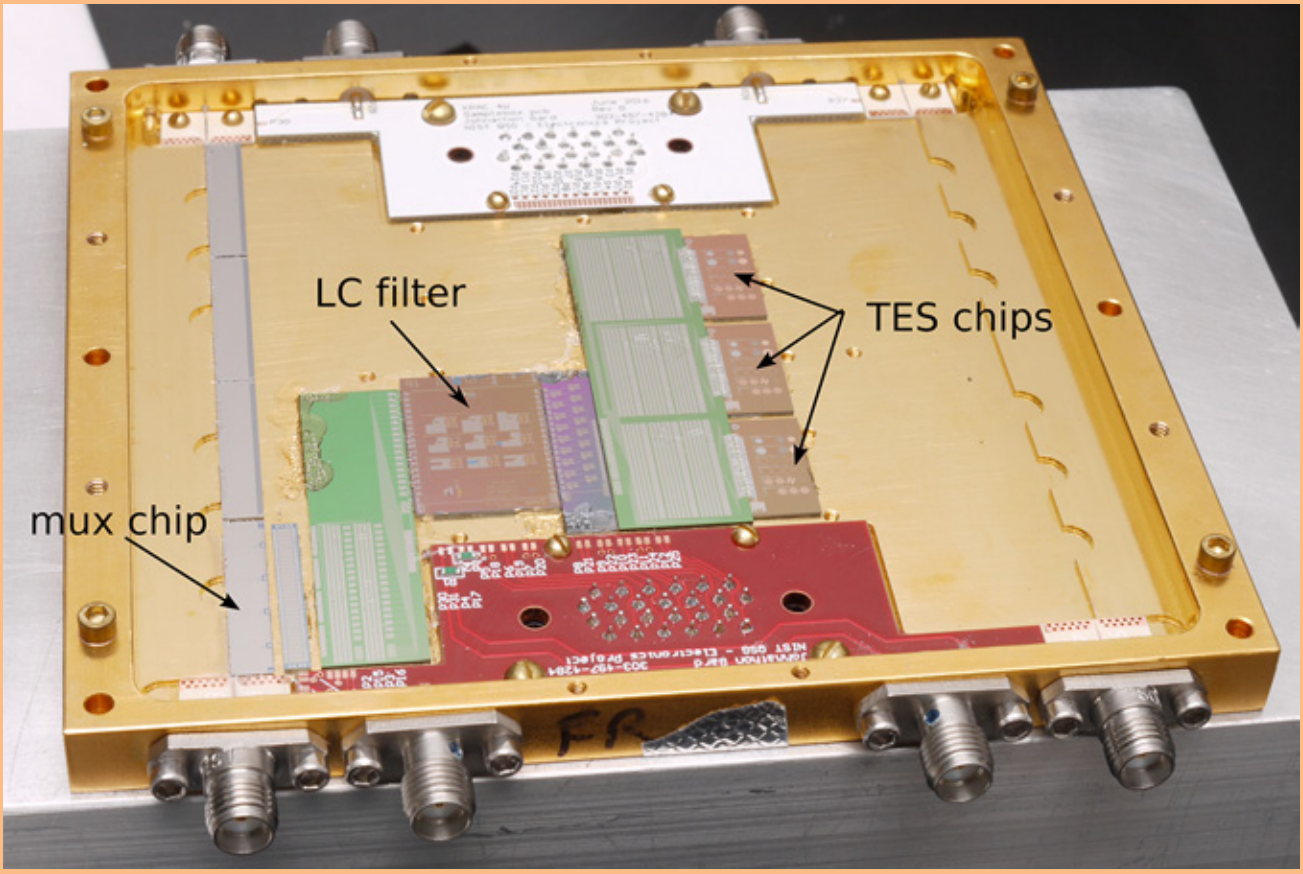

Fig. 4. *Microwave SQUID multiplexing readout chip integrated with AC-biased TESs using the SRON LC filter and transformer chips (MUX, multiplexer).*

In addition, GSFC and SRON scientists began testing new GSFC X-ray microcalorimeters using an existing test set-up at SRON. A new array was measured at SRON, consisting of different TES sizes (50, 100, 120, and 140 μm), targeted at understanding the influence of TES geometry on the performance under AC bias. These designs were first tested at GSFC under DC bias so the two bias strategies could be directly compared. It was observed in these early measurements that the resonance width of the AC-bias LC chip with the X-ray TESs connected was wider than predicted and also wider than had been observed in previous TESs optimized for bolometry. The wider resonance widths imply additional loss in the resonance circuit that decrease the effective signal-to-noise ratio of the FDM readout. Mitigating this effect is a high priority for the X-IFU and a focus of our team's recent efforts.

Many different TESs of different sizes with different configurations of the normal metal structures have now been tested in the FDM setup at GSFC. A summary of the loss inferred from measured resonator widths is shown in Fig. 5. There is a clear trend of increasing loss with increased AC-bias frequency as was observed in previous measurements at SRON. The other obvious trend is that devices without the X-ray absorbing layers have lower loss. The absorbing layer is 4 μm of bismuth on top of a 1.7-μm layer of gold that is cantilevered above the TES. These two results are strong evidence for eddy-current loss in the absorber due to the AC bias of the TES. Each of the points in Fig. 5 represents a separate measurement on a different device. This large body of AC-biased measurements was enabled by this program.

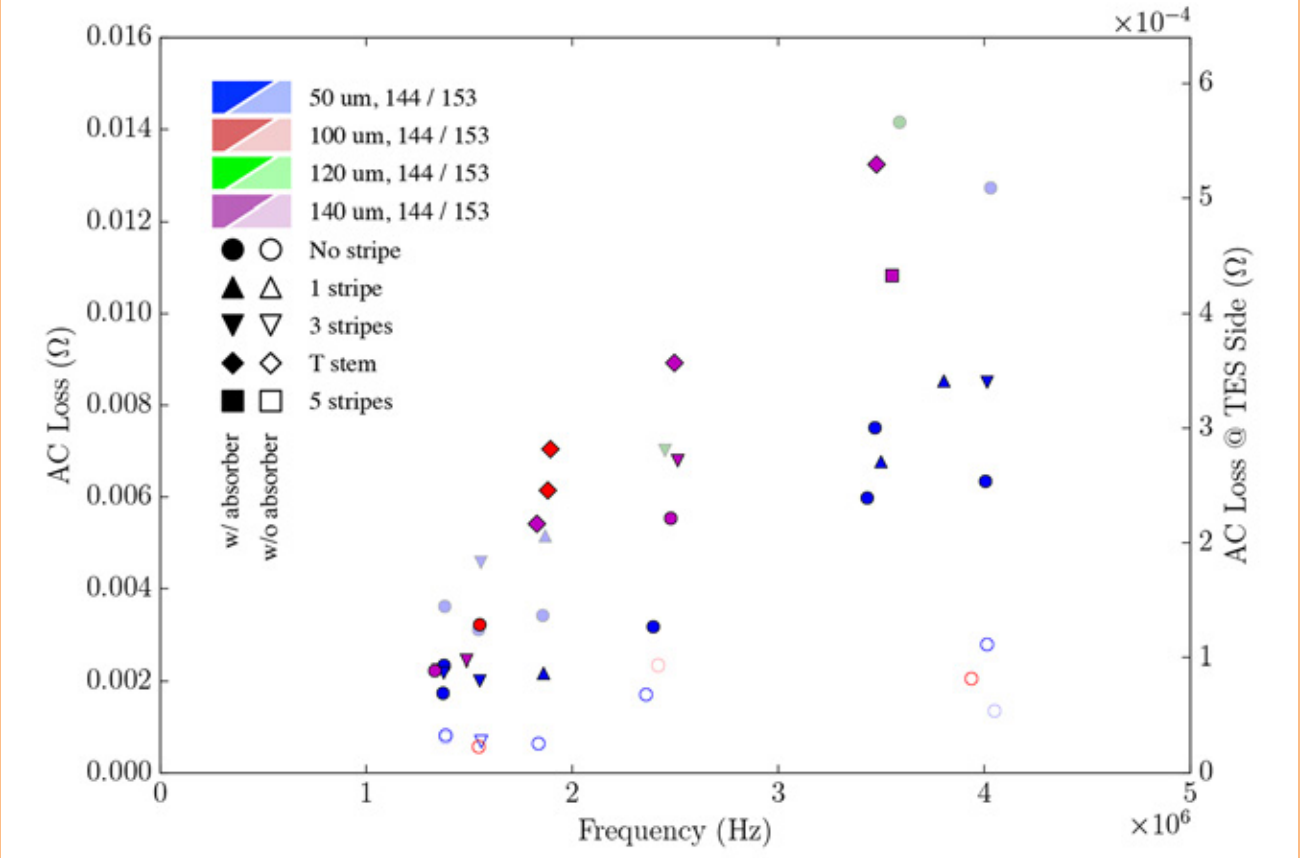

Fig. 5. *Measured AC Loss (left axis) and AC Loss referred to the TES side of the transformer (right axis) as a function of AC-bias frequency for TESs of different sizes, different configurations of normal metal features, and with and without X-ray absorbers.*

To further test the eddy current hypothesis, NIST designed and fabricated TESs that will allow the eddy-current loss mechanism to be separated from other resistive mechanisms, to definitively isolate the structures in which the loss is occurring, and to test mitigation strategies. An example of one of the new designs is shown in Fig. 6 (left). In this design, the molybdenum/copper bilayer is replaced with a superconducting molybdenum layer and the normal-metal features are electrically disconnected from the superconducting film. If the loss is similar to the standard electrically connected design, then this confirms the eddy-current hypothesis. Alternatively, if the loss is reduced, then the in-transition superconductivity of the TES film must play some role. Another of the new designs, shown in Fig. 6

(center), has a very simple structure consisting of a superconducting ring surrounding a disc of normal metal. Eddy-current generation in this geometry is easy to simulate numerically. Different metals can be used for the disk to explore how the resistivity of the metal affects loss. The first measurement of one of these designs is shown in Fig. 6 (right).

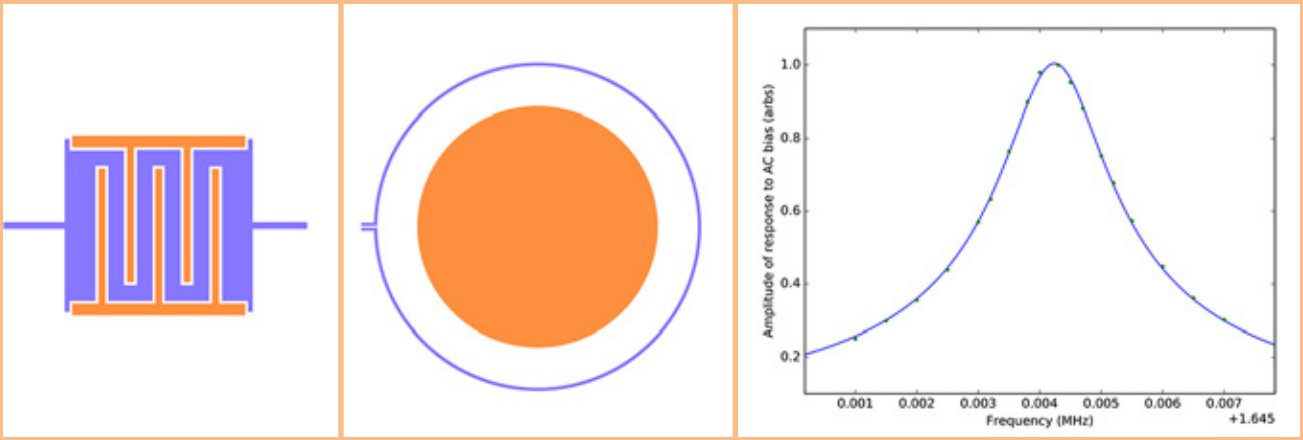

Fig. 6. Left: *Schematic of device design where normal metal is electrically disconnected from superconducting film.* Center: *Device design where effects of eddy-current heating are easier to model numerically.* Right: *Measurement (green points) of the response of an AC-bias LC resonator connected to the device shown at the center, along with a fit to the circuit model (blue line) to extract the effective resistance. Frequency values on the x-axis are defined relative to an offset frequency of 1.645 MHz.*

Frequency-domain measurements provide a natural measure of both the in-phase current (which should contain the TES signal component) and any out-of-phase current. If the TES were a purely resistive element with no reactive elements, there should be no out-of-phase component. However, detailed measurement of TES IV curves show the presence of oscillatory structure and discontinuities in the measurements of the out-of-phase current that are not attributable to the bias circuit. Thus, the out-of-phase current is thought to be related to the physical properties of the TES.

Theoretical efforts to understand these effects have focused on understanding the Josephson-junction-like properties of these TESs under AC excitation. We now believe these reactive features are a direct result of the non-linear Josephson inductance of the TES. In a theoretical analysis by McDonald and Clem [7], the non-linear nature of the differential equations that describe a Josephson junction are shown to result in bifurcations effects, resulting in a 2π phase slip of the superconducting phase difference (oscillating in time) across the junction for certain values of the AC drive signal. These phase slips manifest as discontinuities in the time-averaged reactance, quite similar to the effects observed in TES data. Efforts are ongoing to compare the TES measurements to these theoretical models and extend the models to better reflect the more complex extended geometries of a TES.

Evidence of these discontinuities (Fig. 7, left) are also observed in the in-phase current (real part of the impedance) of the measured transition as small steps. The discontinuities show a corresponding feature in the derivative of resistance with respect to temperature at constant current, known as α (Fig. 7, right). When the sensor response traverses these features, the energy resolution is degraded. In some devices, bias points above 30% of the normal resistance (R_n) can avoid these features. When operating in the

continuous regions around them, the AC spectral resolution is as good as 2.9 eV FWHM at 6 keV [8]. Biasing the TES array at 30% R_n could potentially limit the resolution and dynamic range of the X-IFU instrument. The best performance for the equivalent DC-biased TESs is achieved for bias points around 10% of the normal resistance. Additionally, in some TESs the features extend to much higher fractions of R_n and there are no bias points that achieve the target resolution. While the theory of McDonald and Clem provides a qualitative understanding of these features, achieving the goals of the X-IFU instrument will likely require the development of stronger quantitative and predictive capabilities.

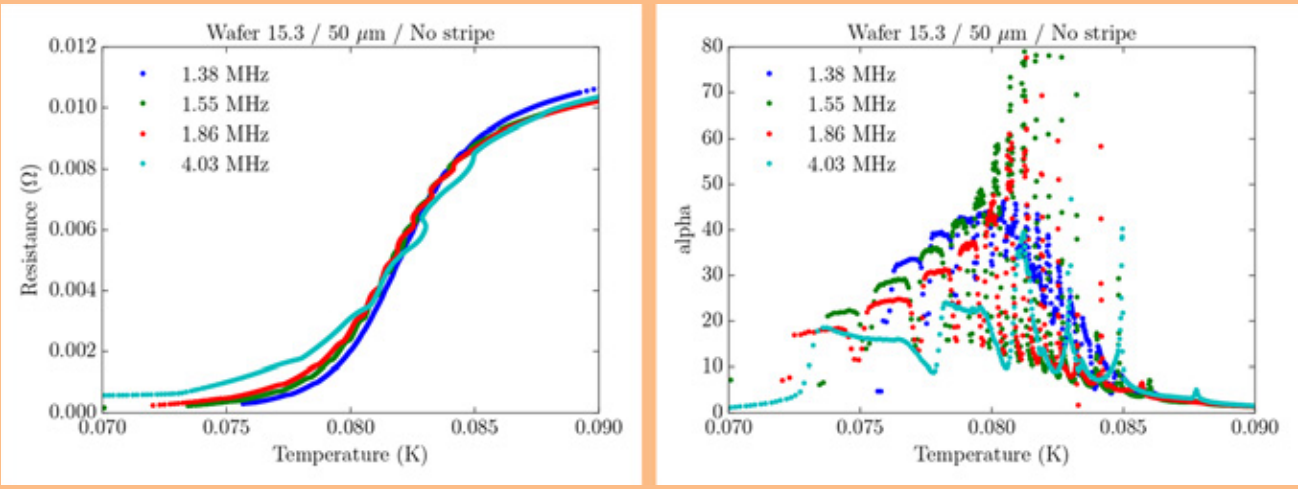

Fig. 7. Left: *Measured resistance as a function of temperature as inferred from IV curves for a 50-μm TES.* Right: α_{IV} *as a function of the same temperature.*

Path Forward

The complementary capabilities of the GSFC AC-bias setup to perform direct comparison with the SRON FDM, and the NIST AC-bias setup to separate the effects of an AC-biased TES from the readout implementation will continue to provide significant insight into AC-biased TESs. The important discovery of a source of resistive loss under AC bias has caused us to focus many of our resources on characterizing and mitigating this loss mechanism in candidate Athena TES designs. The increased measurement capability for AC-biased TESs has already proven useful by enabling measurement of a large number of TES for these loss studies. Future work will identify how different structures and materials within TESs contribute to this loss. Additionally, sharp steps observed in the transition, that originate in basic superconductivity physics, currently limit the bias range and useful dynamic range of AC-biased TESs. Understanding how to mitigate these steps and recover the full dynamic range of the TES will be another major focus of this work as it continues as part of NASA's role in the Athena mission.

References

[1] K. Nandra et al., "*ATHENA, the Advanced Telescope for High ENergy Astrophysics*," recently accepted mission proposal submitted to ESA's L2 large mission opportunity (2014)

[2] D. Barret et al., "*The Hot and Energetic Universe: The X-ray Integral Field Unit (X-IFU) for Athena+*," *astro-ph arXiv:1308.6784* (2013)

[3] R. den Hartog et al., "*Baseband Feedback for Frequency-Domain-Multiplexed Readout of TES X-ray Detectors*," AIP Conf. Proc. **1185**, 261-264 (2009)

[4] H. Akamatsu et al., "*Single Pixel Characterization of X-Ray TES Microcalorimeter Under AC Bias at MHz Frequencies*," IEEE Trans. Appl. Supercon. **23**, 2100503 (2013)
[5] H. Akamatsu et al., "*Performance of TES X-ray Microcalorimeters with AC Bias Read-Out at MHz Frequencies,*" J. Low Temp. Phys. **176**, 591 (2014)
[6] J. Mates et al., "*Demonstration of a multiplexer of dissipationless superconducting quantum interference devices*," Appl. Phys. Lett. **92**, 023514 (2008)
[7] J. McDonald and J.R. Clem, "*Microwave response and surface impedance of weak links*," Physical Review B **56**, 14723 (1997)
[8] H. Akamatsu et al., "*TES-Based X-ray Microcalorimeter Performances Under AC Bias and FDM for Athena*," J. Low Temp. Phys. **184**, 1, 436-442 (2016)

For additional information, contact Joel Ullom: *joel.ullom@nist.gov*

Next-Generation X-ray Optics: High Angular Resolution, High Throughput, and Low Cost

Prepared by: William W. Zhang (PI; NASA/GSFC)

Summary

This work continues technology development of X-ray optics for astronomy. Since Fiscal Year (FY) 2012, the Strategic Astrophysics Technology (SAT) program has funded this effort, which the Constellation-X project initiated and the International X-ray Observatory (IXO) project continued. This is an effort by GSFC with collaboration from MSFC.

The objective is to advance astronomical X-ray optics by at least an order of magnitude in one or more of three key metrics from the state of the art represented by the four major X-ray missions: Chandra, X-ray Multi-mirror Mission-Newton (XMM-Newton), Suzaku, and Nuclear Spectroscopic Telescope Array (NuSTAR). These metrics are: (1) angular resolution, (2) mass per unit area, and (3) production cost per unit area. The modular nature of this technology renders it appropriate for missions of all sizes—from Explorers that can be implemented by the end of this decade, to Probes and Flagship missions that can be implemented during the next decade.

Key areas of technology development include: (1) fabrication of substrates, (2) thin-film coating of these substrates to make X-ray mirror segments, (3) alignment and (4) bonding of mirror segments into mirror modules, and (5) systems engineering to ensure all spaceflight requirements are met.

Major accomplishments in the past year include: (1) successful fabrication of mirror substrates shown by optical metrology to have sub-arcsec point spread function (PSF); and (2) successful alignment, bonding, and X-ray testing of a pair of mirrors using four precisely machined spacers, achieving a 4.5" image, the best with lightweight X-ray mirrors. These accomplishments demonstrate the feasibility of making diffraction-limited X-ray mirrors using mono-crystalline silicon and the validity of the meta-shell approach. We expect to continually improve both image quality and overall Technology Readiness Levels (TRLs) over the coming years.

Background

The last five centuries of astronomy are a history of technological advancements in optical fabrication and optical-systems integration. Furthering our understanding of the cosmos requires telescopes with ever-larger collecting area and ever-finer angular resolution. In the visible and other wavelength bands, where radiation can be reflected at normal incidence, a large mirror area alone directly translates into a large photon-collecting area. However, due to its grazing-incidence nature, an X-ray telescope requires a combination of both large area and thin mirrors to increase photon-collecting area.

Three metrics capture the essence of an X-ray optics technology: (1) angular resolution, (2) mass per unit collecting area, and (3) production cost per unit collecting or mirror area. The X-ray optics of every successful observatory represents a scientifically useful compromise between the three metrics that was implementable in its specific technological, budgetary, schedule, and spaceflight opportunity context. The objective of this effort is to ready an X-ray telescope fabrication process that ever tilts the compromise toward better performance for given amounts of resources in terms of money and mass.

Our effort started in 2001, with the epoxy replication process developed for Suzaku. Instead of using thermally formed aluminum substrates, we used thermally formed (or slumped) thin glass for substrates. Taking advantage of the already smooth surface of float-glass sheets, by 2007 we were able to make glass substrates that no longer needed the epoxy replication process, saving both time and money. In late 2007, we X-ray-tested a pair of glass mirrors and produced X-ray images better than 15" half-power diameter (HPD), meeting the requirement of the Constellation-X mission. Between 2007 and 2011, we continued to improve the glass slumping technique, culminating in a process that consistently makes glass mirrors of 6" HPD. Between 2011 and 2015, we developed a mirror alignment and bonding process that has produced technology-development modules with three pairs of mirrors, making X-ray images better than 8" HPD. Compared with Chandra, this technology would lower mass and cost per unit collecting area by nearly two orders of magnitude. Compared with XMM-Newton, it would reduce mass per unit collecting area by a factor of eight and cost by a factor of three, while significantly improving angular resolution. Compared with Suzaku and NuSTAR, it would improve angular resolution by an order of magnitude, while preserving their advantages in mass and cost per unit collecting area.

In 2016, based on successful development work funded by an Astrophysics Research and Analysis (APRA) grant, we changed our mirror technology from using slumped glass to using mono-crystalline silicon. The major reasons for this change include:

1. Polished silicon mirrors have the potential for much better angular resolution than slumped-glass mirrors.
2. Silicon has far superior material properties compared to those of glass: lower density, higher thermal conductivity, higher elastic modulus, and lower coefficient of thermal expansion.
3. The silicon fabrication process does not require mandrels as needed for the glass-slumping process, saving time and money.

In conjunction with the change of substrates from slumped glass to polished silicon mirrors, we have also changed the overall approach to making an X-ray mirror assembly. Figure 1 is an illustration contrasting the old approach with the new one. Both start with small mirror segments, but they differ in the intermediate step. In the old approach, a large number of wedge-like modules are built, tested, and then integrated to form the final mirror assembly. In the new approach, a relatively small number of meta-shells are built, tested, and then integrated.

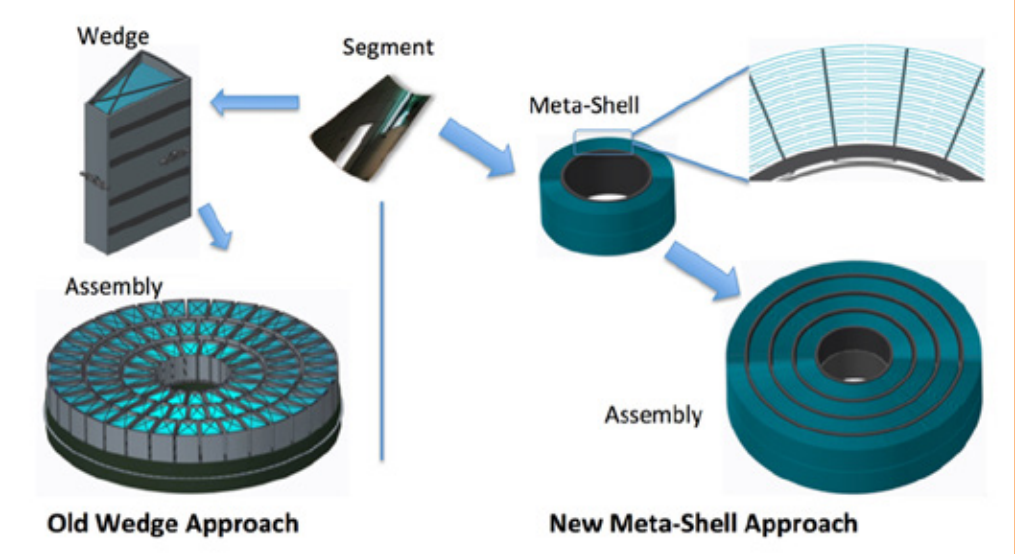

Fig. 1. *Illustration of two ways to build a large X-ray mirror assembly from a large number of small mirror segments. The wedge approach has been widely adopted and therefore has been the "standard" way, whereas the "meta-shell" approach has significant advantages.*

The new approach has several major advantages. First, each mirror segment is kinematically supported at four locations during the alignment and bonding process, minimizing distortion by gravity. Second, because of the optimized locations of the four mirror supports, any frozen-in distortion and thus distortion after gravity release is minimized, making it possible to build and test sub-arcsec lightweight X-ray mirror assemblies in a gravity environment. Third, this construction process naturally defines the optical axis, making it much easier to both build and integrate meta-shells into a final mirror assembly. Fourth, the construction process proceeds naturally from inner shells to outer shells, making it much easier to baffle against stray light and realize much smaller inter-shell spacing, essential for achieving maximum packing efficiency.

Objectives and Milestones

The objective of this effort is to perfect a process for making mirror meta-shells that meet spaceflight environmental requirements and have progressively better performance in terms of angular resolution and effective area. We expect to achieve better than 5" HPD in the near term (next two years). In the longer term (next five to 10 years), we expect to continue and improve every aspect of the process toward better angular resolution from 5" to less than 1", reaching 0.1" or better in the 2020s.

The same set of milestones can be used to measure progress toward realizing both near-term and long-term objectives. They differ only in the X-ray image quality measured in arcsec. Each step or milestone has two metrics: image quality and consistency. The steps are as follows.

1. Fabricating mirror substrates.
2. Maximizing X-ray reflectivity by coating substrates with thin-film iridium or other material.
3. Aligning individual mirror segments and pairs of mirror segments.
4. Bonding mirror segments to a mechanical structure.
5. Constructing meta-shells, requiring co-alignment and bonding of multiple mirror segments.
6. Environmental-testing meta-shells, with X-ray performance tests before and after environmental tests.

Environmental tests include vibration, acoustic, and thermal-vacuum. X-ray performance tests include measurement of PSF and effective area at representative X-ray energies – e.g., 1.5 keV (aluminum Kα), 4.5 keV (titanium Kα), and 8.0 keV (copper Kα).

Progress and Accomplishments

In the past year, we made progress in every area of the technology: substrate fabrication; coating; mirror alignment; mirror bonding; and meta-shell design, analysis, construction, and testing.

Substrate Fabrication

In the past year, we validated a complete substrate fabrication process: starting with a block of commercially procured mono-crystalline silicon and ending with an X-ray mirror, with an image quality of about 0.4" HPD, shown in Fig. 2. This is about 20 times better than the best slumped-glass mirrors, comparable to or slightly better than the Chandra mirrors, and therefore the best astronomical X-ray mirror in the world. We expect to continually refine and perfect this process, not only improving the mirror quality but also reducing production time and cost.

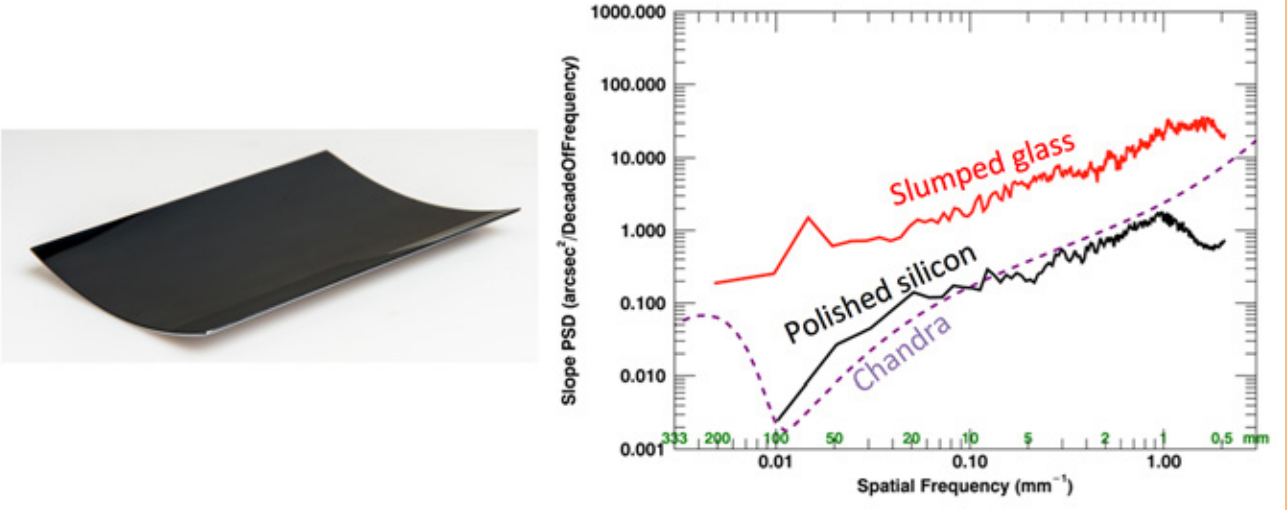

Fig. 2. *Status of lightweight mono-crystalline silicon mirror fabrication.* Left: *Photo of a 0.9-mm-thick mirror.* Right: *The axial-slope power-spectral density (PSD) in comparison with typical slumped-glass mirrors and that of the Chandra mirrors. As of June 2017, the silicon mirror is about 20 times better than the best slumped-glass mirrors and comparable to or slightly better than the Chandra mirrors.*

The substrate fabrication process consists of the following steps:

1. Figure generation.
2. Slicing or light-weighting.
3. Edge- and backside lapping.
4. Acid etching.
5. Stress-polishing.
6. Trimming.
7. Edge-polishing.
8. Ion-beam figuring.

Our work in the coming years is to refine and perfect each step, not only improving quality but also reducing production time and cost.

Coating

Mirror substrates require an optical coating (e.g., 15-nm iridium) to enhance X-ray reflectivity. The stress of an iridium film, typically several Giga-Pascal, severely distorts the figure of a thin substrate, greatly degrading its imaging quality. Over the last few years we have experimented with different ways of reducing the figure distortion, including balancing the front- and back-side coating stress and thermal annealing. In the past year, we set up two magnetrons in a vacuum chamber to coat the front side (concave) and the back side (convex) of the mirror simultaneously. Initial test with this setup has shown that coating thickness uniformity of better than 1 nm can be achieved across a 100 mm by 100 mm mirror surface. This work will continue into the next year with results expected by the middle of 2018.

Mirror-Segment Alignment and Bonding

Traditionally, the alignment of a mirror is achieved by using a 6-dof (degrees of freedom) stage that can translate and orient a rigid body in all possible ways. We used this traditional method until early 2016, when we switched to using the fact that an X-ray mirror segment, or more generally a cylindrical

mirror segment, can be supported at four posts (or spacers) with its orientation uniquely determined. The orientation of the mirror can be fine-tuned by precise adjustment of the radial height of one or more of these posts. Figure 3 shows our implementation of this concept, where each mirror segment is supported by four spacers whose radial heights are precisely machined. In practice, this is an iteration process guided by Hartmann measurements.

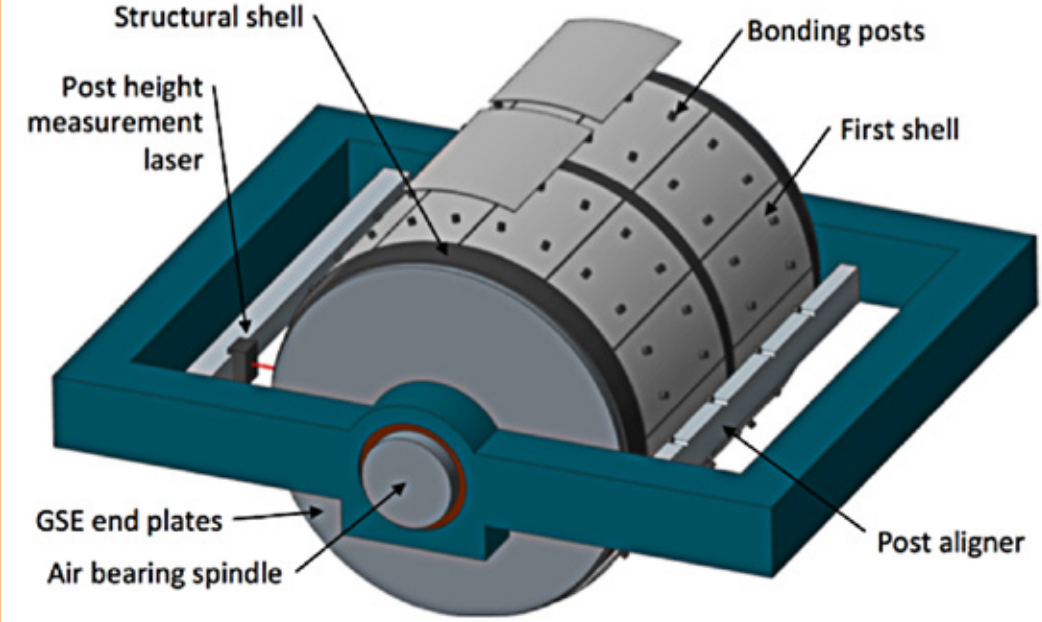

Fig. 3. *Illustration of the mirror alignment and bonding process. Each mirror segment is supported and aligned by four spacers. The radial heights of these spacers are precisely and iteratively machined in-situ, guided by Hartmann measurements (GSE, ground-support equipment).*

As shown in Fig. 3, once the four spacers have been machined to achieve alignment for the mirror segment, a minute amount of epoxy is applied to each spacer. The mirror segment is then placed on the spacers and a small vibration jiggles the mirror into its optimal alignment. Once the epoxy cures, the mirror is permanently bonded.

In the past year, we demonstrated with stand-alone experiments several key elements of this alignment and bonding process. First, the alignment is uniquely determined by the four spacers. A mirror was repeatedly placed and removed to show that the images of the different placement trials precisely reproduce the same quality and location. Second, a grinding and buffing process can deterministically change the height of a spacer with sub-μm precision. Third, the application of epoxy on the spacer does not change the alignment of the mirror, implying that the epoxy thickness variation from spacer to spacer is acceptably small. Our effort culminated in the buildup and X-ray testing of a module of consisting of a single pair of silicon mirrors, as shown in Fig. 4. The pair of mirrors aligned, bonded, and tested here have not gone through the ion-beam figuring step of the fabrication process, as such its performance prediction based on normal incidence optical metrology is about 4.5”, agreeing well with the X-ray test result. In the coming year, we will conduct several tests of this kind using the best possible X-ray mirrors, expecting the image quality to be substantially better than 4.5”.

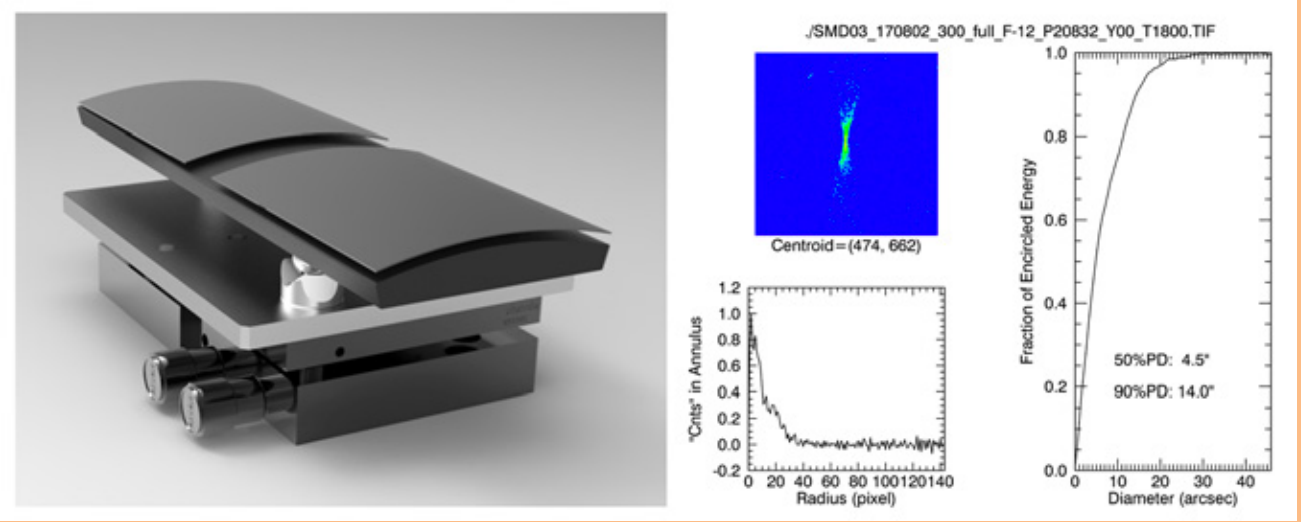

Fig. 4. Left: *a pair of mono-crystalline silicon mirrors aligned and bonded using four spacers each on a silicon plate.* Right: *X-ray image and its properties of the pair of mirrors on the left when fully illuminated with 4.5 keV X rays in a 600-m X-ray beam line in Area 200 at GSFC (EED, Encircled Energy Diameter). The 4.5" HPD image is the best image produced by lightweight X-ray mirrors in the world.*

Meta-Shell Design, Analysis, and Test

Since the conception of the meta-shell approach a little over a year ago, we have conducted a design, analysis, and test exercise. Figure 5 shows the preliminary design of a mirror assembly with an outer diameter of 1.3 m. It consists of six meta-shells, each having about 20 layers of mirrors, not all of which are drawn. A set of preliminary structural, thermal, and performance analyses has led to the following conclusions:

1. Each meta-shell, with its relatively thick structural shell and interlocked mirror segments, is stiff and has good mechanical integrity. Assuming the use of a standard aerospace epoxy, such as Hysol 9309, and a reasonable bond area for each spacer, about 2 mm in diameter, the meta-shell can sustain launch loads. This conclusion has been empirically verified by a set of vibration tests of articles shown in Fig. 6.
2. The meta-shell construction process, as shown in Fig. 3, where the optical axis is horizontal, does not freeze in any significant amount of distortion, meaning that when the meta-shell is turned vertical, the frozen figure distortion is sub-arcsec.
3. A meta-shell can be X-ray-tested in a horizontal beam line. The images of some of the mirrors show minimal distortion. By rotating the meta-shell, we expect to be able to fully characterize the imaging performance of the entire meta-shell.
4. Because the meta-shell is made of silicon, with only trace amounts of different materials such as epoxy and iridium, a bulk temperature change of 1°C changes the imaging performance by only 0.1" HPD.

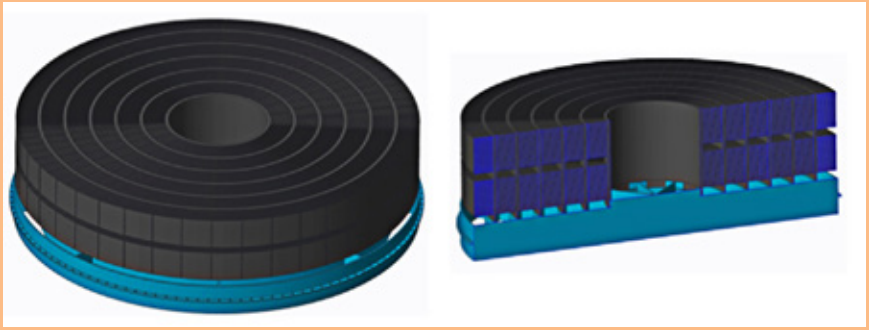

Fig. 5. *Illustration of a mirror assembly consisting of six meta-shells. Each meta-shell is flexure-mounted onto an aluminum (or composite) structure wagon-wheel. The spokes of the wagon-wheel are all hidden behind the spacers and cause no additional blockage.*

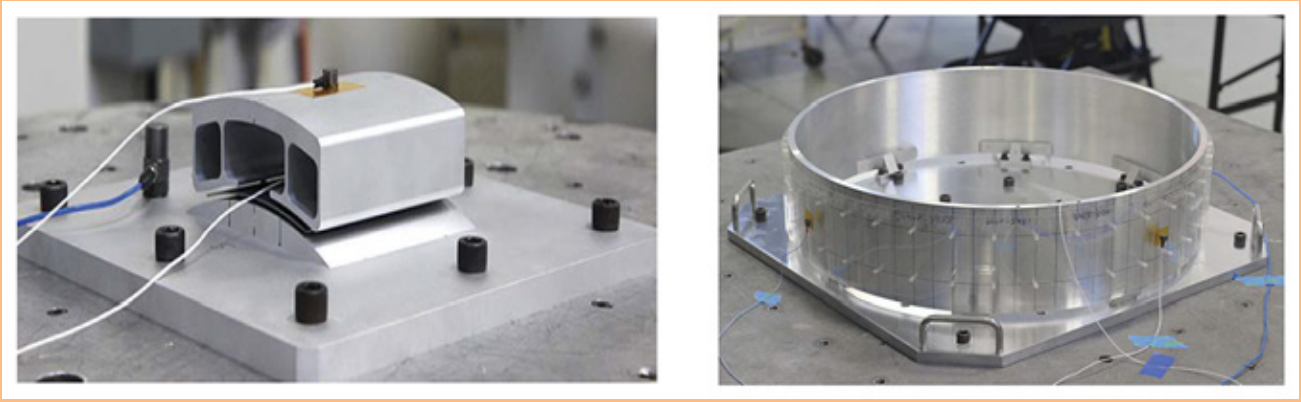

Fig. 6. *Two articles tested on a vibration table to prove the concept of bonding thin brittle mirror segments with four spacers.* Left: *a thick silicon mirror segment bonded by four spacers to an aluminum base plate simulating the structural shell and by another four spacers to a light-weighted aluminum block simulating the mechanical effect of additional mirror segments.* Right: *an aluminum cylinder bonded with 54 small clear glass mirror segments in three layers simulating silicon mirror segments. Both articles were vibrated to, and survived, a quasi-static level of 12.3 g, demonstrating that the meta-shell construction meets a significant and necessary requirement.*

Overall, the analysis and test results have shown that the meta-shell approach is sound in every aspect: performance, thermal, and structural. We note that this approach incorporates the merits of all four currently operating missions' X-ray mirror assemblies.

Path Forward

Based on our previous work, as well as heritage of previous missions, such as Chandra, XMM-Newton, Suzaku, and NuSTAR, we have conceived and validated the meta-shell approach for our technology development. Numerous stand-alone experiments and finite element analyses, both structural and thermal, have validated the approach. In the coming year, we will start building and testing mirror modules, or meta-shells, based on this approach. Initially, we will continue to build and test single pairs. Then, we will proceed to build a meta-shell with three layers of mirrors, with a total of 72 mirror segments. We will then X-ray-test this meta-shell, environmentally test it, and repeat the X-ray test to verify the environmental testing did not degrade its performance.

For additional information, contact William Zhang: *william.w.zhang@nasa.gov*

Planar Antenna-Coupled Superconducting Detectors for CMB Polarimetry

Prepared by: James J. Bock (JPL, California Institute of Technology)

Summary

We are developing advanced antenna-coupled superconducting detector-array technology for the NASA Inflation Probe (IP), a future satellite dedicated to comprehensive measurements of Cosmic Microwave Background (CMB) polarization in NASA's Physics of the Cosmos (PCOS) Program. This Strategic Astrophysics Technology (SAT) project will extend the demonstrated frequency range of antennas down to 40 GHz and up to 350 GHz, and develop dual-band antennas that offer larger wafer formats with a higher density of detectors, a valuable resource in a 100-mK space-borne focal plane.

Antenna-coupled detectors have the requisite attributes – sensitivity, frequency coverage, and control of systematic errors – called for in community studies of space-borne CMB-polarization experiments. The arrays provide integral beam-formation, spectral-band definition, and polarization analysis; and scale to operate over the wide frequency range of 30 to over 300 GHz required to remove galactic foregrounds at near-background-limited sensitivity. The devices have rapid response speed and 1/f noise stability for slow-scanning observations without requiring an additional level of signal modulation.

Our program rapidly infuses new detector technology into scientific observations, the fastest way to learn about real-world performance in demanding applications. Simultaneously, the program develops aspects of the technology uniquely required for space-borne operations. We are expanding the frequency coverage of the antennas, and applying these devices to improved foreground separation between the galaxy and the CMB. We are developing broadband antennas to better exploit full access to the electromagnetic spectrum in space. We are expanding the development of focal-plane modules that integrate detectors and readouts into a package for large focal planes, and fielding these devices in the Background Imaging of Cosmic Extragalactic Polarization 3 (BICEP3) experiment. We are furthering our measurements of cosmic-ray susceptibility, based on our experience with the detectors on the European Space Agency (ESA) Planck satellite. Finally, we are starting to develop arrays on larger 150-mm wafers, expanding to the larger formats demanded by CMB scientists.

This two-year grant began in October 2015, and includes Jeff Filippini at the University of Illinois Urbana-Champaign (UIUC); and Krikor Megerian, Hien Nguyen, Roger O'Brient, Anthony Turner, and Alexis Weber at JPL. The program actively engages postdocs and students at Caltech, including Bryan Steinbach, Jon Hunacek, Howard Hui, and Sinan Kefeli. The students characterize the devices at cryogenic temperature, and then use the arrays in astrophysical measurements of CMB polarization.

Scientifically, the devices have led the way in state-of-the-art (SOTA) CMB measurements from ground-based and balloon-borne observations. Last year, the BICEP2/Keck Array collaboration published the first results incorporating measurements in two spectral bands, 95 and 150 GHz. These measurements constrain the amplitude of the Inflationary gravitational-wave background more strongly from CMB polarization data than with CMB temperature information, a transition predicted in the 1990s.

The collaboration is completing a paper that uses new data at 95, 150, and 220 GHz from 2015 observations. This paper will provide the first constraints using ground-based data at 220 GHz to constrain the polarized galactic foreground from interstellar-dust emission. The two receiver-years from 2015 used in this analysis provide similar constraints on polarized dust emission to the best 353-GHz data from the Planck satellite. New 220-GHz data from 2016 have now surpassed Planck. In January 2015, the Suborbital Polarimeter for Inflation Dust and the Epoch of Reionization (Spider) balloon experiment flew with six full focal planes operating at 95 and 150 GHz. The detectors performed well in the scientific environment closest to space, with low photon backgrounds, slow-scanned observations, and a difficult cosmic-ray environment.

Background

The importance of CMB-polarization research has been recognized in national reports including the 1999 National Academy Report; the 2001 Decadal Survey; and the 2003 National Research Council (NRC) report, "*Connecting Quarks with the Cosmos*." In 2005, the Task Force on CMB Research stated that its first technology recommendation was "*technology development leading to receivers that contain a thousand or more polarization-sensitive detectors,"* and that *"highest priority needs to be given to the development of bolometer-based polarization sensitive receivers.*" The Astro2010 decadal report endorsed a CMB technology program of $60M-$200M, its second-ranked medium initiative for space. In addition, the decadal report states the amount could be increased to $200M following a mid-decade review of the state of CMB-polarization measurements. The CMB Technology Roadmap ranked detector arrays as its highest CMB-technology priority, recommending a program that takes maximum advantage of operating the arrays in sub-orbital and ground-based CMB-polarization experiments.

The IP will measure CMB polarization over the entire sky to cosmological and astrophysical limits. The CMB is thought to carry a B-mode polarization signal imparted by a gravitational-wave background produced by the Inflationary expansion ~10^{-32} seconds after the Big Bang. The Inflationary polarization signal is sensitive to the energy scale and shape of the Inflationary potential, and can be clearly distinguished from polarization produced by matter-density variations due to its distinctive B-mode spatial signature. A detection of the Inflationary polarization signal would do more than just confirm Inflation—the amplitude of gravitational waves depends on the model and energy scale of Inflation, so detection would distinguish between models and constrain the physical process underlying Inflation. Such a measurement has profound implications for cosmology and bears on the current frontiers of fundamental physics: the union of general relativity and quantum mechanics, string theory, and the highest accessible energies.

The IP will also map the CMB-polarization pattern produced by gravitational lensing. Intervening matter between us and the surface-of-last-scattering slightly distorts the background CMB polarization, imparting a B-mode signal that peaks at arcmin angular scales and probes the evolution of large-scale structure, which is sensitive to neutrino mass and dark energy. The CMB lensing signal is related to the projected gravitational potential of this matter, and provides a powerful combination with dark-energy surveys such as baryon acoustic oscillations and weak lensing.

The most recent definition study of the IP in 2008-2009 developed the basis for space-borne CMB-polarization measurements, incorporating high-sensitivity detector arrays as the key technology, operating over a wide range of frequencies to accurately measure and remove polarized galactic foregrounds. The detector system must demonstrate extreme 1/f noise stability, forward-beam definition with stray-light immunity, radio-frequency (RF) and magnetic shielding, excellent spectral-band and time-constant

matching, and cosmic-ray insusceptibility. Alternate implementations have been proposed, including an ESA medium-class mission and the Japanese Aerospace eXploration Agency (JAXA) Lite (Light) satellite for the studies of B-mode polarization and Inflation from cosmic background Radiation Detection (LiteBIRD) concept. NASA began a new study of the IP in 2017 for the Probe mission class.

Antenna-coupled Transition-Edge-Sensor (TES) bolometer arrays (Fig. 1) are a scalable, planar focal-plane architecture that coherently sums an array of individual slot antennas with a microstrip feed network, controlling the phase and electric-field amplitude distributed to each slot. The planar antenna enables customized shaping of the detector beam-pattern for controlling detector illumination on critical optical surfaces. The antenna operates in two polarizations: an array of horizontal slots couples to one detector, and an interleaved array of vertical slots couples to another. The spectral band is defined by a three-pole RF microstrip filter. Power from the antenna is deposited in a meandered Au resistor on a thermally isolated bolometer, detected by a Ti/Al TES detector and read out by a multiplexed Superconducting-QUantum-Interference-Device (SQUID) current amplifier. As shown in Fig. 1, this technology has now been demonstrated in scientific observations in spectral bands centered at 95, 150, and 220 GHz. A fourth band at 270 GHz has been developed under the SAT program and started first-light observations in 2017.

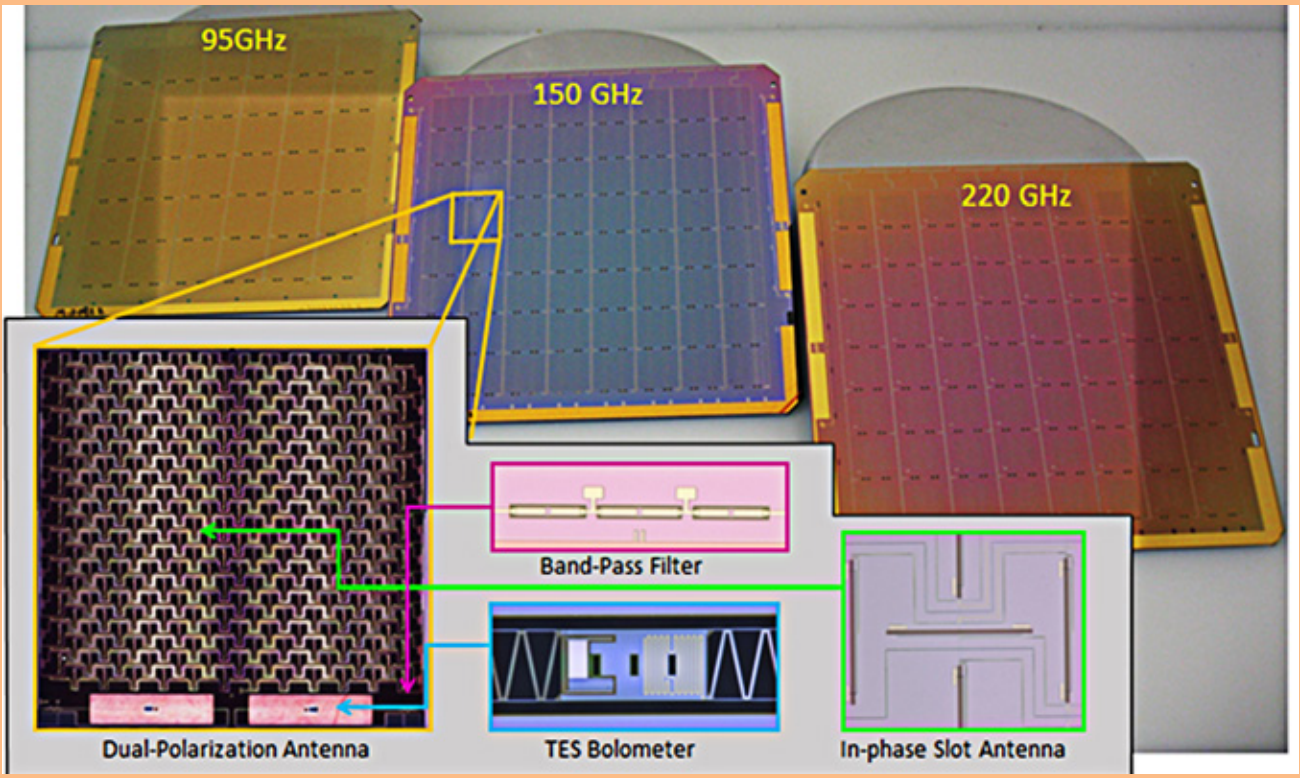

Fig. 1. *Focal-plane array wafers designed for operation at 95, 150, and 220 GHz. Each wafer is based on planar dual-polarization antennas consisting of an array of slot antennas coherently combined with a feed network. The output of the antenna passes through a lithographed band-defining filter and terminates in a resistive meander located on an island thermally isolated on micro-machined silicon-nitride beams. Power deposited on the bolometer is sensed with a voltage-biased TES bolometer readout with multiplexed SQUID current amplifiers.*

Planar antennas are entirely lithographed and avoid coupling optics such as feedhorns or hyper-hemispherical lenses, ideal for a low-mass 100-mK focal plane. The devices can cover the wide range of frequencies by scaling the antenna with wavelength and keeping the detector element essentially

unchanged. The antennas demonstrate excellent polarization properties and the lithographed filters provide reproducible control of the spectral band. The Ti TES detectors give predictable noise properties and low-frequency noise stability appropriate for slow-scanned observations from space.

Current State of CMB Polarization Measurements

In recent years, CMB-polarization measurements have broken new ground in placing constraints on a background of gravitational waves produced in some models of Inflation. Antenna-coupled TES bolometer-array technology is ideal, because the architecture scales in frequency, and we have developed science-grade arrays in three frequency bands (Fig. 1). In 2016, polarization measurements using this technology surpassed constraints based on CMB-temperature measurements. In Fig. 2 we show the latest scientific measurements from the BICEP2/Keck experiment obtained at these three frequencies from data up to 2016. These data at 220 GHz have now surpassed the sensitivity of the Planck satellite in constraining polarized interstellar dust emission. The maps demonstrate SOTA sensitivity, while serving as valuable tests for controlling systematic errors. Indeed, the sensitivity at 150 GHz, below 50 nK in a square degree, is comparable to the sensitivity expected for the IP satellite. Instead of studying a small region, however, the IP will map the entire sky in multiple bands at this sensitivity.

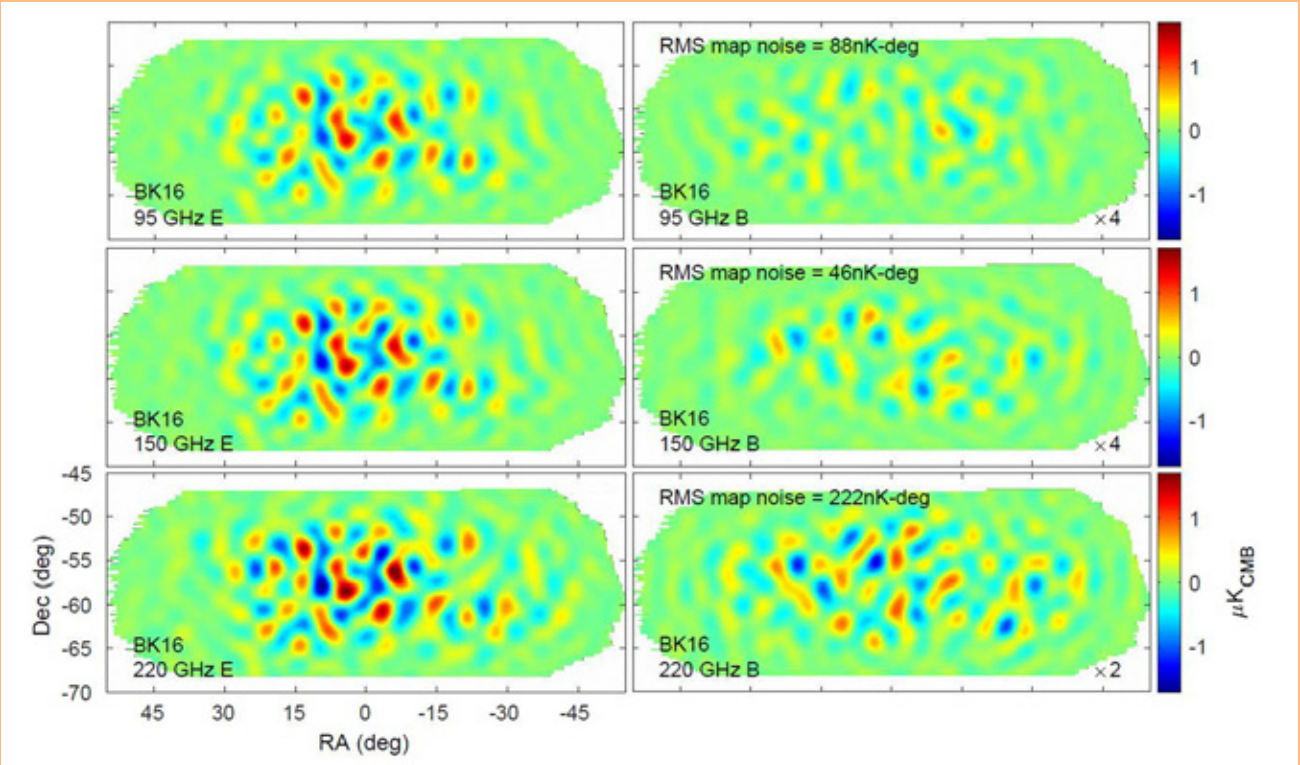

Fig. 2. *New CMB maps (Dec, declination; RA, right ascension; deg, degrees; RMS, root mean square) from BICEP-Keck using data through 2016 (but excluding additional BICEP3 data). E-mode polarization is clearly visible and reproduced in all three frequencies (left column of images). The B-mode polarization maps indicate the map noise level in nK-deg based on Q/U data over an effective area of 390 sq. deg (right column of images). Note the B-mode map scales are increased by 2-4 to show the fainter structures and noise. The 2016 maps at 220 GHz have over ×3 better power spectral sensitivity than the 2015 data, and have overtaken Planck 353-GHz data for measurements of polarized emission from galactic dust, a foreground contaminant. The 220-GHz band also is closer in frequency to the 95- and 150-GHz CMB channels, reducing possible errors in extrapolating the dust spectrum.*

Objectives and Milestones

This SAT program advances the detector attributes needed for space-borne observations, specifically, developments related to frequency coverage, focal-plane packaging, RF susceptibility, beam control, cosmic-ray susceptibility, and wafer formats. The tasks for our 2017 SAT program build on current antenna-coupled detector technology to address specific challenges for a space mission as follows:

- Extend the frequency range to bands at 40 GHz and 350 GHz;
- Develop dual-band devices operating broadband antennas;
- Develop larger focal-plane modules for 150-mm wafers with larger formats;
- Characterize and reduce focal-plane RF susceptibility;
- Develop more highly tapered antennas for coupling to ambient-temperature optics;
- Measure cosmic-ray particle susceptibility in arrays; and
- Scale the fabrication process up to 150-mm-diameter wafers.

Progress and Accomplishments

Focal-plane technology developed under this SAT program has made strong scientific progress in the past year, with focal-plane modules operating successfully in the Keck Array and BICEP3 experiments. BICEP3 operates 20 modules, a technology developed under the SAT program, in a large focal plane to achieve high sensitivity at 95 GHz. The modular design enabled component-wise development and testing. Arrays operating at 220 GHz in the Keck Array produced SOTA polarization measurements at the South Pole last observing season (Austral summer 2016/17) (Fig. 2). These maps, the deepest produced at this frequency to date, will provide leading constraints on Inflationary polarization by providing new information on the brightness and polarization of the galactic-dust foreground.

This year, we completed fabrication of full devices on 150-mm-diameter wafers (Fig. 3), following earlier engineering tests of film uniformity on this larger wafer size. The wafers are based on 40-GHz antennas, and are now being prepared for testing at 300 mK. They will be characterized for uniformity in thermal conductivity, transition temperature, normal resistance, spectral response, beam response, and optical efficiency.

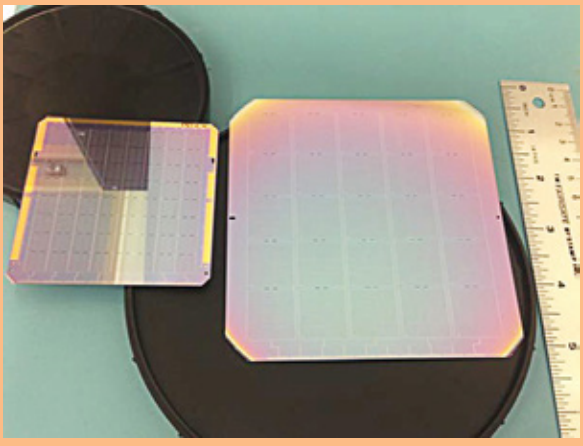

Fig. 3. *The first antenna-coupled TES bolometer array fabricated on a 150-mm-diameter wafer (right). As this photo illustrates, going from 100-mm to 150-mm wafers more than doubles the active area per wafer, which also doubles the number of detectors per Micro Devices Laboratory (MDL) fabrication hour. The larger wafers present challenges for materials uniformity, particularly for the TES and dielectric layers (evident by the change in color at the outside corners caused by variations in the dielectric layer). The array was developed for 35 GHz to test end-to-end process uniformity.*

We have completed the design of a new focal-plane module to accommodate the larger 150-mm-diameter wafers (Fig. 4). The design incorporates the detector wafer, the multiplexed SQUID readout, an anti-reflection wafer, and a $\lambda/4$ optical back-short in a compact package that uses the space behind

the wafer to maximize areal packing. The detector signals exit from a single flexible cable out the back, and the detector bias, SQUID bias, and row commands are all sent via the same cable. The module must provide magnetic shielding of the sensitive SQUIDs. Finally, the edges of the module are corrugated to minimize artefacts from beam interactions. The module was developed to operate flexibly with a variety of formats. In order to accommodate the density of traces and interconnects, we use a lithographed silicon wafer, serving as a high-density single-layer printed circuit board. The silicon SQUID multiplexer chips mount on the silicon circuit board, which is populated and wire-bound in different configurations. The magnetic shielding of the module was calculated using a finite-element electromagnetic field analysis package.

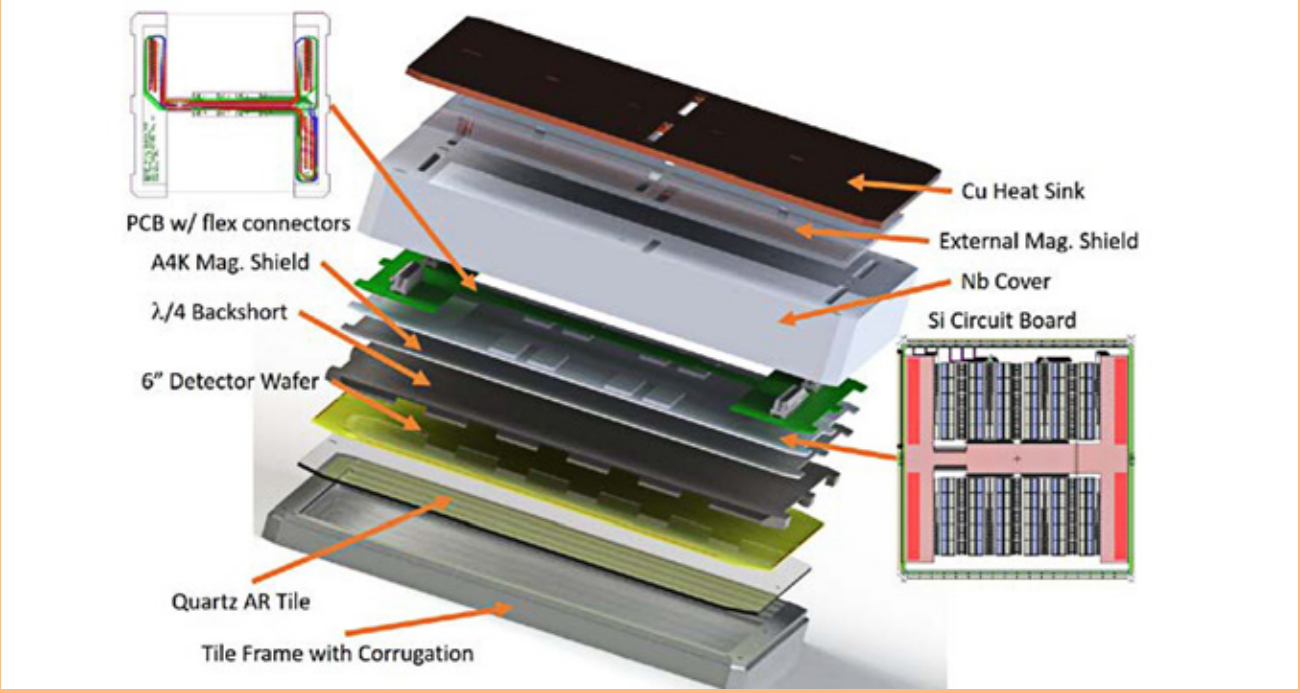

Fig. 4. *Module design for accommodating arrays from 150-mm-diameter wafers. The design employs a silicon circuit board for a dense design, routing between the detector wafer and Time Division Multiplexing (TDM) SQUID chips with aluminum traces. The silicon wafer interfaces to a conventional connectorized printed circuit board (PCB) for bias lines, row address, and SQUID signal outputs. The row address lines route through 10 columns of N-chained base-11 SQUID chips. This allows us to flexibly allocate channels in multiple configurations such as 35, 95, and 150 GHz with 64, 288, and 648 channels (AR, anti-reflection).*

We have also developed and fabricated a family of 200-to-300-GHz antennas. As shown in Fig. 5, we characterized a new broadband 200-to-300-GHz antenna. The spectral response agrees with calculated performance, though a spectral dip results from using a single anti-reflection layer in the test configuration. A two-layer anti-reflection stack should eliminate this feature. We have also found we can realize a uniform broadband response with a single anti-reflection layer by the choice of antenna design and by tuning the silicon-device-wafer thickness. This approach is attractive at lower frequencies, where the wafers are not too thin for fabrication.

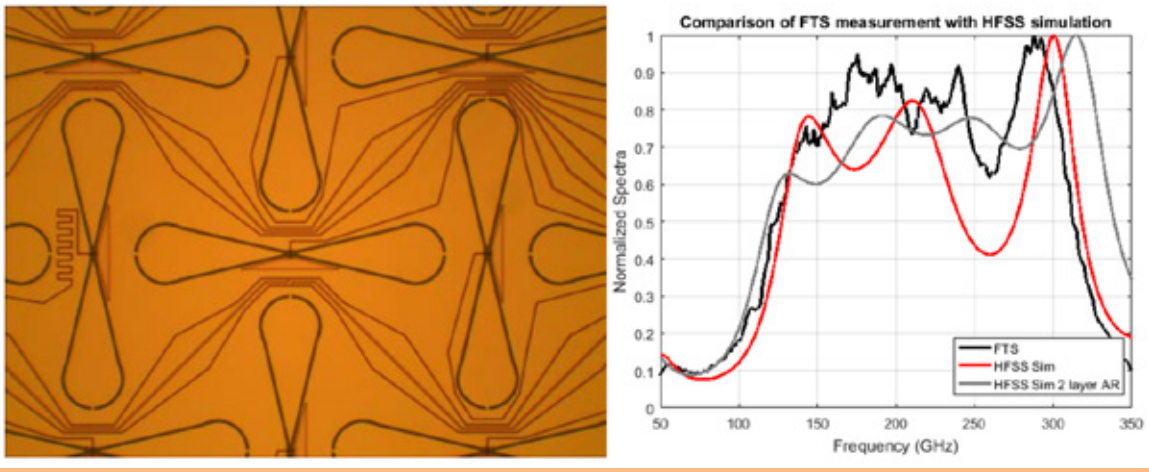

Fig. 5. Left: *Broadband 200-to-300-GHz antenna designed from unit "bowtie" slot sub-antennas in a base Nb ground plane, back-illuminated through the Si wafer. The sub-antennas connect to a feed network of microstrip lines. Note the design detects vertical and horizontal polarizations, which are interleaved in two feed networks.* Right: *Measured spectral response of the antenna (black) scaled to the calculated response (red) for a single-layer AR coating. We calculate that a two-layer AR stack (grey) will remove the prominent dip at 260 GHz (FTS, Fourier-transform spectroscopy; HFSS, high-frequency structural simulator).*

We developed a science-capable focal-plane array for 270 GHz. This band is nicely accommodated in the upper half of the 200-to-300-GHz atmospheric window (Fig. 6). The 270-GHz frequency band may ultimately be able to obtain slightly higher sensitivity to galactic dust than 220 GHz, due to its steeply rising spectrum. However, its main scientific purpose is to provide additional spectral information on galactic dust emission in conjunction with 220 GHz, to constrain model parameters. The detector arrays were tested for optical efficiency, spectral response, and differential beam matching (Fig. 6). The array is now operating at the South Pole in one of the Keck Array receivers as a first test of observing in this band. Preliminary analysis indicates that sensitivity is comparable to that of a 220-GHz receiver.

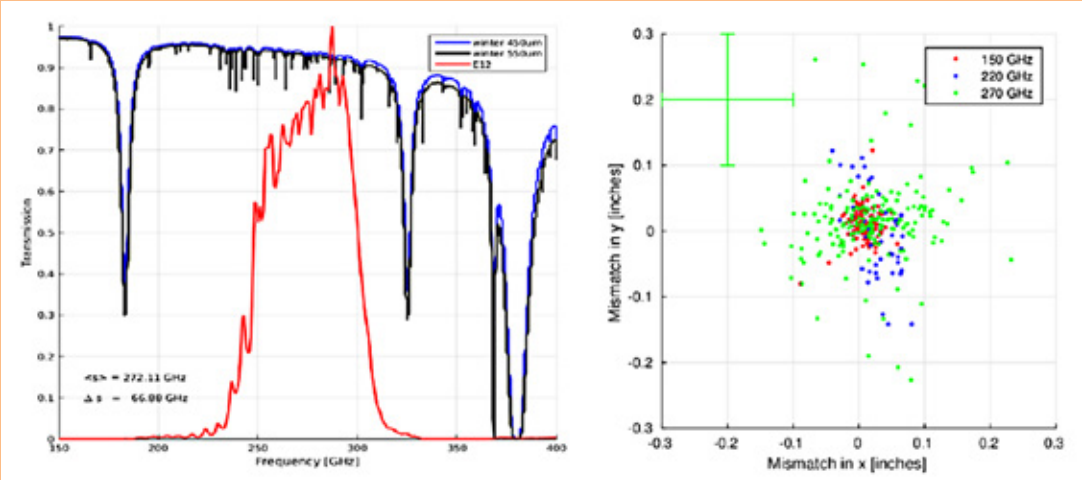

Fig. 6. Left: *Normalized spectral response of detectors on the 270-GHz focal-plane array compared with atmospheric transmission.* Right: *Dipole beam distribution, measured in the far field of the antennas. The scatter at 270 GHz, limited by measurement errors shown by the cross, is similar to that at 220 GHz.*

Recent results from Spider and BICEP3 showed a degree of RF susceptibility at system level. The current design uses the ground plane of the antennas as an RF shield, connected to the housing through a series of wire bonds. We developed a new design, where a bandpass filter placed over the detector array provides additional RF attenuation. This filter, developed at Cardiff University, has a high-pass inductive grid that reflects long-wavelength RF power. The filter grid is electrically connected to the housing frame. Because RF susceptibility is really a system issue, due to the many potential paths to the detector, characterizing this device requires a dedicated measurement. As shown in Fig. 7, the filter has been completed and shown to provide a suitable spectral band with a high-pass edge that blocks low-frequency RF power. The RF performance has been tested at component level at room temperature, showing no discernable leakage compared with a metal sheet.

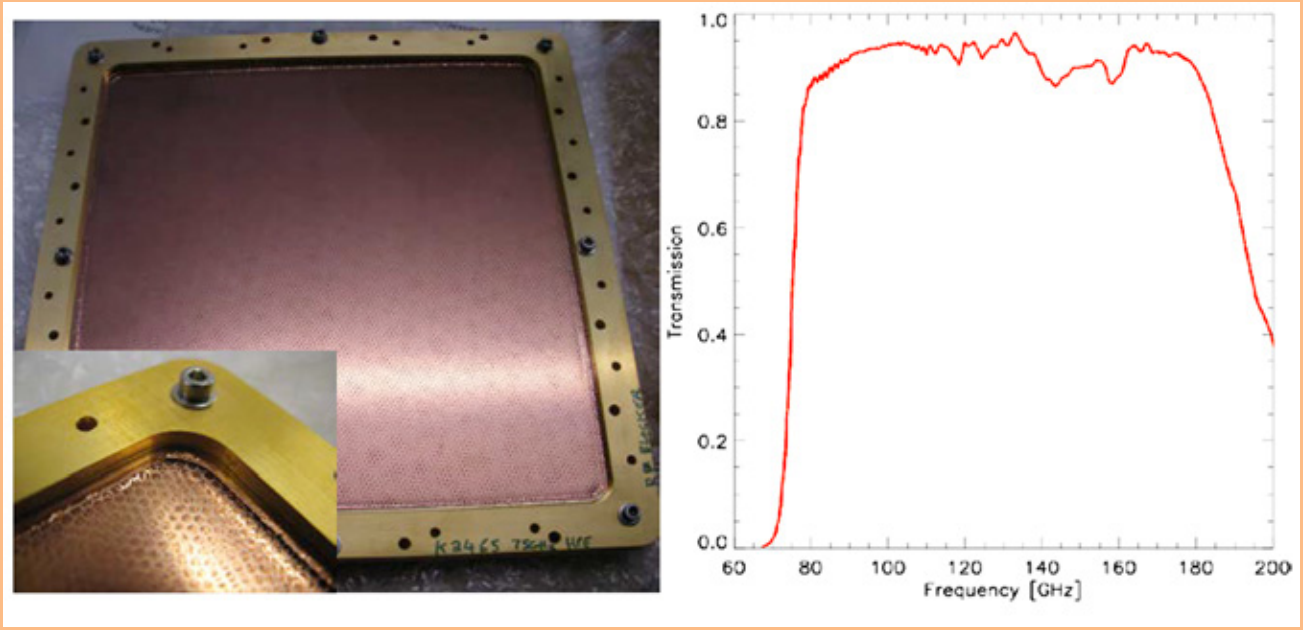

Fig. 7. Left: *RF-mitigation filter designed from an inductive mesh in a band-pass filter that is placed in front of the detector array. The inset at the lower left shows the inductive screen that is electrically shorted to the brass module frame.* Right: *The band-pass filter provides comparable transmission to the low-pass edge filters we are currently using. The low-frequency edge blocks RF from impinging on the detectors. We also electrically connect the detector Nb ground plane to the frame for additional RF mitigation.*

A cryogenic test bed has been developed at the University of Illinois to test cosmic-ray susceptibility in the array frames. The design is completed and the system is now being fabricated.

Table 1 shows project milestones by topic, with each milestone's schedule and status.

Topic	Milestone	Schedule and Status
Antennas for Extended Frequencies	**40-GHz Arrays** Demonstrate antennas for the 40-GHz frequency band	**October 2014 – August 2015** Completed
	270-GHz Arrays Develop arrays for 270 GHz	**August 2014 – June 2016** Completed
	350-GHz Arrays Develop arrays for 350 GHz	**March 2016 – December 2017** High-frequency loss test of devices in process
Multi-Color Antennas	**Wide-Band Antenna** Develop wide-band antenna for 220/270 GHz	**August 2014 – June 2016** Completed
	Diplexer and Filters Develop and test diplexer + filter components	**August 2014 – December 2015** Dichroic tested separately
Large-Focal-Plane Modules	**Large-Format Modules** Develop and test designs for operating 150-mm wafers with larger formats	**January 2016 – November 2016** Design completed, prototype in development
RF Susceptibility	**Focal-Plane RF-Susceptibility Mitigation** Test and improve RF susceptibility	**January 2016 – April 2016** Fabricated and tested at room temperature; system-level test in process
Beam Spillover	**Highly Tapered Antennas** Develop and test highly tapered 95-GHz antennas at device level	**January 2016 – November 2017** Design has not started
Particle Susceptibility	**Frame Response of Single-Element Device** Test Planck devices with modified frame to minimize events	**January 2014 – August 2015** Completed
	Array Frame Hits Measure frame susceptibility in arrays	**January 2016 – December 2017** Developing cryogenic test bed at UIUC
150-mm-Diameter Wafers	**150-mm Wafer Fabrication Process** Determine engineering parameters for fabricating 150-mm-diameter wafers	**January 2016 – October 2017** Completed uniformity tests. Full-device wafer fabricated and awaiting test

Table 1. *Project milestones, schedule, and status by topic.*

Path Forward

The design of the 150-mm-diameter module is complete, including a detailed analysis of its corrugations and magnetic shielding. We will start fabrication of a prototype unit for characterization. We will continue to analyze data at 270 GHz this season. If we find that the atmospheric conditions are suitable (as expected), we will make improvements to the focal plane using new wafers for a second season of observations. The RF filter, having passed component-level testing, is now being readied for a system-level test in one optical barrel of the Spider cryostat. Future developments of 350-GHz and highly-tapered antennas will begin with fabrication of wafers with devices for measuring loss at high frequencies, followed by optical testing.

Publications

1. P. Ade et al., "*Antenna-Coupled TES Bolometers Used in BICEP2, Keck Array, and SPIDER*," ApJ, **812**, 176B (2015)
2. BICEP2 and Keck Array Collaborations, "*BICEP2/Keck Array IX: New Bounds on Anisotropies of CMB Polarization Rotation and Implications for Axion-Like Particles and Primordial Magnetic Fields*," arXiv 1705.02523 (2017)

3. J.M. Nagy et al., "*A New Limit on CMB Cicular Polarization from SPIDER*," arXiv 1704.00215 (2017)
4. BICEP2 and Keck Array Collaborations, "*BICEP2/Keck Array VIII: Measurement of Gravitational Lensing from Large-Scale B-Mode Polarization*," ApJ, **833**, 228B (2016)
5. BICEP2 and Keck Array Collaborations, "*BICEP2/Keck Array VII. Matrix Based E/B Separation Applied to BICEP2 and the Keck Array*," ApJ, **825**, 66B (2016)
6. BICEP2/Keck Collaborations, "*Improved Constraints on Cosmology and Foregrounds from BICEP2 and Keck Array CMB Data with Inclusion of 95 GHz Band*," PRL, **116**, 1302B
7. BICEP2/Keck and Planck Collaborations, "*Joint Analysis of BICEP2/Keck Array and Planck Data*," PRL, **114**, 1301 (2015)
8. BICEP2/Keck Array Collaboration, "*BICEP2/Keck Array V: Measurements of B-Mode Polarization at Degree Angular Scales and 150 GHz by the Keck Array*," ApJ, **811**, 126B (2015)
9. BICEP2 Collaboration, "*BICEP2 III: Instrumental Systematics*," ApJ, **814**, 110B (2015)
10. BICEP2/Keck Collaboration, "*BICE2/Keck Array VIII: Measurement of Gravitational Lensing from Large-Scale B-Mode Polarization*," arXiv 1606.01968K (2016)
11. BICEP2/Keck Array Collaboration, "*BICEP2/Keck Array IV: Optical Characterization and Performance of the BICEP2 and Keck Array Experiments*," ApJ, **806**, 206B (2015)
12. W.L.K. Wu et al., "*Initial Performance of BICEP3: A Degree Angular Scale 95 GHz Band Polarimeter*," JLTP, **184**, 765W (2016)
13. K.S. Karkare et al., "*Optical Characterization of BICEP3 CMB Polarimeter at the South Pole*," SPIE **9914E**, 30K (2016)
14. H. Hui et al., "*BICEP3 Focal Plane Design and Detector Performance*," SPIE **9914E**, 0TH (2016)
15. J.A. Grayson et al., "*BICEP3 Performance Overview and Planned Keck Array Upgrade*," SPIE **9914**, 0SG (2016)

For additional information, contact James Bock: *james.j.bock@jpl.nasa.gov*

High-Efficiency Feedhorn-Coupled TES-based Detectors for Cosmic Microwave Background Polarization Measurements

Prepared by: Edward J. Wollack (PI; GSFC), David T. Chuss (Villanova University), Kevin L. Denis and S. Harvey Moseley (GSFC), Karwan Rostem (GSFC, JHU), and Tobias A. Marriage and Charles L. Bennett (JHU)

Summary

The relic radiation from the Big Bang, the Cosmic Microwave Background (CMB), has provided a Rosetta stone for deciphering the content, structure, and evolution of the early universe. Our current theoretical understanding suggests that the universe underwent a rapid exponential expansion, called "Inflation," in the first fraction of a second. Such an inflationary epoch would result in an observable stochastic background of gravitational waves that impress a faint polarized signature on the CMB. The cosmological importance of undertaking this measurement was highlighted in the 2010 National Research Council Decadal Survey, "*New Worlds, New Horizons in Astronomy and Astrophysics*" (NWNH) [1]. NASA consequently recognized characterization of the CMB as a high-priority science objective and a dedicated Inflation Probe (IP) mission was called out in the NASA Astrophysics Roadmap, "*Enduring Quests, Daring Visions*" [2]. These efforts are international in their scope, with collaborative mission concepts under consideration by both the Japanese and European Space Agencies. The development of enabling technologies, including large-format focal planes, for space-borne polarization missions is a priority of the NASA Physics of the Cosmos (PCOS) technology roadmap.

This two-year technology maturation effort, initiated by the Strategic Astrophysics Technology (SAT) program in January 2016, focuses on the implementation of polarization-sensitive focal-plane arrays that are compatible with the space environment. We have developed and demonstrated superconducting Transition-Edge Sensor (TES) detectors that utilize a unique combination of highly symmetric electromagnetic design elements and single-crystal-silicon that results in high transmission efficiency, the required sensitivity, and low cross-polarization response. Our objective is to advance these devices to a Technology Readiness Level (TRL) of 6.

Background

The polarized signature of Inflation in the CMB offers an important tool to investigate the physics of the inflationary epoch of the early universe. Discovery of this signature would provide the first direct evidence for Inflation, and would rule out most competing explanations for the initial conditions of the early universe. Characterization of this signal provides a path to probe and quantify the physics of the first ~10^{-32} second of the universe, when energy scales vastly exceeded those accessible to current Earth-bound particle accelerators.

The measurement is arguably challenging, as the polarized signal from Inflation is anticipated to be faint, likely a mere ~10^{-8} of the 2.725 K isotropic component of the CMB. High sensitivity is a prerequisite; however, any mission that targets this measurement will also have to distinguish this

minute polarized signal from both instrumental effects and other astrophysical sources. This requires high sensitivity and stability, multiple spectral bands for astrophysical foreground removal, control over potential systematic measurement and calibration errors, and compatibility with unique space-borne environmental conditions. Large detector arrays as well as development of calibration and observational techniques to achieve these instrumental attributes are key enabling technology considerations. We have developed a sensor architecture that addresses these needs of an IP mission.

The basic design and the fabrication processes that have been developed have been reported in the literature [3-5]. Figure 1 provides an illustration of the architecture. Radiation from the optics is coupled by the feedhorn of each sensor into microstrip circuitry. Each linear polarization is coupled to an independent microstrip line, filtered to set the desired spectral passband, and detected in a TES. This configuration directly addresses the requirements of the IP mission as follows:

- **Polarization Sensitivity**: The symmetric planar ortho-mode transducer (OMT) coupled scalar feedhorn ensures that each polarization has symmetric beams and high isolation over the full spectral band.
- **Sensitivity**: The TES bolometers operate at ~150 mK to ensure that the noise limit is set by the fluctuations in the CMB when operated in an appropriately stabilized space-borne system. In addition, the signal-mode sensor's large fractional bandwidth (60%) and high transmission efficiency (~90%) enable improved throughput relative to alternative implementations. The architecture is demonstrably scalable to the large focal planes required for an IP mission.
- **Systematic Error Control**: On-chip thermal blocking and bandpass filters ensure that the spectral band is well-defined for radiation coupling through the optics. Boxed microstrip and electrical closeouts for the TES detectors ensure that stray (out-of-band) radiation does not couple directly to the detector. The design has been scaled to three broadband designs that span the CMB spectrum. Multiple spectral channels will be necessary to separate the CMB signal from astrophysical foregrounds such as galactic dust and synchrotron radiation. A highly uniform dielectric layer provides the control required to realize broadband circuit elements across the array reliably.
- **Prevention of Surface and Deep Dielectric Charging**: Damage can occur from interaction between exposed dielectric surfaces and ambient space plasma. The conductive elements in the design, including the feedhorns and integrated degenerately doped silicon package, greatly limit exposure of dielectric structures to energetic electrons in the environment. In addition, the comprehensive filtering strategy, stray light control, and metallic beam-forming elements minimize the number of quasi-optical dielectric elements required by the instrument design.
- **Mitigation of Cosmic-Ray Events**: High-energy ionizing particles that electromagnetically interact with the detector have the potential to induce signal contamination. It is not practical to mitigate cosmic-ray events via shielding. The approach adopted here is the implementation of structures having simple (easily understood) and fast thermal response, to reduce the affected portion of the data.

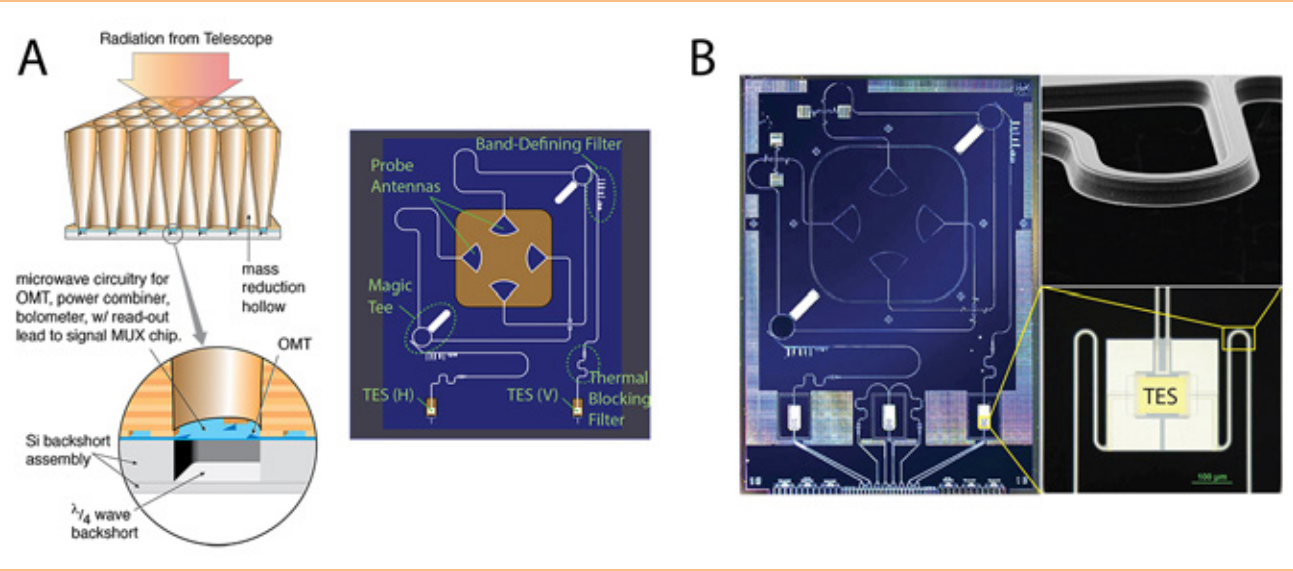

Fig. 1. (A) *The detector architecture combines the excellent beam-forming properties of feedhorns with the sensitivity of TES devices (MUX, multiplexer).* (B) *Photographs of the various parts of a device are shown.*

The basic operation of these detectors has been demonstrated at 40 GHz and is currently being employed in a ground-based telescope. This work focuses on extending their capabilities through a series of architectural improvements and corresponding validation.

Objectives and Milestones

This development effort centers on three targeted improvements in the focal-plane architecture. The first is to extend stray-light rejection bandwidth up to the 700-GHz gap frequency of the superconducting niobium circuitry. Measurements indicate that the achieved limit is ~500 GHz, limited by the closeout approach adopted in the current generation of device structures. This response has been refined by implementing vias in the silicon substrate that enable the micro-machined backshort assembly to be bonded directly to the ground plane. These vias complete the electromagnetic closeout of the detector and eliminate unintended coupling paths for out-of-band radiation. Second, we implemented direct access to the microwave ground plane to provide greater signal fidelity. This architectural improvement has been demonstrated to improve the noise performance of the devices in a prototype structure. The final architectural improvement extends the use of "crossovers," which allow the microstrip from waveguide-coupling probes to be routed on-chip to higher frequencies.

In our 40- and 90-GHz detectors, this detail has been handled using a novel "via-less" crossover [6]. To extend these design concepts to higher frequencies, we implemented "air-bridge" crossovers, in which one line crosses over the other with an air gap between them. Efforts are also underway to enhance the TES topology and device thermalization. In addition, fabrication-process improvements were targeted to improve yield, reliability, and uniformity. These upgrades will be incorporated into focal-plane arrays as they are demonstrated.

Progress and Accomplishments

Fabrication processes for the ground-plane contacts and backshort assembly vias (Fig. 2) have been developed and validated. The ground-plane contacts and backshort-assembly vias have been integrated into detector arrays at 90 GHz (Fig. 3) and have passed continuity and environmental tests. These features have also been implemented in the dichroic 150/220-GHz detector designs, and are currently in production (Fig. 4). Air-bridge crossover designs have been fabricated and tested [7]. In addition, the via-less crossover has been refined and integrated into detector arrays. The TES membrane thermal design has been improved in both the 90- and 150/220-GHz arrays. This improvement decreases the thermalization time scale for the membrane, and leads to improved noise performance at low frequencies. Finally, a cryogenic thermal calibration source was developed and validated from ~30-300 GHz for validating the optical-efficiency polarimetric sensors [8].

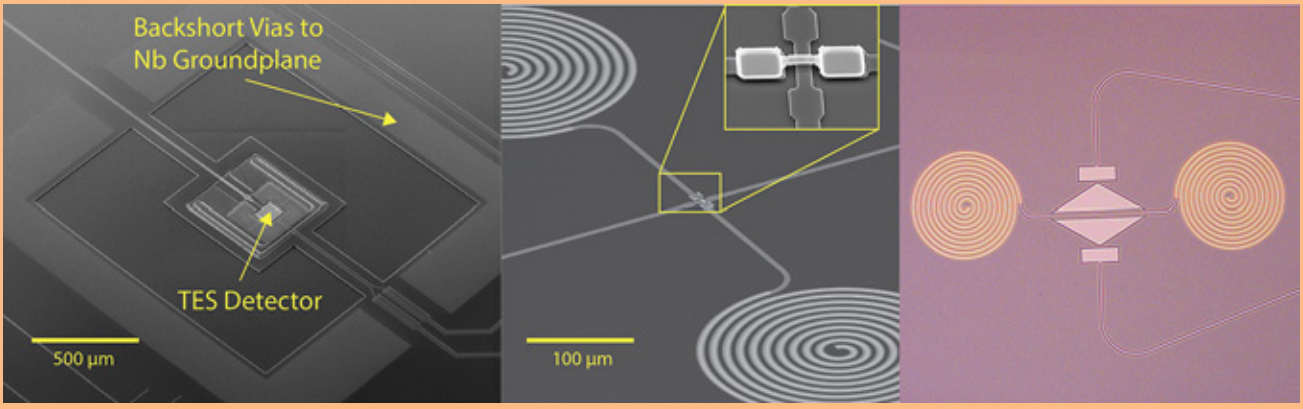

Fig. 2. Left: *Backshort vias are used to connect the backshort assembly wafer directly to the detector wafer ground plane. This forms a complete electromagnetic shield to mitigate stray radiation from coupling to the detector.* Center: *The air-bridge crossover fabrication process has been demonstrated. These millimeter-wave circuit structures on silicon have limited radiation loss and increased coupling bandwidth.* Right: *An alternate via-less crossover approach has been designed and fabricated.*

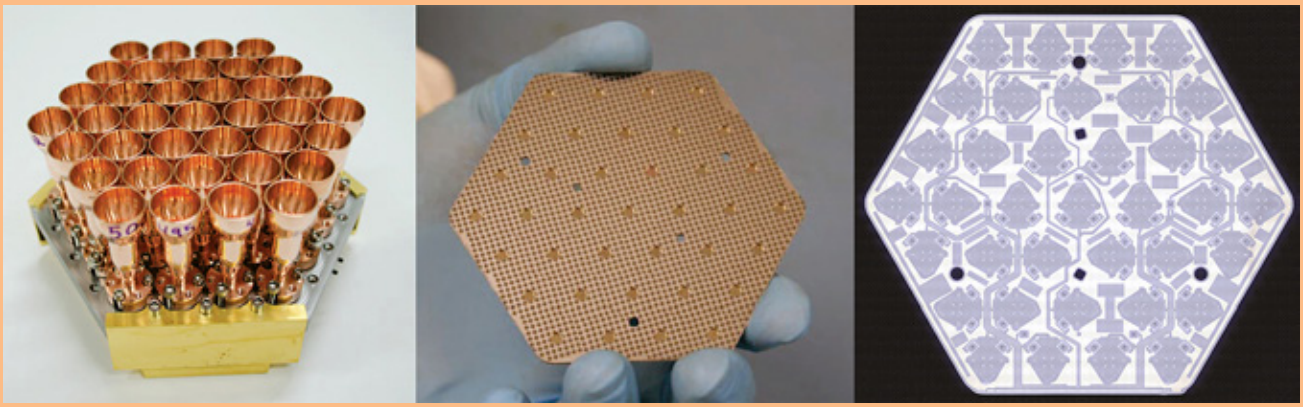

Fig. 3. Left: *A complete 90-GHz sub-array prototype module is shown.* Center: *The 37-element integrated wafer.* Right: *This wafer includes the vias and ground-plane contacts described in the text.*

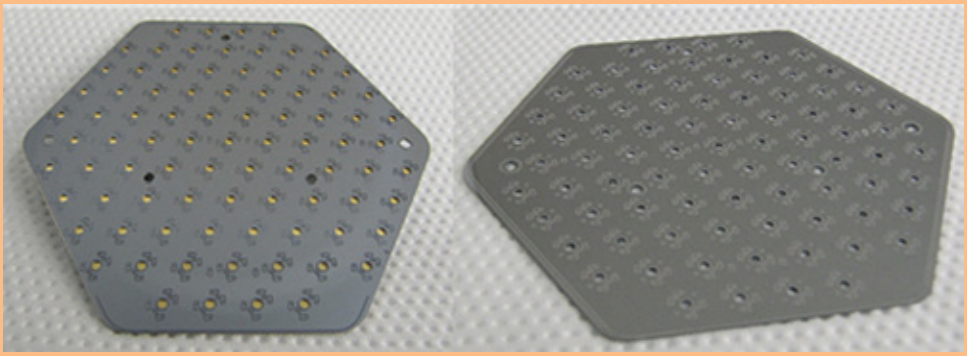

Fig. 4. *Dichroic arrays operating at 150/220 GHz are currently being fabricated.* Left: *Micro-machined backshort assembly.* Right: *Micro-machined photonic choke wafer.*

Path Forward

As a component of this effort, a multi-channel readout system has been commissioned for validating both the 90-GHz and 150/220-GHz arrays [9]. Optical efficiency and electronic characterization are underway for the 90-GHz prototypes, and the 150/220-GHz arrays are nearing completion. Representative focal-plane arrays will be integrated into the Cosmology Large Angular Scale Surveyor (CLASS) telescope [10] to achieve and demonstrate the TRL objectives for this technology. Targeted test structures are planned to investigate the sensors' electron-phonon coupling properties in greater detail, with an eye toward improved device performance and achieving greater control over key fabrication parameters. In addition to the performance improvements achieved on individual devices, these research efforts have driven the maturation of the processes required to realize large focal planes with improved reliability and yield.

References

[1] Blandford et al., "*New Worlds, New Horizons in Astronomy and Astrophysics*," National Academy of Sciences (2010)

[2] National Aeronautics and Space Administration, "*Enduring Quests, Daring Visions*," Astrophysics Roadmap (2013)

[3] D.T. Chuss et al., "*Cosmology Large Angular Scale Surveyor (CLASS) Focal Plane Development*," Journal of Low Temperature Physics, 101007/s10909-015-1368-9 (2016)

[4] K.L. Denis et al., "*Fabrication of Feedhorn-Coupled Transition Edge Sensor Arrays for Measurement of the Cosmic Microwave Background Polarization*," Journal of Low Temperature Physics, 10.1007/s10909-015-1366-y (2016)

[5] K. Rostem et al., "*Scalable Background-Limited Polarization-Sensitive Detectors for mm-wave Applications*," Proc. SPIE **9153**, 91530B (2014)

[6] K. U-yen, E.J. Wollack, S.H. Moseley, T.R. Stevenson, W.-T. Hsieh, and N.T. Cao, "*Via-less microwave crossover using microstrip-cpw transitions in slotline propagation mode*," in Microwave Symposium Digest, MTT '09, IEEE MTT-S International, 1029-1032 (2009)

[7] K.L. Denis, A.D. Brown, M.P. Chang, R. Hu, K. Rostem, K. U-Yen, and E.J. Wollack, "*Fabrication of Superconducting Vacuum-Gap Crossovers for High Performance Microwave Applications*," IEEE Transactions on Applied Superconductivity, **27**, 4, 1-4 (2017)

[8] D.T. Chuss, K. Rostem, E.J. Wollack, L. Berman, F. Colazo, M. DeGeorge, K. Helson, and M. Sagliocca, "*A Compact Cryogenic Thermal Source for Detector Array Characterization*," RSI, accepted (2017)

[9] K. Rostem, A. Ali, J.W. Appel, C.L. Bennett, A. Brown, M.P. Chang, D.T. Chuss, F.Colazo, K.L. Denis, T. Essinger-Hileman, R. Hu, T.A. Marriage, S.H. Moseley, T.R. Stevenson, K. U-Yen, E.J. Wollack, and Z. Xu, "*Silicon-based antenna-coupled polarization-sensitive millimeter-wave bolometer arrays for cosmic microwave background instruments*," Proc. SPIE, **9914**, 99140D-99140D-10 (2016)

[10] K. Harrington et al., "*The Cosmology Large Angular Scale Surveyor*," Proc. SPIE, **9914**, 99141K, (2016)

For additional information, contact Edward Wollack: *Edward.J.Wollack@nasa.gov*

High-Speed, Low-Noise, Radiation-Tolerant CCD Image Sensors for Strategic High-Energy Astrophysics Missions

By Mark Bautz (MIT)

NASA's 2016 Physics of the Cosmos Program Annual Technology Report (PATR) identifies 'fast, low-noise, megapixel X-ray imaging arrays' as a top-priority technology development need for future strategic astrophysics missions. The Lynx large mission concept now under study by NASA for presentation to the 2020 Decadal Survey in Astronomy and Astrophysics, in particular, includes a notional high-definition X-ray imaging instrument requiring a combination of readout rate, noise, spatial resolution and size that cannot be furnished by currently-mature technologies.

We have been developing a new generation of charge-coupled device (CCD) detectors with the aim of meeting this need. X-ray imaging CCDs have been flown successfully for more than twenty years, and state of the art devices provide low noise and near-theoretical spectral resolution, as well as spatial resolution and size approaching that required for Lynx. However, Lynx requires detector readout rates more than two orders of magnitude faster than current technology, with no compromise in noise or spectral resolution. This performance must be achieved within the instrument power and mass constraints and maintained over the expected lifetime of a strategic mission.

We propose to advance the readiness of CCD technology to meet these requirements by capitalizing on developments at MIT Lincoln Laboratory for other applications which also require fast, large format, low-noise, low-power imagers. Building on high-speed prototype CCD X-ray detectors currently operating in our laboratory, we aim to fabricate and demonstrate devices with lower noise, better low-energy quantum efficiency, and improved radiation tolerance.

For additional information, contact Mark Bautz: *mwb@space.mit.edu*

Superconducting Antenna-Coupled Detectors for CMB Polarimetry with the Inflation Probe

By James J. Bock (JPL)

We propose to develop advanced, high-sensitivity millimeter-wave detector arrays for measuring the polarization of the cosmic microwave background (CMB). The arrays are based on planar antennas that provide beam collimation, polarization analysis, and spectral band definition in a compact lithographed format that eliminates discrete fore-optics such as lenses and feedhorns. The antennas are coupled to transition-edge superconducting (TES) bolometers, read out with multiplexed SQUID current amplifiers. This development is directed to advance the technology readiness of the Inflation Probe mission in NASA's Physics of the Cosmos program. The Inflation Probe is a fourth-generation CMB satellite that will measure the polarization of the CMB to astrophysical limits, characterizing the inflationary polarization signal, mapping large-scale structure based on polarization induced by gravitational lensing, and mapping Galactic magnetic fields through measurements of polarized dust emission. The inflationary polarization signal is produced by a background of gravitational waves from the epoch of inflation, an exponential expansion of space-time in the early universe, with an amplitude that depends on the physical mechanism producing inflation. The inflationary polarization signal may be distinguished by its unique 'B-mode' vector properties from polarization from the density variations that predominantly source CMB temperature anisotropy.

Observations with these detectors currently provide the world's leading constraints on the inflationary B-mode polarization signal and, in turn, constraints on inflationary physics. Devices have been developed that demonstrate sensitivity, stability, and tolerance of energetic particles in an long-duration balloon environment. Ground-based receivers using these detectors demonstrate precise control of systematic errors at sensitivities in small sky patches that are representative of the Inflation Probe. New arrays operating at 220 and 270 GHz are now providing the most sensitive determinations of polarized emission from interstellar dust.

We propose to advance specific aspects of antenna-coupled superconducting detectors so that they have high technology readiness for space applications, including the NASA Inflation Probe and upcoming international satellite opportunities. For this proposal we will develop a diplexed 30/40 GHz dual-polarization antenna that saves focal plane area, a premium at low frequencies where devices are physically large. We will design, fabricate, and test a new focal plane module for housing arrays made on 150 mm diameter wafers that is compatible with 30, 40, 95 and 150 GHz layouts. Both the diplexed 30/40 GHz antennas and the modules are well-suited for immediate use in sub-orbital and ground-based science experiments. We will design and characterize a passive resonator chip for measuring propagation loss in Nb and dielectric materials. The chip is designed for rapid and routine process monitoring on production wafers. Finally we will develop spatially uniform AlMn TES films, and characterize array cosmic ray susceptibility at 100 mK, extending successful performance measurements at 300 mK.

For additional information, contact James Bock: *james.j.bock@jpl.nasa.gov*

Appendix D
Acronyms

A

AAS . . . . . American Astronomical Society
AC . . . . . Alternating Current
ACAs . . . . . Anisotropic Conductive Adhesives
ACF . . . . . Anisotropic Conductive Film
ACIS . . . . . Advanced CCD Imaging Spectrometer
ADC. . . . . Analog-to-Digital Converter
ADR. . . . . Adiabatic Demagnetization Refrigeration
AEGIS . . . . . Astrophysics Experiment for Grating and Imaging Spectroscopy
AEI . . . . . Albert Einstein Institute (Hannover)
AFM. . . . . Atomic-Force-Microscopy
AGN. . . . . Active Galactic Nuclei
AIM . . . . . Advanced Interferometry and Metrology
AIP . . . . . American Institute of Physics
AIP . . . . . Astrophysics Implementation Plan
ALD . . . . . Atomic Layer Deposition
ANU. . . . . Australian National University
AO. . . . . Announcement of Opportunity
AOM . . . . . Acousto-Optic Modulator
APD. . . . . Astrophysics Division
APRA. . . . . Astrophysics Research and Analysis
APS . . . . . Active Pixel Sensor
AR . . . . . Anti-Reflection
ASCA . . . . . Advanced Satellite for Cosmology and Astrophysics
ASE . . . . . Amplitude-Stimulated Emission
ASST . . . . . Athena Science Study Team
Athena . . . . . Advanced Telescope for High-ENergy Astrophysics
AXAF . . . . . Advanced X-ray Astrophysics Facility
AXRO . . . . . Adjustable X-ray Optics
AXSIO . . . . . Advanced X-ray Spectroscopic Imaging Observatory

B

BI . . . . . Back-Illuminated
BICEP . . . . . Background Imaging of Cosmic Extragalactic Polarization
BOX. . . . . Buried Oxide
BRDF. . . . . Bidirectional Reflectance Distribution Function

C

CAD. . . . . Computer-Aided Design
CAT . . . . . Critical-Angle Transmission
CATXGS. . . . . Critical-Angle Transmission X-ray Grating Spectrometer
CCD. . . . . Charge-Coupled Device

CDA . . . . . Centroid Detector Assembly
CDF . . . . . Concurrent Design Facility
CDM . . . . . Code-Division Multiplexing
CDR . . . . . Critical Design Review
CDS . . . . . Correlated Double Sampling
CGH . . . . . Computer-Generated Hologram
CLASS . . . . . Cosmology Large-Angular-Scale Surveyor
CMB . . . . . Cosmic Microwave Background
CMOS . . . . . Complementary Metal Oxide Semiconductor
CNR . . . . . Carrier-to-Noise (density) Ratio
CNT . . . . . Carbon Nanotube
COPAG . . . . . Cosmic Origins Program Analysis Group
COR . . . . . Cosmic Origins
COTS . . . . . Commercial off the Shelf
CR . . . . . Cosmic Rays
CRESST . . . . . Center for Research and Exploration in Space Science & Technology
CST . . . . . Community Science Team
CTA . . . . . Cherenkov Telescope Array
CTE . . . . . Coefficient of Thermal Expansion
CY . . . . . Calendar Year

D

DAM . . . . . Detector Assembly Mount
DC . . . . . Direct Current
Dec . . . . . Declination
deg . . . . . Degrees
DLR . . . . . Dienstleistungszentrum L.ndlicher Raum (German Aerospace Center)
DM . . . . . Demonstration Model
dof . . . . . degree of freedom
DRIE . . . . . Deep Reactive Ion Etching
DWS . . . . . Differential Wavefront Sensing

E

E . . . . . Energy
E-beam . . . . . Electron-beam
e-ROSITA . . . . . extended ROentgen Survey with an Imaging Telescope Array
EBEX . . . . . The E and B Experiment
EC . . . . . Executive Committee
ECL . . . . . External Cavity Laser
EED . . . . . Encircled Energy Diameter
eLISA . . . . . evolved Laser Interferometer Space Antenna
EM . . . . . Electromagnetic
EM . . . . . Engineering Model
EOM . . . . . ElectroOptic Phase Modulator
ENSCI . . . . . Euclid NASA Science Center at IPAC
ERP . . . . . Event Recognition Processor
ESA . . . . . European Space Agency

EUSO . . . . . Extreme Universe Space Observatory
ExEP . . . . . Exoplanet Exploration Program
ExoPAG . . . . . Exoplanet Exploration Program Analysis Group

F

FDM . . . . . Frequency-Division Multiplexed
FDM . . . . . Frequency-Domain Multiplexing
FEA . . . . . Finite Element Analysis
FI. . . . . Front-Illuminated
FLL . . . . . Flux-Lock-loop
FOV . . . . . Field of View
FPA . . . . . Focal-Plane Array/Assembly
FPGA . . . . . Field Programmable Gate Array
FTS . . . . . Fourier-Transform Spectroscopy
FWHM . . . . . Full-Width at Half-Maximum
FY . . . . . Fiscal Year

G

GAS . . . . . Grating-Array Structure
GEMS. . . . . Gravity and Extreme Magnetism Small Explorer
GEVS . . . . . General Environmental Verification Standard
GFE . . . . . Government-Furnished Equipment
GLAST . . . . . Gamma-ray Large-Area Space Telescope
GOAT. . . . . Gravitational Observatory Advisory Team
GOF. . . . . Guest-Observer Facility
GPS . . . . . Global Positioning System
GR . . . . . General Relativity
GRACE. . . . . Gravity Recovery and Climate Experiment
GRACE-FO . . . . . GRACE Follow-On
GRB. . . . . Gamma-Ray Burst
GRS . . . . . Gravitational Reference System
GRS . . . . . Gravitational Reference Sensor
GSE . . . . . Ground Support Equipment
GSFC . . . . . Goddard Space Flight Center
GW . . . . . Gravitational Wave

H

HabEx . . . . . Habitable Exoplanet
HDXI . . . . . High-Definition X-ray Imager
HETGS. . . . . High-Energy Transmission-Grating Spectrometer
HFDFC. . . . . High-Fidelity Deterministic Figure Control
HFSS . . . . . High-Frequency Structural Simulator
HPD . . . . . Half-Power Diameter
HQ . . . . . Headquarters
HRMA . . . . . High-Resolution Mirror Assembly

I

IAU . . . . . International Astronomical Union
IBS . . . . . Ion-Beam Sputtering

IF. . . . . Intermediate Frequency
INFN . . . . . Istituto Nazionale di Fizica Nucleare (Italian National Institute for Nuclear Physics)
I/O . . . . . Input/Output
IP . . . . . Inflation Probe
IPAC . . . . . Infrared Processing and Analysis Center
IR . . . . . Infrared
IR&D / IRAD . . . . . Internal Research and Development
ISS. . . . . International Space Station
ITT . . . . . Invitation to Tender
I-V . . . . . Current-Voltage
IXO . . . . . International X-ray Observatory
IXPE . . . . . Imaging X-ray Polarimeter Explorer

J

JANUS . . . . . Joint Astrophysics Nascent Universe Satellite
JAXA . . . . . Japanese Aerospace eXploration Agency
JEM . . . . . Japanese Experiment Module
JHU . . . . . Johns Hopkins University
JPL. . . . . Jet Propulsion Laboratory
JUICE. . . . . JUpiter ICy moons Explorer
JWST . . . . . James Webb Space Telescope

K

KAGRA . . . . . KAmioka GRAvitational-wave telescope

L

LADEE . . . . . Lunar Atmosphere and Dust Environment Explorer
LAOP . . . . . Large-Area Optical Performance
LBNL . . . . . Lawrence Berkeley National Laboratory
LCD . . . . . Liquid Crystal Display
LCRD . . . . . Laser Communication Relay Demonstration
LD . . . . . Laser Diode
LED . . . . . Light-Emitting Diode
LEO . . . . . Low Earth Orbit
LIGO . . . . . Laser Interferometer Gravitational-wave Observatory
LISA. . . . . Laser Interferometer Space Antenna
LiteBIRD . . . . . Lite (Light) satellite for the studies of B-mode polarization and Inflation from cosmic background Radiation Detection
LLC . . . . . Limited Liability Company
LP . . . . . Line Processor
LPA . . . . . Large-Pixel Array
LPF . . . . . LISA Pathfinder
LRI. . . . . Laser-Ranging Interferometer
LRP . . . . . Laser-Ranging Processor
LSF . . . . . Line Spread Function
LSS . . . . . Lower Sideband-Sideband
LTP . . . . . LISA Technology Package
LUPI . . . . . Laser Unequal Path-length Interferometer

LUVOIR . . . . . Large UV/Optical/IR
LVS . . . . . Leon Van Speybroeck
L1 . . . . . Level 1
L2 . . . . . Level 2
L2 . . . . . Second large space mission of ESA's Cosmic Vision program
L3 . . . . . Third large space mission of ESA's Cosmic Vision program
L3ST . . . . . L3 Study Team

M

MAXI . . . . . Monitor of All-sky X-ray Image
MBE. . . . . Molecular-Beam Epitaxy
MCC. . . . . Magnetically Coupled (micro-)Calorimeter
MCR. . . . . Mission Consolidation Review
MDL. . . . . Micro-Devices Laboratory
MEMS . . . . . Micro-Electro-Mechanical System
MIDEX. . . . . Medium-class Explorer
MIT . . . . . Massachusetts Institute of Technology
MKI . . . . . MIT Kavli Institute
MO . . . . . Mission of Opportunity
MOPA . . . . . Master Oscillator Power Amplifier
MPPC. . . . . Multi-Pixel Photon Counter
MSFC . . . . . Marshall Space Flight Center
MSM . . . . . Magnetic Smart Material
mux. . . . . multiplexer

N

NANOGrav. . . . . North American Nanohertz Observatory for Gravitational waves
NASA. . . . . National Aeronautics and Space Administration
Near-IR . . . . . Near-Infrared
NGO . . . . . New Gravitational-wave Observatory
NISP . . . . . Near-Infrared Spectrometer and Photometer
NIST . . . . . National Institute of Standards and Technology
NITPC . . . . . Negative-Ion Time Projection Chamber
NPP . . . . . NASA Postdoctoral Program
NPR. . . . . NASA Procedural Requirements
NPRO . . . . . Non-planar Ring Oscillator
NRC. . . . . National Research Council
NSF . . . . . National Science Foundation
NuSTAR . . . . . Nuclear Spectroscopic Telescope ARray
NWNH . . . . . New Worlds, New Horizons in Astronomy and Astrophysics (2010 Decadal Survey)
N-XGS . . . . . Notional X-ray Grating Spectrometer

O

OAP. . . . . Off-Axis Parabola
OBA . . . . . Optical Bench Assembly
OBF. . . . . Optical Blocking Filter
OCT. . . . . Office of the Chief Technologist
OEM . . . . . Original Equipment Manufacturer

OGRE . . . . . Off-plane Grating Rocket Experiment
OLED. . . . . Organic Light-Emitting Diode
OMT . . . . . Ortho-Mode Transducer
OP-XGS . . . . . Off-Plane X-ray Grating Spectrometer
OSIRIS-REx . . . . . Origins, Spectral Interpretation, Resource Identification, and Security-Regolith Explorer
OST . . . . . Origins Space Telescope
OWL . . . . . Orbiting Wide-angle Light collectors

P

PAG . . . . . Program Analysis Group
PATR . . . . . Program Annual Technology Report
PBS . . . . . Polarizing Beam-Splitter
PCB . . . . . Printed Circuit Board
PCI . . . . . Peripheral Component Interconnect
PCOS. . . . . Physics of the Cosmos
PD . . . . . Photodetector
PD . . . . . Pinhole Density
PDL . . . . . Product Design Lead
PDLs . . . . . Product Development Leads
PDR. . . . . Preliminary Design Review
PER . . . . . Polarization Extinction Ratio
PHARAO . . . . . Projet d'Horloge Atomique par Refroidissement d'Atomes en Orbit (On-Orbit Cooled-Atom Atomic Clock Project)
PhysPAG . . . . . Physics of the Cosmos Program Analysis Group
PI . . . . . Principal Investigator
PIPER . . . . . Primordial Inflation Polarization Explorer
PLC . . . . . Planar Linear Cavity
PLL . . . . . Phase Locked Loop
PM. . . . . Project Manager
PMS . . . . . Phase-Measurement System
PMT. . . . . Photomultiplier Tube
POD . . . . . Pixel Optical Density
POET. . . . . Polarimetry of Energetic Transients
PRAXyS . . . . . Polarimeter for Relativistic Astrophysical X-ray Sources
PRN. . . . . Pseudo-Random Noise
PRT . . . . . Platinum Resistance Thermometer
PSD . . . . . Power Slope Density
PSD . . . . . Power-Spectral Density
PSF . . . . . Point Spread Function
PSM. . . . . Point-Source Microscope
PSU . . . . . Penn State University
Pt. . . . . Platinum
PTB . . . . . Physikalisch-Technische Bundesanstalt (German National Metrology Institute)

Q

QE. . . . . Quantum Efficiency

R

RA . . . . . Right Ascension
RAM . . . . . Random Access Memory
R&D. . . . . Research and Development
REXIS . . . . . REgolith X-ray Imaging Spectrometer
RF . . . . . Radio Frequency
RFI . . . . . Request for Information
RFI . . . . . Radio Frequency Interference
RGS . . . . . Reflection-Grating Spectrometer
RIN . . . . . Relative Intensity Noise
RIO . . . . . Redfern Integrated Optics
rms . . . . . root mean square
ROC. . . . . Radius of Curvature
ROSES . . . . . Research Opportunities in Earth and Space Science
RTD. . . . . Resistance Temperature Detector
RTF . . . . . Roman Technology Fellowship
RXTE . . . . . Rossi X-ray Timing Explorer

S

SAC-B . . . . . Satelite de Aplicaciones Cientificas-B
SAO . . . . . Smithsonian Astrophysical Observatory
SAT . . . . . Strategic Astrophysics Technology
SBIR . . . . . Small Business Innovation Research
SBS . . . . . Stimulated Brillouin Scattering
S/C . . . . . Spacecraft
SEM . . . . . Scanning Electron Micrograph
SGO. . . . . Space-based Gravitational-wave Observatory
SGR . . . . . Soft-Gamma Repeater
SiPM . . . . . Silicon Photomultiplier
SLF . . . . . Stray-Light Facility
SMART-X . . . . . Square Meter, Arcsecond Resolution Telescope for X-rays
SMBH . . . . . Supermassive Black Hole
SMD. . . . . Science Mission Directorate
SMEX. . . . . Small Explorer
SOI . . . . . Silicon-on-Insulator
SOTA . . . . . State of the Art
SPA . . . . . Small-Pixel Array
SPC . . . . . Science Program Committee
Spider . . . . . Suborbital Polarimeter for Inflation Dust and the Epoch of Reionization
SPIE. . . . . Society of Photo-Optical Instrumentation Engineers
SPO . . . . . Silicon Pore Optic
SQUID . . . . . Superconducting QUantum Interference Device
SRON. . . . . Space Research Organization Netherlands
SR&T . . . . . Supporting Research and Technology
SSL . . . . . Space Sciences Laboratory
STD . . . . . Solar Time Delay

STDT . . . . . Science and Technology Definition Team
STI. . . . . SpaceTech International (Germany)
STMD. . . . . Space Technology Mission Directorate
STOP . . . . . Structural Thermal and Optical Performance
ST-7 . . . . . Space Technology 7

T

TBA . . . . . To Be Announced
TBD. . . . . To Be Determined
TC . . . . . Thermocouple
TDM . . . . . Time-Division Multiplexing/Multiplexed
TDM . . . . . Technology Development Module
TDR. . . . . Technology Development Roadmap
TES . . . . . Transition-Edge Sensor
TES . . . . . Transition-Edge Superconducting
TFB . . . . . Tapered Fiber Bundle
TFT . . . . . Thin-Film Transistors
TIS. . . . . Total Integrated Scatter
TM. . . . . Test Mass
TMB. . . . . Technology Management Board
TPC . . . . . Time Projection Chamber
TPCOS . . . . . Technology development for Physics of the Cosmos
TRL . . . . . Technology Readiness Level
TVAC . . . . . Thermal Vacuum

U

UHECR . . . . . Ultra-High-Energy Cosmic Ray
UIUC . . . . . University of Illinois Urbana-Champaign
UK. . . . . United Kingdom
UROP . . . . . Undergraduate Research Opportunities
US . . . . . United States
USO. . . . . Ultra-Stable Oscillator
USRA . . . . . Universities Space Research Association
USS . . . . . Upper Sideband-Sideband
UV . . . . . Ultraviolet

V

V5 . . . . . Virtex-5 (FPGA)

W

WDM . . . . . Wavelength-Division Multiplexer
WFI . . . . . Wide-Field Imager
WFIRST . . . . . Wide-Field Infrared Survey Telescope
WFS. . . . . Wavefront Sensor
WHIM . . . . . Warm-Hot Intergalactic Medium
WHIM . . . . . Warm-Hot Interstellar Medium

X

XARM . . . . . X-ray Astronomy Recovery Mission
XCSR . . . . . X-ray mission Concepts Study Report

XGS . . . . . X-ray Grating Spectrometer
X-IFU . . . . . X-ray Integral Field Unit
XMM-Newton . . . . . X-ray Multi-mirror Mission-Newton
XMS . . . . . X-ray Microcalorimeter Spectrometer
XRS . . . . . X-Ray Surveyor
XRT . . . . . X-Ray Telescope
XTiDE . . . . . X-ray Time Domain Explorer

Other

3NT . . . . . Three-Noise Tester